

International Conference

Progress in Organic and Macromolecular Compounds

**Dedicated to the 105th anniversary of
Acad. Cristofor I. Simionescu (1920-2007)**

Proceedings

ISSN 2810 – 2126 ISSN – L 2810 – 2126



**International Conference Progress in Organic and Macromolecular Compounds
30th Edition**

ICMPP – Petru Poni Institute of Macromolecular Chemistry

Iasi | Romania | September 23 - 26, 2025

Edited by

Marcela MIHAI | *Editor-in-Chief*

Radu-Dan RUSU | *Editor*

Cover by

Catalin-Paul CONSTANTIN

Technical editing by

Marcela MIHAI | Radu-Dan RUSU | Marius-Mihai ZAHARIA

Copyright © 2025

All rights reserved. Except as permitted under current legislation no part of this publication may be photocopied, reproduced or distributed in any form or by any means or stored in a database or retrieval system, without the prior permission from the copyright holders.

This book contains information obtained from authentic and highly regarded sources. Reprinted material is quoted with permission as signed by authors, and sources are indicated. Copyright for individual articles remains with the authors as indicated. A wide variety of references are listed. Reasonable efforts have been made to publish reliable data and information, but the authors, editors, and the publisher cannot assume responsibility for the validity of all materials or the consequences of their use.



Dear colleagues from Romania and abroad

It is our pleasure to invite you to attend at the 30th edition of the International Conference Progress in Organic and Macromolecular Compounds, MACRO Iasi 2025, a traditional event organized by the Petru Poni Institute of Macromolecular Chemistry, between 23 and 26 September 2025, in Iasi.

The International Conference addresses polymer and organic chemists and physicists from academia, research institutes and industry, being intended as a dynamic platform for the presentation and sharing of their research and ideas.

MACRO Iasi 2025 gives a broad overview of major topics in organic and polymer synthesis and physics, multifunctional polymeric architectures, engineering of polymeric materials and their applications.

Also, as part of the MACRO Iasi conference, the workshop “POLYSACCHARIDE BASED (BIO)HYBRID NANOSTRUCTURES” (September 23, 2025) will be organized, to which you are welcome to participate (please contact the organizers - hybsac.pnrr@icmpp.ro).

This meeting could not have been organized without the generous and tireless support and contribution of many individuals and groups within and outside the ICMPP. Therefore, we would like to acknowledge to all the invited lecturers, speakers, board and committee members, chairpersons, sponsors and all the people that have been involved in the organization and presentation of relevant results and perspectives.

Best wishes for a professionally rewarding conference!

Valeria HARABAGIU and Marcela MIHAI

Chairpersons of MACRO Iasi 2025



International Scientific Board

- David HADDLETON (U Warwick, UK)
- Eric GUIBAL (CME, Ales, France)
- Dieter SCHLUTER (ETH Zurich, Switzerland)
- Andreas FERY (IPF, Dresden, Germany)
- Stergios PISPAS (NHRF, Athens, Greece)
- Patrick NAVARD (CEMEF, Sophia Antipolis, France)
- Svetlana BRATSKAYA (ICB FEBRAS, Vladivostok, Russia)
- Olya STOILOVA (IP-BAS, Sofia, Bulgaria)
- Aleksandra WOLINSKA-GRABCZYK (CPCM-PAS, Zabrze, Poland)
- Tania BUDTOVA (CNRS, Sophia Antipolis, France)
- Carmen TEODOSIU (TU, Iasi, Romania)
- Raluca-Ioana STEFAN-VAN STADEN (INCEMC, Bucharest, Romania)
- Florica MANEA (UPT, Timisoara, Romania)
- Gabi DROCHIOIU (UAIC, Iasi, Romania)
- Calin DELEANU (CCO, Bucharest, Romania)
- Anton AIRINEI (ICMPP, Iasi, Romania)
- Maria CAZACU (ICMPP, Iasi, Romania)
- Mariana PINTEALA (ICMPP, Iasi, Romania)
- Sergiu COSERI (ICMPP, Iasi, Romania)
- Luminita MARIN (ICMPP, Iasi, Romania)
- Gheorghe FUNDUEANU-CONSTANTIN (ICMPP, Iasi, Romania)
- Mariana Dana DAMACEANU (ICMPP, Iasi, Romania)
- Mariana CRISTEA (ICMPP, Iasi, Romania)

Organizing Board

Program

- Marcela MIHAI
- Sergiu COSERI
- Radu-Dan RUSU

Editorial

- Marius-Mihai ZAHARIA
- Catalin Paul CONSTANTIN
- Catalin BUZDUGAN – IT support

Executive

- Narcisa Laura MARANGOCI
- Mirela ZALTARIOV
- Florica DOROFTEI
- Alina-Petronela MORARU
- Timeea-Anastasia CIOBANU
- Melinda-Maria BAZARGHIDEANU
- Dumitru POPOVICI



CONTENT

INVITED LECTURERS.....	12
CRISTOFOR I. SIMIONESCU, THE MAN WITHIN	
Bogdana Simionescu	16
PLENARY LECTURES	
MAGNETIC AND LUMINESCENT MOLECULAR MATERIALS CONSTRUCTED FROM LANTHANIDES: NEW SYNTHETIC APPROACHES	
Marius Andruh	20
EMERGING FUNCTIONAL HYBRID NANOMATERIALS BASED ON GALLIUM NITRIDE AND AEROGALNITE	
Ion Tiginyanu, Tudor Braniste	22
EMERGING FUNCTIONAL HYBRID NANOMATERIALS BASED ON GALLIUM NITRIDE AND AEROGALNITE	
Michele Laus, Riccardo Chiarcos, Michele Perego	25
TURNING LIQUIDS SOLID: FROM EMULSIONS TO MICROMIXERS	
Cristian Silvestru, Gabriel Dunes, Alpar Pöllnitz, Alexandru Sava, Yann Sarazin	28
EFFECTS OF MONOMER SEQUENCE AND CHEMICAL COMPOSITION ON THERMORESPONSIVE PHASE TRANSITION OF OEGMA-BASED SYMMETRIC PENTABLOCK TERPOLYMERS	
Shaobai Wang, Theoni K. Georgiou	31
ENGINEERING FUNCTIONAL NANOPLATFORMS FOR BIOIMAGING AND THERAPEUTIC AGENT DELIVERY	
Mariana Pinteala, Dragos Peptanariu, Bogdan Craciun, Denisse-Iulia Bostiog, Tudor Vasiliu, Petru Tirnovan, Razvan Puf, Cristina Uritu, Teodora Rusu, Adrian Fifere, Andrei Neamtu	34
RESPONSIVE POLYMERIC NANOCAPSULES AND MULTI-COMPARTMENTS AS CELLULAR MIMICS	
Brigitte Voit.....	39
POLYMER MEMBRANES FOR ENERGY APPLICATIONS CHARACTERIZED BY NEUTRON SCATTERING TECHNIQUES	
Aurel Radulescu	42



NEW WAYS FOR FUNCTIONAL NANOMATERIALS: THE JOURNEY FROM LINEAR TO STAR-SHAPED POLYMERS

Barbara Mendrek, Marcelina Bochenek, Natalia Oleszko-Torbus, Agnieszka Kowalczyk 45

POLYMER PRECISION IN POLYMER SYNTHESIS: FROM SUSTAINABLE POLYMERS TO BIOACTIVE GLYCOPOLYMERS

C. Remzi Becer 48

PLENARY LECTURES WORKSHOP HYBSAC

POLYMER-PROTEIN COMPLEXES AS VERSATILE CARRIERS FOR TARGETED PROTEIN AND DRUG DELIVERY CHARACTERIZED BY SMALL-ANGLE NEUTRON SCATTERING

Aurel Radulescu 50

MULTIFUNCTIONAL POLYSACCHARIDE-BASED HYBRID HYDROGELS WITH POROSITY TAILORED BY CRYOTROPIC GELATION

Maria Valentina Dinu, Maria Marinela Lazar, Claudiu Augustin Ghiorghita, Irina Elena Raschip, Ioana Victoria Platon..... 53

REACHING FOR THE STARS WITH NEW GENERATIONS OF FUNCTIONAL POLYMETHACRYLATES

Anna Celny, Paulina Teper, Barbara Mendrek, Agnieszka Kowalczyk 56

FROM TREES TO TECH: THE SILENT REVOLUTION OF CELLULOSE NANOFIBERS IN BIOELECTRONICS

Sergiu Coseri 58

LECTURES

RETRACTION OF VISCOELASTIC FLUID AFTER THE RUPTURE OF THE FILAMENT

Ciprian Mateescu, Doru-Daniel Cristea, Nicoleta Tanase, Corneliu Balan..... 61

SUPRAMOLECULAR ORGANIC SEMICONDUCTING MATERIALS FOR BIO-ELECTRONICS

Aurica Farcas, Ana-Maria Resmerita 64

MAKING LINEAR CIRCULAR: FROM CELLULOSE/LIGNIN TO BIOPLASTICS, BIO-H2 AND AROMATICS

Xiaoyan Ji, Leon Engelbrecht, Yonglei Wang, Francesca Mocci, Narcis Cibotariu, Aatto Laaksonen..... 67

ENGINEERING POLY(2-OXAZOLINE) NANOSTRUCTURES FOR BIOMEDICAL USE

Marcelina Bochenek, Natalia Oleszko-Torbus, Barbara Mendrek, Alicja Utrata-Wesołek, Wojciech Wałach, Violeta Mitova, Neli Koseva, Agnieszka Kowalczyk 70



USING EPR SPECTROSCOPY TO INVESTIGATE COMPLEX SUPRAMOLECULAR SYSTEMS

Gabriela Ionita, Sylvain R. A. Marque, Jean-Patrick Joly, Iulia Matei,
Alexandru Gabriel Bucur 73

MULTIPLE TARGET LIGANDS WITH AZAHEREROCYCLES SKELETON

Ionel I. Mangalagiu, Dorina Amariuca-Mantu, Vasilichea Antoci, Gheorghita Zbancioc,
Costel Moldoveniu, Violeta Mangalagiu 76

ORAL COMMUNICATIONS

INACCURACIES IN INTERPRETING THERMORHEOLOGICAL BEHAVIOR OF SOME POLYMERS: TO WHAT EXTENT THEY INFLUENCE THE CONCLUSIONS

Daniela Ionita, Mariana Cristea, Costel Gaina 79

SORPTION PERFORMANCE OF ZWITTERIONIC RESINS FOR HEAVY METAL DECONTAMINATION OF POLLUTED WATERS

Marius-Mihai Zaharia, Alina-Petronela Moraru, Ramona Ciobanu, Florin Bucatariu,
Marcela Mihai 82

SENSING COATINGS BASED ON A HARD-SOFT COPOLYIMIDE FOR TOLUENE DETECTION

Irina Butnaru, Adriana-Petronela Chiriac, Loredana Vacareanu, Mariana-Dana Damaceanu .. 85

NANOMETRIC EM-VESICLES WITH ENHANCED BIOPHARMACEUTICAL ATTRIBUTES

Vera-Maria Platon, Anda M. Craciun, Irina Rosca, Natalia Simionescu, Luminita Marin 88

OLD COMPOUNDS, NEW PURPOSE: IODINE-SUBSTITUTED PYRROL-2-ONES FOR TARGETED ANTITUMOR THERAPY

Cristina M. Al-Matarneh, Natalia Simionescu, Ashraf Al-Matarneh, Ionel I. Mangalagiu 91

THE EFFECT OF MICELLIZATION ON THE EPR SPECTRA OF NITRONYL NITROXIDES WITH ALKYL CHAINS RADICALS

Alexandru Gabriel Bucur, Alexandru V. F. Neculae, Mihaela Lavinia Ciutu,
Georgiana Alexandra Sanda, Sevasti Matsia, Gabriela Ionita 94

LIGNIN CARBON-BASED STRUCTURES: SYNTHESIS ROUTE AND PHYSICOCHEMICAL FEATURES

Irina Apostol, Narcis Anghel 97

SUSTAINABLE PET RECYCLING THROUGH DESIGN THINKING: CIRCULAR CHEMISTRY SOLUTIONS

Andra-Cristina Enache, Petrisor Samoila, Corneliu Cojocaru, Ionela Grecu,
Valeria Harabagiu 100



MODULATED TEMPERATURE DSC: FROM THEORY TO APPLICATIONS IN POLYMER CHARACTERIZATION Paul Lazar.....	103
PLASMA-ACTIVATED POLYMERS AND FORMULATIONS FOR CANCER TREATMENT Camelia Miron, Luminita Marin, Taishi Yamakawa, Koki Ono, Ryo Wakatsukasa, Manuela Iftime, Kenji Ishikawa, Shinya Toyokuni, Masaru Hori, Hiromasa Tanaka	106
SUPRAMOLECULAR GOLD AGGREGATES WITH ENHANCED VISIBLE-LIGHT ABSORPTION FOR PHOTOTHERMAL APPLICATIONS Elena-Laura Ursu	109
ENHANCEMENT OF AUTOPHAGY-INDUCING COMPOUNDS BY NITROGEN REACTIVE SPECIES FROM ATMOSPHERIC PRESSURE PLASMA Taishi Yamakawa, Ayako Tanaka, Camelia Miron, Kenji Ishikawa, Masaru Hori, Hiromasa Tanaka.....	112
MULTIFUNCTIONALITY OF XANTHAN-BASED CRYOGELS ENRICHED WITH ANTHOCYANINS Ioana-Victoria Platon, Irina Elena Raschip, Nicusor Fifere, Maria Valentina Dinu	115
INTERACTION STUDIES OF CHITOSAN-g-PNIPAM MULTIRESPONSIVE CHAINS WITH A MODEL PROTEIN Florin Bucatariu, Marius-Mihai Zaharia, Larisa-Maria Petrila, Marcela Mihai, Stergios Pispas	118
EVALUATION OF BACCAUREA PLANT FOR THEIR USE AS ANTIOXIDANT COMPOUNDS IN POLYMERIC MATERIALS Daniela Pamfil, Elena Butnaru, Benedict Samling, Sim Siong Fong, Shafri Bin Semawi Mihai Brebu, Elena Stoleru	121
SYNTHESIS OF AN INDOLOBENZAZOCINE DERIVATIVE FOR INHIBITION OF TUBULIN POLYMERIZATION Marin-Aurel Trofin, Irina Kuznetcova, Ioana-Antonia Iftimie, Mihaela Balan-Porcarasu, Mihaela Dascalu, Gheorghe Roman, Maria Cazacu, Vladimir Arion	124
MULTIFUNCTIONAL PULLULAN-POLYVINYL ALCOHOL HYDROGELS WITH MULTIPLE CROSSLINKING STRATEGIES Ioana-Sabina Trifan, Gabriela Biliuta, Raluca Baron, Sergiu Coseri	127
DUAL FUNCTIONAL PHENOXAZINE-BASED POLYMERS: BRIDGING NIR ELECTROCHROMIC AND ENERGY STORAGE APPLICATIONS Catalin-Paul Constantin, Andra-Elena Bejan, Adriana-Petronela Chiriac.....	130
NOVEL BIOCATALYSTS AS LACCASE/POLYSACCHARIDE NANOASSEMBLIES Larisa-Maria Petrila, Maria Karayianni, Tudor Vasiliu, Stergios Pispas, Marcela Mihai	133



ORAL COMMUNICATIONS WORKSHOP HYBSAC

CHITOSAN-g-POLY(N-ISOPROPYLACRYLAMIDE) POLYPLEXES WITH DNA MOLECULES OF DIFFERENT LENGTHS Maria Karayianni, Elena-Daniela Lotos, Marcela Mihai, Stergios Pispas.....	136
GREEN SYNTHESIS OF GOLD NANOPARTICLES STABILIZED BY AMYLOPECTIN-g- POLY (ACRYLIC ACID) COPOLYMER Melinda-Maria Bazarghideanu, Marius-Mihai Zaharia, Alina-Petronela Moraru, Florin Bucatariu, Stergios Pispas, Marcela Mihai.....	139
NEW THERMORESPONSIVE COMPOSITES CONTAINING CHITOSAN-g-PNIPAM AND <i>IN SITU</i> FORMED GOLD NANOPARTICLES Marius-Mihai Zaharia, Melinda-Maria Bazarghideanu, Alina-Petronela Moraru, Florin Bucatariu, Marcela Mihai, Stergios Pispas.....	142
SYNTHESIS AND CHARACTERIZATION OF pH-RESPONSIVE GRAFT COPOLYMER BASED ON POTATO STARCH AND POLY (ACRYLIC ACID) Diana Felicia Loghin, Stefania Racovita, Silvia Vasiliu, Mihaela Iuliana Avadanei, Ana-Maria Macsim, Melinda-Maria Bazarghideanu, Stergios Pispas, Marcela Mihai	145
NEW POLYSACCHARIDE GRAFTING METHOD PAIRING CHITOSAN WITH PNIPAM BEARING CARBOXYL END GROUP Elena-Daniela Lotos, Maria Karayianni, Marcela Mihai, Stergios Pispas.....	148

POSTERS

FLUORESCENCE PROPERTIES OF CARBON DOTS SYNTHESIZED <i>VIA</i> HYDROTHERMAL TREATMENT OF TRYPTOPHAN/N-HYDROXYPHTHALIMIDE PRECURSORS WITH MANGANESE DOPING: AN EXCITATION-EMISSION MATRIX STUDY Adina Coroaba, Ioan-Andrei Dascalu, Oana-Elena Carp, Narcisa-Laura Marangoci	151
THEORETICAL NORFLOXACIN LOADED BIODEGRADABLE CHITOSAN/QUATERNIZED CHITOSAN NANOFIBERS FUNCTIONALIZED WITH AN ANTIFUNGAL ALDEHYDE AS WOUND DRESSINGS Vera-Maria Platon, Sandu Cibotaru, Alexandru Anisie, Irina Rosca, Isabela-Andreea Sandu, Corneliu-George Coman, Liliana Mititelu-Tartau, Bianca-Iustina Andreica, Luminita Marin.	154
DEVELOPMENT AND CHARACTERIZATION OF A MULTIFUNCTIONAL BIOACTIVE COMPLEX AS A REGULATOR FOR MELANOGENESIS Alexandra Vieru, Alina Gabriela Rusu, Alina Ghilan, Liliana Mititelu-Tartau, Alexandru Serban, Loredana Elena Nita.....	157
NEXT-GENERATION ANTIBACTERIAL MATERIALS: TAILORED DESIGN AND SYNTHESIS OF PULLULAN DERIVATIVES Gabriela Biliuta, Raluca Ioana Baron, Sergiu Coseri.....	160



IDENTIFICATION OF FLUORESCENCE ORIGIN IN CARBON DOT SYNTHESIS

– CASE STUDY

Ioan-Andrei Dascalu, Maurusa Ignat, Adina Coroaba, Narcisa-Laura Marangoci..... 163

INVESTIGATION OF AMINE-RESPONSIVE PROPERTIES OF FUNCTIONALIZED AZULENES FOR POTENTIAL SENSING APPLICATIONS

Mihaela Homocianu, Dragos Lucian Isac, Anton Airinei, Mihaela Cristea 166

POLY(VINYL ALCOHOL)/GELATIN/TANNIC ACID/LIGNIN NANOPARTICLES HYDROGELS FOR AGRICULTURE APPLICATION

Cosmina-Maria Bogza, Maria-Cristina Popescu..... 169

NEW NANOCOMPOSITE MATERIALS WITH MULTIPLE THERMOREGULATION MECHANISMS

George Theodor Stiubianu, Bianca-Iulia Ciubotaru, Alexandra Bargan, Mihaela Dascalu, Adrian Bele, Cristian Ursu, Roxana Solomon 172

VERSATILE POLYIMIDE-BASED SENSING COATINGS FOR PHENOL VAPOURS DETECTION

Adriana-Petronela Chiriac, Irina Butnaru, Mariana-Dana Damaceanu 175

HYBRID THERMOREVERSIBLE POLYURETHANE-PEPTIDE HYDROGELS WITH SELF-HEALING PROPERTIES

Alexandra Lupu, Luiza Madalina Gradinaru, Vasile-Robert Gradinaru, Maria Bercea 178

POLY(2-OXAZOLINE)S CONJUGATED WITH CHELATORS FOR THE DESTRUCTION OF BACTERIAL CELL MEMBRANES

Marcelina Bochenek, Barbara Mendrek, Wojciech Wałach, Aleksander Foryś, Jerzy Kubacki, Łukasz Jałowicki, Jacek Borgulat, Grażyna Płaza, Agnieszka Klama-Baryła, Anna Sitkowska, Agnieszka Kowalczyk, Natalia Oleszko-Torbus 181

SIMULTANEOUS QUANTITATIVE DETERMINATION OF URSOLIC, POMOLIC, OLEANOLIC AND ROSMARINIC ACIDS IN PEPPERMINT EXTRACTS. A COMPARATIVE STUDY OF 2D-NMR AND HPLC DATA

Veaceslav Kulcitki, Adrian Topala, Vladilena Girbu, Alic Barba, Alina Nicolescu, Calin Deleanu..... 184

SILSESQUIOXANES-BASED HYBRID MATERIALS FOR ENVIRONMENTAL APPLICATIONS (CO₂ CAPTURE)

Alexandra Bargan, Mihaela Dascalu, Bianca-Iulia Ciubotaru, Mirela-Fernanda Zaltariov, Adrian Bele, George Theodor Stiubianu, Muslum Demir, Maria Cazacu 187

DESIGN AND ENGINEERING OF FLOATABLE HYBRID AEROGELS BASED ON CELLULOSE NANOFIBERS

Andreea L. Chibac-Scutaru, Violeta Melinte, Gabriela Biliuta, Madalina E. Bistriceanu, Raluca I. Baron, Sergiu Coseri..... 190



3D PRINTED SCAFFOLDS BASED ON FUNCTIONALISED GELATIN AND XANTHAN GUM FOR SOFT TISSUE ENGINEERING

Isabella Nacu, Anca Toma, Maria Butnaru, Loredana Elena Nita, Liliana Verestiuc 193

PROJECTS

POLYSACCHARIDE-BASED (BIO)HYBRID NANOSTRUCTURES – HYBSAC

Marcela Mihai, Stergios Pispas 197

INTELLIGENT SYSTEMS FOR CANCER DIAGNOSIS AND TREATMENT – IntelDots

Adina Coroaba, Narcisa-Laura Marangoci 200

METAL COMPLEXES AS MICROTUBULE- AND DUAL MICROTUBULE-R2 RNR-TARGETING DRUGS FOR CANCER TREATMENT – Metubin

Mihaela Dascalu, Vladimir Arion 203

MULTIFUNCTIONAL HYBRID 3D ARCHITECTURES BASED ON HOLLOW GAN NANO-MICRO-TETRAPODS FOR ADVANCED PPLICATIONS AT PETRU PONI INSTITUTE OF MACROMOLECULAR CHEMISTRY – MultiPodGaN

Narcisa-Laura Marangoci, Alexandru Rotaru, Tudor Braniste, Ion Tighineanu 206

BIOMAT4CAST DEVELOPMENT ALIGNED WITH CUTTING-EDGE SCIENTIFIC PERSPECTIVES

Teodora Rusu, Mariana Pinteala, Ana – Nicoleta Bondar, Aatto Laaksonen 209

FOSTERING EUROPEAN TALENTS FOR WIDENING CIRCULAR ECONOMY

Magdalena Aflori, Raluca-Oana Andone, Dan-Radu Rusu, Tachita Vlad-Bubulac, Valeria Harabagiu 212



INVITED LECTURERS (alphabetical order)

Marius ANDRUH studied Chemistry at the University of Bucharest and received his PhD in 1988. He was a post-doc in Orsay with Professor Olivier Kahn, and an Alexander von Humboldt fellow in Göttingen, in the group of Professor Herbert W. Roesky. His major research interests are focused on metallo-supramolecular chemistry, molecular magnetism and crystal engineering. He was Chair of the Inorganic Chemistry Department at the University of Bucharest. Since 2021, Professor Andruh is Director of the C. D. Nenitzescu Institute of Organic and Supramolecular Chemistry of the Romanian Academy. He is member of the Romanian Academy (and Vice-President since 2022), member of the Academia Europaea, and member of the European Academy of Sciences. Marius Andruh is author of more than 330 papers, H index 53.



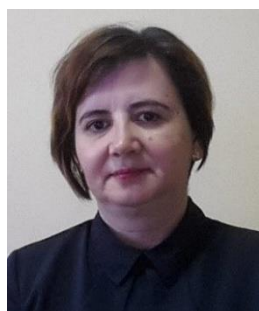
C. Remzi BECER has completed his PhD at Eindhoven University of Technology, the Netherlands (2009). He received a Marie Curie Research Fellowship (2009–2011) and joined University of Warwick, UK. He was awarded a Science City Senior Research Fellowship (2011–2013) to start up his independent research group at the same university. He was appointed (2013–2018) as a Senior Lecturer at Queen Mary, University of London. He is currently a Professor in Sustainable Polymer Chemistry at the University of Warwick (2019–), acting as an editor of European Polymer Journal (2018–) and chair of the RSC Macro Group UK. For more information visit <https://warwick.ac.uk/fac/sci/chemistry/research/becer/becergroup/>



Sergiu COSERI is a senior researcher and head of the Polyaddition and Photochemistry Department at the “Petru Poni” Institute of Macromolecular Chemistry of the Romanian Academy in Iasi. His work centers on polysaccharide chemistry—especially selective, mild oxidations of cellulose—free-radical processes, and nanocellulose-based materials for environmental and energy applications. He earned his PhD in organic chemistry in 2001 and completed a habilitation in 2016 on nitroxyl-radical-mediated functionalization of biopolymers. Dr. Coseri has led the department since 2019 and previously held an NSERC fellowship at the National Research Council of Canada with Keith U. Ingold. He has authored influential reviews and research articles, including the widely cited “Cellulose: To Depolymerize... or Not?” (Biotechnology Advances, 2017) and a groundbreaking study on nanocellulose as a key material for soft robotics, published in Advanced Functional Materials in 2022, and has contributed perspective pieces on the evolution of cellulose research in Romania.



Maria Valentina DINU studied Chemistry at “Al. I. Cuza” University of Iasi, and received her Ph.D. in 2009 from Romania Academy, Petru Poni Institute of Macromolecular Chemistry. During her Ph.D. studies, an important part of the work was carried out at Istanbul Technical University, Turkey, and Wroclaw University of Technology, Poland. She done a post-doctoral fellowship financially supported by the European Social Fund – Cristofor I. Simionescu Postdoctoral Fellowship Programme. Within the research activities performed during this post-doctoral fellowship (2010-2013), she spent some months in Leibniz Institute of Polymer Research Dresden, Germany, and in Institute of Macromolecular Chemistry, Prague, Czech Republic. After a postdoc in the Department of Chemistry, University of Basel, Switzerland, she returned to the Functional Polymers Department, in 2015, as a Senior Researcher. Since 2021 she habilitated and member of the School of Advanced Studies of the Romanian Academy. Dr. Dinu is highly active in the field of synthesis and functionalization of various hydrogel-based systems, composite materials, and (bio) functional self-organized polymeric nanostructures, being co-author of 104 papers, with an H-index of 34. In 2012, she



received the “Nicolae Teclu” Romanian Academy Award. Currently, Dr. Dinu is Group Leader in the Department of Functional Polymers, and is acting as an editor of Reactive and Functional Polymers from Elsevier, B.V. For more information visit: <https://icmpp.ro/laboratories/14/g2/topics.php>.

Theoni GEORGIU is a Professor in Polymer Chemistry at the Department of Materials at Imperial College London. She obtained a BSc in Chemistry and a PhD in Polymer Chemistry from the University of Cyprus. Following her PhD studies, she joined Professor Antonios (Tony) Mikos' group at Rice University in USA as a postdoctoral fellow. In October 2007 she moved to UK when she was awarded a five-year RCUK Fellowship in Colloidal Nanotechnology at the University of Hull. In 2014 she joined Imperial College as a Lecturer where she is now a professor since 2022. She has been an active member of the scientific community; was a member of the Macro group committee from 2017 to 2022 and the chair of the committee from 2019 and 2022. She was also a member of the Materials Chemistry Division Council of the Royal Society of Chemistry and of the European Polymer Federation (EPF) council. She is currently a member of the Colloid & Interface Science Group of RSC. In 2017 she was awarded the 2016 Macro Group UK Young Researchers Medal. She is a member of the advisory editorial board of Polymer International, Polymer Chemistry and European Polymer Journal. Finally, she is an Associate Editor for European Polymer Journal since 2022. (ResearcherID: A-4229-2008, <http://orcid.org/0000-0003-4474-6931>)



Agnieszka KOWALCZUK is an Associate Professor at the Centre of Polymer and Carbon Materials PAS, where she leads the Laboratory of Nano- and Microstructural Materials. Her research focuses on developing novel polymers for applications in medicine and nanotechnology. She specializes in anionic and cationic polymerization of oxiranes and cyclic imines, as well as controlled radical polymerization of (meth)acrylates, enabling the synthesis of macromolecules with precise composition, molar mass, and topology. Beyond linear polymers and copolymers, she is interested in designing branched macromolecules, including star-shaped, dendritic, and hyperbranched structures, particularly those responsive to environmental stimuli and functionalized for interactions with bioactive agents.



Michele LAUS graduated in Industrial Chemistry with honours in 1983 and obtained a PhD in Industrial Chemistry in 1987. In 1997 he became Associate Professor of Industrial Chemistry and since November 2005, Full Professor of Industrial Chemistry and Polymeric Materials. He spent periods as visiting professor at Cornell University (invited by Prof. C. K. Ober) and at the Martin Luter University of Freiburg (invited by Prof. W. Gronski). At present, he is the Coordinator of EUPOC (European Polymer Conferences), President of AIM (Italian Association for Science and Technology of Macromolecules) and General Secretary of EPF (European Polymer Federation). At the beginning, his research activity focused on the development of hybrid nanocomposites, functional micro and nanospheres for biomedical and analytical use and superstructural systems organized in 2D and 3D (polymer liquid crystals, monolayers and opals) for optical, microelectronic and sensor applications. Subsequently, the research was directed towards the study of materials for microelectronics through block copolymers and through the use of doping polymers, including the development of new precision polymers. Alongside these activities, two new lines of research have been activated relating to the synthesis of polymers using CO₂ as a monomer and the preparation and study of reversible networks. Prof. M. Laus is author of 280 articles in international journals and 20 patents with an H-index of 44. Furthermore, he has participated as an invited or plenary speaker in more than 100 international conferences.



Mariana PINTEALA studied chemical engineering and received her PhD at “Gheorghe Asachi” Technical University, Iasi, Romania, in 1995. She has been active in “Petru Poni” Institute of Macromolecular Chemistry since 1987 and from 2010 is the Head of the “IntelCenter” integrated into institute (www.intelcentru.ro). She has published more than 200 papers, 1 book and 12 book chapters, is evaluator for national projects in the chemistry field. The scientific and managerial activities include the successful coordination of two EU projects, 8 national projects and 4 bilateral projects, as well as the participation to a NSF grant and others. In addition, she has implemented the IntelCentre infrastructure project based on EU Structural Funds. The research interests are focused on the development of polymer-based biomaterials, supramolecular assemblies of hydrophobic and hydrophilic (co)polymers; pseudo- and polyrotaxanes, (co)polymers containing cyclodextrins, and more recently on biomedical-oriented nanotechnologies (non-viral vectors for gene and drug delivery systems; nanoparticles based on metal and metal oxides for tumors imaging and therapy; development of fullerene, cyclodextrin, and polymer derivatives for medical applications; design of cyclodextrin inclusion complexes with different drugs as potential drug delivery systems).



Aurel RADULESCU is a senior scientist at Forschungszentrum Jülich GmbH in Germany and is primarily responsible for the small-angle neutron diffractometer KWS-2 at the Jülich Centre for Neutron Science at the Heinz Maier-Leibnitz Zentrum in Garching, Germany. He received his PhD in nuclear physics from the University of Bucharest, Romania, in 2000 and received a Young Scientist Award from the European Neutron Scattering Association in 1999. Between 2016 and 2021, he also served as a specially appointed professor at the University of Osaka, Japan. His current work focuses on semi-crystalline polymers, polymer-protein complexes and methodological developments in neutron scattering.



Cristian SILVESTRU research (born on 1955, Baia-Mare) is Professor at Babeş-Bolyai University of Cluj-Napoca. His research activities concentrated on development of organometallic and coordination chemistry, with particular focus on Main Group metal compounds. In collaboration with foreign research groups, he brought significant contributions to the chemistry of hypervalent Main Group organometallics, reporting on the first examples of some new types of compounds as alkoxides, halochalcogenides, metal heterocycles, etc. as well as CO₂ fixation, and C–H bond activation. He published more than 250 original articles and reviews in international journals (more than 4700 citations; Hirsch index of 36). From 2016 he is representative of Romanian Chemical Society in the Division of Organometallic Chemistry of EuCheMS. He is member of the Romanian Academy (from 2017), the European Academy of Sciences and Arts (Salzburg, Austria; from 2019) and European Academy of Sciences (Brussels, Belgium; from 2021).



Ion TIGINYANU is received his Ph.D. degree in Semiconductor Physics from Lebedev Institute of Physics, Moscow, in 1982. Starting from 2001, he serves as the founding Director of the National Center for Materials Study and Testing, Technical University of Moldova. In 2019 he was elected president of the Moldova Academy of Sciences. Professor Tiginyanu's research interests are related to nanotechnologies, smart nanomaterials and development of photonic and electronic novel device structures for various applications, including microfluidic and biomedical applications. He is Fellow of the International Science Council, honorary member of the Romanian Academy, honorary professor of Shizuoka University (Japan), member of the Academia Europaea, Fellow of the International Society for Optics and Photonics (SPIE), and member of AAAS, IEEE, Optica (formerly OSA) etc. For more information visit <https://asm.md/en/membru?id=52>.



Brigitte VOIT received her PhD in Macromolecular Chemistry 1990 from University Bayreuth, Germany.



After postdoctoral work in 1991/1992 at Eastman Kodak in Rochester, USA, she joined Technische Universität München. After habilitation in 1996, she was appointed 1997 full professor for "Organic Chemistry of Polymers" at Technische Universität (TU) Dresden as well as Director of the Division Macromolecular Chemistry at the Leibniz Institute of Polymer Research (IPF) Dresden. From 2002 to 2022 she was also Scientific Director of IPF. At TU Dresden she is member of the Center for Advancing Electronics Dresden (CFAED), Dresden International Graduate School for Biomedicine and Bioengineering (DIGS BB), and the DFG Graduate School Hydrogel-based Microsystem. She is active in the European Polymer Federation (president 2014/2015), elected member of ACATECH, and holder of the Staudinger Award. Her scientific interest is in functional polymer architectures and responsive polymers for e.g. biomedicine, smart systems and organic electronics



CRISTOFOR I. SIMIONESCU, THE MAN WITHIN

Bogdana Simionescu

Petru Poni Institute of Macromolecular Chemistry, Romanian Academy, Iasi, Romania
bogdana.simionescu@icmpp.ro

For others – the professor, the scientist, the mentor, the rector, the president, the director, the authority. For me – my grandfather. And that was more than enough.

He was born in Plopeni, a small village in Northern Moldova, on July 17, 1920. His family was poor, but hardworking, from both his parents learning – since an early age – to read, write, work the land, take care of the domestic animals, help in the household and be disciplined.

Between 1927–1931, he attended the primary school in Plopeni, having his mother as a teacher. Starting from 1931, he attended, for two years, the „Ștefan cel Mare” High School in Suceava, in 1933 relocating to Iași and becoming part of the National High School, in accordance to the burning wish of his mother who wanted her son to train „in a big city, in the spirit of the French culture”.

Even as a young boy in high school, he was eager to learn and discover the great cultural/scientific personalities of his time, so he made a habit in attending, with great delight, in the „Al. I. Cuza” University Hall, the speeches/conferences/lectures of George Călinescu, Nicolae Iorga, Ion Th. Simionescu, Ștefan Procopiu, Horia Hulubei, Petre Andrei and many others. Later in life, he confessed that he was deeply touched and shaped by these prominent figures.

Before graduating, he came to the conclusion that students borrow work methods/discipline/habits from their teachers, finding that „between the souls of the teacher and the student weaves an unseen, immaterial cloth, which takes shape in the deeds of children when becoming adults”.

In the fall of 1939, he enrolled at the Industrial Chemistry Faculty in Iași, which he graduated in 1943 with *Magna Cum Laudae*. Between 1941 – 1942, he started his third year of studies in Iași and finished it in Cernăuți, with the move of the Polytechnic Institute from Iași to Bucovina. At that time, Cernăuți presented the characteristics of a Western city, the students enjoying a number of facilities, among which the large Mulhendorf Bookshop. In the fourth year of studies (1942 – 1943), giving in to the repeated requests of dr. Mihai Dima, the young student Cristofor I. Simionescu returns to Iași to take over the responsibility of leading the laboratory works on oil technology.

Starting with 1944, Cristofor I. Simionescu carried out his activity in higher education, serving the Technical University of Iași for 52 years, with nothing but professionalism, devotion, perseverance, courage and great strategic vision.

- 1944 – 1952 – assistant, lecturer
- 1953 (age 33) – 1995 – full professor
- 1949 (29 years old) – he founded the Department of Cellulose Chemistry and Technology

From now on, his life was composed by a series of responsibilities, as he described it. At only 33 years old, in 1954, he became general director in the Ministry of Education, alongside his mentor, fellow rector and Romanian Academy member and president (1963 – 1966), whom he greatly admired, professor Ilie G. Murgulescu.

- 1951 (age 31) – 1952 – vice-rector, Iași Polytechnic Institute
- 1952 (32 years) – 1994 – head of Department



- 1953 – 1976 – rector, Iași Polytechnic Institute
- 1955 (35 years old) – corresponding member of the Romanian Academy (youngest member)
- 1955 (35 years old) – he founded, with prof. Ion Curievici, the “Polytechnic Museum” (nowadays “Ștefan Procopiu” Museum of Science and Technic” – Palace of Culture, Iași)
- 1955 (35 years old) – co-founded the “Polytehnica Iași” Football Club
- 1956 – 1970 – head of Laboratory, Petru Poni Institute of Chemistry (he changed the institute’s name in 1964)
- 1963 (43 years old) – full member of the Romanian Academy
- 1963 – he founded the Department of Organic and Macromolecular Chemistry
- 1970 – 2000 – director, “Petru Poni” Institute of Macromolecular Chemistry
- 1963 – 1974, 1989 – 2001 – president of the Romanian Academy Iași Branch
- 1974 – 1990 – vice-president of the Romanian Academy
- 1977 – 1980 – president (with delegation) of the Romanian Academy
- 1967 – founding editor – Cellulose Chemistry and Technology
- 1976 – Gold Centennial Medal from the American Chemical Society.

The founding father of the polymer science school in Romania

Professor Cristofor I. Simionescu was the first who introduced the emerging polymer chemistry and physics in Romanian high education programs. At only 28 years old, he gave the first lecture on polymers on March 16, 1948, in the Iași Polytechnic Institute’s Aula Magna.

On his initiative, the Institute of Chemistry – which was established by professor Radu Cernătescu, built/developed by professor Cristofor I. Simionescu and modernized/extended by professor Bogdan C. Simionescu – was transformed, in 1964, into an Institute entirely dedicated to polymer research, i.e., the “Petru Poni” Institute of Macromolecular Chemistry. From this starting point and for 30 years (1970 – 2000) under his leadership, this Institute became one of the most internationally known Romanian research centers, advancing and broadening the long tradition of fundamental and applied research in various areas of polymer science.

Along with his enthusiastic team of co-workers, he has been highly appreciated by the international scientific/academic community for his innovative approaches in the investigation of biopolymers, the origins of life (“the cold theory”), controlled synthesis of complex macromolecular architectures, semi- and photo-conducting polymers, new bi-(or multi)-functional initiators for the synthesis of graft and block copolymers, polymers with potential biomedical applications, and so on. Under his supervision, his collaborators initiated and developed studies on wood and lignin chemistry, cellulosic fibers, capitalization of the Danube Delta reed, electro-insulating papers, vegetal cancer, etc. Almost at the same time with the investigations on natural polymers, the first Romanian contributions on the synthesis of vinyl polymers by radical polymerization were published. Great achievements were also accomplished on the synthesis and modification of polymers through mechanochemistry reactions, electrochemistry, and plasma chemistry.

Cristofor I. Simionescu’s research group was also the first to report the preparation of ultrahigh molecular weight polymers (*pleistomers*) with chain lengths exceeding by far those ever reported.

During his extended remarkable career, he has mentored more than 100 PhD students (some of them being foreign citizens). All past generations of students remember his dedication and communication skills, his appreciation of solid values and encouragement for research, his heartfelt advices. No matter how busy life was and how many high positions he occupied – both in Iași and/or Bucharest – he never missed a course, considering that teaching his students always came first.

He has published more than 800 scientific papers and 27 books/book chapters, has obtained 70 patents and numerous national and international distinctions. In recognition of his merits in both scientific and



cultural/social activities, he was awarded more than 30 relevant medals/prizes, such as the *Centennial Medal* of the American Chemical Society, *Honorary Diploma* from the High School of Slovakia, *Honorary Diploma* from the Société de Chimie Industrielle de Paris, and the *Diploma* of the Bulgarian Academy of Sciences. He was elected member of several international scientific organizations, including Société Chimique de France, American Chemical Society, International Union of Pure and Applied Chemistry (IUPAC) Macromolecular Division, International Academy of Wood Science, and International Society for the Study of the Origin of Life. Professor Simionescu also received an honorary doctoral degree from the Polytechnical School of Sofia, Bulgaria. He was honorary member of the Hungarian Academy of Sciences, of German (DDR) Academy of Sciences, of the Academy of Sciences of the Republic of Moldova.

Cristofor I. Simionescu may be considered the greatest builder of the XXth century historical region Moldova. He has thought, co-designed, searched/found the proper location for, fought to convince the authorities to accept the architectural plans and approve the financing of the – nowadays – “Gh. Asachi” Technical University of Iași unique modern campus that included over 50 faculties large buildings, pilot installations, micro-production halls, dozens of dormitories, a sports field and a huge canteen designed to serve over 2000 students daily. He is also responsible for building the Romanian Academy Iași Branch, great part of the “Petru Poni” Institute of Macromolecular Chemistry, the Bârlad train station and many important factories/industrial complexes such as the fine curtains factory in Pașcani that worked, for decades, mainly for the international market.

Professor Cristofor I. Simionescu was, in those complicated times, the longest-serving rector in Europe (1953 – 1976) until his execution/purge for political reasons, 1976 marking the beginning of very difficult years for him and our family.

He proved to be brave and wise during historical times of tremendous challenge. He embodied brilliant leadership qualities and radiated an impressive sense of vitality, masculinity and will, accompanied by an irresistible personal charm. The complicated years after the World War II have had a huge impact on the scientific community, as well. These times demanded a new direction in science and visionary brave leaders able to transcend the adversarial communism approaches in order to solve the numerous problems. The historical decades he lived in asked for courageous decisions and commanded will power, wisdom and spirit. His drive to change “*the status quo*” quite often met with political resistance, but he was helped by a deep understanding of the human nature. This is why, almost miraculously, his determination to withstand resistance always prevailed.

During all his adult life, my grandfather’s unnamed and most valuable lifelong partner/collaborator was his wife – my grandmother – Natalia (Talia). He used to say that she put up with him, as difficult as he was, as absent from the household duties and deaf to daily problems as he was. Discretely, she was his rock who “has raised two fundamentally good, modest men with a soft soul and impeccable demeanor”; she wisely intervened in difficult times, with both advice and criticism, knowing exactly what to say and how to say it. For that, and many more, he was forever grateful.

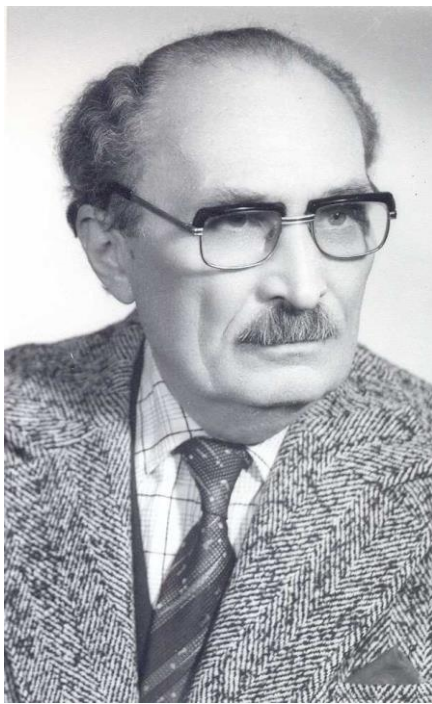
My grandfather was passionate about literature, history and ornithology, owning dozens of canaries and parrots. He had a uniquely irony filled sense of humor, was set on appreciating high core values, was a man of rare integrity and honor, an enthusiastic promoter of emerging fields, a visionary and courageous man who knew to take risks and responsibilities all his life, a true patriot. He always tirelessly helped others, even when involving personal risks and damaging public slanders. He even chose to endure political persecutions and to be removed from different academic positions in order to protect others.

Nowadays, 18 years after he’s left, I’m still stopped on the street by complete strangers and told how much he changed their lives and how much they still owe him. He continues, therefore, to teach valuable lessons, even after all this time.



His lifelong driving force and, I might add, obsession, was to leave a solid scientific/academic/cultural/social/human legacy for the generations to come.

“I want to leave the image of a brave, active and voluble man, who was dignified and defended his beliefs”.
Now, at his 105th anniversary, I can honestly say – Grand dad, you have definitely succeeded.



CRISTOFOR I. SIMIONESCU

1920 - 2007



MAGNETIC AND LUMINESCENT MOLECULAR MATERIALS CONSTRUCTED FROM LANTHANIDES: NEW SYNTHETIC APPROACHES

Marius Andruh^{1,2}

¹*Costin D. Nenitescu Institute of Organic and Supramolecular Chemistry,
Romanian Academy, Bucharest, Romania*

²*Inorganic Chemistry Laboratory, Faculty of Chemistry, University of Bucharest,
Bucharest, Romania
marius.andruh@acad.ro*

1. Introduction

The lanthanide(III) ions are largely employed in designing multifunctional materials [1]: the magnetically anisotropic Ln^{III} ions (e. g. Tb^{III}, Dy^{III}, Ho^{III}) are excellent ingredients to construct single molecule magnets (SMMs) and single chain magnets (SCMs); the isotropic Gd^{III} ion, with a high spin ($S = 7/2$), generates compounds with a large magnetocaloric effect; most of the Ln^{III} complexes display visible and/or NIR luminescence (Figure 1). The properties of these molecular materials can be modulated by combining the lanthanides with other spin carriers, such as 3d metal ions or paramagnetic radicals [2,3].

2. Results and discussion

In this lecture I will present the main synthetic strategies towards magnetic and luminescent molecular materials, currently developed in our laboratory: (1) Design of new paramagnetic ligands (from the nitronyl-nitroxide family) and their metal complexes: 2p-3d; 2p-4f. 2p-3d-4f (Figures 2 and 3); (2) Heterobi- and heterotrimetallic complexes; (3) Coordination compounds containing two different lanthanides into the same molecular entity using specially designed ligands (Figure 3); (4) Model compounds for magnetostructural correlations.

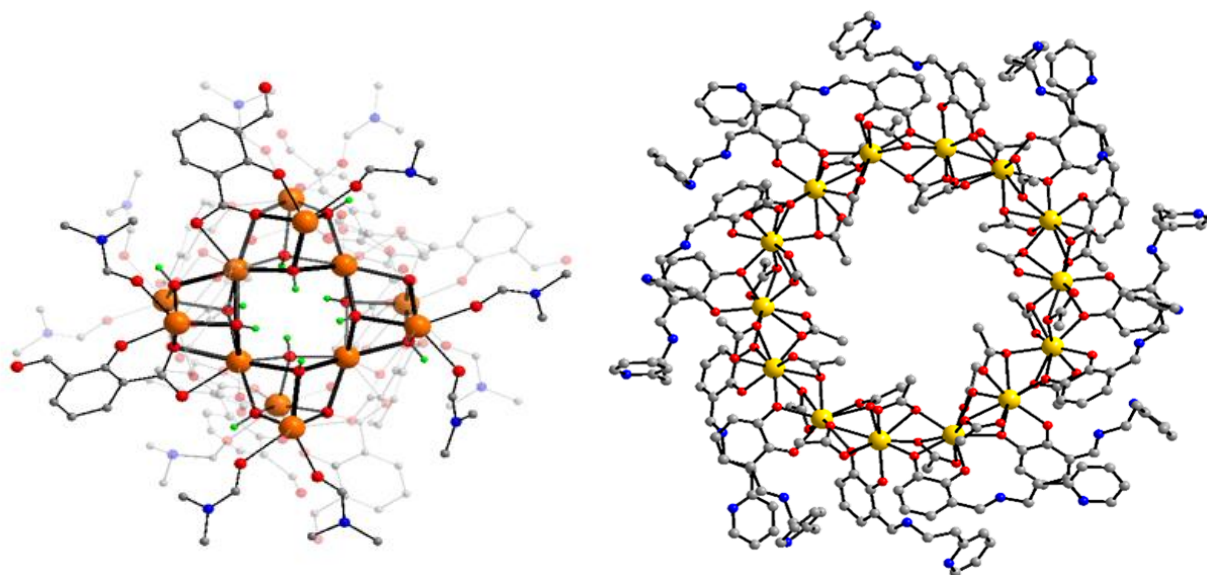


Figure 1. Homometallic clusters constructed from 12 (left), and 14 lanthanide ions (right).



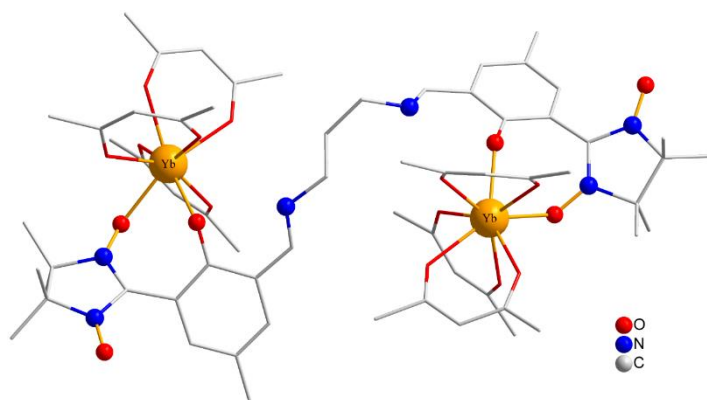


Figure 2. Schiff-base bi-radicals and their binuclear complexes.

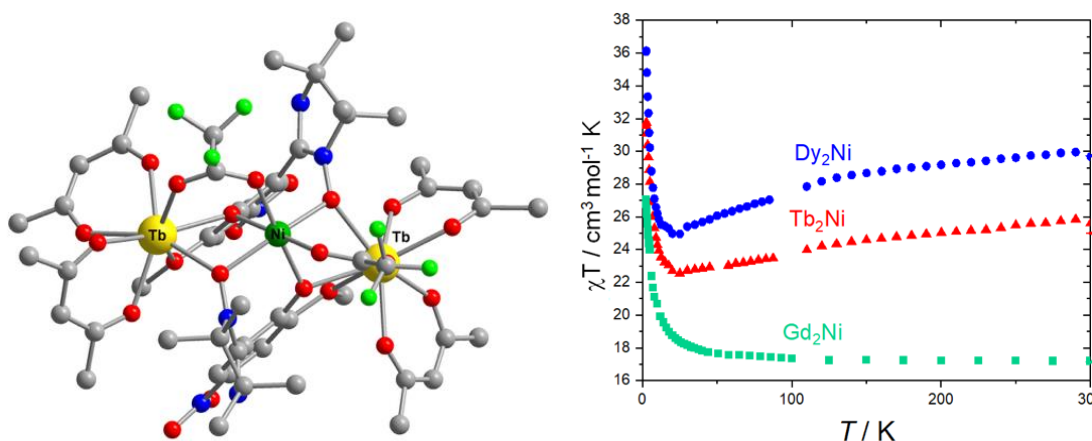


Figure 3. A new family of 2p-3d-4f heterotrispin complexes (left) and their magnetic properties (right).

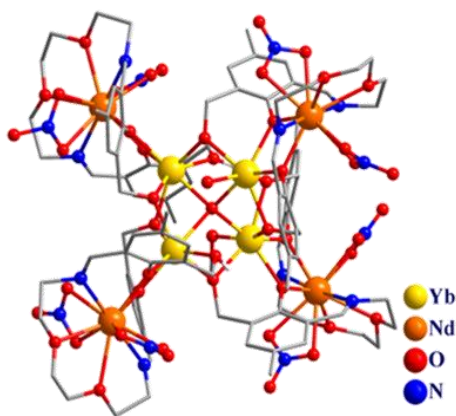


Figure 4. 4f-4f heterometallic complexes constructed from heterotopic, side-off compartmental ligands.

References

- [1]. Marin R, Brunet G, Murugesu M. Shining New Light on Multifunctional Lanthanide Single-Molecule Magnets. *Angew. Chem., Int. Ed.* 60, 1728–1746, 2021.
- [2]. Andruh M. Heterotrimetallic complexes in molecular magnetism. *Chem. Commun.* 54, 3559–3577, 2018.
- [3]. Vaz MGF, Andruh M. Molecule-based magnetic materials constructed from paramagnetic organic ligands and two different metal ions. *Coord. Chem. Rev.*, 427, 213661–213618, 2021.



EMERGING FUNCTIONAL HYBRID NANOMATERIALS BASED ON GALLIUM NITRIDE AND AEROGALNITE

Ion Tiginyanu,* Tudor Braniste

Petru Poni Institute of Macromolecular Chemistry, Romanian Academy, Iasi, Romania

**ion.tighineanu@icmpp.ro*

1. Introduction

Aerogels represent a new class of nanomaterials with ultra-light weight porous structure, mechanical robustness, high electrical conductivity, facile scalability and huge potential in practical applications. The field of aerogel research encompasses several fascinating materials, each with unique properties that make them highly valuable in various applications. Among the most studied are silica aerogels, renowned for their exceptional thermal insulation and transparency, making them ideal for insulation and windows. Carbon aerogels also garner significant attention due to their high electrical conductivity and large surface area, which are advantageous in energy storage and filtration technologies. Metal oxide aerogels, such as alumina, titania, and zirconia, are extensively investigated for their catalytic properties and use in sensors and environmental cleanup efforts. Polymer aerogels are gaining interest because of their lightweight and flexible nature, broadening their potential in insulation and biomedical fields. Meanwhile, graphene-based aerogels stand out for their remarkable strength, conductivity, and potential in electronics and energy storage systems. Overall, these 3D structures are at the forefront of research, contributing to innovative scientific and industrial solutions. Over the last decade, our group has been involved in the development of 3D nanoarchitectures based on GaN, introducing such terms as aerogalnite, or aero-GaN, that represents an interconnected network of hollow microtetrapods based on GaN with wall thickness in the range of 10-100 nm. GaN is a wide-bandgap semiconductor material known for its excellent electronic and optical properties. The material is used in high-power and high-frequency electronic devices because of its ability to handle high voltages, operate at high temperatures, and efficiency in optoelectronic applications. Its robustness and efficiency make GaN an essential material in telecommunications, radars, laser technology, and power electronics, offering faster switching speeds and greater energy efficiency compared to traditional semiconductor materials like Si.

2. Results and discussion

In the realm of advanced materials, aero-GaN emerges as a key player, offering unique capabilities for various applications. The interconnected network of hollow microtubes of aero-GaN proves to have very good response for pressure sensors, making it highly valuable in precise measurement devices [1]. The material is super-repellent to water on its surface, yet water-attracting at its ends – a unique combination of properties found in aero-GaN, opening doors to specialized uses [2]. Aero-GaN emerged as a promising EMI shielding material across different frequency bands due to its unique combination of properties. In the X-band, it offers comparable shielding effectiveness to traditional materials, with the advantage of a significantly reduced weight and tunable shielding capabilities based on porosity. Furthermore, aero-GaN exhibits excellent shielding performance in the Terahertz (THz) and Gigahertz (GHz) ranges, primarily through absorption, solidifying its potential for applications in advanced electronics, aerospace, and automotive industries where lightweight, effective, and stable EMI shielding solutions are critical [3].

The processes for creating aero-GaN material is depicted in Figure 1a. The initial step is converting the sacrificial ZnO template architecture, composed of interconnected zinc oxide tetrapods, into aero-GaN. The process is conducted in a horizontally-heated HVPE reactor with multiple temperature zones. The process uses metallic gallium and NH₃ gas as precursors, along with hydrogen chloride (HCl) and hydrogen (H₂)



as carrier gases. Two chemical reactions occur during these processes. The first reaction involves the formation of GaCl from the interaction of gaseous HCl and liquid Ga at high temperatures in the reactor's source zone. The second reaction results in the nucleation of GaN on the surface of ZnO microtetrapods through the interaction between GaCl and NH₃ gas at 600 °C in the reaction zone. Subsequently, GaN layers are formed by raising the temperature in the reaction zone to 850 °C, gradually decomposing and removing the sacrificial ZnO template.

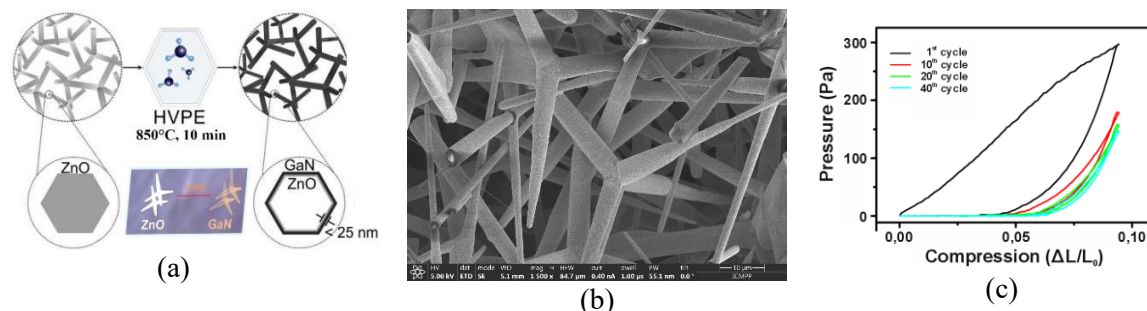


Figure 1. Schematics of the aerogalnite synthesis process (a), the scanning electron microscopy picture of the aero-GaN (b) and the compressive stress – strain response of the Aero-GaN network under 40 loading and unloading cycles (c) [2].

The 3D aero-GaN nano-micro-architecture, despite its low specific density, is highly flexible, showing reversible elastic behavior after several loading cycles. Its unique hierarchical structure, combining micrometer and nanometer features, along with elasticity, piezoelectricity, and flexoelectricity, contributes to its impressive mechanical and electromechanical properties. The material also exhibits strong yellow luminescence, characteristic of ultrathin GaN membranes, while traces of ZnO have minimal impact on its optical properties. This combination of features suggests potential for advanced nanostructured electronic and photonic applications [2].

Carbon-based aerogels and aeromaterials are highly investigated. Aerographite represents a flexible ultralightweight 3D nanoarchitecture based on carbon material characterized by remarkable compressibility and elasticity, while maintaining electrical conductivity, making it promising for applications in batteries, sensors, EMI shielding, and lightweight structures. When combining GaN with aerographite, it results in forming adaptable networks perfect for micro-opto-electro-mechanical systems and other bendable electronics. The 3D Aerographite-GaN hybrid nanoarchitectures with a flexible, interconnected network was successfully created by directly growing GaN nano- and micro-structures on Aerographite tubes using the HVPE techniques [4]. This process resulted in a uniform growth of highly crystalline GaN on both the inner and outer surfaces of the graphitic tubes, strongly attached to prevent clumping, while maintaining multiple growth directions indicative of free growth. The resulting hybrid material exhibits strong UV and yellow emissions, retains the flexibility of the Aerographite template, and demonstrates stress-dependent electrical conductivity, making it suitable for various applications such as sensors, self-reporting materials, and next-generation lightweight conducting composites for electronic and photonic devices. Aerographite, known for its Ohmic behavior, forms a hybrid network with GaN that displays a slightly non-linear current-voltage (I–V) response, indicating successful integration of GaN nano- and microstructures [4]. A non-linear I–V behavior is observed, and can be attributed to the non-Ohmic contact points between GaN structures and Aerographite. SEM images in Figure 2 illustrate the growth of GaN structures on both the outer and inner surfaces of the microtubular Aerographite network. Given the flexibility of the hybrid network, its resistivity under compression has been measured, as shown in Figure 2c.

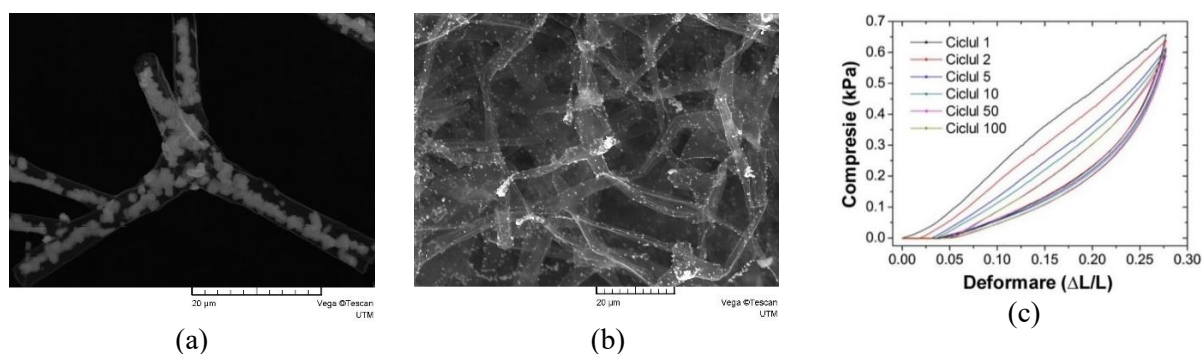


Figure 2. SEM pictures of aerographite-GaN hybrid nanostructures (a), (b); cyclic loading-unloading response (compressive) of the AG-GaN network under compressive stress (c) [4]

Compression reduces the resistivity of the AG-GaN 3D hybrid network, mainly due to an increase in the number of electrical contacts. Once the stress is removed, the resistivity returns to its original value. The network's mechanical flexibility causes cyclic variations in electrical current. The stress-dependent electrical conductivity of this synthesized hybrid network offers potential for applications in pressure sensors, actuators, and self-reporting materials. In conclusion, Gallium Nitride, through its variety of 3D nano-micro-architectures, proves to be a versatile and promising material poised to drive innovations in sensorics, electronics, optoelectronics, and beyond. The 3D nano-micro-architectures based on GaN, obtained under a precise control over the material growth on different substrates, allows the fine-tuning of the materials' properties and foster the development of novel practical applications [5].

Acknowledgements

This work has received funding from the grant of the Romanian National Authority for Research, project no. PNRR-III-C9-2023-I8-161, contract no. 760285/27.03.2024, within the National Recovery and Resilience Plan.

References

- [1]. Dragoman M, Ciobanu V, Shree S, Dragoman D, Braniste T, Raevschi S, Dinescu A, Sarua A, Mishra YK, Pugno N, Adelung R, Tiginyanu I. Sensing up to 40 atm Using Pressure-Sensitive Aero-GaN. *Phys. Status Solidi RRL*. 1900012, 2019.
- [2]. Tiginyanu I, Braniste T, Smazna D, Deng M, Schutt F, Schuchardt A, Stevens-Kalceff MA, Raevschi S, Schurmann U, Kienle L, Pugno NM, Mishra YK, Adelung R. Self-organized and self-propelled aero-GaN with dual hydrophilichydrophobic behaviour. *Nano Energy*, 56, 759–769, 2019.
- [3]. Braniste T, Zhukov S, Dragoman M, Alyabyeva L, Ciobanu V, Aldrigo M, Dragoman D, Iordanescu S, Shree S, Raevschi S, Adelung R, Gorshunov B, Tiginyanu I. Terahertz shielding properties of aero-GaN. *Semicond. Sci. Technol.* 34, 12LT02, 2019.
- [4]. Schuchardt A, Braniste T, Mishra YK, Deng M, Mecklenburg M, Stevens-Kalceff MA, Raevschi S, Schulte K, Kienle L, Adelung R, Tiginyanu I. Three-dimensional Aerographite-GaN hybrid networks: single step fabrication of porous and mechanically flexible materials for multifunctional applications. *Sci Rep.* 6, 5, 8839, 2015.
- [5]. Ursaki V, Braniste T, Marangoci N, Tiginyanu I. Emerging aero-semiconductor 3D micro-nano-architectures: Technology, characterization and prospects for applications. *Appl. Surf. Sci. Advan.* 26, 100708, 2025.

“GRAFTING TO” MECHANISM: AN ENIGMA REVEALED

Michele Laus,^{1*} Riccardo Chiarcos,¹ Michele Perego²

¹*University of East Piemonte, DISIT Dept., Alessandria, Italy*

²*CNR-IMM, Unit of Agrate Brianza, Agrate Brianza, Italy*

**michele.laus@uniupo.it*

1. Introduction

Surfaces and interfaces play a critical role in numerous applications [1]. Tuning the surface hydrophilicity and hydrophobicity, tribology, adhesion and lubricity, as well as its anti-fouling properties, is a fundamental requirement for the successful exploitation of cutting-edge technologies ranging from optoelectronics to sensors and coatings.

The preparation of polymer brushes by grafting to reactions, the chemical reaction of end-functional polymers with a substrate, is an extremely versatile and cost-effective approach for surface design. The elite role of the *grafting to* reaction derives from the control that such approach guarantees over the brush thickness (H) and the number of chains anchored per unit of area, referred to as grafting density (Σ), which are key parameters to determine the polymer brush properties. Σ is commonly estimated by Eq. 1 [2].

$$\Sigma = \frac{H d N_A}{M_n} \quad (1)$$

in which d is the polymer density, N_A is the Avogadro's number and M_n is the number average molecular weight of the graftant polymer. Furthermore, the *grafting to* reaction is generally considered as a self-limiting process, meaning that both H and Σ increase with grafting time until reaching a limiting value.

In spite the large amount of work dedicated to clarifying the fundamental aspects of the polymer brush formation by “*grafting to*”, there are still very important aspects that are commonly accepted without having been adequately analyzed.

2. Results and discussion

The self-limiting nature of the grafting to reaction is conventionally explained by considering the increasing difficulty of a polymer chain to diffuse through the previously grafted chains. As the number of grafted chains increases, diffusion becomes more and more hampered and the growth of the brush layer becomes controlled by the stretching of the chains. This view is widely used to explain the kinetic course of the grafting reaction but indeed it assumes that the grafting reaction is irreversible, as well stated in the Kramer's model [3].

However, it has recently been shown that when the grafting process is carried out under conditions in which the reaction is reversible, the grafting process turns to be of mechanochemical nature [4]. This experimental observation discloses several opportunities to obtain nanoengineered surfaces by exchange reactions between preformed polymer brushes and functional polymers localized on the brush surface by suitably oriented block copolymers.

Another fundamental key point of the grafting process is the assumption that the average molecular weight of the chains that make up the polymer brush is identical to that of the polymer prior to grafting. This hypothesis is implicitly contained in the use of the Eq. 1 to estimate the grafting density from the thickness of the brush layer and the molecular weight of the synthesized polymer.



However, partitioning effects as a function of the molecular weight occur at interfaces and result in the enrichment or surface depletion of species with different molecular weight and/or terminal groups [5]. A significant experiment that was carried out to explain these phenomena is discussed below.

Hydroxy and phosphate -terminated polystyrenes as model polymers were employed to compare the brush evolution during the occurrence of the grafting to reaction performed in melt onto not-deglazed and deglazed silicon substrates. A schematic picture of these processes is provided in Figure 1.

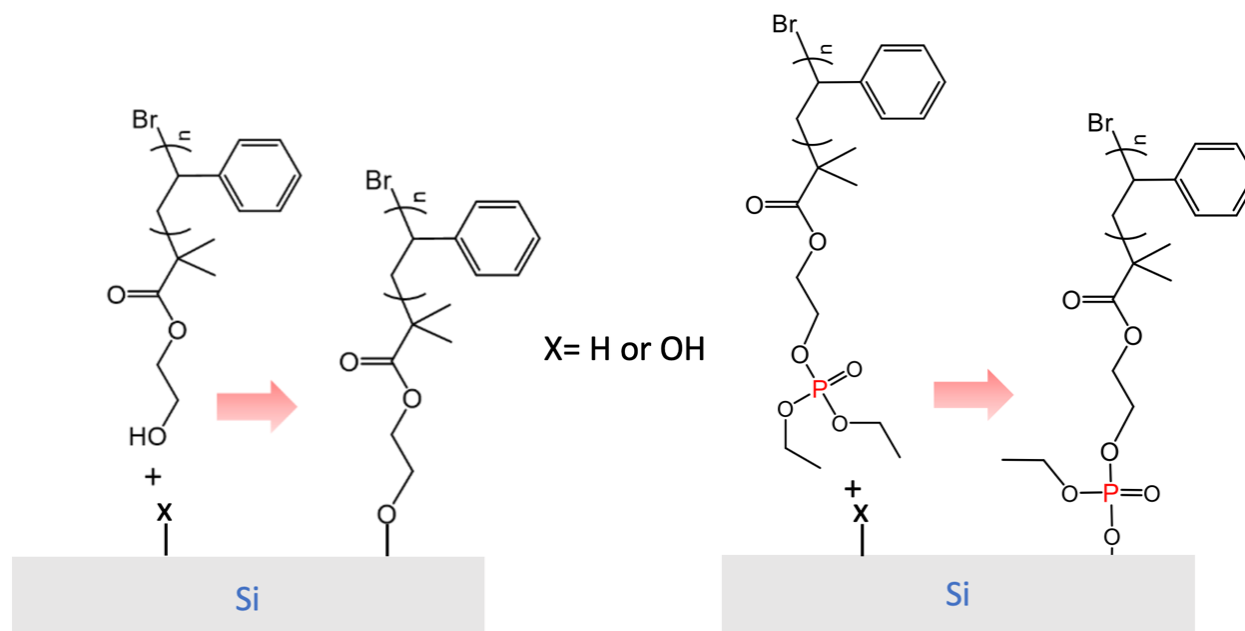


Figure 1. Schematic representation of the *grafting to* reaction of hydroxy or diethylphosphate-terminated polystyrene onto not-deglazed (left) and deglazed (right) silicon substrates.

When the reaction is carried out on polar not-deglazed silicon, a preferential grafting of the shortest component of a disperse polymer sample is systematically observed. This fact was attributed to the lower entropic penalty at which short chains are subjected when their reactive end-group approach the substrate. This reduces the reaction rate constant of the short chains, thus producing preferential grafting.

Furthermore, in the cases of phosphate-terminated polystyrenes, the brush enrichment of short chains is independent from the grafting time at 250 °C, whereas an over enrichment of short chains is observed in the first reaction times at 190 °C. This fact is attributed to a preliminary adsorption of short chains that is due to the affinity between the phosphate group and the surface.

In a completely different way, when the reaction is carried out with phosphate-terminated polystyrenes on apolar deglazed silicon, the obtained brushes result systematically depleted by short chains. In this case, the affinity between the phosphate group and the surface is extremely low and it is supposed to play a role opposite to the one described above.

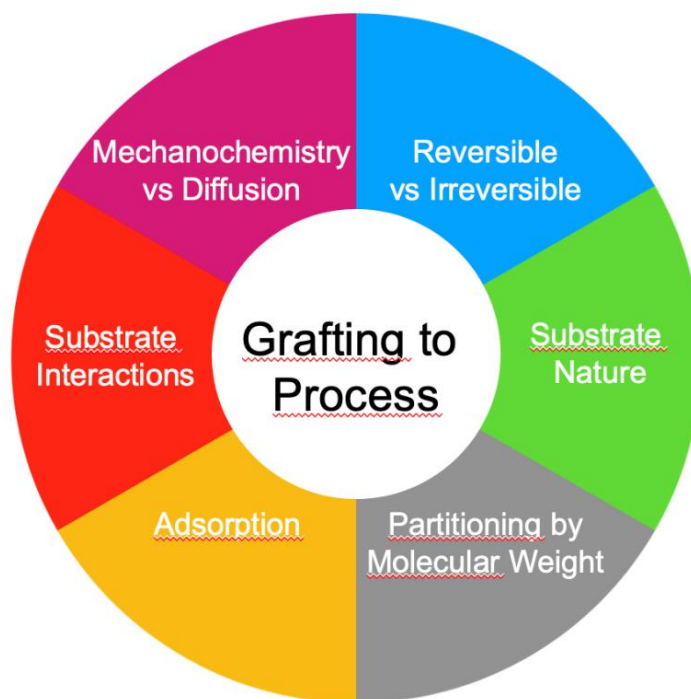


Figure 2. Main parameters and factors affecting the polymer brush characteristics obtained by grafting to reaction.

3. Conclusions

In conclusion, it will be demonstrated that the mechanism of the grafting to process is extremely complex and involves a variety of aspects as schematically illustrated in Figure 2. All of them will be presented and discussed to give a sound guide in the preparation of new surfaces with precisely tuned characteristics.

References

- [1]. Chiarcos R, Perego M, Laus M. Polymer brushes by grafting to reaction in melt: new insights into the mechanism. *Macromol. Chem. Phys.* 224, 2200400, 2023.
- [2]. Michalek L, Barner L, Barner-Kowollik C. Polymer on top: current limits and future perspectives of quantitatively evaluating surface grafting. *Adv. Mater.* 30, 1–18, 2018.
- [3]. Kramer EJ. Grafting kinetics of end-functional polymers at melt interfaces. *Isr. J. Chem.* 35, 49–54, 1995.
- [4]. Laus M, Chiarcos R, Gianotti V, Antonioli D, Sparnacci K, Munaò G, Milano G, De Nicola A, Perego M. Evidence of mechanochemical control in “grafting to” reactions of hydroxy-terminated statistical copolymers. *Macromolecules* 54, 499–508, 2021.
- [5]. Antonioli D, Chiarcos R, Gianotti V, Terragno M, Laus M, Munaò G, Milano G, De Nicola A, Perego M. Inside the brush: partition by molecular weight in grafting to reactions from melt. *Polym. Chem.* 12 6538–6547, 2021.



STRUCTURE AND REACTIVITY OF HEAVY ORGANOPNICTOGENS – FROM CO₂ FIXATION TO C–H BOND ACTIVATION

Cristian Silvestru,^{1*} Gabriel Dunes,^{1,2} Alpar Pöllnitz,¹ Alexandru Sava,¹ Yann Sarazin²

¹*Babes-Bolyai University, Faculty of Chemistry and Chemical Engineering,
Department of Chemistry, Supramolecular Organic and Organometallic Chemistry Centre (SOOMCC),
Cluj-Napoca, Romania*

²*Université de Rennes, CNRS, Institut des Sciences Chimiques de Rennes, Rennes, Cedex, France*

*cristian.silvestru@ubbcluj.ro

1. Introduction

Activation of small molecules (as, for example, H₂, N₂, N₂O, NO, CO, CO₂, ethylene, acetylene, etc.) based mainly on transition metal compounds was and still is a research topic which raised a lot of interest related to synthetic chemistry [1], and different strategies were developed to achieve this task (*e.g.* use of complexes of redox-active ligands, bimetallic and oligonuclear systems [1b], cooperative systems, frustrated Lewis pairs [1c], etc.).

Following the seminal review of Philip P. Power [2] which underlined the similarities between the chemistry of heavier Main Group metal compounds and transition metal complexes, especially regarding the reactivity, under mild conditions, of particular Main Group organometallic species towards saturated (H₂, NH₃) and unsaturated (CO₂, N₂O, olefins, alkynes) small molecules, the interest on the activation of small molecules by compounds of s- and p-block elements has continuously developed [3].

So far, important achievements in this field have been made in (*i*) understanding the importance of ligand design for the stabilization of low-coordinate and/or low-oxidation state species of Main Group metals; (*ii*) the synthesis of well-defined molecular compounds with one or more metallic centres in low-coordinate and/or low-oxidation state, as well as the synthesis of cations, anions and radical species of Main Group metals, or (*iii*) the development of strategies for small molecule activation, *e.g.* the use of frustrated Lewis pairs [4a-c], complexes of redox-active ligands [4d], low-valent main group species [3b,4e], or main group ambiphiles [4f].

2. Results and discussion

The use of transition metals and their compounds as catalysts in synthetic chemistry, both at laboratory and industrial scale, is a topic well established and largely documented. The challenge to develop catalytic applications from the feasible stoichiometric reactions between small molecules and Main Group organometallics was also achieved in some cases. Fascinating results were reported for heavy pnictogen (antimony and bismuth) compounds, including catalytic activity, activation of CO₂ and other small molecules, or C–H activation [5].

Particularly, in the context of *C–H bond activation* using heavy organopnictogen(III) species [6a], a research topic on organobismuth(III) bis(phenolates) and the unusual Bi-oxyaryl species [2,6-(Me₂NCH₂)₂C₆H₃]Bi(C₆H₂BU₂-3,5-O-4) raised interest [5b,h,n]. By contrast, the chemistry of the lighter metalloid, antimony(III), is comparatively less developed [5a]. Here we report on our results on the fixation of CO₂ and C–H bond activation, as well as related chemistry, using low valent organopnictogen compounds [6]. The synthesis, structural characterization and reactivity of organopnictogen(III) bis(phenolates) and related thio and seleno derivatives, ArPn(EAr')₂ (Pn = Sb, Bi; E = O, S, Se) [6e,f], where the Ar groups attached to the metal atom are aromatic ligands with two pendant arms, *i.e.* 2,6-(R₂NCH₂)₂C₆H₃ (R = Me, ⁱPr) or 2,6-{E'(CH₂CH₂)₂NCH₂}₂C₆H₃ (E' = NMe, O), will be presented. The



reactions of ArPnCl_2 with $[2,6\text{-}^t\text{Bu}_2\text{C}_6\text{H}_3\text{O}]\text{K}$ were investigated and special attention was given to the synthesis, structure and reactivity of $[2,6\text{-(Me}_2\text{NCH}_2)_2\text{C}_6\text{H}_3]\text{Sb}(\text{C}_6\text{H}_2^t\text{Bu}_2\text{-3,5-O-4})$ (**1**), an organoantimony(III)-oxyaryl species obtained upon $\text{C}_{\text{sp}^2}\text{-H}$ bond activation in a phenolate ligand [6g]. The mechanism leading to the formation of **1** is highly sensitive to steric considerations as probed experimentally and by DFT calculations. All data agrees with a process involving charged species, rather than free radicals as previously considered for congeneric bismuth species. The nucleophilic behaviour of the oxyaryl ligand in **1** was illustrated in derivatisation reactions, *e.g.* insertion of CS_2 in the $\text{Sb-C}_{\text{oxyaryl}}$ bond, thus generating a new C–C bond in $[2,6\text{-(Me}_2\text{NCH}_2)_2\text{C}_6\text{H}_3]\text{Sb}(\text{S}_2\text{C-C}_6\text{H}_2^t\text{Bu}_2\text{-3,5-O-4})$ (**2**) (Figure 1).

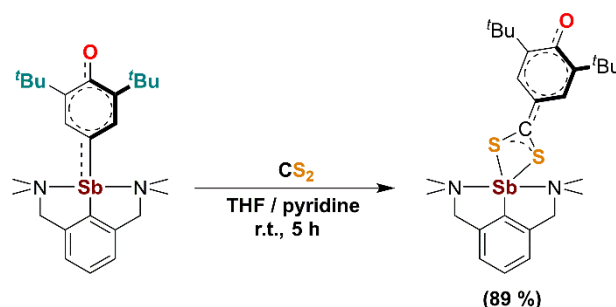


Figure 1. Reaction of the organoantimony(III)-oxyaryl species **1** with CS_2 , generating a new C–C bond in $[2,6\text{-(Me}_2\text{NCH}_2)_2\text{C}_6\text{H}_3]\text{Sb}(\text{S}_2\text{C-C}_6\text{H}_2^t\text{Bu}_2\text{-3,5-O-4})$ (**2**) [6g].

Acknowledgements

This work was supported by a grant of the Romanian Ministry of Education and Research, CNCS – UEFISCDI, project number PN-III-P4-ID-PCE-2020-2651, within PNCDI III. We are also grateful to the French Agence Nationale de la Recherche for the provision of a research grant to G. D. (BiMeDep project, ANR-21-CE07-0045-02). We thank Dr. Albert Soran and Dr. Alexandra Pop as well as the support provided by the National Centre for X-ray Diffraction (Babes-Bolyai University, Cluj-Napoca, Romania) for the elucidation of the XRD structures of organopnictogen complexes.

References

- [1]. Selected references: (a) Milani B, Licini G, Clot E, Albrecht M. Small molecules activation (editorial). *Dalton Trans.* 45, 14419–14420, 2016; (b) Navarro M, Moreno JJ, Pérez-Jiménez M, Campos J. Small molecule activation with bimetallic systems: a landscape of cooperative reactivity. *Chem. Commun.* 58, 11220–11235, 2022; (c) Carmona M, Perez R, Ferrer J, Rodriguez R, Passarelli V, Lahoz FJ, Garcia-Orduña P, Carmona D. Activation of H–H, HO–H, $\text{C}(\text{sp}^2)\text{-H}$, $\text{C}(\text{sp}^3)\text{-H}$, and RO–H bonds by transition-metal frustrated Lewis pairs based on M/N (M = Rh, Ir) Couples. *Inorg. Chem.* 61, 13149–13164, 2022.
- [2]. Power PP. Main-group elements as transition metals. *Nature* 463, 171–177, 2010.
- [3]. (a) Weetman C, Inoue S. The road travelled: after main-group elements as transition metals. *ChemCatChem*, 10, 4213–4228, 2018; (b) Oberdorf K, Lichtenberg C, Small molecule activation by well-defined compounds of heavy p-block elements. *Chem. Commun.* 59, 8043–8058, 2023.
- [4]. Selected references: (a) Stephan DW. Frustrated Lewis pairs: a new strategy to small molecule activation and hydrogenation catalysis, *Dalton Trans.* 3129–3136, 2009; (b) Stephan D.W. A Perspective on frustrated Lewis pairs. *J. Am. Chem. Soc.* 137, 10018–10032, 2015; (c) Navarro M, Moreno JJ, Campos J. Frustrated Lewis pair systems. In: Parkin G, Meyer K, O'Hare D, editors. *Comprehensive organometallic chemistry IV* – Aldridge S, editor. vol. 10: Groups 14 and 15, Frustrated Lewis pairs. 523–616, 2022; (d) Saha R, Chattaraj PK. Activation of small molecules (H_2 , CO_2 , N_2O , CH_4 , and C_6H_6) by a porphyrinoid-based dimagnesium(I) complex, an electride. *ACS Omega* 3, 17199–171211, 2018; (e) Fujimori S, Inoue S. Small molecule activation by two-coordinate acyclic silylenes. *Eur. J. Inorg. Chem.* 3131–3142, 2020; (f) Dewhurst RD, Légaré M-A, Braunschweig H. Towards the Catalytic Activation of Inert Small Molecules by Main-Group Ambiphiles. *Commun. Chem.* 3, 131, 2020.

[5]. Selected references:

- (i) *catalytic activity*: (a) Rat CI, Silvestru C, Breunig HJ. Hypervalent organoantimony and -bismuth compounds with pendant arm ligands. *Coord. Chem. Rev.* 257, 818–879, 2013; (b) Kindra DR, Evans WJ. Bismuth-based cyclic synthesis of 3,5-Ditert-butyl-4-hydroxybenzoic acid via the oxyarylcarboxy dianion, $(\text{O}_2\text{CC}_6\text{H}_2^t\text{Bu}_2\text{O})^{2-}$. *Dalton Trans.* 43, 3052–3054, 2014; (c) Lichtenberg C. Molecular bismuth(III) monocations: structure, bonding, reactivity, and catalysis. *Chem. Commun.* 57, 4483–4495, 2021; (d) Pang Y, Leutzsch M, Nöthling N, Cornella J. Catalytic activation of N_2O at a low valent bismuth redox platform. *J. Am. Chem. Soc.* 142, 19473–19479, 2020; (e) Hyvl J. Hypervalent organobismuth complexes: pathways toward improved reactivity, catalysis, and applications. *Dalton Trans.* 52, 12597–12603, 2023; (f) Mato M, Cornella J. Bismuth in radical chemistry and catalysis. *Angew. Chem., Int. Ed.* 63, e202315046, 2024;
- (ii) *activation of CO_2 and other small molecules*: (g) Yin SF, Maruyama J, Yamashita T, Shimada S. Efficient Fixation of carbon dioxide by hypervalent organobismuth oxide, hydroxide, and alkoxide. *Angew. Chem., Int. Ed.*, 47, 6590–6593, 2008; (h) Kindra DR, Casely IJ, Fieser ME, Ziller JW, Furche F, Evans WJ. Insertion of CO_2 and COS into Bi–C bonds: reactivity of a bismuth NCN pincer complex of an oxyaryl dianionic ligand, $[2,6-(\text{Me}_2\text{NCH}_2)_2\text{C}_6\text{H}_3]\text{Bi}(\text{C}_6\text{H}_2^t\text{Bu}_2\text{O})$. *J. Am. Chem. Soc.* 135, 7777–7787, 2013; (j) Chen Y, Qiu R, Xu X, Au C-T, Yin S-F. Organoantimony and organobismuth complexes for CO_2 fixation. *RSC Adv.* 4, 11907–11918, 2014; (k) Ramler J, Poater J, Hirsch F, Ritschel B, Fisher I, Bickelhaupt FM, Lichtenberg C. Carbon monoxide insertion at a heavy p-block element: unprecedented formation of a cationic bismuth carbamoyl. *Chem. Sci.* 10, 4169–4176, 2019; (l) Kořenkova M, Hejda M, Erben M, Jirásko R, Jambor R, Růžicka A, Rychagova E, Ketkov S, Dostál L. Reversible C=C bond activation by an intramolecularly coordinated antimony(i) compound. *Chem. Eur. J.* 25, 12884–12888, 2019; (m) Pang Y, Leutzsch M, Nöthling N, Cornella J. Dihydrogen and ethylene activation by a sterically distorted distibene. *Angew. Chem., Int. Ed.* 62, e202302071, 2023;
- (iii) *C–H activation*: (n) Casely IJ, Ziller JW, Fang M, Furche F, Evans WJ. Facile bismuth-oxygen bond cleavage, C–H activation, and formation of a monodentate carbon-bound oxyaryl dianion, $(\text{C}_6\text{H}_2^t\text{Bu}_2\text{O})^{2-}$. *J. Am. Chem. Soc.* 133, 5244–5247, 2011; (o) Hynes T, Masuda JD, Chitnis SS. Mesomeric tuning at planar Bi centres: unexpected dimerization and benzyl C–H activation in $[\text{CN}_2]\text{Bi}$ Complexes. *ChemPlusChem* 87, e202200244, 2022; (p) Oberdorf K, Hanft A, Xie X, Bickelhaupt FM, Poater J, Lichtenberg C. Insertion of CO_2 and CS_2 into Bi–N bonds enables catalyzed CH-activation and light-induced bismuthinidene transfer. *Chem. Sci.* 14, 5214–5219, 2023.
- [6]. (a) Rat CI, Soran A, Varga RA, Silvestru C. C–H bond activation mediated by inorganic and organometallic compounds of main group metals. *Adv. Organomet. Chem.* 70, 233–311, 2018; (b) Breunig HJ, Königsmann L, Lork E, Philipp N, Nema M, Silvestru C, Soran A, Varga RA, Wagner R. Hypervalent organobismuth(iii) carbonate, chalcogenides and halides with the pendant arm ligands 2-(Me_2NCH_2) C_6H_4 and 2,6-(Me_2NCH_2) C_6H_3 . *Dalton Trans.* 1831–1842, 2008; (c) Breunig HJ, Nema MG, Silvestru C, Soran A, Varga RA. Organobismuth compounds with the pincer ligand 2,6-(Me_2NCH_2) C_6H_3 : monoorganobismuth(iii) carbonate, sulfate, nitrate, and a diorganobismuthenium(iii) salt. *Dalton Trans.* 39, 11277–11284, 2010; (d) Strimb G, Pöllnitz A, Rat CI, Silvestru C. A general route to monoorganopnictogen(iii) ($\text{M} = \text{Sb}, \text{Bi}$) compounds with a pincer (N,C,N) group and oxo ligands. *Dalton Trans.* 44, 9927–9942, 2015; (e) Dunes G, Soran A, Silvestru C. Organopnictogen(III) bis(arylthiolates) containing NCN-aryl pincer ligands: from synthesis and characterization to reactivity. *Dalton Trans.* 51, 10406–10419, 2022; (f) Dunes G, Silvestru C. NCN-Pincer Organopnictogen(III) bis(aryloxides). *New J. Chem.* 68, 5523–5529, 2024; (g) Dunes G, Cordier M, Kahlal S, Pöllnitz A, Saillard J-Y, Silvestru C, Sarazin Y. C–H Bond activation at antimony(III): synthesis and reactivity of Sb(III)-oxyaryl species. *Dalton Trans.* 53, 15427–15440, 2024.



EFFECTS OF MONOMER SEQUENCE AND CHEMICAL COMPOSITION ON THERMORESPONSIVE PHASE TRANSITION OF OEGMA-BASED SYMMETRIC PENTABLOCK TERPOLYMERS

Shaobai Wang,* Theoni K. Georgiou

Department of Materials, Imperial College London, London, UK

**sw120@ic.ac.uk*

1. Introduction

Thermoresponsive block copolymers have been extensively studied for their potential in biomedical applications. Their thermoresponsive performance can be finely tuned by varying the structural features, such as monomer sequence and chemical composition. The efficacy of this strategy has been widely demonstrated in diblock and triblock systems [1]. Our previous work showed that the tetrablock terpolymers could exhibit an enhanced gelation performance compared to their triblock counterparts, as long as the additional block was appropriately positioned and composed [2]. However, likely due to challenges in the synthesis, the effect of the structural features of pentablock terpolymers remains poorly explored.

In this study, we systematically investigated the effects of monomer sequence and chemical composition on the thermoresponsive phase transition of symmetric pentablock terpolymers, using a complete set of in-house prepared symmetric pentablock terpolymers comprised of hydrophilic (oligo(ethylene glycol) methyl ether methacrylate) (average MM of monomer = 300 g/mol, OEGMA300, unit A), hydrophobic *n*-butyl methacrylate (BuMA, unit B), and less-thermoresponsive (di(ethylene glycol) methyl ether methacrylate) (DEGMA, unit C). This abstract, condensed from our two published articles [3,4], highlights a novel monomer sequence with superior gelation performance. Further compositional variation also identified interesting time-dependent evolution patterns of the gelation performance.

2. Experimental

The terpolymers were synthesised via one-pot group transfer polymerisation by sequential addition of OEGMA300, DEGMA, and BuMA in a pre-determined sequence and amount. A bifunctional initiator was incorporated to prepare the symmetric pentablock terpolymers, while a monofunctional initiator was employed to synthesise triblock terpolymers as controls. The thermoresponsive properties of the resulting polymers, including cloud point temperature (T_{cp}), visual gel point, rheology properties, and the evolution of hydrogel network structure, were systematically investigated. Small angle X-ray scattering (SAXS) experiments for the structural analysis were performed on Beamline B21, Diamond Light Source, Didcot, UK.

3. Results and discussion

For clarity in the following discussion, the obtained terpolymers were labelled according to their monomer sequence. This includes six pentablock terpolymers: ABCBA, CBABC, ACBCA, BCACB, BACAB, and CABAC, as well as three triblock controls: ABC, ACB, and CAB. All terpolymers share a consistent composition of 45-25-30 wt% (OEGMA300-DEGMA-BuMA) and M_n of approximately 9200 g/mol. GPC and ¹H-NMR analysis confirmed that the chemical structures met the requirements of this study.

The thermo-induced phase transition of the terpolymers was investigated by turbidimetry at 1 wt% in deionised (DI) water. As shown in Figure 1(a), ACBCA, BCACB, ABCBA, ACB, and ABC exhibit relatively higher T_{cp} values, while the others display lower T_{cp} s in the range of 40-43 °C. This difference



can be attributed to the core-shell micelle conformation of these terpolymers in aqueous media. Taking ACBCA as an example, the outermost layer of the micelles is dominated by the poly(OEGMA300) blocks, as illustrated in Figure 1(b). In this case, the micelles could remain stable at higher temperatures, resulting in a higher T_{cp} . In contrast, the micelles formed by CABAC possess a poly(DEGMA)-rich outermost layer. Due to the lower LCST of poly(DEGMA), the micelle shell may dehydrate and collapse at lower temperatures, thereby lowering the T_{cp} .

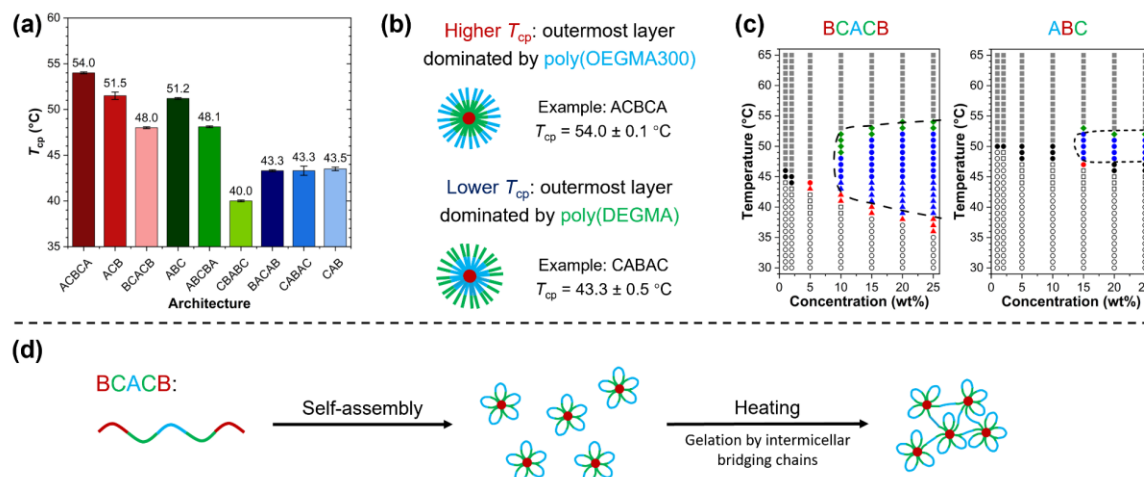


Figure 1. (a) Comparison of T_{cp} values of the pentablock terpolymers and triblock controls, measured by turbidimetry at 1 wt% in DI water; (b) schematic of micelle conformation formed by ABCBA and CABAC in aqueous media; (c) phase diagrams of the two gellable terpolymers in PBS (pH = 7.4, 1×), with gellable temperature and concentration range highlighted in blue colour; (d) schematic representation of thermogel formation by BCACB. Redrawn based on Ref. [3].

The gelation properties of the pentablock terpolymers was initially investigated by visual tests in PBS (pH = 7.4, 1×). Among them, it was found that BCACB was the only gellable pentablock terpolymers. This terpolymer demonstrated enhanced gelation performance over the ABC triblock control, showing a broader range of gellable temperature and concentration (Figure 1(c)). This enhanced gelation is likely due to its unique ability to form stable intermicellar bridging chains, which facilitates the formation of hydrogel network (Figure 1(d)). Notably, the lower boundary of the gellable temperature range is close to physiological conditions, highlighting the potential of the BCACB pentablock terpolymer as thermogelling agent for biomedical applications.

Further variations in the composition of the BCACB sequence also altered the gelation performance of the resulting terpolymers. While both the hydrophobic terpolymer with a composition of 40-25-35 wt% (named as ODB(40-25-35)) and the hydrophilic one of 45-30-25 wt% (named as ODB(45-25-30)) began to form hydrogel at 10 wt% in PBS, the intermediate terpolymer of 40-30-30 wt% (named as ODB(40-30-30)) exhibited gelation at a lower concentration of 5 wt% in PBS. Moreover, ODB(40-30-30) consistently showed higher values of maximum storage modulus (G'_{max}) than the other two across all the gellable concentrations.

Since thermoresponsive hydrogels are typically intended for long-term applications, such as sustained drug release and tissue engineering, it is important to understand their time-dependent behaviour. Notably, time-resolved rheometry and SAXS revealed three distinct evolutionary patterns of the BCACB hydrogels (Figure 2). For the intermediate ODB(40-30-30), the storage modulus (G') reached a maximum and stabilised from around 900 s. This trend closely mirrored its time-dependent volume fraction (ϕ) of correlated micelles, as derived from SAXS models. This relationship between G' and ϕ suggests that the elastic-active bridging chains govern the development of the hydrogel network formed by ODB(40-30-30). In contrast, G' of ODB(40-25-35) hydrogel gradually decreased after peaking at about 600 s, while its ϕ

showed a slight but steady increase. This negative elastic-active relationship was attributed to the large-scale defects within the hydrogel network caused by excessive micellar association. ODB(45-25-30) consistently exhibited the lowest G' , despite a linear increase in ϕ . This suggests that the ODB(45-25-30) hydrogel was configured by weak, dynamic entanglements within overlapping micelle shells, instead of elastic-active bridging chains.

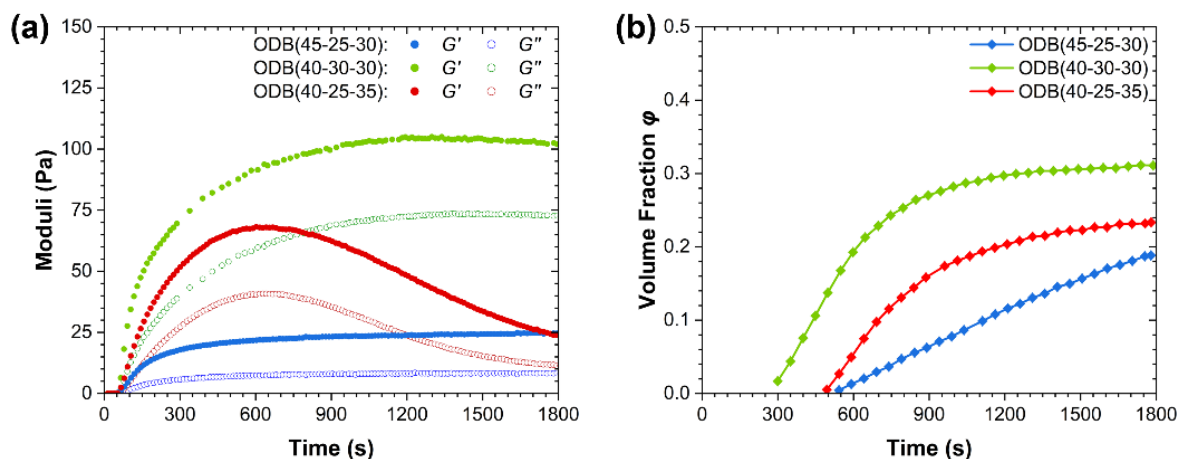


Figure 2. (a) Moduli-time plot of the three BCACB terpolymers at 10 wt% in PBS at 44 °C, recorded by time-resolved rheometry; (b) the time-dependent variation in the volume fraction of correlated micelles, derived from time-resolved SAXS analysis. Redrawn based on Ref. [4]

4. Conclusions

The presented work demonstrates the effect of monomer sequence on thermoresponsive performance of symmetric pentablock terpolymers composed by OEGMA300 (unit A), BuMA (unit B), and DEGMA (unit C). Notably, the BCACB terpolymer exhibits superior gelation performance over other counterparts. Further compositional variations on this terpolymer highlight the importance of a balanced ratio of hydrophilic and hydrophobic components in the configuration of resilient thermoresponsive hydrogel network.

Acknowledgements

The authors thank Diamond Light Source for the allocation of beam time under the proposal number SM38094 and the assistance of Dr Nathan Cowieson during the SAXS experiments.

References

- [1]. Yuan Y, Raheja K, Milbrandt NB, Beilharz S, Tene S, Oshabaheebwa S, Gurkan UA, Samia ACS, Karayilan M. Thermoresponsive polymers with LCST transition: synthesis, characterization, and their impact on biomedical frontiers. *RSC Appl. Polym.* 1, 158–189, 2023.
- [2]. Constantinou AP, Sam-Soon NF, Carroll DR, Georgiou TK. Thermoresponsive tetrablock terpolymers: effect of architecture and composition on gelling behavior. *Macromolecules* 51, 7019–7031, 2018.
- [3]. Wang S, Liu X, Wang S, Georgiou TK. Effect of architecture on the thermo-induced phase transition of methacrylate-based symmetric pentablock terpolymers. *Polym. Chem.* 15, 4894–4907, 2024.
- [4]. Wang S, Georgiou TK. Temperature- and time-dependent evolution of hydrogel network formed by thermoresponsive BCACB pentablock terpolymers: effect of composition. *Polymer* 328, 128426, 2025.



ENGINEERING FUNCTIONAL NANOPLATFORMS FOR BIOIMAGING AND THERAPEUTIC AGENT DELIVERY

Mariana Pinteala,^{1*} Dragos Peptanariu,¹ Bogdan Craciun,¹ Denisse-Iulia Bostiog,¹

Tudor Vasiliu,¹ Petru Tirnovan,¹ Razvan Puf,¹ Cristina Uritu,²

Teodora Rusu,¹ Adrian Fifere,¹ Andrei Neamtu³

¹*Petru Poni Institute of Macromolecular Chemistry, Romanian Academy, Iasi, Romania*

²*Prof. Ostin C. Mungiu Advanced Center for Research and Development in Experimental Medicine,
Grigore T. Popa University of Medicine and Pharmacy, Iasi, Romania*

³*Department of Physiology, Grigore T. Popa University of Medicine and Pharmacy, Iasi, Romania*

**pinteala@icmpp.ro*

1. Introduction

Personalized medicine as a concept began in 1953, when Watson and Crick discovered the DNA double helix (Figure 1). Further, the concept was developed by the Human Genome Project (1990–2003), which provided an understanding of the fact that the effect of a drug is different from patient to patient, being related to each individual's genome. This understanding, along with progress in biomarkers, pharmacogenomics, and molecular diagnostics, has resulted in our days conception of tailoring medications to each patient's unique profile.

2. Results and discussion

In this environment, in 1998, John Funkhouser, as Chief Executive Officer of PharmaNetics, in a press release, introduced the notion of theranostics, which integrates treatment and diagnostics, subsequently actualized using multifunctional non-viral vectors [1]. As an important observation, theranostics is the next step of personalized medicine; it not only delivers the treatment but also shows, through imaging, how the treatment is working in real time. This way, theranostics turns personalized medicine into a practical tool at the bedside. In parallel, Felgner in 1987 introduced cationic lipids as non-viral vectors in lipofection, as secure alternatives to viral carriers, and later in 1995, Boussif introduced polyethylenimine [2,3]. Collectively, these advancements established the groundwork for precision medicine founded on secure, focused, and cohesive treatment frameworks (Figure 1).

Personalized medicine can be achieved through several complementary strategies (Figure 2). Genomic profiling enables sequencing to identify mutations and molecular targets. Biomarker identification using proteins, metabolites, or imaging signals allows patient stratification. Non-viral vectors (e.g., polymeric, gold, silica, carbon dot nanoparticles) serve as reliable platforms for medication and gene delivery. Targeted delivery is achieved by functionalization with ligands, antibodies, or peptides to ensure cell and tissue selectivity. By continuously modifying therapy, adaptive treatment is made possible by real-time monitoring using PET, SPECT, MRI, and CT. Finally, multimodal theranostics amalgamates therapy, imaging, and feedback into a single platform to facilitate personalized treatment.

Theranostics combines therapy and diagnosis into a unified system, facilitating real-time assessment of treatment efficacy and enhancing individualized medicine with increased accuracy and fewer adverse effects.



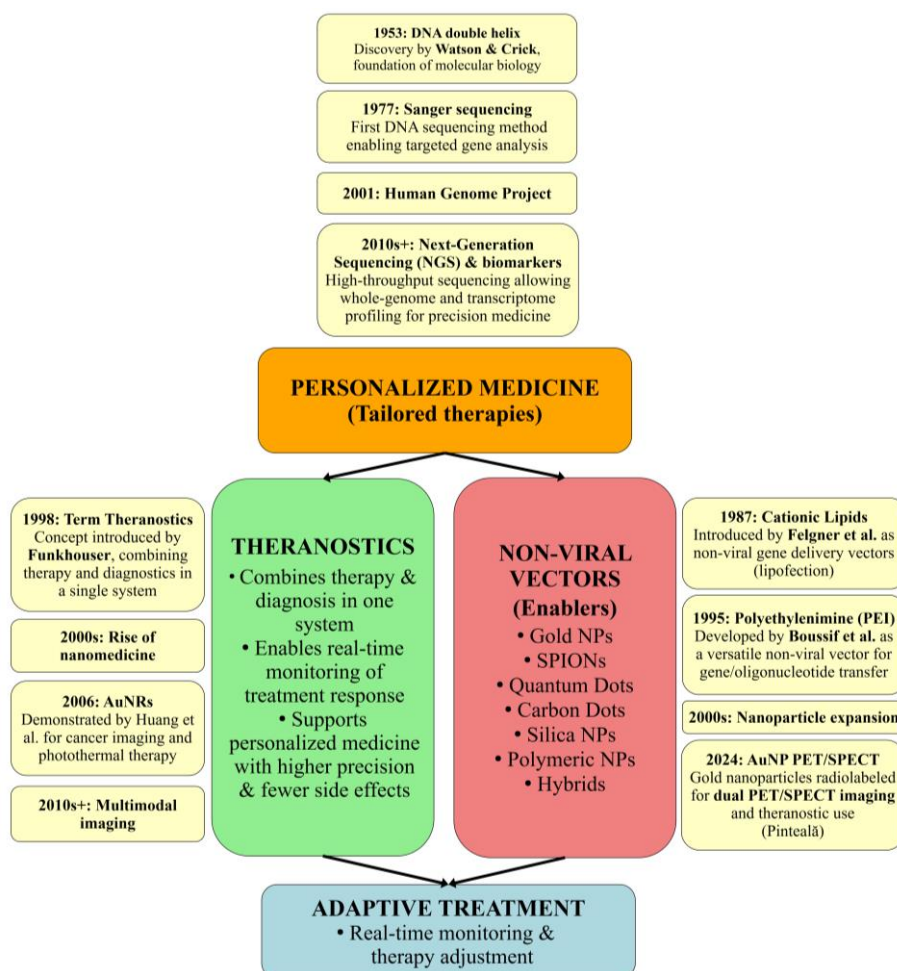


Figure 1. The evolution of personalized medicine toward theranostics and non-viral vectors.

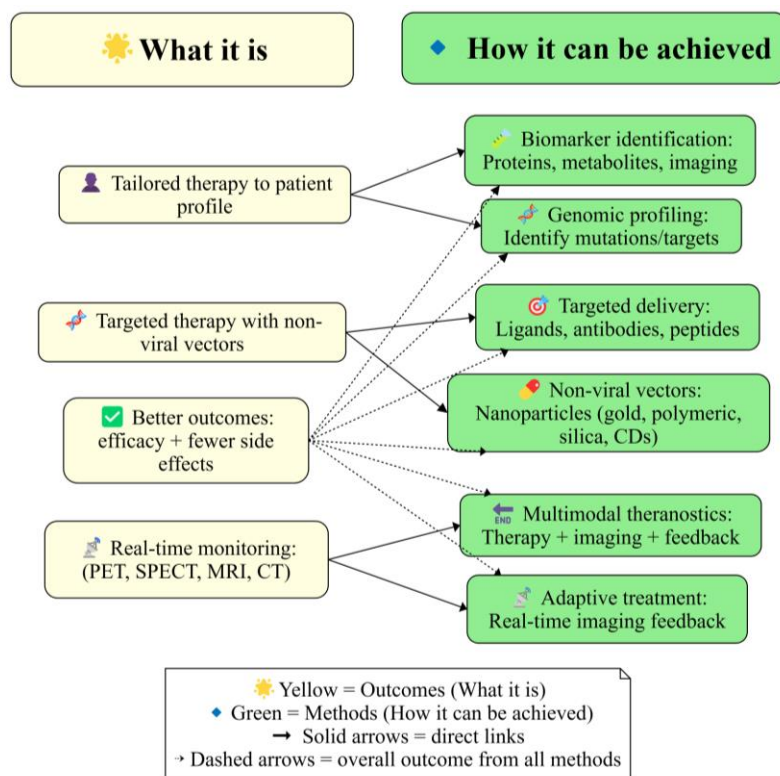


Figure 2. How personalized medicine can be achieved.

Non-viral vectors, from gene to precision care, named “engines of personalized medicine”, are central tools that make personalized medicine (Figure 3) practical by ensuring safe, targeted, and adaptable delivery of therapies, often combined with diagnostic imaging (theranostics).

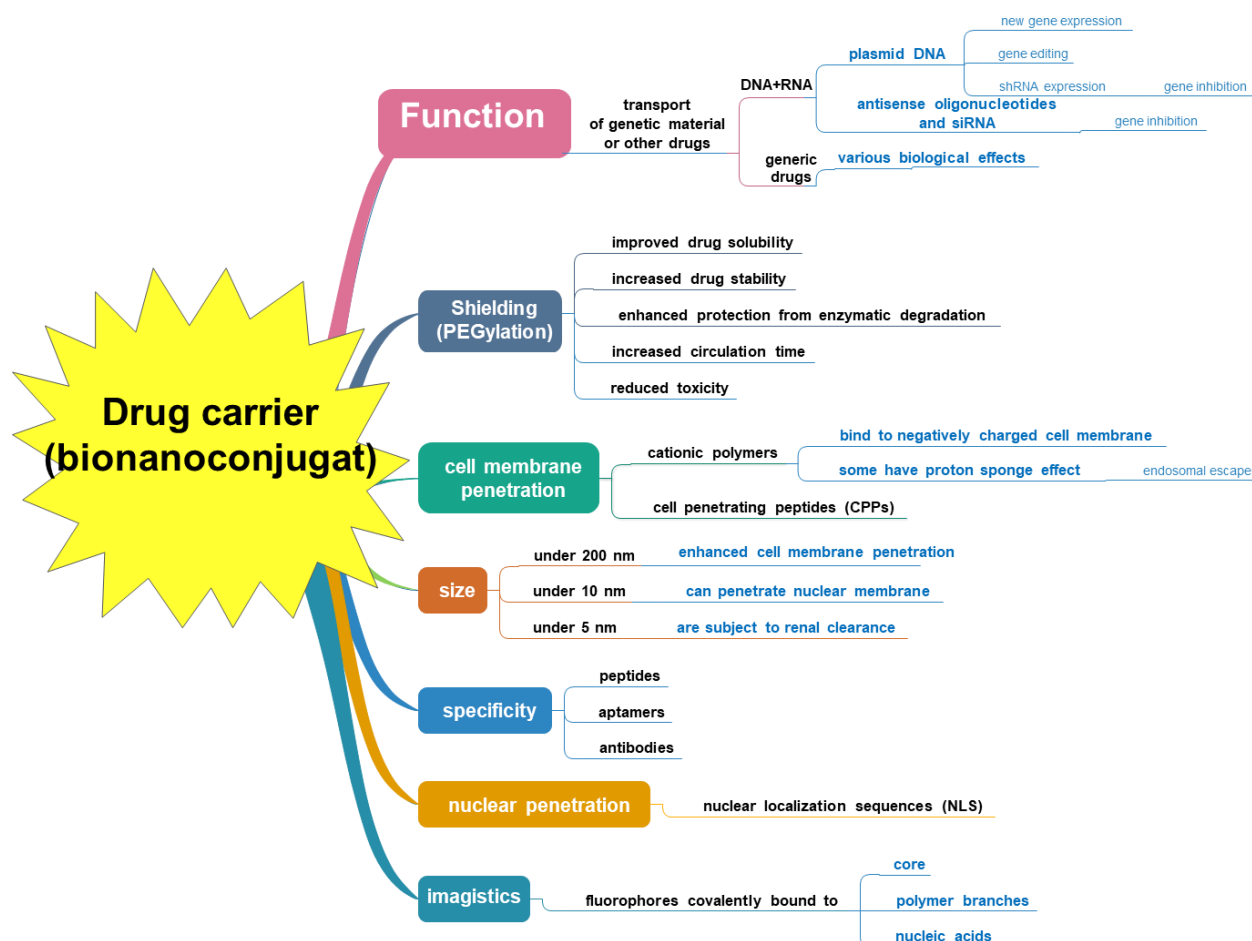


Figure 3. Non-viral delivery vectors: foundations of personalized medicine.

Briefly, the use of non-viral vectors in personalized medicine has the following advantages:

- Safety to use → deliver DNA, RNA (siRNA, mRNA) or drugs without the risks of viral integration or strong immune reactions.
- Can be designed as a function of the genetic profile of patients, the type of disease, and the needed treatment.
- Can be designed to deliver genes and drugs, essential for gene silencing, gene editing, and controlled drug delivery.
- Can be designed for theranostics applications → can be radiolabeled or functionalized for imaging (PET, SPECT, MRI) while simultaneously carrying therapeutic payloads.

Several types of nanoparticles could be utilized as theranostic platforms (Table 1). Among them, gold nanoparticles are versatile carriers for gene and drug delivery and act as imaging agents. Iron oxide nanoparticles combine MRI contrast with magnetic hyperthermia, while quantum and carbon dots can offer tunable fluorescence for bioimaging and mesoporous silica nanoparticles are able to load a high drug amount with controlled release.

Polymeric nanoparticles, such as PLGA, are biodegradable carriers already in clinical use. Hybrid systems integrate multiple functions, allowing simultaneous therapy and diagnosis.



Table 1. Nanoparticle types, applications, and limitations as a theranostic platforms.

Nanoparticle type	Therapy applications	Imaging modalities	Key references	Limitations / disadvantages
Gold nanoparticles (AuNPs)	Photothermal therapy, drug/gene delivery	CT, PET/SPECT, optical	[4,5]	High cost; limited penetration depth of light; possible long-term accumulation
Iron oxide nanoparticles (SPIONs)	Magnetic hyperthermia, drug delivery	MRI	[6,7]	Aggregation tendency; risk of long-term tissue accumulation
Quantum Dots (QDs)	Drug/gene delivery	Fluorescence, optical	[8,9]	Toxicity due to heavy metals; limited clinical translation
Carbon Dots (CDs)	Drug/gene delivery, photothermal/photodynamic	Fluorescence, NIR imaging	[10,11]	Lower stability vs. QDs; moderate drug loading capacity
Mesoporous Silica NPs (MSNs)	High-capacity drug delivery, stimuli-responsive release	MRI (doped), PET/SPECT, fluorescence	[12,13]	Slow clearance; potential inflammatory response
Carbon-based nanomaterials (graphene, CNTs, nanodiamonds)	Photothermal, photodynamic, drug/gene delivery	Raman, fluorescence, multimodal	[14,15]	Toxicity and biodegradability concerns; regulatory hurdles
Polymeric NPs (PLGA, PEG, dendrimers)	Controlled drug delivery, gene carriers	PET/SPECT, fluorescence, MRI (labeled)	[16,17]	Need for labeling for imaging; sometimes limited stability in circulation
Hybrid NPs (Au@Fe ₃ O ₄ , silica-coated Au)	Multi-therapy (photothermal + hyperthermia + drug delivery)	Multimodal (MRI + CT + PET/SPECT)	[18,19]	Complex synthesis; high cost; scalability issues

AuNPs = gold nanoparticles; SPIONs = superparamagnetic iron oxide nanoparticles; QDs = quantum dots; CDs = carbon dots; MSNs = mesoporous silica nanoparticles; CNTs = carbon nanotubes; PLGA = poly(lactic-co-glycolic acid); PEG = polyethylene glycol; MRI = magnetic resonance imaging; CT = computed tomography; PET = positron emission tomography; SPECT = single-photon emission computed tomography; NIR = near-infrared; PTT = photothermal therapy.

3. Conclusions

Personalized medicine signifies a transformative change in healthcare, providing a patient-oriented methodology whereby treatments are customized according to each individual's genetic and clinical characteristics. Advancements in precision targeting allow medicines to focus on particular mutations, biomarkers, or pathways, hence improving effectiveness. Simultaneously, reduced side effects are obtained by better dosage and targeted administration methods. Dynamic monitoring, including imaging modalities and biomarkers, enables real-time adjustment of treatment plans. The integration of theranostics, which combines diagnosis and treatment into a unified platform, enhances the capacity of customized medicine to revolutionize contemporary clinical practice.



Acknowledgements:

This paper is supported by European Union's Horizon Europe research and innovation programme under grant agreement No 101086667, project BioMat4CAST - "Petru Poni" Institute of Macromolecular Chemistry Multi-Scale In Silico Laboratory for Complex and Smart Biomaterials.

References

- [1]. Song Y, Zou J, Castellanos EA, Matsuura N, Ronald JA, Shuhendler A, Weber WA, Gilad AA, Müller C, Witney TH, Chen X. Theranostics – a sure cure for cancer after 100 years? *Theranostics* 14(6), 2464–2488, 2024.
- [2]. Felgner PL, Gadek TR, Holm M, Roman R, Chan HW, Wenz M, Northrop JP, Ringold GM, Danielsen M. Lipofection: a highly efficient, lipid-mediated DNA-transfection procedure. *Proc. Natl. Acad. Sci.* 84(21), 7413–7417, 1987
- [3]. Boussif O, Lezoualc'h F, Zanta MA, Mergny MD, Scherman D, Demeneix B, Behr JP. A versatile vector for gene and oligonucleotide transfer into cells in culture and in vivo: Polyethylenimine. *Proc. Natl. Acad. Sci.* 92(16), 7297–7301, 1995.
- [4]. Huan X, El-Sayed IH, Qian W, El-Sayed MA. Cancer cell imaging and photothermal therapy in the near-infrared region by using gold nanorods. *J. Am. Chem. Soc.* 128(6), 2115–2120, 2006
- [5]. Uritu CM, Al-Matarneh CM, Bostiog DI, Coroaba A, Ghizdov V, Filipiuc SI, Simionescu N, Stefanescu C, Jalloul W, Nastasa V, Tamba BI, Maier SS, Pinteala M. Multi-layered gold nanoparticle conjugates as biocompatible dual PET/SPECT tracers for theranostic applications. *J. Mat. Chem. B* 12(23), 5120–5132, 2024
- [6]. Gupta AK, Gupta M. Synthesis and surface engineering of iron oxide nanoparticles for biomedical applications. *Biomaterials* 26(18), 3995–4021, 2005.
- [7]. Laurent S, Forge D, Port M, Roch A, Robic C, Vander Elst L, Muller RN. Magnetic iron oxide nanoparticles: synthesis, stabilization, vectorization, physicochemical characterizations, and biological applications. *Chem. Rev.* 108(6), 2064–2110, 2008.
- [8]. Michalet X, Pinaud FF, Bentolila LA, Tsay JM, Doose S, Li JJ, Sundaresan G, Wu AM, Gambhir SS, Weiss S. Quantum dots for live cells, in vivo imaging, diagnostics. *Science*, 307(5709), 538–544, 2005.
- [9]. Yong KT. Quantum dots for biomedical applications: current status and future perspectives. *Nanomedicine* 4(4), 455–471, 2009.
- [10]. Lim SY, Shen W, Gao Z. Carbon quantum dots and their applications. *Chem. Soc. Rev.* 44(1), 362–381, 2015.
- [11]. Hola K, Zhang Y, Wang Y, Giannelis EP, Zboril R, Rogach AL. Carbon dots-emerging light emitters for bioimaging, cancer therapy and optoelectronics. *Nano Today* 9(5), 590–603, 2014.
- [12]. Slowing II, Vivero-Escoto JL, Wu CW, Lin VSY. Mesoporous silica nanoparticles for drug delivery and biosensing applications. *Adv. Funct. Mater.* 18(23), 3745–3753, 2008.
- [13]. Mamaeva V, Sahlgren C, Lindén M. Mesoporous silica nanoparticles in medicine-recent advances. *Adv. Drug Delivery Rev.* 65(5), 689–702, 2013.
- [14]. Li N, Zhang Q, Gao S, Song Q, Huang R, Wang L, Liu L, Dai J, Tang M, Cheng G, Jiang G. Three-dimensional graphene foam as a biocompatible and conductive scaffold for neural stem cells. *Theranostics* 3(6), 481–489, 2013.
- [15]. Liu Z, Sun X, Nakayama-Ratchford N, Dai H. (2007). Supramolecular chemistry on water-soluble carbon nanotubes for drug loading and delivery. *ACS Nano* 1(1), 50–56, 2007.
- [16]. Makadia HK, Siegel SJ. Poly lactic-co-glycolic acid (PLGA) as biodegradable controlled drug delivery carrier. *Polymers* 3(3), 1377–1397, 2011.
- [17]. Duncan R, Izzo L. Dendrimer biocompatibility and toxicity. *Adv. Drug Delivery Rev.* 57(15), 2215–2237, 2005.
- [18]. Lee DE, Koo H, Sun IC, Ryu JH, Kim K, Kwon IC. Multifunctional nanoparticles for multimodal imaging and theragnosis. *Chem. Soc. Rev.* 41(7), 2656–2672, 2012.
- [19]. Rengan AK, Jagtap M, De A, Banerjee R, Srivastava R, Paul A. Multifunctional gold-coated iron oxide nanoparticles for combined hyperthermia and photothermal therapy in cancer treatment. *Sci. Rep.* 5, 11605, 2015.



RESPONSIVE POLYMERIC NANOCAPSULES AND MULTI-COMPARTMENTS AS
CELLULAR MIMICS

Brigitte Voit

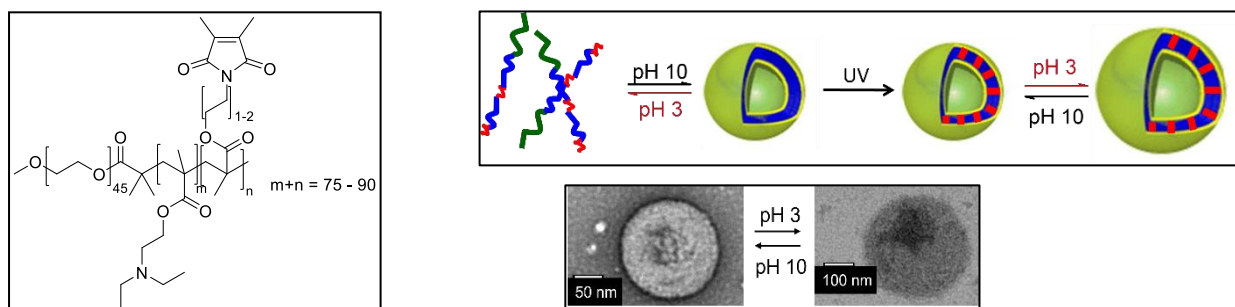
Leibniz-Institut fuer Polymerforschung Dresden e.V., Hohe Strasse 6, 01069 Dresden, Germany,
voit@ipfdd.de

1. Introduction

Polymeric micro- or nanocapsules and multicompartment systems are highly interesting in the field of nanoreactors and in mimicking biological systems and processes. Of special interest is the introduction of a stimuli-responsiveness into the capsule shell to be able to control the traffic through the membranes.

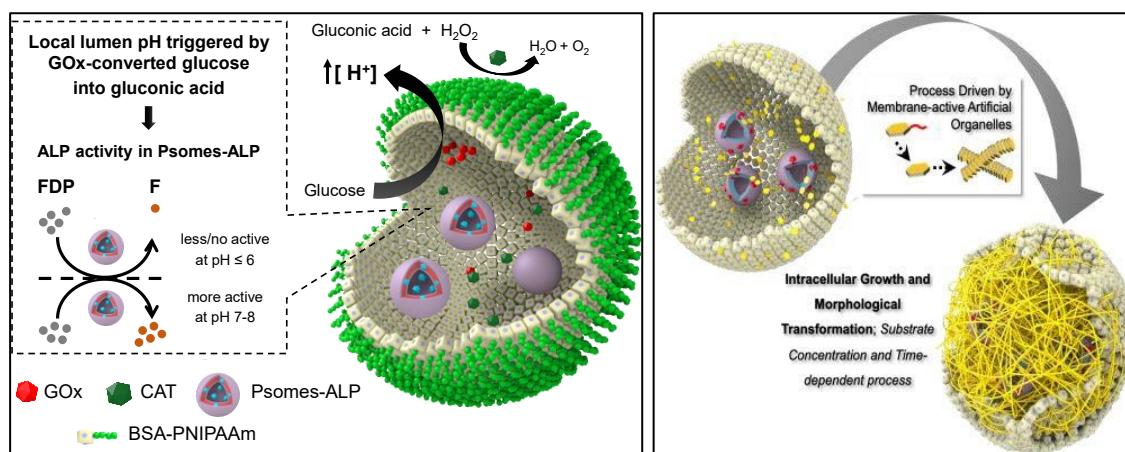
2. Results and discussion

Photocrosslinked, pH sensitive polymersomes: Robust, pH-responsive and multifunctional photocrosslinked polymersomes will be reported, which are interesting for studies in synthetic biology, but also for application as nanoreactors in microsystem devices and in nanotechnology. While pH sensitive polymersomes usually disassemble upon acidification, ours show a definite swelling, since the cross-linked membrane remains intact, and they allow pH-dependent diffusion of small molecules through the membrane (Scheme 1). Thus, cascade enzyme reactions could be carried out under pH control using polymersome-encapsulated enzymes and specific features of organelles could be mimicked¹ and the effectivity of the cascade enzymatic reactions could be increased by clustering [2]. In such pH-responsive and photo-crosslinked polymersomes various functions can be integrated e.g. additional light or redox responsiveness, and they can be decorated with various functionalities and bioactive biomacromolecules to achieve specific binding properties, targeting or therapeutic action [3-5].



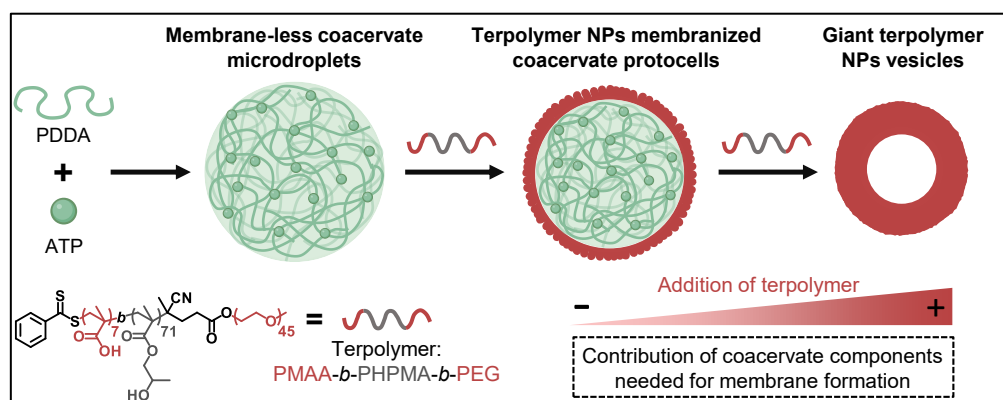
Scheme 1. left: pH-sensitive and crosslinkable block copolymer; top: schematic presentation of the self-assembly into polymersomes and UV crosslinking of the pH sensitive block copolymer; bottom: TEM images of the collapsed and swollen polymersomes [1].

Proteinosomes as multicompartments: Larger proteinosomes (up to 50 micrometer), prepared by pickering emulsion from BSA-PNIPAAm bioconjugates, have been realized as synthetic cell wall, and those compartments have been equipped with the smaller pH-responsive polymersomes, mimicking organelle structures in a cell [6-10]. Examples will be given how these multicompartments can be used to study complex cellular functions controlling cellular traffic, including the formation of cytoskeleton-like structures within the proteinosomes (Scheme 2) [9].



Scheme 2: Multicompartments based on polymersomes-in-proteinosome; left: enzymes loaded into the polymersomes allowed to trigger feed-back loop reactions based on pH differences [7]; right: generation of a cytoskeleton-like structure in proteinosomes from intracellular membrane-active artificial organelles [10].

Coacervates: The dynamics of membranes are integral to regulating biological pathways in living systems, particularly in mediating intra- and extracellular communication between membrane-less and membranized nano- and microcompartments. The membranization of membrane-less coacervates and further demembranization under control of the coacervate architecture paves the way for the exploitation of complex protocells. Different coacervate-based protocell transformations will be presented making use of ionic interactions of charged terpolymers with the coacervate components. Two different terpolymers are used with variations in the hydrophobic blocks but the same hydrophilic block [11,12].



Scheme 3. Transformation process of membrane-less coacervates (MLC) to terpolymer membranized coacervates (TMCs) and giant terpolymer vesicles (GTVs): MLCs are established *via* mixing of cationic PDDA and anionic ATP; subsequent addition of a terpolymer (PMAA-*b*-PHPMA-*b*-PEG) solution leads to formation of TMCs and the further reconfiguration into GTVs; membrane formation by aggregated terpolymer NPs on outer surface of coacervates is only possible when coacervate components participated [11].

The first transformation process is orchestrated by altering the balance of non-covalent interactions through varying concentrations of an anionic terpolymer, leading to the deposition of terpolymer nanoparticles (NPs) at the coacervate surface to fabricate membranized coacervates and, finally, giant vesicles (Scheme 3) [11].

A second strategy presents the controlled demembranization of membranized coacervate droplets [12]. After the formation of a solid-like membrane of coacervates by terpolymer-based nanospheres, the addition

of an anionic polysaccharide triggers the demembranization process arising from electrostatic competition with the membrane components, resulting in demembranized polysaccharide-containing coacervate droplets. These membranization/demembranization processes not only allow for the controlled structural reconfiguration of the coacervate entities, but also varies their permeability towards (biological) (macro)molecules and nano- and micro-scale objects. Additionally, integrating a polymersome membrane facilitates the creation of bilayer and "Janus-like" membranized coacervates. This is a strong advancement toward the creation of synthetic cells with different diffusible compartments and the development of coacervate protocells with hierarchical and asymmetric membrane structures.

Acknowledgements

The strong contributions of Dietmar Appelhans and Silvia Moreno is heartfully acknowledged, as well as those of all involved PhD students, coworkers and cooperation partners.

References

- [1]. Gaitzsch J, Appelhans D, Wang L, Battaglia G, Voit B. Synthetic bio-nanoreactor: mechanical and chemical control of polymersome membrane permeability. *Angew. Chem. Int. Ed.* 51, 4448–4451, 2012.
- [2]. Wang P, Moreno S, Janke A, Boye S, Wang D, Schwarz S, Voit B, Appelhans D. Probing crowdedness of artificial organelles by clustering polymersomes for spatially controlled and pH-triggered enzymatic reactions. *Biomacromolecules* 23, 9, 3648–3662, 2022.
- [3]. Moreno S, Sharan P, Engelke J, Gumz H, Oertel U, Wang P, Banerjee S, Klajn R, Voit B, Lederer A, Appelhans D. Light-driven proton transfer for cyclic and temporal switching of enzymatic nanoreactors. *Small* 16, 2002135, 2020.
- [4]. Moreno S, Gaitzsch J, Voit B. The chemistry of cross-linked polymeric vesicles and their functionalization towards biocatalytic nanoreactors. *Colloid Polym. Sci.* 299, 309–324, 2021.
- [5]. Geervliet E, Moreno S, Baiamont L, Booijin R, Boye S, Wang P, Voit B, Lederer A, Appelhans D, Bansal R. Matrix metalloproteinase-1 decorated polymersomes, a surface-active extracellular matrix therapeutic, potentiates collagen degradation and attenuates early liver fibrosis. *J. Controlled Release* 332, 594–607, 2021.
- [6]. Wang X, Moreno S, Boye S, Wen P, Formanek P, Lederer A, Voit B, Appelhans D. Feedback-induced and oscillating pH regulation of a binary enzyme–polymersomes system. *Chem. Mater.* 33, 6692–6700, 2021.
- [7]. Wang D, Moreno S, Boye S, Voit B, Appelhans D. Detection of subtle extracellular glucose changes by artificial organelles in protocells. *Chem. Commun.* 57, 8019–8022, 2021.
- [8]. Xu X, Moreno S, Boye S, Wang P, Voit B, Appelhans D. Artificial organelles with digesting characteristics: imitating simplified lysosome- and macrophage-like functions by trypsin-loaded polymersomes. *Adv. Sci.* 2207214, 2023.
- [9]. Zhang K, Moreno S, Wang X, Zhou Y, Boye S, Formanek P, Voigt D, Voit B, Appelhans D. Biomimetic cell structures: probing induced pH-feedback loops and pH self-monitoring in cytosol using binary enzyme-loaded polymersomes in proteinosome. *Biomacromolecules* 24, 6, 2489–2500, 2023.
- [10]. Wang D, Moreno S, Gao M, Guo J, Xu B, Voigt D, Voit B, Appelhans D. Protocells capable of generating a cytoskeleton-like structure from intracellular membrane-active artificial organelles. *Adv. Funct. Mater.* 33, 2306904, 2023.
- [11]. Zhou Y, Zhang K, Moreno S, Temme A, Voit B, Appelhans D. Continuous transformation from membrane-less coacervates to membranized coacervates and giant vesicles: toward multicompartmental protocells with complex (membrane) architectures. *Angew. Chem. Int. Ed.* 63, e202407472, 2024.
- [12]. Zhou Y, Maitz M, Zhang K, Voit B, Appelhans D. Dynamic and diverse coacervate architectures by controlled demembranization. *J. Am. Chem. Soc.* 147, 12239, 2025.



POLYMER MEMBRANES FOR ENERGY APPLICATIONS CHARACTERIZED BY NEUTRON SCATTERING TECHNIQUES

Aurel Radulescu

*Forschungszentrum Jülich GmbH, Jülich Centre for Neutron Science (JCNS) at
Heinz Maier-Leibnitz Zentrum (MLZ), Garching, Germany
a.radulescu@fz-juelich.de*

1. Introduction

Nafion is the commercial benchmark for proton exchange membranes (PEM) in fuel cell applications. However, due to its fluorine content, it has a high environmental impact. The transition from fluorinated materials to environmentally friendly hydrocarbon membranes while maintaining conductivity, mechanical stability, and chemical resistance is desirable in energy conversion applications. Syndiotactic polystyrene is a relatively new semi-crystalline material that becomes hydrophilic through appropriate functionalization by sulfonation and is therefore proton-conductive upon hydration. The solid-state sulfonation process enables homogeneous functionalization of the amorphous phase across the entire membrane thickness without compromising crystallinity. Under conditions of high functionalization, s-sPS exhibits ion conductivity and mechanical stability comparable to Nafion.

In order to understand the ion transport properties of s-sPS membranes under various application-relevant conditions and to identify optimization conditions, we first wanted to understand the morphology of the hydrated domains and the molecular dynamics of water at the microscopic level. Scattering methods using neutrons provide complete information about the meso- and nanoscale structures and molecular dynamics over a wide time scale in such materials. The particularly strong difference in neutron scattering cross section between the hydrogen isotopes protium (^1H) and deuterium (^2H or D) offers the unique advantage of D-labeling (contrast variation) of hydrocarbon materials such as synthetic or natural polymers. The combination of small-angle neutron scattering (SANS) over an extended Q range in structural investigations with quasi-elastic neutron spectroscopy (QENS) with variable resolution in molecular dynamics investigations is the ideal experimental approach for understanding s-sPS ion membranes at the microscopic level.

2. Experimental

This report covers SANS and QENS experiments on functionalized (sulfonated) syndiotactic polystyrene (s-sPS) conducted at various neutron scattering instruments installed at either stationary (reactor) or pulsed (spallation) neutron sources [1]. The polymer membranes were exposed in situ to controlled variation in relative humidity (RH) and temperature (T) within the range of application relevant conditions.

The experimental data were interpreted using structural and dynamic models to extract the parameters of interest, such as the size and shape of the hydrated domains, the volume fraction of water in the membrane and the hydrophilic phase, and the dilution law from a structural point of view, but also the type of dynamics, the characteristic time and diffusion coefficients of various motion processes, and the number of water molecules involved in different dynamic modes from a microdynamic standpoint. Deuterated sPS films were used, which kept the incoherent background at a low level. In addition, this enabled reliable recording of coherent structural information during neutron contrast manipulation in both the functionalized amorphous and crystalline phases by using H_2O or $\text{H}_2\text{O}/\text{D}_2\text{O}$ mixtures in different ratios for membrane hydration and doping the crystalline form (clathrate with guest molecules) with protonated guest molecules to highlight the crystalline scattering properties. Moreover, using deuterated films, the water dynamics in the QENS experiments could be specifically investigated using H_2O in the membrane hydration.



3. Results and discussion

SANS provides information about the size, shape, orientation, and density of the scattering objects, as well as their organization into higher-order units/aggregates. To separate the contributions of the crystalline and hydrated amorphous phases for a robust analysis, uniaxially deformed polymer films were used. In this way, the scattering contributions of different morphological components, such as crystalline lamellae or the crystal lattice, appear at different scattering angles depending on their size and are distributed to specific detector sectors depending on their orientation and alignment with the sample deformation. Examples of SANS patterns collected over an extended Q range from a uniaxially deformed s-SPS membrane at RH = 85% are shown in Figure 1a, as measured across the equatorial and meridian sectors of the detector.

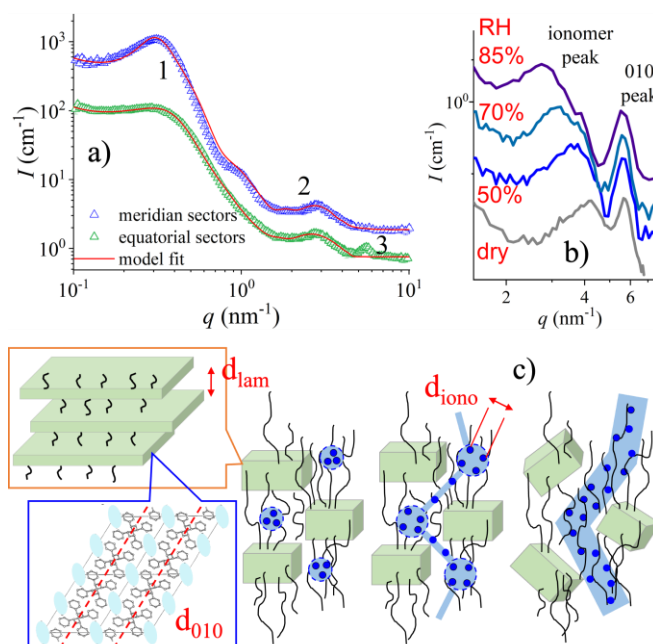


Figure 1. SANS patterns (a and b) measured on uniaxially deformed s-SPS membranes under various RH conditions, and the morphology resulting from the model interpretation of the scattering data (c); the meaning of the parameters and labels is explained in the text.

The three scattering characteristics specific to this type of membrane are recognizable: 1 – the interlamellar correlation peak, which can be observed in the meridian sector and is caused by the correlation between aligned lamellae along the deformation axis over the distance d_{lam} ; 2 – the ionomer peak, which can be observed in both the meridian and equatorial sectors and indicates the correlation length d_{iono} between the ionic clusters that are randomly distributed within the functionalized amorphous phase; and 3 – the 010 crystal peak due to the correlation between the crystal planes in the lamellae over the distance d_{010} , which are aligned along the axis perpendicular to the deformation direction. The ionomer peak is a direct indication of the ionic character of the material and its hydrophilicity: the more water is absorbed by the membrane, the larger the correlation length between the ion clusters, causing the peak position in the scattering experiment to shift to lower Q values (Figure 1b). Furthermore, the preservation of the crystalline peak 010 at the same position (Figure 1b) regardless of the treatment conditions of the membrane (RH and T) indicates a high mechanical stability of the membrane. The model interpretation of a large number of scattering data from membranes under different degrees of functionalization, neutron contrast, RH, and T conditions is shown in Figure 1c: In contrast to NAFION, which is characterized by a bicontinuous distribution of hydrophilic and hydrophobic phases, water accumulates in the s-SPS membranes in spherical clusters that increase in size with increasing RH and connect with each other until they eventually develop into cylindrical channels when the membranes are equilibrated in water. Due to this special morphology of

the hydrated domains, the high ion conductivity in s-SPS can only be maintained at a high degree of hydration, as was also demonstrated by conductivity measurements.

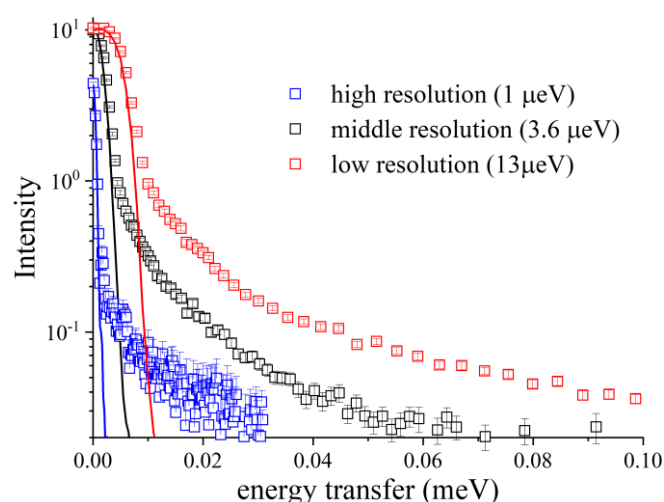


Figure 2. QENS spectra (symbols) of a deuterated s-SPS membrane hydrated in situ with H₂O vapors at a RH = 85%, measured with different instrumental resolutions (lines).

Figure 2 shows examples of QENS spectra from water dynamics in s-SPS membranes: the broadening towards higher energy transfers of the elastic line centered at zero energy transfer indicates quasi-elastically scattered neutrons due to energy exchange with the mobile water molecules: the better the experimental resolution, the slower the movements of the water molecules could be detected. The model interpretation of the experimental data enabled the characterization of several dynamic modes in terms of the characteristic time between nanoseconds and picoseconds, the corresponding diffusion coefficient, the spatial extent of the movement, and the number of water molecules involved in each mode, whereby the amount of water absorbed by the membrane was known.

4. Conclusions

The application of neutron scattering techniques to investigate the structure and morphology of hydrated domains at the meso- and nanoscale as well as the water micro-dynamics on a time scale between ns and ps in sulfonated syndiotactic polystyrene membranes is extensively reviewed.

References

- [1]. Schiavone MM, Lamparelli, DH, Daniel C, Golla M, Zhao Y, Iwase H, Arima-Osonoi H, Takata S, Szentmiklosi L, Maroti B, Allgaier J, Radulescu A. Extended Q-range small-angle neutron scattering to understand the morphology of proton exchange membranes: the case of functionalized syndiotactic-polystyrene model system. *J Appl Cryst.* 56, 947–960, 2023.



NEW WAYS FOR FUNCTIONAL NANOMATERIALS: THE JOURNEY FROM LINEAR TO STAR-SHAPED POLYMERS

Barbara Mendrek, Marcelina Bochenek, Natalia Oleszko-Torbus, Agnieszka Kowalczyk*

Centre of Polymer and Carbon Materials, Polish Academy of Sciences, Zabrze, Poland

**akowalczyk@cmpw-pan.pl*

1. Introduction

The journey from linear to star-shaped polymers is not just a change in macromolecular architecture, but also an important step in polymer science with wide theoretical and practical impact. Although the concept of non-linear macromolecules, such as branched and star-like polymers, was already proposed more than eighty years ago, the interest in these complex structures remained modest for a long time. Their synthesis posed significant challenges, and controlling their architecture was difficult. At the same time, dendrimers — perfectly branched, monodisperse macromolecules — emerged as a new class of materials with intriguing properties, further stimulating interest in branched polymers and challenging chemists to develop polymeric analogues with comparable functionality but improved accessibility and cost-efficiency.

Among the various classes of branched polymers, star polymers represent a particularly interesting and versatile architecture [1,2]. These macromolecules consist of multiple linear polymer arms — either homopolymers or copolymers — covalently attached to a central core. This core, often referred to as the branching centre serves as the structural “nucleus” around which the star-like architecture is formed. For many years, scientific interest in star polymers primarily centered on mastering their structural control rather than exploring their functional or biological potential. However, recent advancements in polymerization techniques and molecular design have shifted this focus. The growing accessibility of synthetic methods, coupled with the ability to achieve high molar masses and multifunctionality, has positioned star polymers as promising candidates for a wide range of biorelated applications. One of the most attractive features of these polymers is the tunability of their macromolecular parameters. By adjusting the molar mass or modifying the chemical nature and functionality, it is possible to tailor the physical, chemical, and biological properties of the resulting polymeric nanostructures. In the case of stars, the linear arms themselves can be composed of a wide polymer types, including various block or random copolymers, allowing for fine control over solubility, degradability, and compatibility with various biological environments. Thanks to this architectural flexibility and the growing ease of synthesis, star polymers are no longer just a topic of academic interest. They are now recognized as functional nanomaterials with high potential for biomedical applications, smart materials, and nanotechnology. Their unique combination of branched structure, tunable chemistry, and multifunctionality opens new routes for innovation in polymer science and engineering.

2. Results and discussion

The aim of this work was to develop functional polymers of various topologies and to investigate the ability of selected nanostructures for interactions with bioactive substances, cells and bacteria. Star polymers with both low molecular weight cores as well as hyperbranched polymeric cores have been successfully obtained, and a wide variety of star topologies have been synthesized. Linear homopolymers and copolymers of different architectures (block, random, gradient) were used as arms, while the synthesis strategies were primarily based on controlled/living polymerization techniques. Methods such as cationic and anionic living polymerization, atom transfer radical polymerization (ATRP), and degenerative chain transfer polymerization (IDT) were employed, enabling precise control over the number and length of star arms as well as the molar mass.



Initially, star polymers were synthesized by the “arm-first” approach, in which living chains were terminated with multifunctional agents [3]. In our subsequent works, emphasis was placed on the “core-first” strategy, where multifunctional initiators induced the polymerization of monomers, ensuring the absence of unreacted linear chains in the product. By this method, stars with polystyrene [4], poly(meth)acrylate [5-7], polyacid [8], polyether [9], and poly(2-substituted 2-oxazoline) [10] arms were obtained. The functionality of the stars was evaluated by selective alkaline hydrolysis of ester linkages, allowing the determination of the real number of arms. For poly(tert-butyl methacrylate) and poly(N,N'-dimethylaminoethyl methacrylate) (PDMAEMA) stars, the calculated functionalities were close to the expected values (26–28), while for stars with poly[(oligoethylene glycol) methacrylate] P(DEGMA-co-OEGMA) arms, a lower functionality (20–22) was observed, most likely due to steric hindrance limiting access to initiating groups. The solution behavior of the synthesized macromolecules was also investigated. GPC-MALLS and light scattering methods confirmed that star-shaped polymers occupied smaller hydrodynamic volumes than their linear analogues of the same molar mass. For various systems, branching parameters were calculated, and scaling laws describing their size in solution were established. The existence of core-shell morphologies was demonstrated for stars with hydrophobic cores and hydrophilic arms, which influenced their tendency to aggregate in selective solvents. Thermoresponsive behavior was observed for poly(2-oxazoline), polyether, and PDMAEMA-based stars [5-7,10,11], with transition temperatures being dependent on arm length, composition, and solvent conditions. pH-responsivity was also detected in polyacid- and PDMAEMA-containing stars, where aggregation in aqueous environments was governed by the ionization state of the arms [6,8,11,12]. The biorelevant properties of star polymers were systematically examined.

Cytotoxicity studies confirmed that PDMAEMA and P(DEGMA-co-OEGMA) stars were non-toxic to selected human fibroblast and fibrosarcoma cell lines [6,11,13]. Several bioapplications were successfully demonstrated. Cisplatin was conjugated with poly(acrylic acid) arm stars with high efficiency (up to 80%, corresponding to 45 wt% platinum), and the drug was continuously released over more than a week. PEGylation of the outer shell enhanced drug loading and prolonged release [8,14]. PDMAEMA-based stars were employed as carriers for nucleic acids, where the formation of stable polyplexes with DNA and RNA was confirmed [6,15]. Cytotoxicity was reduced by the incorporation of oligo(ethylene glycol) units, while efficient cellular uptake and gene delivery were achieved [7]. In another application, PDMAEMA stars were used to reduce silver ions to stable silver nanoparticles, resulting in hybrid nanomaterials with enhanced antimicrobial activity [16]. Nanostructures formed from polymers with chelate-functionalized poly(2-oxazoline) arms also exhibited satisfactory antibacterial activity, which opens the way for their use as potential antimicrobial agents [17]. Furthermore, P(DEGMA-co-OEGMA) stars demonstrated their potential as drug nanocarriers by encapsulating fluorescent dyes, remaining stable in aqueous solution [5].

3. Conclusions

To summarize, star polymers of diverse compositions and functionalities were synthesized by controlled polymerization techniques. Their structural parameters were precisely tuned, their solution behavior was elucidated, and biorelated properties were extensively evaluated. The unique characteristics of these macromolecular architectures - including low toxicity, responsiveness to external stimuli, and ability to act as carriers of drugs, nucleic acids, and nanoparticles demonstrate their promise for future applications in medicine, particularly in drug delivery and gene therapy.

Acknowledgements

This work was supported by the National Science Centre, project 2021/43/B/ST4/01493.

References

- [1]. Wu W, Wang W, Li J. Star polymers: Advances in biomedical applications. *Prog. Polym. Sci.* 46, 55–85, 2015.



- [2]. Ren J, McKenzie T, Fu Q, Wong E, Xu J, An Z. Star Polymers. *Chem. Rev.* 116, 6743–836, 2016.
- [3]. Dworak A, Kowalczyk-Bleja A, Trzebicka B, Wałach W. Amphiphilic core-shell PEO stars by Williamson etherification reaction. *Polym. Bull.* 49, 9–16, 2002.
- [4]. Kowalczyk-Bleja A, Trzebicka B, Komber H, Voit B, Dworak A. Controlled radical polymerization of p-(iodomethyl)styrene – a route to branched and star-like structures *Polym.* 45, 9–18, 2004.
- [5]. Kowalczyk A, Mendrek B, Żymełka-Miara I, Libera M, Marcinkowski A, Trzebicka B, Smet M, Dworak A. Solution behavior of star polymers with oligo(ethylene glycol) methyl ether methacrylate arms. *Polymer* 53, 5619–5631, 2012.
- [6]. Mendrek B, Sieroń Ł, Libera M, Smet M, Trzebicka B, Sieroń A, Dworak A, Kowalczyk A. Polycationic star polymers with hyperbranched cores for gene delivery. *Polymer* 55, 4551–4562, 2014.
- [7]. Mendrek B, Sieroń Ł, Żymełka-Miara I, Binkiewicz P, Libera M, Smet M, Trzebicka B, Sieroń A, Kowalczyk A, Dworak A. Non-viral plasmid DNA carriers based on N,N'-dimethylaminoethyl methacrylate and di(ethylene glycol) methyl ether methacrylate star copolymers. *Biomacromolecules* 16, 3275–3285, 2015.
- [8]. Kowalczyk A, Stoyanova E, Mitova V, Shestakova P, Momekov G, Momekova D, Koseva N. Star-shaped nanoconjugates of cisplatin with high drug payload. *Int. J. Pharm.* 404, 220–230, 2011.
- [9]. Libera M, Trzebicka B, Kowalczyk A, Wałach W, Dworak A. Synthesis and thermoresponsive properties of four-arm, amphiphilic poly(tert-butyl glycidyl ether)-block-polyglycidol stars. *Polym.* 52, 250–257, 2011.
- [10]. Kowalczyk A, Kronek J, Bosowska K, Trzebicka B, Dworak A. Star poly(2-ethyl-2-oxazoline)s – synthesis and thermosensitivity. *Polym. Int.* 60, 1001–1009, 2011.
- [11]. Mendrek B, Fus A, Klarzyńska K, Sieroń AL, Smet M, Kowalczyk A, Dworak A. Synthesis, characterization and cytotoxicity of novel thermoresponsive star copolymers of N,N'-dimethylaminoethyl methacrylate and hydroxyl-bearing oligo(ethylene glycol) methacrylate. *Polymers* 10, 1255, 2018.
- [12]. Kowalczyk A, Trzebicka B, Rangelov S, Smet M, Dworak A. Star macromolecules with hyperbranched poly(arylene oxindole) cores and polyacid arms: synthesis and solution behavior. *J. Polym. Sci., Part A: Polym. Chem.* 49, 5074–5086, 2011.
- [13]. Mendrek B, Żymełka-Miara I, Sieroń Ł, Fus A, Balin K, Kubacki J, Smet M, Trzebicka B, Sieroń AL, Kowalczyk A. Stable star polymer nanolayers and their thermoresponsiveness as a tool for controlled culture and detachment of fibroblast sheets. *J. Mater. Chem. B* 6, 641–655, 2018.
- [14]. Stoyanova V, Mitova V, Shestakova P, Kowalczyk A, Momekov G, Momekova D, Marcinkowski A, Koseva N. Reversibly PEGylated nanocarrier for cisplatin delivery. *J. Inorg. Biochem.* 120, 54–62, 2013.
- [15]. Fus-Kujawa A, Teper P, Botor M, Klarzyńska K, Sieroń Ł, Verbelen B, Smet M, Sieroń AL, Mendrek B, Kowalczyk A. Functional star polymers as reagents for efficient nucleic acids delivery into HT-1080 cells. *Int. J. Polym. Mater. Polym. Biomater.* 70(5), 356, 2021.
- [16]. Teper P, Sotirova A, Mitova V, Oleszko-Torbus N, Utrata-Wesołek A, Koseva N, Kowalczyk A, Mendrek B. Antimicrobial activity of hybrid nanomaterials based on star and linear polymers of N,N'-dimethylaminoethyl methacrylate in situ produced silver nanoparticles. *Materials* 13(13), 3037, 2020.
- [17]. Bochenek M, Mendrek B, Kowalczyk A, Wałach W, Jałowicki Ł, Borgulat J, Plaza G, Kubacki J, Sikora M, Fus A, Sieroń Ł, Gawron K, Oleszko-Torbus N. Designing antibacterial polymeric systems: (co)poly(2-oxazoline) conjugates with acyclic and macrocyclic polyamino polycarboxylic chelators. *Biomater. Sci.* 13(14), 3876–3886, 2025.



PRECISION IN POLYMER SYNTHESIS: FROM SUSTAINABLE POLYMERS TO BIOACTIVE GLYCOPOLYMERS

C. Remzi Becer

*Department of Chemistry, University of Warwick, Coventry, CV4 7AL, United Kingdom
remzi.becer@warwick.ac.uk*

1. Introduction

Sequence controlled polymers have been attracting more and more attention to deliver the desired properties to the advanced materials by the help of their precisely controlled compositions and architectures. Understanding the specific multivalent carbohydrate-protein interactions is crucial to determine the structure-property relationships and to design accordingly the next generation of functional glycomaterials.

2. Results and discussion

We investigate the structure-property relationships between the mammalian lectins and multivalent carbohydrate polymers, which may have applications for anti-adhesion therapy [1,2]. Moreover, we have investigated the affinity of poly(mannose-methacrylate), helical glycopolypeptides, gp120, star shaped glycopolymers, and cyclodextrin centered glycopolymers with a selected mannose binding lectin (DC-SIGN) that exists on dendritic cells, using SPR technique. Selected members of a glycopolymer library were used to demonstrate the interactions between DC-SIGN and mannose rich polymers.

We extend this study to a broader set of polymers to examine the effect of chain length, end group, architecture, thermoresponsive block, and number of arms in the star shaped polymers on the lectin binding (Figure 1).

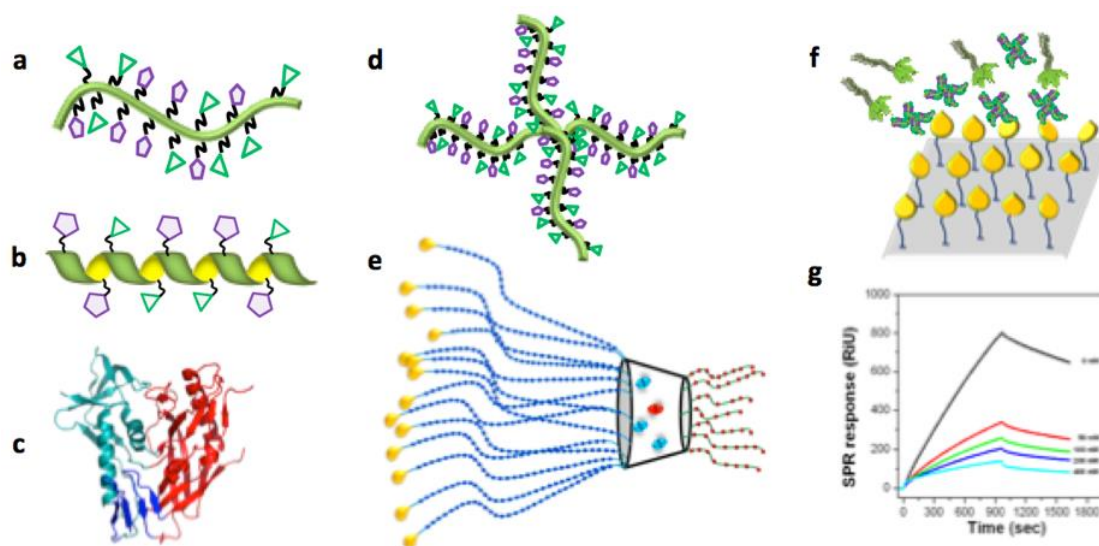


Figure 1. Schematic representation of (a) linear GP, (b) helical glycopolypeptide, (c) glycoprotein 120 (gp120), (d) star shaped GP, (e) cyclodextrin centred GP, (f) SPR measurement on glycopolymer - DCSIGN competition in solution, (g) SPR response-time for the interaction of DC-SIGN & gp120.

Poly(2-oxazoline)s are promising class of polymers that allows several design possibilities. Functional 2-oxazoline monomers with initiator or chain transfer agents allow creating macroinitiators for brush copolymers. In this talk, we will highlight various combinations of 2-oxazolines that are polymerized by



cationic ring opening polymerization and acrylates/acrylamides that are polymerized by controlled radical polymerization techniques (Figure 2) [3].

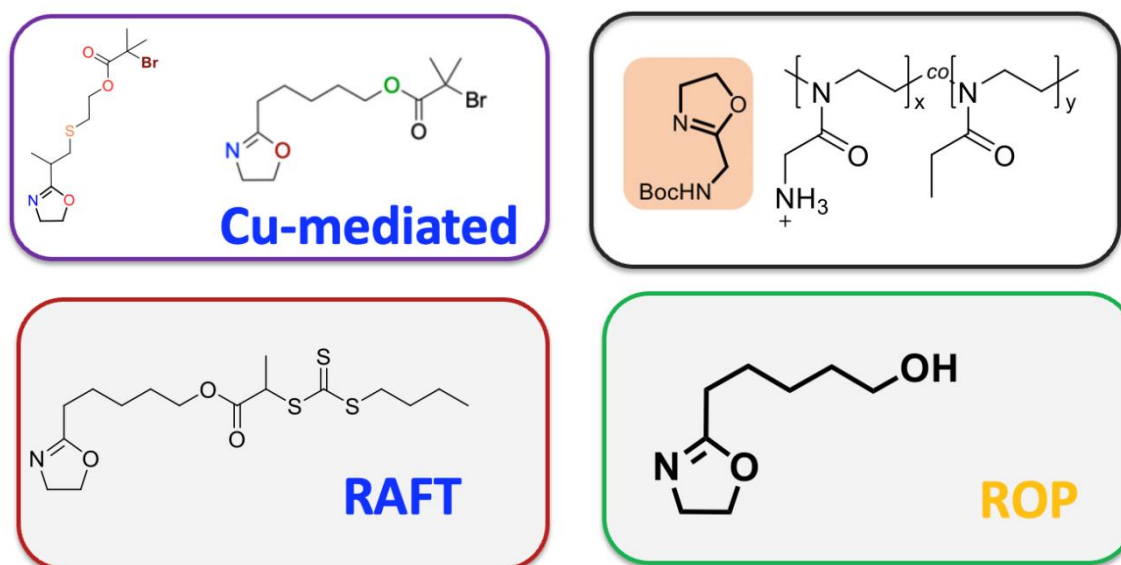


Figure 2. Structures of functional 2-oxazoline monomers that allow synthesis of hybrid 2-oxazoline and acrylate copolymers.

References

- [1]. Hartweg M, Jiang Y, Yilmaz G, Jarvis CM, Nguyen HVT, Primo GA, Monaco A, Beyer VP, Chen KK, Mohapatra S, Axelrod S, Gómez-Bombarelli R, Kiessling LL, Becer CR, Johnson JA, Synthetic glycomacromolecules of defined valency, absolute configuration, and topology distinguish between human lectins. *JACS Au*, 1 (10), 1621–1630, 2021.
- [2]. Abdouni Y, TerHuurne GM, Yilmaz G, Monaco A, Redondo-Gómez C, Meijer EW, Palmans ARA, Becer CR, Self-assembled multi- and single-chain glyconanoparticles and their lectin recognition. *Biomacromolecules*, 22 (2), 661–670, 2021.
- [3]. Concilio M, Nguyen N, Hall SCL, Huband S, Becer CR. Synthesis of oxazoline/methacrylate-based graft-copolymers via grafting-through method and evaluation of their self-assembly in water and dodecane. *Macromolecules*, 56, 7961–7972, 2023.



POLYMER-PROTEIN COMPLEXES AS VERSATILE CARRIERS FOR TARGETED PROTEIN AND DRUG DELIVERY CHARACTERIZED BY SMALL-ANGLE NEUTRON SCATTERING

Aurel Radulescu

*Forschungszentrum Jülich GmbH, Jülich Centre for Neutron Science (JCNS),
Heinz Maier-Leibnitz Zentrum (MLZ), Garching, Germany
a.radulescu@fz-juelich.de*

1. Introduction

Micro- and nano-gels made from biopolymers such as polysaccharides combine the properties of nanoparticles and hydrogels and respond to external stimuli such as pH, ionic strength or temperature (T) as their network structure enables swelling/deswelling transitions and they possess the appropriate dimensions for encapsulation and nano-delivery. The addition of proteins to polysaccharides and their coupling to form more complex morphologies opens up possibilities for fine-tuning gel properties by physically cross-linking the components and modifying the gel network structure. In general, complexes of proteins with natural or biodegradable synthetic polymers can result in micelles, vesicles or more complex morphologies. These systems find application in nanomedicine for the targeted delivery and controlled release of proteins thanks to the pH-responsiveness of the formed structures. Moreover, the presence of a polymer/protein layer enables the encapsulation of ionic drugs within such particles. Furthermore, proteins protect bio-active molecules such as vitamins through non-covalent interactions. Vitamins D2 and D3 (VD2 and VD3) play an important role in human and animal nutrition by regulating the circuit of calcium and phosphorus cycling in the body and incorporation into the skeleton. Challenges of administering vitamins D include its poor water solubility, chemical degradation at elevated temperatures, and variable oral bioavailability. Micro- and nanogels composed of polysaccharides and various proteins protect vitamins D from degradation than the protein alone, which is susceptible to structural changes triggered by modifications in its environment, such as pH and T.

Understanding the physicochemical properties of these polymer-protein complexes under different conditions, with and without encapsulated components, is therefore crucial for their optimization and utilization. Small-angle neutron scattering (SANS) provides comprehensive information about the meso- and nanoscale structures of such materials. The particularly strong difference in the neutron scattering cross section between the hydrogen isotopes protium (¹H) and deuterium (²H or D) offers the unique advantage of D-labeling (contrast variation) of hydrocarbon materials such as polymers and proteins. This work demonstrates how contrast variation SANS can uniquely resolve the complex structure and morphology under application-relevant pH and T conditions in polymer-protein complexes based on bio- and synthetic polymers with encapsulated drugs or vitamins.

2. Experimental

This report covers experimental SANS studies on complexes of biodegradable polymers such as PEO-PDMAEMA or PEO-QPDMAEMA and insulin [1], as well as on biopolymers such as different types of carrageenan and BSA or HSA proteins. Complexes encapsulating drugs such as protoporphyrin-IX or VD3 vitamins have also been investigated. SANS experiments are presented that were performed under contrast variation conditions over a wide Q range between 2×10^{-4} and 1.0 \AA^{-1} at small-angle diffractometers installed either at stationary (reactor) or pulsed (spallation) neutron sources. This approach covered a broad length scale in real space between a few Å and mm. To apply the contrast variation method selected components in the complex morphology in a partially or fully deuterated state were used. Neutron contrast conditions were used with an appropriate mixing of deuterated and protonated components in aqueous solutions,



allowing either full contrast, thus the full morphology “visible” in D₂O when all components were used in protonated state; the visibility of the PE block in 70% D₂O - 30% H₂O when deuterated QPDMAEMA block was matched out; or protonated protein, which was matched out in 35-40% D₂O content, thus only the polymer was visible. Samples were analyzed under different pH, temperature and concentration conditions. Scattering patterns were interpreted using appropriate structural models to extract the shape, size and density of the polymer-protein morphologies. Encapsulation and controlled drug release was checked by fluorescence spectroscopy. To support the structural findings, cryo-TEM was also used for some of the complexes in addition to neutrons.

3. Results and discussion

Figure 1a shows the scattering patterns of a sample containing the diblock copolymer with a weakly charged block and insulin in D₂O for two pH conditions. Scattering of polyelectrolyte-protein complexes is observed at pH = 7.4, whereas at pH = 11, superposition of scattering of the two components individually is observed, since no complex is formed at this pH.

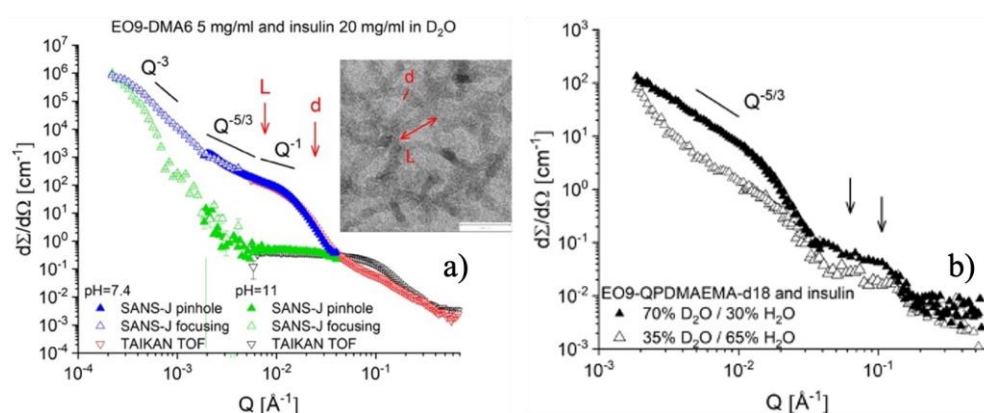


Figure 1. Scattering patterns from the combination of weakly charged diblock copolymer and protein in full contrast (a) and selected contrast matching conditions (b). The cryo-TEM image is shown as an inset in (a). The power law behavior of the scattering and the estimated thickness and length of the complex morphology are indicated in (a). Arrows in (b) indicate the scattering features representing correlation effects between the charged components of the complex.

Data collected with two different instruments at reactor (SANS-J) and spallation (TAIKAN) sources in Japan sources are shown in parallel using different color scheme. Very good agreement is observed between the scattering data at medium and low Q and the cryo-TEM images (inset in Figure 1a) regarding the medium- and large-scale morphology of the polyelectrolyte-protein complexes: one-dimensional flexible morphologies are formed (Q^{-1} power law behavior of the scattered intensity), which, on a larger length scale, behave like a branched morphology resembling that of a solvent-swollen self-avoiding polymer coil ($Q^{-5/3}$ power law). The thickness and segment length can be estimated from the analysis of the cryo-TEM image, while the power law behavior of the scattering patterns at medium Q and pH = 7.4 agrees well with the morphology revealed by the micrograph. At low Q , an increase in the scattering pattern is observed under both pH conditions, presumably due to the association of the one-dimensional flexible morphologies into a larger network. The contrast matching results (Figure 1b) for the QPDMAEMA block (full symbols) or insulin (open symbols) confirm the morphology formation scenario described above: over an extended Q range, a $Q^{-5/3}$ power law behavior is observed when alternately visualizing either the charged block or the protein, i.e. both oppositely charged species jointly assemble the complex, while the PEO block forms a kind of shell and network of the morphology. The broad peak-like scattering feature at high Q appears under both contrast conditions, albeit with different intensities, indicating correlation effects between the interacting charged components in the complex system, which are made visible or invisible in the scattering

experiment depending on the contrast condition.

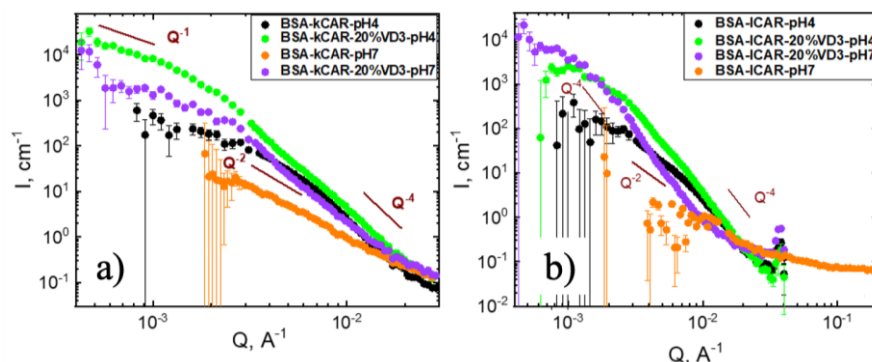


Figure 2. SANS profiles from (a) BSA- κ -carrageenan complexes and (b) BSA- λ -carrageenan complexes upon 20% VD3 encapsulation and pH adjustment from pH = 4 to pH = 7.

Figure 2 shows the scattering patterns of two systems containing BSA protein and either the polysaccharide κ -carrageenan (a) or λ -carrageenan (b) at two pH conditions, pH = 4 and pH = 7, and with 20% VD3 encapsulation. It shows that the addition of VD3 led to the stabilization of larger complex morphologies, likely because VD3 acts as an additional cross-linking point for association of already formed complexes or induces further structural rearrangements within the BSA component. Furthermore, SANS data showed complex disruption at pH = 7, as indicated by the significant drop in scattering intensity (orange symbols). However, when VD3 was encapsulated in the complexes, increasing the pH did not lead to complete disruption, as scattering from large aggregates is still visible at low Q , suggesting that VD3 increases the stability of the complexes. This stabilization effect was more pronounced in case of λ -CAR complexes than in case of κ -CAR complexes, since even at pH = 7, larger stable morphologies could be identified based on the strong scattering observed at low Q .

4. Conclusions

The application of contrast variation SANS to investigate the structure and morphology of polymer-protein complexes and their drug encapsulation properties using biopolymers such as carrageenan polysaccharides or synthetic PEO-based di-block copolymers is described in details.

References

- [1]. Murmiliuk A, Iwase H, Kang JJ, Mohanakumar S, Appavou MS, Wood K, Almasy L, Len a, Schwärzer K, Allgaier J, Dulle M, Gensch T, Förster B, Ito K, Nakagawa H, Wiegand S, Förster S, Radulescu A. Polyelectrolyte-protein synergism: pH-responsive polyelectrolyte/insulin complexes as versatile carriers for targeted protein and drug delivery. *J Coll Interface Sci.* 665, 801–813, 2024.



MULTIFUNCTIONAL POLYSACCHARIDE-BASED HYBRID HYDROGELS WITH POROSITY TAILORED BY CRYOTROPIC GELATION

**Maria Valentina Dinu,* Maria Marinela Lazar, Claudiu Augustin Ghiorghita,
Irina Elena Raschip, Ioana Victoria Platon**

Petru Poni Institute of Macromolecular Chemistry, Romanian Academy, Iasi, Romania

**dinu.valentina@icmpp.ro*

1. Introduction

Hydrogels are three-dimensional polymer networks that have attracted significant attention due to their structural similarity to living tissues and their responsiveness to environmental stimuli [1]. These features make them valuable for a wide range of biomedical, environmental, and technological applications [1]. However, conventional hydrogels are often limited by poor mechanical strength and slow responsiveness, which restrict their broader use. To overcome these challenges, hybrid hydrogel architectures and cryotropic gelation strategies have been developed to introduce multifunctionality, mechanical stability, and tailored porosity [2,3]. Cryogenically structured hydrogels, in particular, exhibit unique features such as high elasticity, toughness, rapid water sorption, and interconnected macroporosity that support efficient mass transport without diffusion-related issues [2].

In this lecture will be discussed the development of multifunctional polysaccharide-based hybrid cryogels, with focus on three main categories: (i) interpenetrating polymer networks (IPNs), in which polysaccharides are integrated into synthetic networks to generate mechanically resilient and porous materials; [2,4,5]; (ii) polysaccharide–inorganic filler hybrids, engineered for selective sorption, pollutant removal, and catalytic properties [6-8], and (iii) polysaccharide–plant extract hybrids, where bioactive phytochemicals impart antioxidant, and antimicrobial properties with applications ranging from healthcare to food packaging [9-14].

By combining semi-IPN strategies, cryotropic gelation, and functional biopolymer–filler integration, we demonstrate how porosity can be engineered to yield advanced hybrid hydrogels tailored for applications in medicine, environment, and food systems.

2. Results and discussion

Interpenetrating polymer networks (IPNs)

Semi-IPN cryogels formed by embedding polysaccharides such as dextran, dextran sulfate, and chitosan (CS) into cross-linked polyacrylamide matrices exhibit finely controlled porosity and ultra-fast swelling, making them promising for drug delivery and environmental remediation [2]. More complex hybrid architectures were obtained by introducing triple-cationic systems (CS, polyethyleneimine, and PDMAEMA) reinforced with hydrated iron oxide nanoparticles, achieving remarkable phosphate sorption capacity, and recyclability [4]. Similarly, tricomponent polyelectrolyte complex cryogels combining CS, ionene polycations, and carboxymethylcellulose efficiently removed oxyanions and heavy metal ions while exhibiting complete antibacterial activity against both Gram-positive and Gram-negative bacteria [5].

Polysaccharide–inorganic filler hybrids

Polysaccharide–inorganic filler hybrids, particularly CS-based cryogels, have been also developed as multifunctional platforms for both controlled drug release and environmental remediation. Incorporation of natural zeolite produced hybrid networks with adjustable morphology, swelling behavior, and drug release kinetics, while ion-imprinted cryogels offered highly selective and reusable sorbents for removal of Cu²⁺ ions [6]. Functionalization with aminopolycarboxylic acids further extended the removal spectrum to Pb²⁺, Cd²⁺, Zn²⁺, and Ni²⁺ ions, maintaining efficiency in both batch and continuous column operations, including



real wastewater treatment (Figure 1A,B) [7,8].

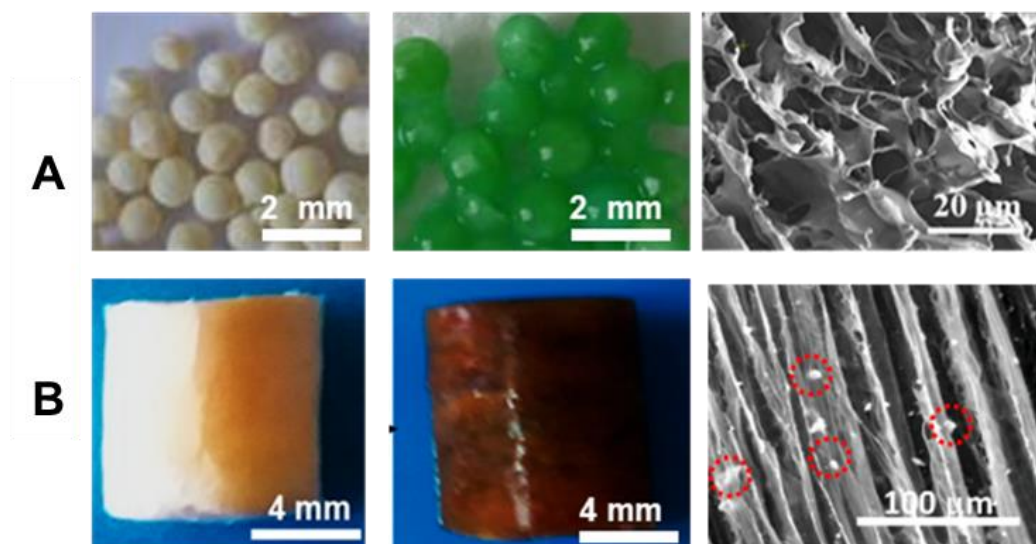


Figure 1. (A) Aminopolycarboxylic acid-functionalized CS-based composite cryogels with heterogeneous morphology, used as beads for selective sorption of Cu^{2+} ions from aqueous solutions; (B) CS-acid-activated zeolite hybrid cryogels with anisotropic pores, employed as monoliths for the simultaneous removal of metal ions from industrial wastewater.

Maximizing resource efficiency and transforming waste into high-value products for new applications represent central principles of circular economy. Thus, thiourea-functionalized CS cryogels, after Cu(II) or Ag(I) uptake were converted into Cu- and Ag-nanoparticle-loaded cryogels, yielding recyclable and highly active catalysts for 4-nitrophenol hydrogenation.

Polysaccharide-plant extract hybrids

Hybrid hydrogels that integrate mechanical stability with antioxidant, antimicrobial, and sensor functionality were also developed by the incorporation of bioactive plant extracts into polysaccharide cryogels. CS/dextrin cryogels loaded with *Thymus vulgaris* essential oil showed a more than fortyfold increase in elasticity compared to neat polysaccharide films, while providing significant antifungal and antioxidant activity [9]. Xanthan/PVA cryogels containing red grape pomace extracts demonstrated polyphenol-mediated pore stabilization, enhanced mechanical performance, and strong bioactivity, supporting applications in food packaging [10]. For healthcare applications, thiourea-CS cryogels enriched with *Hypericum perforatum* extracts exhibited outstanding liquid uptake, mechanical resilience, antioxidant potential, and broad-spectrum antibacterial activity [13]. Most recently, anthocyanin-rich bilberry extracts were incorporated into xanthan-based cryogels, producing ultra-light, highly porous constructs with antimicrobial activity, antioxidant capacity, and pH-responsive color changes [14].

3. Conclusions

Our research demonstrates that the combination of polysaccharides with synthetic polymers, inorganic fillers, or plant-derived bioactive compounds through cryotropic gelation enables the creation of multifunctional hybrid hydrogels with precisely engineered porosity. IPN-based architectures provide resilience and sorption of multiple contaminants; polysaccharide-inorganic hybrids enable both pollutant remediation and catalytic valorization, while polysaccharide-plant extract hybrids bridge biomedical, food, and environmental domains with bioactivity and visual monitoring functions.

Acknowledgements

The authors are grateful for the financial support from project PN-IV-P1-PCE-2023-1968 (4PCE/2025).



References

- [1]. Thakur VK, Thakur MK. Recent trends in hydrogels based on psyllium polysaccharide: a review. *J. Clean Prod.* 82, 1–15, 2014.
- [2]. Dragan ES, Dinu MV. Advances in porous chitosan-based composite hydrogels: Synthesis and applications. *React. Funct. Polym.* 146, 104372, 2020.
- [3]. Behrendt F, Gottschaldt M, Schubert US. Surface functionalized cryogels – characterization methods, recent progress in preparation and application. *Mater. Horiz.* 11, 4600, 2024.
- [4]. Dragan ES, Humelnicu D, Dinu MV. Designing smart triple-network cationic cryogels with outstanding efficiency and selectivity for deep cleaning of phosphate. *Chem. Eng. J.* 426, 131411, 2021.
- [5]. Ghiorghita CA, Humelnicu D, Dinu MV, Ignat M, Bonardd S, Díaz Díaz D, Dragan ES. Polyelectrolyte complex composite cryogels with self-antibacterial properties and wide window for simultaneous removal of multiple contaminants. *Chem. Eng. J.* 459, 141562, 2023.
- [6]. Dinu MV, Dinu IA, Lazar MM, Dragan ES. Chitosan-based ion-imprinted cryo-composites with excellent selectivity for copper ions. *Carbohydr. Polym.* 186, 140–149, 2018.
- [7]. Humelnicu D, Lazar MM, Ignat M, Dinu IA, Dragan ES, Dinu MV. Removal of heavy metal ions from multi-component aqueous solutions by eco-friendly and low-cost composite sorbents with anisotropic pores. *J. Hazard. Mater.* 381, 120980, 2020.
- [8]. Dinu MV, Humelnicu I, Ghiorghita CA, Humelnicu D, Aminopolycarboxylic acids-functionalized chitosan-based composite cryogels as valuable heavy metal ions sorbents: fixed-bed column studies and theoretical analysis. *Gels* 8, 221, 2022.
- [9]. Dinu MV, Gradinaru AC, Lazar MM, Dinu IA, Raschip IE, Ciocarlan N., Aprotosoia AC. Physically cross-linked chitosan/dextrin cryogels entrapping *Thymus vulgaris* essential oil with enhanced mechanical, antioxidant and antifungal properties. 184, 898-908, 2021.
- [10]. Raschip IE, Fifere N, Varganici CD, Dinu MV. Development of antioxidant and antimicrobial xanthan-based cryogels with tuned porous morphology and controlled swelling features. *Int. J. Biol. Macromol.* 156, 608-620, 2020.
- [11]. Dragan ES, Platon IV, Nicolescu A, Dinu MV. Structural, mechanical, antioxidant and antibacterial properties of double cross-linked chitosan cryogels as hosts for thymol. *Int. J. Biol. Macromol.* 304, 140968, 2025.
- [12]. Ghiorghita CA, Platon IV, Lazar MM, Dinu MV, Aprotosoia AC. Trends in polysaccharide-based hydrogels and their role in enhancing the bioavailability and bioactivity of phytochemicals. *Carbohydr. Polym.* 334, 122033-122033, 2024.
- [13]. Platon IV, Ghiorghita CA, Lazar MM, Aprotosoia AC, Gradinaru AC, Nacu I, Verestiuc L, Nicolescu A, Ciocarlan N, Dinu MV. Highly compressible, superabsorbent, and biocompatible hybrid cryogel constructs comprising functionalized chitosan and St. John's Wort extract. *Biomacromolecules* 25, 5081–5097, 2024.
- [14]. Raschip IE, Platon IV, Fifere N, Darie-Nita RN, Aprotosoia AC, Dinu MV. Stabilization of anthocyanins in xanthan-based systems for synergistic cryogels with enhanced physicochemical and biological properties for visual freshness monitoring of Prussian carp (*Carassius gibelio*). *Food Hydrocoll.* 168, 111566, 2025.



REACHING FOR THE STARS WITH NEW GENERATIONS OF FUNCTIONAL
POLYMETHACRYLATESAnna Celny, Paulina Teper, Barbara Mendrek, Agnieszka Kowalczyk**Centre of Polymer and Carbon Materials, Polish Academy of Sciences, Zabrze, Poland***akowalczyk@cmpw-pan.pl***1. Introduction**

In the recent years, significant progress has been achieved in the precise synthesis of star polymers with tailored functional arms and the development of effective strategies for their covalent immobilization on solid substrates enabling their successful application in biomedical field. Concurrently, the development of efficient systems for protecting genetic material from degradation and for delivering nucleic acids to specific targets still remains a major challenge in gene transfection research. While viral vectors have demonstrated promising outcomes, their use is often limited by immunogenic side effects, highlighting the need for safe and less pathogenic synthetic alternatives.

Polycationic polymers have emerged as a promising solution, as their amino groups enable the condensation of DNA or RNA into compact biohybrid structures known as polyplexes. Recent advances in the synthesis and detailed characterization of star-shaped polymers, along with their immobilization onto functional polymer surfaces, have facilitated the creation of star polymer-based vectors for gene therapy. Among these, polycationic star polymers constructed from poly(N,N-dimethylaminoethyl methacrylate) (PDMAEMA) have been the most extensively investigated.

2. Results and discussion

Star-shaped amino-functionalized polymethacrylates were synthesized using modern controlled polymerization techniques, and their solution behavior under varying pH and temperature conditions was systematically investigated to assess their potential biomedical applications. A series of star polymers with a hyperbranched poly(arylene oxindole) core and PDMAEMA arms differing in molar mass and arm length was obtained using atom transfer radical polymerization (ATRP).

Dynamic light scattering measurements revealed that stars existed as single macromolecules in acetone, while small aggregates were observed in aqueous or alcoholic media, with sizes remaining suitable for biomedical use. PDMAEMA stars were found to be pH-sensitive, with higher pH reducing positive charge and decreasing nanostructure size. At pH 13, uncharged stars exhibited thermosensitivity, and phase transition temperatures decreased with increasing arm length.

Obtained polycationic star polymers electrostatically bound negatively charged nucleic acids to form compact polyplexes, enabling safe and efficient genetic material delivery into cells. Polyplexes reached a constant size of approximately 150 nm above N/P = 6. Cryo-TEM imaging showed that stars with shorter arms formed elongated clusters, whereas longer-arm stars produced larger, regular spherical polyplexes. Transfection efficiency, assessed via luciferase activity, correlated with polymer cytotoxicity, and longest-arm stars provided maximal gene expression while maintaining full cell viability [1]. To reduce cytotoxicity, non-ionic di(ethylene glycol) methacrylate (DEGMA) was incorporated into the arms, yielding smaller and less compact polyplexes with significantly reduced cytotoxicity and high gene expression at elevated N/P ratios [2].

Over the past decade, research on nano- and microstructured star polymer layers on solid surfaces has advanced considerably. This progress includes the precise synthesis of star polymers with tailored



functional arms, the development of effective immobilization strategies, comprehensive characterization of the resulting layers, and their successful bioapplication [3].

Therefore, in our further research we obtained the layers composed of poly(oligo(ethylene glycol) methacrylate) (POEGMA) stars which supported fibroblast and HT-1080 cell growth, with noninvasive detachment controlled solely by temperature changes. Detachment from star POEGMA layers occurred faster than from linear brushes [4]. These thermoresponsive layers were subsequently used for deposition of DNA-polymer carriers, enabling polyplex formation and efficient nucleic acid delivery, with transfection efficiency several times higher than controls. Detached transfected cells maintained viability and adherence upon reseeding [4].

Finally, for further development of research on functional polymethacrylates, POEGMA-O star polymers with functionalities of 4 and 12 were grafted onto modified silicon surfaces and silicon-based sensors used for QCM studies. Nanolayers were characterized by ellipsometry, AFM, and contact angle measurements, confirming high homogeneity and increased hydrophilicity with increasing arm number and polymer molar mass. Protein adsorption tests using lysozyme and fibrinogen demonstrated significantly enhanced resistance to nonspecific interactions, particularly for 12-arm polymers, which achieved up to 100% protein removal. These findings highlight the potential of POEGMA-OH star polymers as effective antifouling layers for biomedical and sensor applications.

3. Conclusions

Functional methacrylate-based star polymers provide versatile platforms for biomedical and sensor applications. PDMAEMA stars enabled efficient, safe gene delivery, with DEGMA incorporation reducing cytotoxicity and enhancing transfection. POEGMA star nanolayers exhibited homogeneity, thermoresponsiveness, and strong antifouling properties, improved by higher arm number and molar mass. These findings demonstrate that functional star polymethacrylates, with tunable architecture and chemistry, offer multifunctional nanomaterials for gene therapy, tissue engineering, and antifouling surfaces.

References

- [1]. Mendrek B, Sieroń Ł, Libera M, Smet M, Trzebicka B, Sieroń A, Dworak A, Kowalczyk A. Polycationic star polymers with hyperbranched cores for gene delivery. *Polymer* 55, 4551–4562, 2014.
- [2]. Mendrek B, Sieroń Ł, Żymelka-Miara I, Binkiewicz P, Libera M, Smet M, Trzebicka B, Sieroń A, Kowalczyk A, Dworak A. Non-viral plasmid DNA carriers based on N,N'-dimethylaminoethyl methacrylate and di(ethylene glycol) methyl ether methacrylate star copolymers. *Biomacromolecules* 16, 3275–3285, 2015.
- [3]. Mendrek B, Oleszko-Torbus N, Teper P, Kowalczyk A. Towards next generation polymer surfaces: nano- and microlayers of star macromolecules and their design for applications in biology and medicine. *Prog. Polym. Sci.* 139, 101657, 2023.
- [4]. Mendrek B, Żymelka-Miara I, Sieroń Ł, Fus A, Balin K, Kubacki J, Smet M, Trzebicka B, Sieroń AL, Kowalczyk A. Stable star polymer nanolayers and their thermoresponsiveness as a tool for controlled culture and detachment of fibroblast sheets. *J. Mater. Chem. B* 6, 641–655, 2018.
- [5]. Mendrek B, Fus-Kujawa A, Teper P, Botor M, Kubacki J, Sieroń AL, et al. Star polymer-based nanolayers with immobilized complexes of polycationic stars and DNA for deposition gene delivery and recovery of intact transfected cells. *Int. J. Pharm.* 589, 119823, 1–16, 2020.



FROM TREES TO TECH: THE SILENT REVOLUTION OF CELLULOSE NANOFIBERS IN BIOELECTRONICS

Sergiu Coseri

Petru Poni Institute of Macromolecular Chemistry, Romanian Academy, Iasi, Romania

coseris@icmpp.ro

1. Introduction

The rapid growth of the bioelectronics sector has ushered in a new era of functional devices that seamlessly interface with biological systems. From wearable sensors to implantable neural probes, the demand for flexible, biocompatible, sustainable, and electrically conductive materials has never been greater [1]. Traditional electronic materials, which are often based on rigid synthetic polymers or scarce metals, struggle to meet these requirements, especially with regard to long-term environmental and biomedical compatibility. This has driven the exploration of bio-derived alternatives, with cellulose nanofibers (CNFs) emerging as a promising option [2].

Cellulose is the most abundant biopolymer on Earth [3]. It is a structural component of plant cell walls, and it is naturally renewable, biodegradable, and non-toxic. Through controlled mechanical, enzymatic, or chemical processing, cellulose can be deconstructed into nanoscale fibers with diameters typically below 100 nanometers (nm). These cellulose nanofibers (CNFs) exhibit a unique combination of high mechanical strength, a large surface area, tunable surface chemistry, and optical transparency. These properties position CNFs as versatile building blocks for next-generation bioelectronic devices. CNFs can be processed into flexible films, aerogels, hydrogels, and composite structures, enabling integration into diverse device architectures [4]. In addition to their attractive mechanical and environmental attributes, CNFs offer functionalities that are highly relevant to bioelectronics. Their hydrophilic and porous nature allows them to interact closely with cells, tissues, and ionic environments - a prerequisite for stable bioelectronic interfaces. Moreover, CNFs can be chemically modified. They can also be combined with conductive polymers, nanoparticles, or carbon-based nanomaterials. This combination can impart electronic conductivity. They can do so without compromising their intrinsic sustainability and biocompatibility. Recent advances for wearable sensors, biodegradable electrodes, ion-conducting membranes, and implantable devices have underscored the broad technological potential of CNF-based substrates. The silent revolution of cellulose nanofibers (CNFs) lies in their ability to transform an age-old natural resource into cutting-edge technological solutions. By bridging the gap between biological systems and electronics, CNFs represent a paradigm shift in material design, merging sustainability with performance.

This paper explores the progress, challenges, and future opportunities of CNFs in bioelectronics, emphasizing how this tree-derived material is poised to transform the landscape of sustainable electronic technologies.

2. Experimental

The cellulose sources employed for the preparation of cellulose nanofibers (CNFs) included microcrystalline cellulose (MCC; Avicel PH-101, Sigma-Aldrich, 99% hydrolyzed, crystallinity index (Cr.I.) = 78, degree of polymerization (DP) = 140), cotton linter (CL; microcrystalline cellulose powder, 20 μ m, Sigma-Aldrich, Cr.I. = 86, DP = 465, viscosity = 8.4 cPs), eucalyptus pulp (EYPT; commercial bleached eucalyptus cellulose, Sodra Company, Sweden, Cr.I. = 52, DP = 2742, viscosity = 865 dm³/kg), and α -cellulose (α -CEL; powder, Sigma-Aldrich, purity 95%, Cr.I. = 68, DP = 950). The reagents used for TEMPO-mediated oxidation included 2,2,6,6-tetramethylpiperidine-1-oxyl (TEMPO; Sigma-Aldrich), sodium bromide (NaBr; Sigma-Aldrich), and an 8% sodium hypochlorite solution (NaClO; Chemical



Company). All chemicals and solvents were utilized as received, without further purification. To fabricate the highly stretchable, self-healing, and conductive hydrogel, 4-(bromomethyl)phenylboronic acid (PBA) and 1-vinylimidazole were sourced from Sigma-Aldrich and applied directly without additional purification. Ethyl acetate, acrylamide (AM), N,N'-methylene bisacrylamide (MBA, 97%), ammonium persulfate (APS, 99.5%), and N,N,N',N'-tetramethylethylenediamine (TEMED, $\geq 99.5\%$) were obtained from Shanghai Aladdin Biochemical Technology Co., Ltd.

3. Results and discussion

The scientific literature contains a wide variety of experimental approaches that report the production of nanoscale cellulose derivatives, including nanocrystalline and nanofibrillated cellulose, using sources that are exotic in some areas of the world but common in others. Among these categories of natural materials, non-agricultural sources play a special role (Figure 1). These sources include tunicates and red algae, as well as agricultural sources such as spinifex grass, miscanthus, coconut coir, and pineapple leaves. To eliminate problems related to immense source variability and ensure better data reproducibility, we opted to use commercial cellulose sources available to anyone, which provide predictable results.

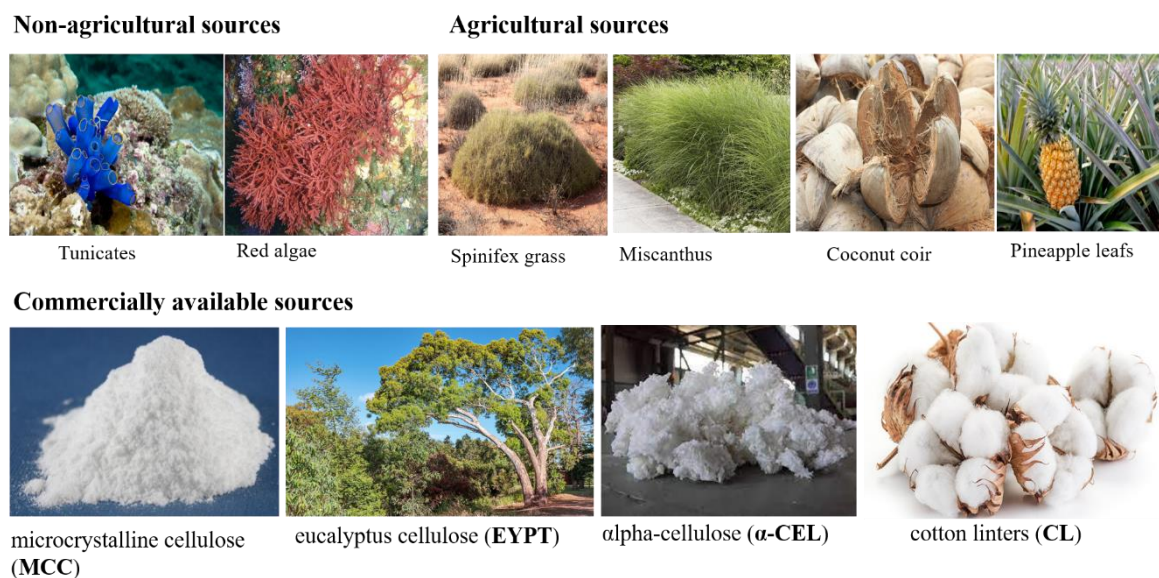


Figure 1. The different cellulose sources used in the preparation of fibrillated nanocellulose, including non-agricultural sources, agriculturally derived sources, *versus* commercially available sources.

Through the use of pretreatment processes followed by chemical oxidation using the TEMPO-NaBr- NaClO_4 system, the nanofibrillated cellulose fractions could be isolated from each of the starting materials, each with their own particular morphological and structural characteristics. By incorporating cellulose nanofibers (CNFs) into a system containing acrylic monomers and tailor-made ionic liquids, a robust cross-linked hydrogel network can be constructed. The structural integrity and multifunctionality of the hydrogel arise from the integration of multiple crosslinking mechanisms, including dynamic covalent boronic ester bonds, noncovalent interactions (hydrogen bonding and electrostatic forces), and chain entanglements within the interpenetrating CNF-based polymer networks. This synergistic combination provides an optimal balance between mechanical performance and multifunctional properties.

Furthermore, the coexistence of conductive ionic liquids and negatively charged surface carboxylate groups on CNFs facilitates ion transport by establishing efficient conductive pathways. Owing to its homogeneous microstructure, the hydrogel exhibits high optical transmittance ($>95\%$), which is critical for optical signal accessibility. Leveraging these features, the tailor-made ionic liquid serves not only as a structural



component but also as a functional element for constructing high-performance ionic conductive hydrogels (ICHs). The resulting ICH-based sensors demonstrate reliable, sensitive, and stable monitoring of human motion. Overall, this study highlights a versatile design strategy for developing next-generation intelligent sensors and electronic skins.

4. Conclusions

One objective of this study was to optimize the isolation of carbon nanofibers (CNFs) from four commercially available cellulose sources by integrating TEMPO-mediated selective oxidation with alkaline–acid and ultrasonic pretreatments, and to elucidate how the structural characteristics of the resulting CNFs influence their self-assembly behavior. Our results demonstrate that the dimensions, morphologies, and surface carboxyl group densities of the CNFs are strongly dependent on the cellulose precursor.

A second objective was to incorporate CNFs into hydrogel-like architectures using ionic liquids functionalized with boron-containing moieties, thereby imparting enhanced functionality and structural versatility. The resulting hydrogels exhibited outstanding electrical and mechanical performance, including ultra-high extensibility, elevated tensile strength, pronounced viscoelasticity, intrinsic self-healing capability, and reversible adhesion. Furthermore, experimental investigations revealed that the synergistic combination of these features enables the fabrication of ionically conductive hydrogels that function as highly sensitive, stable, and reproducible wearable sensors capable of detecting and discriminating diverse human motions in real time.

Acknowledgements

This work was supported by a grant of the Ministry of Research, Innovation and Digitization, CNCS-UEFISCDI, project number PN-IV-P1-PCE-2023-0558, within PNCDI IV.

References

- [1]. Yao X, Zhang S, Wei N, Qian L, Coseri S. Cellulose-based conductive hydrogels for emerging intelligent sensors, *Adv. Fiber Mater.*, 6, 1256–1305, 2024.
- [2]. Yao X, Zhang S, Qian L, Wei N, Nica V, Coseri S, Han F. Super stretchable, self-healing, adhesive ionic conductive hydrogels based on tailor-made ionic liquid for high-performance strain sensors. *Adv. Funct. Mater.*, 32, 2204565, 2022.
- [3]. Biliuta G, Coseri S. Cellulose: a ubiquitous platform for ecofriendly metal nanoparticles preparation. *Coord. Chem. Rev.*, 383, 155–173, 2019.
- [4]. Biliuta G, Dascalu A, Stoica I, Baron RI, Bejan D, Bercea M, Coseri S. Structural and rheological insights of oxidized cellulose nanofibers in aqueous suspensions. *Wood Sci. Technol.*, 57, 1443–1465, 2023.



RETRACTION OF VISCOELASTIC FLUID AFTER THE RUPTURE OF THE FILAMENT

Ciprian Mateescu,^{1,2} Doru-Daniel Cristea,^{1,2} Nicoleta Tanase,² Corneliu Balan^{2*}

¹Carol Davila University of Medicine and Pharmacy, Bucharest, Romania

²Politehnica National University of Science and Technology, Energetics, Bucharest, Romania

*corneliu.balan@upb.ro

1. Introduction

The aim of the paper is to investigate the retraction of viscoelastic surface which remains attached to the plates of a rheometer after the rupture of the filament. The breakup of fluids filament was intensively treated in literature in the past decades, mainly in relation to measurements of extensional viscosity and elasto-capillarity [1,2], slender filament retraction, breakup of fluid jets and droplets formation [2-4]. The present experimental study is focused to the analysis of free surface topology of a viscoelastic fluid during the post pinch-off dynamic in a CaBER like configuration [2].

2. Experimental

The liquid sample used in experiments is a viscoelastic oil based on a petroleum compound (density $\rho = 950 \text{ kg/m}^3$, surface tension $\gamma = 0.034 \text{ N/m}$) (Figure 1).

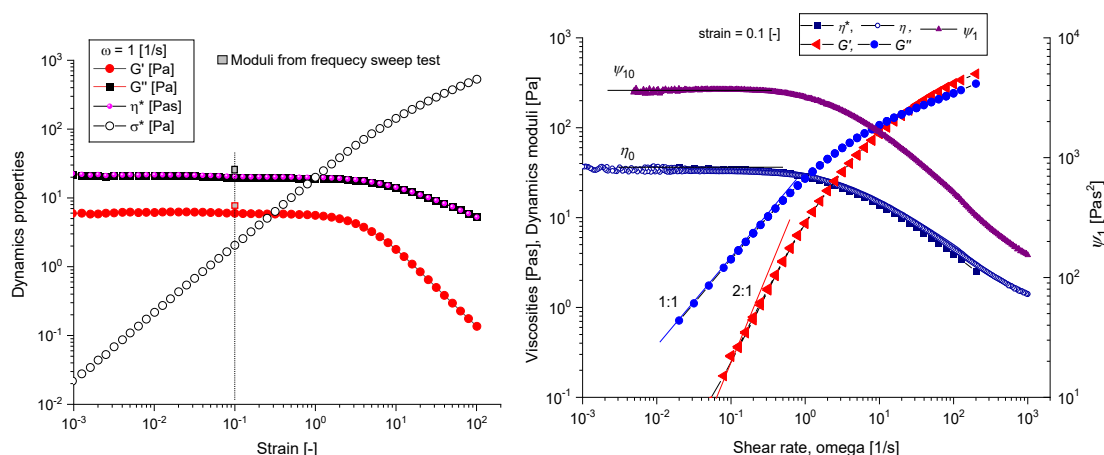


Figure 1. Rheological characterization of the viscoelastic sample in strain/ ω -frequency sweeps and shear rate ramp (G' elastic modulus, G'' viscous modulus, η^* complex viscosity, σ^* complex shear stress, η shear viscosity, ψ_1 first normal stress coefficient). The fluid sample discloses shear thinning and well defined zero viscosity and zero first normal stress difference.

The sample fills the gap of 1 mm between the plates of MCR 301 Anton Paar rheometer before the mobile plate (40 mm diameter) is lifted at height 100 mm from the fix plate. The fluid attached at the upper plate starts to retract after the rupture of the filament due to the action of adhesion, capillary and elastic forces against gravity, Figure 2. The high-speed cameras used for image acquisition of the interface dynamics are Phantom VEO-E 340L (1024×1024 pixels at 2800 fps) and FASTCAM mini-UX100 (1280×1024 pixels at 4000 fps), equipped with different optic devices and lighting setups. Series of images are extracted from the movies and the interface profiles liquid-air are obtained using a special code implemented in the commercial ImageJ and MATLAB software (Figure 2.b and Figure 3).

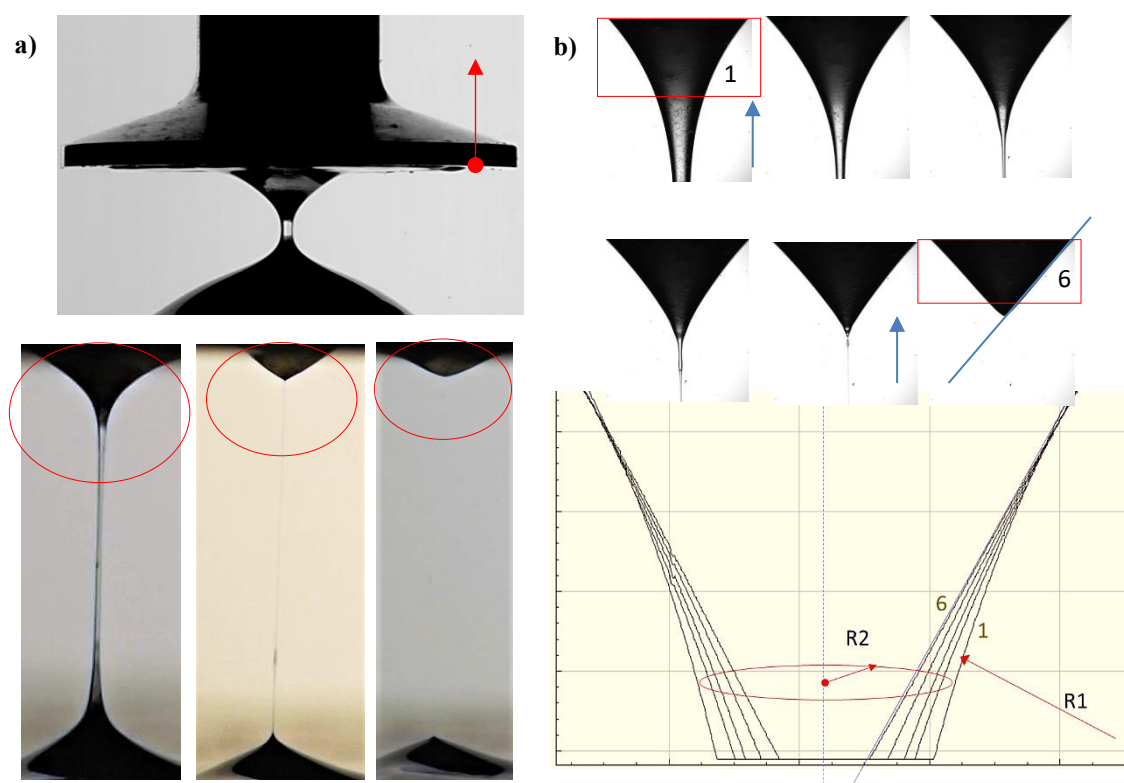


Figure 2. (a) CaBER like configuration (plate-plate rheometer), evolution of the filament between the two plates at rest; (b) details in vicinity of the upper plate at rest; interface profiles attached on the upper plate (configurations 1 → 6) during the thinning of the filament until its rupture (6).

3. Results and discussion

An axial-symmetric surface in space is characterized by two radii of curvature, their change in time being the only geometrical quantities which define the surface/interface kinematics, [5]. The first radius R_1 defines the lateral surface of the interface and the second radius R_2 is almost identical (for slow motions) with half diameter of the liquid body, (Figure 2.b, Figure 3).

Following the idea that pinch-off and rupture of liquid filaments disclose some universal characteristics, independently of the liquid properties [4], we observe that at the moment of filament rupture the fluid domain which remains attached at the upper plate is described by a conical surface, i.e. $R_1 \rightarrow \infty$ and R_2 has a smooth increasing from $R_2 = 0$ at the cone tip (where the rupture takes place) to maximum value at the plate. Before rupture the liquid surface is concave and during the first part of retraction (after rupture) discloses an inflexion point, at the end the surface being convex (Figure 3). We remarked that change of interface curvature for all tested liquid samples (not shown in this paper), so $R_1 \rightarrow \infty$ might be a general characteristic for this type of configuration which indicates the onset of retraction after rupture time of the filament (the liquid bridge between the two plates). We also observed that liquid retraction follows in time an exponential decay of the tip distance from the plate, $h(t) \sim e^{-t/\lambda}$, $\lambda = 0.92$ s, Figure 3.b. This means that retraction velocity of the surface after pinch-off is proportional to the film height attached at the solid surface, i.e. $\dot{h}(t) \sim h(t)$, the dynamics being defined by the relaxation time τ . The phenomenon is different on the lower plate, since gravity and adhesion fluid-solid force have the same direction. One remarks that retraction is dominated by interfacial forces (capillarity and elasticity), on both plates the friction force due viscosity is acting against inertia.

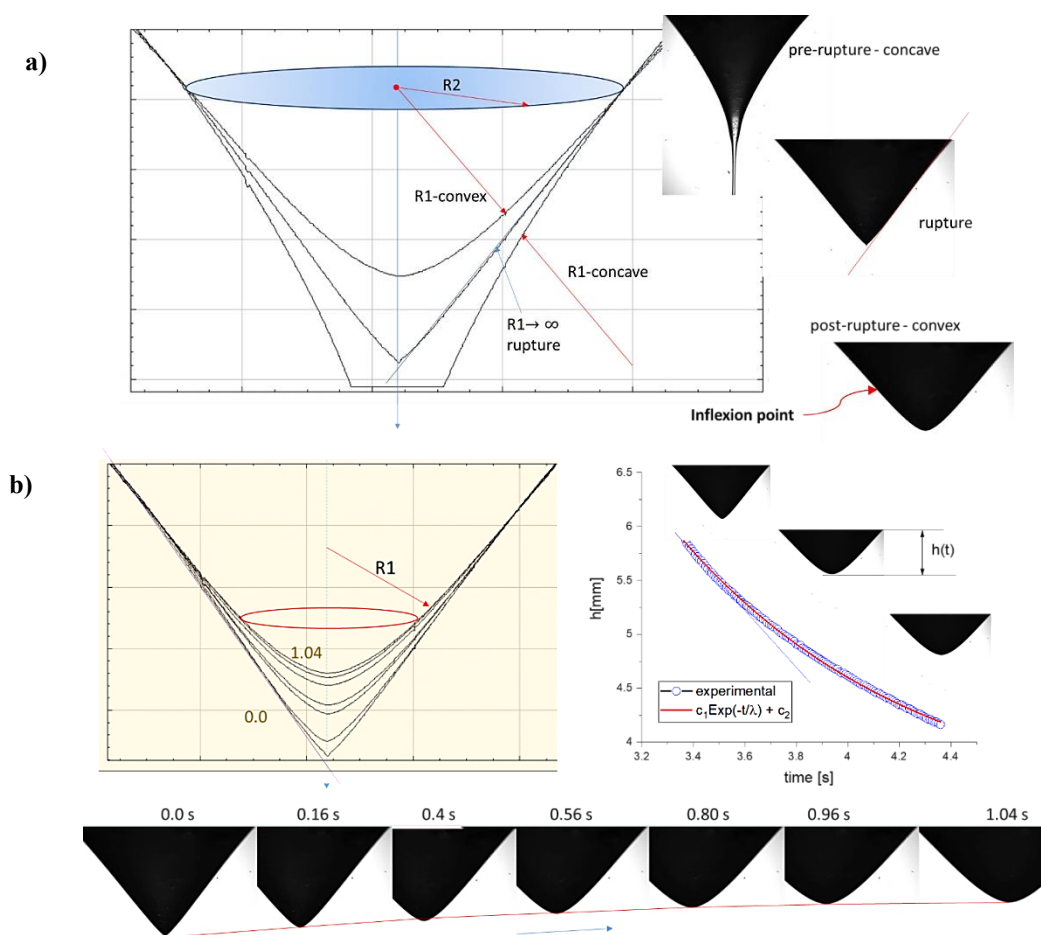


Figure 3. (a) Variation of the interface profile in vicinity of the filament rupture;
(b) retraction of viscoelastic samples after the rupture of the filament.

4. Conclusions

The evolution of viscoelastic interface in an extensional dynamic process can be divided in two stages: (i) formation of the filament, (ii) rupture of the filament followed by fluid retraction and generation of droplets. This work investigates the second stage of dynamics, i.e. the retraction of the viscoelastic fluid in the vicinity of the rheometer plate after its lifting. The profile of the interface is analyzed using an adapted image processing method and the variation of the maximum fluid thickness is recorded, which discloses an exponential decay curve characterized by a particular relaxation time. The study will be future applied to characterize and test the gel samples used in the 3D printing, where retraction of the fluid interface plays a major role the quality control of the printed object.

References

- [1]. Anna SL, McKinley GH. Elasto-capillary thinning and breakup of model elastic liquids. *J. Rheol.* 45, 115–138, 2001.
- [2]. Mckinley GH, Sridhar T. Filament-stretching rheometry of complex fluids, *Annu. Rev. Fluid Mech.* 34, 375–415, 2002.
- [3]. Sen U, Datt C, Segers T, Wijshoff, Snoeijer JH, Versluis, Lohse D. The retraction of jetted slender viscoelastic liquid filaments. *J. Fluid Mech.* 929, A25, 2021.
- [4]. Eggers J. Universal pinching of 3D axisymmetric free-surface flow. *Phys. Rev. Lett.* 71(21), 3458–3460, 1993
- [5]. Bran A, Balan C. Fluid rheology prediction using interface detection and machine learning regression. *Phys. Fluids* 37, 033114, 2025.

SUPRAMOLECULAR ORGANIC SEMICONDUCTING MATERIALS
FOR BIO-ELECTRONICSAurica Farcas,* Ana-Maria Resmerita*Petru Poni Institute of Macromolecular Chemistry, Romanian Academy, Iasi, Romania*

*afarcas@icmpp.ro

1. Introduction

The great interest in organic semiconducting materials (OSMs), which is mostly based on π -conjugated small molecules or polymers, is motivated by reason of their tunable physicochemical and semiconducting properties [1]. Despite the enormous interest in OSMs materials, many aspects remain poorly understood, especially their strong tendency to aggregate, which affect the photoluminescence efficiency, electrical transport, and their environmental stability, which considerably limit their applications [2]. In this regard, control of intermolecular interactions increased attention as an important factor for the exploitation of OSMs. In the past decade, the field of polymer science has witnessed remarkable innovations and progress, alongside major advances in the complementary field of supramolecular science, which offer great opportunity for new concepts, new materials with unique properties and novel practical applications. Among the wide range of possibilities, the construction of mechanically interlocked assemblies such as conjugated polypseudorotaxane (PPs) or polyrotaxane (PRs) architectures provides an alternative to the modification of the polymer backbone with substituents. PPs and PRs are a class of supramolecular compounds consisting of macrocycles (hosts) threaded over conjugated monomers/oligomers or polymers cores (guests) through non-covalent interactions. A wide variety of host molecules have the ability to encapsulate the conjugated backbones into their cavities based on intermolecular interactions, thus leading to thermodynamically unstable inclusion complexes (ICs). Native cyclodextrins (CDs) are by far the most intensively investigated host molecules in the synthesis of such supramolecular architectures. The second investigated groups of host molecules are composed of chemically modified CDs, such as partially randomly methylated β -CD (RM- β -CD) or fully modified derivatives 2,3,6-tri-*O*-methyl CD (TM-CD) and 2,3,6-tri-*O*-trimethylsilyl CD (TMS-CD) [3-7]. Through chemical modification, the hydrophilic character of native CDs decreases, while the binding ability for hydrophobic guest molecules increases. Despite the great effort devoted to CDs-based PPs or PR architectures, less attention has been paid to cucurbiturils (CBs) as host molecules. Due to their hydrophobic cavities and two hydrophilic carbonylated rims, CBs are a new family of host molecules, able to complex neutral insulated/conjugated guests by hydrophobic interactions similar to those of CDs. According to their characteristic molecular structure (electron-deficient cavity, no bonds, or lone pairs inside), CBs have a good capability to bind various π -conjugated monomers, oligomers, or polymers to form longer supramolecular assemblies even individual molecular wires [8-11]. The incorporation of non-covalent interactions in the construction of supramolecular architectures has an impact on the behavior of OSMs backbones and subsequently generates smart polymeric functional materials.

Herein, we continue to provide extensive insights into the effect of macrocyclic encapsulations using different host molecules on the photophysical, surface morphology, wetting properties, as well as film forming ability of conjugated polyazomethines (PAMs), polythiophenes (PTs), polyfluorenes (PFs) homo- or copolymers and poly(3,4-ethylenedioxythiophene) (PEDOT). For the sake of comparison, the photophysical properties of these supramolecular OSMs will be compared with those of their non-threaded homologs. The unique photophysical characteristics of these newly developed supramolecular architectures, together with ready synthetic routes, are contributing forces to their applications in bioelectronics.



2. Experimental

The synthesis of PPs and PRs architectures were performed according to previously reported procedures [3-11].

3. Results and discussion

The synthesis of such supramolecular structures is based on the molecular recognition principle and is the result of the cooperation of various non-covalent interactions. The first step in the preparation of PRs structures is the threading of macrocyclic compounds (hosts) onto linear chains (guests) when thermodynamically unstable ICs or pseudorotaxanes are obtained. To avoid dethreading in the second step, a blocking reaction of both ends of the guest molecule with bulky groups (also known as stoppers) is required. The presence of macrocycles suppresses intermolecular interactions and effectively inhibits interstrand interactions by increasing separation distances between the conjugated backbones. The electronic properties of such supramolecular materials are strongly affected by the chemical nature of the surrounding encapsulated segments.

This presentation summarizes our recent endeavors, related on the design, synthesis, properties, and the Langmuir monolayer formations at the air-water interface of PAMs, PTs, PFs homo- or copolymers, and PEDOT (Figure 1).

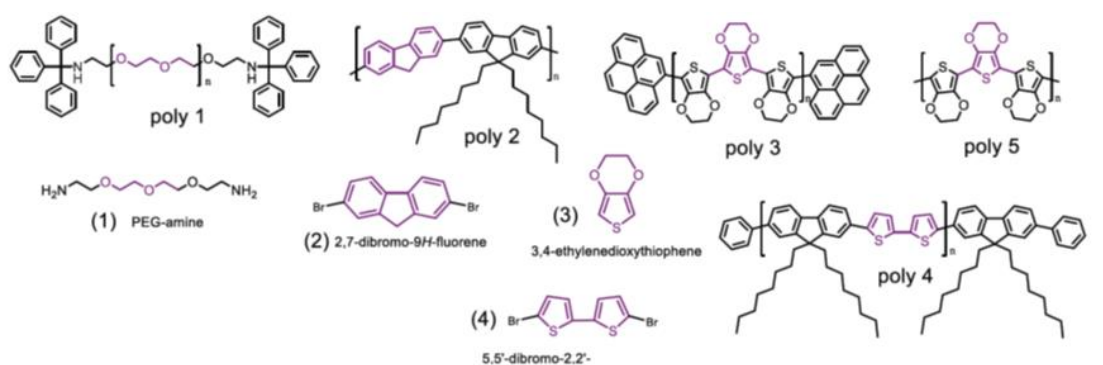


Figure 1. Chemical structures of OSMs used for the synthesis of PRs.

In addition, an overview of the ICs synthesis using CDs and their lipophilic derivatives as well CB7 will be considered. For the sake of comparison, the photophysical properties of these supramolecular compounds will be compared to those of their non-threaded homologs. The supramolecular OSMs materials were under widespread investigation as active components in photovoltaic and as hole-transporting layers in *p-n* hybrid diode. In addition, Nanopore resistive pulse-sensing technique and computational modeling demonstrate the strong interactions of the PEDOT PPs with a biological aerolysin nanopore. This approach could provide an unexpected opportunity to develop new classes of biomimetic ionic channels useful for broad applications in the field of nanobiotechnology

4. Conclusions

The study demonstrated that the supramolecular encapsulation of OSMs backbones is effective in preventing aggregation and hindering fluorescence quenching, even when only a small fraction of the conjugated backbone is encapsulated. These findings offer tremendous opportunities for extending the understanding of the factors, which control the charge transport within and between encapsulated conjugated SMPs chains that is relevant for the application in organic electronics. In addition, these supramolecular compounds exhibit a crucial importance for further development of OSMs and represent a key bottom-up strategy to build and process relatively soft functional materials providing clear information about improvements of photophysical and transport properties relevant to applications in bioelectronics.

Acknowledgements

This work was supported by a grant of the Ministry of Research, Innovation and Digitization, CNCS – UEFISCDI, project number PN-IV-P1-PCE-2023-0300.

References

- [1]. Berggren M, Crispin X, Fabiano S, Jonsson MP, Simon DT, Stavrinidou E, Tybrandt K, Zozoulenko I. Organic electrochemical devices: Ion electron-coupled functionality in materials and devices based on conjugated polymers. *Adv. Mater.* 31, 1805813, 2019.
- [2]. Noriega R, Rivnay J, Vandewal K, Koch FPV, Stingelin N, Smith P, Toney MF, Salleo A. A general relationship between disorder, aggregation and charge transport in conjugated polymers. *Nat. Mater.* 12, 1038–1044, 2013.
- [3]. Farcas A, Tregnago G, Resmerita AM, Dehkordi ST, Cantin S, Goubard F, Aubert PH, Cacialli F. Effect of permethylated β -cyclodextrin on the photophysical properties of poly[2,7-(9,9-dioctylfluorene)-alt-(5,5'-bithiophene)] main chain polyrotaxanes. *J. Polym. Sci. A Polym. Chem.* 52, 460–471, 2014.
- [4]. Farcas A, Resmerita AM, Aubert PH, Ghosh I, Cantin S, Nau WM. Synthesis, photophysical, and morphological properties of azomethine-persilylated α -cyclodextrin main-chain polyrotaxane. *Macromol. Chem. Phys.* 216, 662–670, 2015.
- [5]. Putnin T, Lec H, Bui T-T, Jakmunee J, Ounnunkad K, Peralta S, Aubert PH, Goubard F, Farcas A. Poly(3,4-ethylenedioxythiophene/permethylated β -cyclodextrin) polypseudorotaxane and polyrotaxane: synthesis, characterization and application as hole transporting materials in perovskite solar cells. *Eur. Polym. J.* 105, 250–256, 2018.
- [6]. Farcas A, Liu Y-C, Nilam M, Balan-Porcarasu M, Ursu EL, Nau WM, Hennig A. Synthesis and photophysical properties of inclusion complexes between conjugated polyazomethines with γ -cyclodextrin and its tris-O methylated derivative. *Eur. Polym. J.* 113, 236–243, 2019.
- [7]. El Haitami A, Resmerita AM, Ursu LE, Asandulesa M, Cantin S, Farcas A. Novel insight into the photophysical properties and 2D supramolecular organization of poly(3,4-ethylenedioxythiophene)/permethylated cyclodextrins polyrotaxanes at the air water interface. *Materials* 16, 4447, 2023.
- [8]. Farcas A, Aubert P-H, Mohanty J, Lazar AI, Cantin S, Nau W.M. Molecular wire formation from poly[2,7(9,9-dioctylfluorene)-alt-(5,5'-bithiophene/cucurbit[7]uril)] polyrotaxane copolymer. *Eur. Polym. J.* 62, 124-129, 2015.
- [9]. Farcas A, Assaf KI, Resmerita AM, Sacarescu L, Asandulesa M, Aubert PH, Nau WM. Cucurbit[7]uril-threaded poly(3,4-ethylenedioxythiophene): a novel processable conjugated polyrotaxane. *Eur. J. Org. Chem.* 2019, 3442–3450, 2019.
- [10]. Farcas A, Damoc M, Asandulesa M, Aubert PH, Tigoianu RI, Ursu EL. The straightforward approach of tuning the photoluminescence and electrical properties of encapsulated PEDOT end-capped by pyrene. *J. Mol. Liq.* 376, 121461, 2023.
- [11]. Farcas A, Ouldali H, Cojocar C, Pastoriza-Gallego M, Resmerita AM, Oukhaled A. Structural characteristics and the label-free detection of poly(3,4-ethylenedioxythiophene/cucurbit[7]uril) pseudorotaxane at single molecule level. *Nano Res.* 16, 2728–2737, 2022.



MAKING LINEAR CIRCULAR: FROM CELLULOSE/LIGNIN TO BIOPLASTICS, BIO-H₂ AND AROMATICS

Xiaoyan Ji,¹ Leon Engelbrecht,² Yonglei Wang,³ Francesca Mocci,²
Narcis Cibotariu,⁴ Aatto Laaksonen^{5*}

¹Division of Energy Science, Energy Engineering, Luleå University of Technology, Luleå, Sweden

²Department of Chemical and Geological Sciences, University of Cagliari, Monserrato, Italy

³National Supercomputing Center (NSC), Linköping University, Linköping, Sweden

⁴Petru Poni Institute of Macromolecular Chemistry, Romanian Academy, Iasi, Romania

⁵Department of Chemistry, Stockholm University, Stockholm, Sweden

*aatto@su.se

1. Introduction

Global petroleum-based plastic production exceeds 400 million metric tons per year, with less than 10% recycled. The rest of it piles up on land and floats in the oceans. Gradually it becomes fragmented by radiation from Sun to tiny particles, microplastics, now also found in the human food chain, ultimately entering living cells. It is estimated that ~200,000 particles per person are ingested per year, with still not known effects to our health [1,2]. All of this is result from our linear short-sighted “take–make–waste” way of using the resources. A credible alternative can be developed via circular bioeconomy, where materials remain in biological or technical cycles, starting with renewable biomass and lignocellulose and ending with a model, based on either safe biodegradation or high-quality recycling. In this talk we suggest pathways along circular lines for turning forest and agricultural residues into bioplastics, bio-hydrogen, and high-value aromatic chemicals.

Lignocellulosic biomass is our most abundant renewable carbon source. It does not compete with food when residues such as straw, stover, sawdust and bark are used as raw material. However, there is a catch to use it. It is a material Nature made very robust for reasons. At the molecular level, the linear glucose chains of *cellulose* provide fibrous strength while *hemicellulose* fills the voids and links the chains to make it even stronger. *Lignin*, a cross-linked aromatic network, acts as a hydrophobic rigid matrix [3]. Making use this tough composite material requires a separation of these tightly bound components, followed by upgrading each fraction into products.

In this Lecture we will use ionic liquids (IL) and deep eutectic solvents (DES) in valorizing cellulose into plastics and lignin into aromatic chemicals and energy carriers [4-6]. They are selective, low-volatile, recyclable media, that can loosen crystalline cellulose structure and disrupt the hydrogen-bond networks in it. ILs/DESs can also dissolve hemicellulose and dissolve and solvate lignin's aromatics. They allow ionothermal routes to form/reform materials (e.g., casting or spinning regenerated cellulose films and fibers) under much milder conditions than used in common pulping or petrochemical pathways. Natural DES (NADES), mixtures such as choline chloride + lactic/ levulinic acid are especially promising, offering tunable viscosity and conductivity (important to electrochemistry).

2. Workflow

ISs and DESs are molecularly the most complicated systems, with all types of inter/intramolecular interactions in concert. In comparison to normal liquids their structure and dynamics are highly heterogeneous giving rise to long-range correlations. [3]. They have a key role in this project, as the interactions can be tuned for our purposes. For this we use molecular modelling [3]. For example, we can see that in modelling how imidazolium cations of ILs hydrogen-bond to lignin oxygens while acetate-type anions coordinate to phenolic hydrogens. This explains why the chemistry behind IL/NADES is effective



for lignin dissolution and β -O-4 bond activation. Calculations enable *in-silico* screening and optimization of solvent candidates, prior to laboratory work. The very same IL solvent families can be used *first* to fractionate biomass and *later* they can serve as electrolytes and as reaction media for selective lignin depolymerization. This will greatly simplify the process operations and solvent cycles, as exemplified by sub-projects (A), (B) and (C) below:

(A)romatics from lignin. Lignin can be used as a source of valuable aromatics, rather than waste it as a boiler fuel (as is done regularly in pulp/paper mills). By dissolving/activating lignin in ionic liquids (ILs) or natural deep eutectic solvents (NADES), the dominant β -O-4 linkages can be selectively cleaved to yield monomeric aromatics (e.g., guaiacol, vanillin, syringol) under mild, recyclable conditions. Molecular modelling guides which ion pairs maximize H-bonding to phenolic sites and thus promote dissolution and depolymerization; NADES (e.g., choline chloride + lactic/levulinic acid) offer a complementary, low-volatility platform for delignification and lignin valorization [7].

(B)io-hydrogen co-production. By replacing the energy-intensive oxygen evolution step in water electrolysis by oxidizing lignin at the anode in IL/NADES electrolytes lowers the energy barrier for H₂ generation and yields valuable co-products. The anode generates H⁺/e⁻ from lignin oxidation and produces value-added chemicals, while the cathode combines them to form H₂, thus co-producing hydrogen and aromatics at lower electrical cost per kg H₂. The electrolytes are designed with high lignin solubility, low viscosity, wide potential window and good conductivity. A membrane-separated H-cell is used, letting ions go through while keeping products apart, and the electrodes are graphite felt (or Ni plates). The catalysts are earth-abundant metals (Fe, Co or Ni) [7].

(C)ellulose-based bioplastics. Ionothermal processing and/or minor chemical modification enable regenerated cellulose films and fibers that preserve biodegradability while achieving plastic-like formability. It is possible to create thermoplastic and biodegradable plastics from cellulose by combining (i) chemical modification (e.g., ring-opening to dialcohol cellulose) to lower the glass transition temperature T_g and increase chain mobility, (ii) bio-compatible plasticizers (e.g., glycerol, sorbitol) to weaken inter-chain H-bonding, (iii) use lignin as a natural binder in biocomposites [8], and (iv) ionothermal processing in IL/DES that dissolve/disperse cellulose and enable regeneration of films/fibres under mild, recyclable conditions. ILs can dissolve cellulose by breaking inter/intra-chain H-bond networks (basic anions; aromatic cations) and that IL-water mixtures reduce viscosity while retaining solvency. MD simulations can be used to predict glass transition temperature T_g from variation of density, expansion coefficient, heat capacity and diffusion and reveal H-bond disruption, free-volume gains after ring-opening, and plasticizer migration.

3. Conclusions

In this project we start with forest/agricultural residues to produce aromatics, bio-hydrogen, and bioplastics, by using ionic liquids (ILs) and natural deep eutectic solvents (NADES) as the common, recyclable processing medium. With ILs/NADES we can fractionate lignocellulose, dissolving/activating lignin for selective depolymerization into valuable aromatic molecules, while leaving cellulose accessible. The same solvent family can further serve as an electrolyte/solvent for anodic oxidation of lignin-derived phenolics, which upgrades them to precious chemicals while the cathode co-produces H₂. Further, cellulose can be regenerated or modified to yield biodegradable thermoplastic materials. Molecular modelling is used for screening ions and mixtures for dissolution power and viscosity, mapping H-bond networks and β -O-4 reactivity to maximize aromatic yields, optimizing electrolyte windows for H₂ co-production, and predicting T_g/chain mobility for cellulose formulations. We present an integrated, closed-loop biorefinery concept where one feedstock and one solvent toolbox deliver high-value aromatics, clean hydrogen, and compostable plastics, with a solvent recovery at every step. Molecular modelling is of utmost importance in the project!



Acknowledgements

This work is supported by Kempe Foundations and European Union's Horizon Europe Research and Innovation Programme under grant agreement No 101086667. project BioMat4CAST "Petru Poni" Institute of Macromolecular Chemistry Multi-Scale in Silico Laboratory for Complex and Smart Biomaterials.

References

- [1]. Plastics - European Environment Agency. <https://www.eea.europa.eu/en/topics/in-depth/plastics>. Accessed 27 November 2024.
- [2]. Cox KD, Cloverton GA, Davies HL, Dower JF, Juanes F, Dudas SE. Human consumption of microplastics. *Environ. Sci. Technol.*, 53(12), 7068–70, 2019.
- [3]. Ciesielski PN, Pecha MB, Lattanzi AM, Bharadwaj VS, Crowley MF, Bu L, Vermaas JV, Steirer KX, Crowley MF. Advances in multiscale modeling of lignocellulosic biomass. *ACS Sustainable Chem. Eng.* 8, 3512–3531, 2020.
- [4]. Ma C, Laaksonen A, Liu C, Lu X, Ji X. The peculiar effect of water on ionic liquids and deep eutectic solvents. *Chem. Soc. Rev.* 47 (23), 8685–8720, 2018.
- [5]. Wang YL, Li B, Sarman S, Mocci F, Lu ZY, Yuan J, Laaksonen A, Fayer MD. Microstructural and dynamical heterogeneities in ionic liquids. *Chem. Rev.* 120 (13), 5798–5877, 2022.
- [6]. de Villiers Engelbrecht L, Cibotariu N, Ji X, Laaksonen A, Mocci F. Deep eutectic solvents meet non-aqueous cosolvents: a modeling and simulation perspective — a tutorial review. *J. Chem. Eng. Data* 70 (1), 19–43, 2024.
- [7]. Ali A, Huang G, Zhu J, Laaksonen A, Ji X. Selective electrocatalytic oxidation of phenol to benzoquinone via water splitting using a nonprecious metal-based electrocatalyst. *Adv. Energy Sustainability Res.*, 2500108, 2025.
- [8]. Elf P, Larsson PA, Larsson A, Wågberg L, Hedenqvist MS, Nilsson F. Effects of ring opening and chemical modification on the properties of dry and moist cellulose predictions with MD simulations, *Biomacromolecules* 25 (12), 7581–7593, 2024.



ENGINEERING POLY(2-OXAZOLINE) NANOSTRUCTURES
FOR BIOMEDICAL USE

**Marcelina Bochenek,^{1*} Natalia Oleszko-Torbus,¹ Barbara Mendrek,¹ Alicja Utrata-Wesolek,¹
Wojciech Walach,¹ Violeta Mitova,² Neli Koseva,³ Agnieszka Kowalczyk¹**

¹Centre of Polymer and Carbon Materials, Polish Academy of Sciences, Zabrze, Poland

²Institute of Polymers, Bulgarian Academy of Sciences, Sofia, Bulgaria

³Bulgarian Academy of Sciences, Sofia, Bulgaria

*mbochenek@cmpw-pan.pl

1. Introduction

One of the key challenges in modern medicine and biotechnology is the design of “tailor-made” polymers with precisely defined molar masses and functional groups or bioactive compounds into their structure. One class of such polymers are poly(2-oxazoline)s ((POx)s), analogues of pseudopeptides, which are known for their excellent biocompatibility and wide modification versatility.

Poly(2-oxazoline)s have been known for over 50 years, first reported in the late 1960s by four independent research groups [1–4]. They are synthesized *via* cationic ring opening polymerization (CROP) of five membered cyclic imino ethers containing a double bond at second position (Figure 1) [5]. The living character of this polymerization allows for precise control over poly(2-oxazoline)s molar mass and dispersity what is extremely important in the engineering of polymers with well-defined structures, especially for biomedical applications.

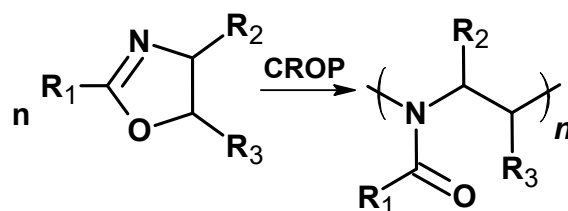


Figure 1. Scheme of cationic ring opening polymerization of 2-oxazoline.

The chemical structure of (POx)s and thus their properties can be tailored in a controlled way. The appropriate selection of an initiator and/or terminating agent enables the synthesis of (co)polymers with functional α - and ω - groups [6,7]. There is an enormous variety of 2-oxazoline monomers with different R1 substituents, ranging from alkyl (linear, branched, or cyclic) or aryl (phenyl or benzyl groups), to those with heteroatoms (oxygen, sulfur, nitrogen, or phosphorus) in the substituent. The nature of R1 substituents in the (co)polymer determines the properties of (POx)s including solubility, thermoresponsiveness, glass transition, melting temperature, and ability to crystallize [7]. Additionally, various methods of modifications of poly(2-oxazoline) side chains have been widely reported, among others so-called “click chemistry” and “thio-click” [8] techniques. These modifications made it possible to introduce appropriate functional groups or compounds to the poly(2-oxazoline) chains.

An important feature of (POx)s are nontoxicity towards many cell lines in a wide range of concentrations. Moreover, rapid blood clearance and remarkably low uptake by the organs have been demonstrated for these polymers. They are considered to be alternatives to polyethylene glycol (PEG), the gold standard among polymers for biomedical applications [9,10].

These properties combined with their relatively straightforward synthesis and the potential for functionalization have led to growing interest in poly(2-oxazoline)s within the fields of medicine and



biotechnology. Their tunable physicochemical characteristics, biocompatibility, and versatility make them promising candidates for various biomedical applications, such as drug delivery systems, tissue engineering, and bioactive coatings. As a result, (POx)s are increasingly being explored as alternatives to traditional polymers, offering both enhanced functionality and structural versatility in advanced therapeutic and diagnostic technologies.

2. Results and discussion

This presentation highlights various examples of (co)polymers of 2-oxazoline featuring diverse chain topologies and microstructures, investigated both in solution and immobilized on surfaces, with a focus on their role as nanomaterials for biomedical applications.

The study investigates amine-functionalized poly(2-oxazoline)s, which possess the ability to form stable polyplexes - complexes of polymers with nucleic acids, making them highly promising candidates for gene therapy applications. These functionalized (POx)s effectively bind to nucleic acids through electrostatic interactions, protecting the genetic material from degradation and facilitating its delivery into target cells. Importantly, obtained polyplexes have demonstrated efficient transfection capabilities, ensuring that the genetic material reaches the cell interior and achieves the desired therapeutic effect. Moreover, amine-functionalized (POx)s and their polyplexes exhibited low cytotoxicity towards the studied cell line, which is the key factor for safe and effective gene delivery. As a result, these materials represent a significant advancement in the development of non-viral gene delivery systems, offering a safer alternative to traditional viral vectors in genetic medicine and therapy [11].

Additionally, conjugates of poly(2-oxazoline)s with chelating agents have been extensively explored as multifunctional nanomaterials due to their unique ability to coordinate metal ions. These POx-based conjugates not only exhibit significant antibacterial activity but also offer high stability and biocompatibility. Developing new 2-substituted-2-oxazoline based polymers functionalized with chelating compounds may offer a novel approach to creating effective antibacterial materials. These polymers are capable of interacting with and disrupting bacterial cell membranes, thereby enhancing their antimicrobial activity. As a result, they have emerged as promising candidates for the development of infection-resistant surface coatings for medical devices, as well as for use as therapeutic agents in the treatment of bacterial infections [12].

Furthermore, the research explores thermoresponsive (co)polymers based on 2-oxazolines, which are covalently grafted onto substrates to create thin nanolayers specifically tailored for cell culture applications. The "smart" polymer-coated surfaces exhibit the unique ability to modulate their properties in response to temperature changes. At physiological temperatures, they promote cell adhesion and growth, being suitable for culturing various cell types. However, when the temperature is lowered, these surfaces undergo a physical transformation that results in the gentle detachment of the cultured cells without the need for enzymatic treatments. The temperature-controlled adhesion and detachment mechanism provides a powerful and non-invasive tool for applications in tissue engineering, regenerative medicine, and advanced cell therapy, enabling the harvesting of intact cell sheets and minimizing damage to cell membranes and extracellular matrices [13].

3. Conclusions

The presented research highlights the versatility and potential of poly(2-oxazoline) based materials in various biomedical applications. Amine-functionalized (POx)s has shown great promise in gene therapy as non-viral vectors, offering efficient nucleic acid delivery. Additionally, POx conjugates with chelating agents exhibit notable antibacterial properties and stability. Moreover, thermoresponsive POx (co)polymers covalently grafted onto surfaces allow for controlled cell adhesion and temperature detachment, providing non-invasive methods for harvesting intact cell sheets. Overall, the multifunctional nature of poly(2-



oxazoline)s, combined with their non-toxicity and tunable chemical properties, makes them a highly attractive platform for the development of advanced materials in modern biomedical science.

Acknowledgements

This work was supported by the National Science Centre, project 2021/43/B/ST4/01493. The bilateral project IC-PL/09/2024-2025 within the scientific cooperation agreement between the Bulgarian Academy of Sciences and the Polish Academy of Sciences is acknowledged.

References

- [1]. Tomalia DA, Sheetz DP. Homopolymerization of 2-alkyl- and 2-aryl-2-oxazolines. *J. Polym. Sci. Part A: Polym. Chem.* 4, 2253–2265, 1966.
- [2]. Seeliger W, Aufderhaar E, Diepers W, Feinauer R, Nehring R, Thier W, Hellman H. Recent syntheses and reactions of cyclic imidic esters. *Angew. Chemie Int. Ed. English* 5, 875–888, 1966.
- [3]. Bruckner J. A bibliogr. cat. seventeenth century. *Ger. Publ. Hall.* 4, 875–888, 2018.
- [4]. Litt M, Herz JJ. Polymerization of cyclic imino ethers: VII. The use of the sessile drop method to investigate the surface structure of poly(N-acyl and aroyl ethyleneimines). *Colloid Interface Sci.* 31, 248–252, 1969.
- [5]. Aoi K, Okada M. Polymerization of oxazolines. *Prog. Polym. Sci.* 21, 151–208, 1996.
- [6]. Guillerme B, Monge S, Lapinte V, Robin J. How to modulate the chemical structure of polyoxazolines by appropriate functionalization. *Macromol. Rapid. Commun.* 33, 1600–1612, 2012.
- [7]. Glassner M, Vergaelen M, Hoogenboom R. Poly(2-oxazoline)s: a comprehensive overview of polymer structures and their physical properties. *Polym. Int.* 67, 32–45, 2018.
- [8]. Lava K, Verbraeken B, Hoogenboom R. Poly(2-oxazoline)s and click chemistry: a versatile toolbox toward multi-functional polymers. *Eur. Polym. J.* 65, 98–111, 2015.
- [9]. Jana S, Uchaman M. Poly(2-oxazoline)-based stimulus-responsive (co)polymers: an overview of their design, solution properties, surface-chemistries and applications. *Prog. Polym. Sci.* 106, 101252, 2020.
- [10]. Hoogenboom R. Poly(2-oxazoline)s a polymer class with numerous potential applications. *Angew. Chem. Int. Ed.* 48, 7978–7994, 2009.
- [11]. Oleszko-Torbus N., Mendrek B., Wałach W., Fus-Kujawa A., Mitova V., Koseva N., Kowalczyk A. Amino-modified 2-oxazoline copolymers for complexation with DNA. *Polym. Chem.* 15, 742–753, 2024.
- [12]. Bochenek M, Mendrek B, Wałach W, Foryś A, Kubacki J, Jałowicki Ł, Borgulat J, Płaza G, Klama-Baryła A, Sitkowska A, Kowalczyk A, Oleszko-Torbus N. Chelate-functionalized poly(2-oxazoline) for the destruction of bacterial cell membranes. *Polym. Chem.* 15, 2387, 2024.
- [13]. Dworak A, Utrata-Wesołek A, Oleszko N, Wałach W, Trzebicka B, Anioł J, Sieroń AL, Klama-Baryła A, Kawecki M. Poly(2-substituted-2-oxazoline) surfaces for dermal fibroblasts adhesion and detachment *J Mater Sci: Mater Med.* 25, 1149, 2014.



USING EPR SPECTROSCOPY TO INVESTIGATE COMPLEX SUPRAMOLECULAR SYSTEMS

**Gabriela Ionita,^{1*} Sylvain R. A. Marque,^{1,2} Jean-Patrick Joly,^{1,2}
Iulia Matei,¹ Alexandru Gabriel Bucur¹**

¹*Ilie Murgulescu Institute of Physical Chemistry, Romanian Academy, Bucharest, Romania*

²*Aix-Marseille University, CNRS, ICR, France*

*gabi2ionita@yahoo.com

1. Introduction

Electron paramagnetic resonance (EPR) spectroscopy represents a sensitive tool that can provide meaningful structural and dynamic insight in various molecular systems with applications in various fields of chemistry, materials science, and the biomedical sciences. In order to use this method, it is necessary for the analyzed systems to contain a paramagnetic species. Since most molecular systems do not have paramagnetic groups, in order to use this method, it is necessary to introduce them either by covalent attachment or as spin probes. In this work, we will present several examples to highlight the usefulness of this method in the study of systems with applications in the biomedical field.

2. Results and discussion

In a series of studies in which EPR spectroscopy was the main tools, we investigated albumin solutions, focusing on various aspects *i*) the interaction of albumins with ionic surfactants and β -cyclodextrin, as a function of different factors including the surfactant/CD concentrations and temperature, *ii*) the ability of a polymeric gel containing CD to remove the surfactant from its complex with the protein (Figure 1a) [1,2] and *iii*) formation and stabilization of nanoparticles in protein solutions [3]. The results support potential applications in optimizing drug formulation processes involving biocompatible compounds. The affinity of certain spin probes for proteins has been exploited to evaluate the correlation between protein profile changes in tears collected from patients with dry eye syndrome with or without associated keratoconus disease by using the spectral changes of spin probes in tear samples before and after treatment (Figure 1b) [4].

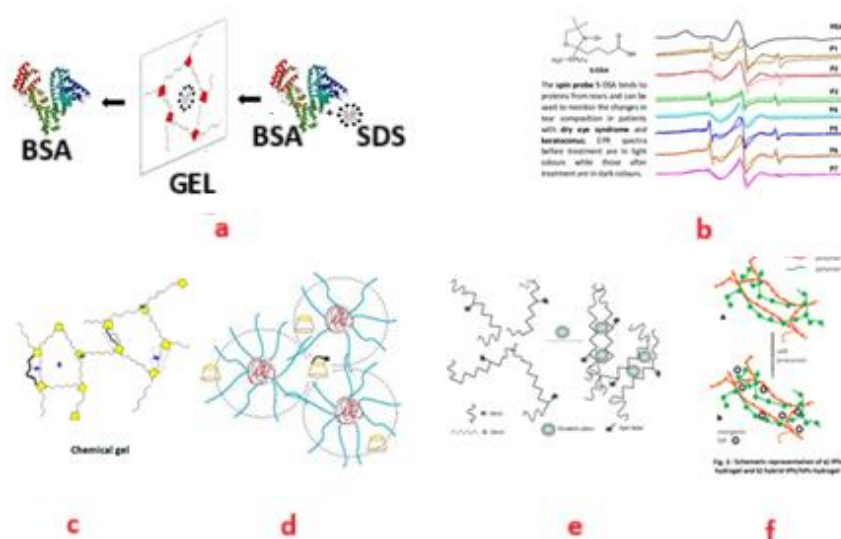


Figure 1. Schematic representation of systems studied by EPR spectroscopy.

The EPR studies revealing interesting structural and dynamic properties of various gel networks outline another research area. These include: covalent gels resulted by crosslinking of CDs with end-capped derivatives of polyethylene glycol, gels resulted by self-assembly of Pluronic F127, supramolecular gels resulted by assembly of low molecular weight gelators, and interpenetrating polymer network (IPN) gels based on polysaccharides (Figure 1, c-f) [5-8]. Host–guest interactions have been exploited to modulate the visco-elastic properties of alginate gels formed in the presence of Ca^{2+} by appending spin labels, adamantane (as guest units) and CD units to alginate chains [9]. Our recent studies are focused on finding supramolecular systems that can be used as contrast agents in OMRI applications. Persistent protease activity is observed in some tumor processes, which has led to the idea of using it to detect tumor formations using the OMRI technique. In some tumors or metastases, human neutrophil elastase (HNE) activity has also been observed, among other things. The activity of this enzyme is being studied because its presence is also associated with the spread and establishment of metastases. Taking these aspects into account, three radical molecules containing a peptide group that can be hydrolyzed by HNE were synthesized (Figure 2).

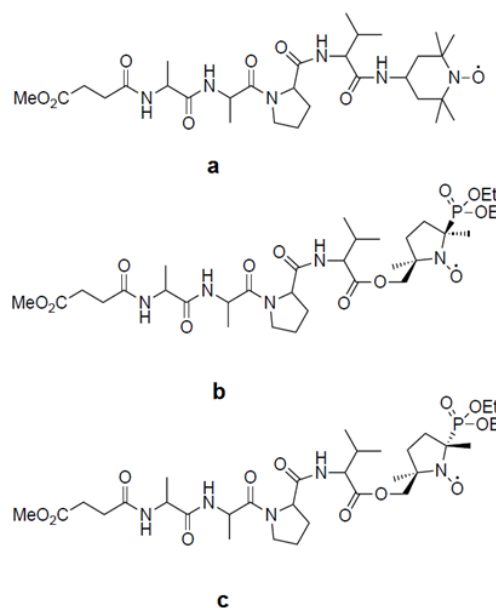


Figure 2. The structures of radicals attached to a peptide chain.

The EPR measurements were performed to highlight changes in spectral parameters as a result of the hydrolysis process in the presence of elastase. In general, nitroxides have some limitations in their use as contrast agents in imaging techniques due to their short relaxation time, possible cytotoxicity, limited tissue penetration, and sensitivity to endogenous reducing agents. To limit these disadvantages, cyclodextrins were introduced into the analyzed systems to generate pseudorotaxane complexes. In the case of radical a (Figure 2), no changes in spectral parameters were observed, which proves that this type of radical is not a solution as contrast agents. Furthermore, complexation stabilizes the radical, as hydrolysis is a slow process. The two diastereoisomers b and c (Figure 2) have different properties in terms of complexation with cyclodextrins. While isomer b does not change its parameters through complexation, isomer c is sensitive to the presence of cyclodextrin. Figure 3 shows the EPR spectra of compound c and the reaction product obtained after enzymatic hydrolysis, illustrating the different EPR parameters in the absence and presence of γ -cyclodextrin. EPR spectrum analysis showed that enzymatic hydrolysis leads to a variation in the hyperfine splitting constant of 1.22 G in the system without cyclodextrin, while in its presence the variation in the splitting constant is 1.9 G. The spectra obtained for the system containing cyclodextrin show two components which illustrate the simultaneous presence of the uncomplexed and complexed species. This concludes that the presence of cyclodextrin further highlights the enzymatic hydrolysis process.

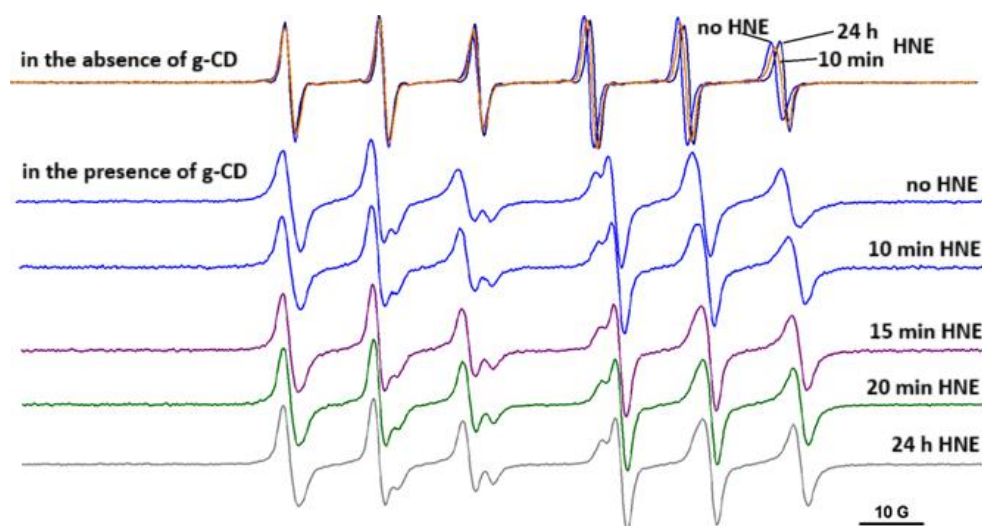


Figure 3. EPR spectra of radical c in the absence and presence of γ -CD; effect of HNE action.

Acknowledgements

We gratefully acknowledge the financial support from project PNRR-III-C9-2023-I8 “Chemical host–guest molecular systems for health applications (OMRI for identification of inflammatory pathologies)”, contract no. 760283/27.03.2024, Romanian National Authority for Research, funded by European Union – NextGenerationEU.

References

- [1]. Matei I, Ariciu AM, Neacsu MV, Collauto A, Salifoglou A, Ionita G. Cationic spin probe reporting on thermal denaturation and complexation–decomplexation of BSA with SDS. Potential applications in protein purification processes. *J. Phys. Chem. B*, 118(38), 11238–11252, 2014.
- [2]. Rogozea A, Matei I, Turcu IM, Ionita G, Sahin VE, Salifoglou A. EPR and circular dichroism solution studies on the interactions of bovine serum albumin with ionic surfactants and β -cyclodextrin. *J. Phys. Chem. B*, 116(49), 14245–14253, 2012.
- [3]. Matei I, Cristina M, Buta CM, Turcu IM, Culita D, Munteanu C, Ionita G. Formation and stabilization of gold nanoparticles in bovine serum albumin solution. *Molecules*, 24(18), 3395, 2019.
- [4]. Constantin MM, Corbu CG, Tanase C, Codrici E, Mihai S, Popescu ID, Enciu AM, Mocanu S, Matei I, Ionita G. Spin probe method of electron paramagnetic resonance spectroscopy – a qualitative test for measuring the evolution of dry eye syndrome under treatment. *Anal. Methods*, 11(7), 965–972, 2019.
- [5]. Ionita G, Ariciu AM, Smith DK, Chechik V. Ion exchange in alginate gels–dynamic behaviour revealed by electron paramagnetic resonance. *Soft Matter*, 11(46), 8968–8974, 2015.
- [6]. Ariciu AM, Staicu T, Micutz M, Neacsu MV, Ionita P, Tecuceanu V, Munteanu C, Ionita G. Investigations on carboxy dibenzylidene sorbitol hydrogels using EPR spectroscopy. *Appl. Magn. Reson.* 46(3), 1395–1407, 2015.
- [7]. Ionita G, Ariciu AM, Turcu IM., Chechik V. Properties of polyethylene glycol/cyclodextrin hydrogels revealed by spin probes and spin labelling methods. *Soft Matter*, 10(11), 1778–1783, 2014.
- [8]. Micutz M, Matalon E, Staicu T, Angelescu D, Ariciu AM, Rogozea A, Turcu IM, Ionita G. The influence of hydroxy propyl β -cyclodextrin on the micellar to gel transition in F127 solutions investigated at macro and nanoscale levels. *New J. Chem.*, 38(7), 2801–2812, 2014.
- [9]. Popescu EI, Aricov L, Mocanu S, Matei I, Hristea E, Baratoiu R, Leonties A, Petcu C, Alexandrescu E, Ionita G. Subtle influence on alginate gel properties through host-guest interactions between covalently appended cyclodextrin and adamantane units. *New J. Chem.*, 45(18), 8083–8091, 2021.



MULTIPLE TARGET LIGANDS WITH AZAHETEROCYCLES SKELETON

**Ionel I. Mangalagiu,^{1*} Dorina Amariuca-Mantu,¹ Vasilichia Antoci,¹ Dumitrelea Diaconu,^{1,2}
Gheorghita Zbancioc,¹ Costel Moldoveanu,¹ Ramona Danac,¹ Violeta Mangalagiu^{1,2}**

¹*Alexandru Ioan Cuza University of Iasi, Faculty of Chemistry, Iasi, Romania*

²*Alexandru Ioan Cuza University of Iasi, Institute for Interdisciplinary Research, CERNESIM and
RECENAIIR Centers, Iasi, Romania*

*ionelm@uaic.ro

1. Introduction

Cancer and microbial (such as malaria, tuberculosis, etc.) illnesses are multifactorial diseases with various etiopathologies, which make them very difficult to treat with drugs that act on a single target [1-3]. One of the modern strategies adopted to fight against multifactorial diseases is Multiple Targeting Drugs (MTD) therapy, where a single chemical entity interacts with two or more distinct biological targets related to a disease. The MTD drugs are usually classified in Hybrid Drugs (HD) and Chimeric Drugs (CD) [1-7]. According to the literature data, azaheterocycles (especially five and six member ring) represent one of the most promising and reliable classes of drug candidates suitable for the MTD approach in our continuous efforts to fight against multifactorial diseases such as cancer, malaria, tuberculosis, etc.

In continuation of our continuous efforts in the field of azaheterocycles of potential interest in the treatment of cancer and microbial diseases, we present herein some selective core results obtained by our group in the last 3 years in the field of hybrid and chimeric MTD molecules with azaheterocycle skeleton of potential interest as anticancer and antimicrobial drugs [8-12].

2. Experimental

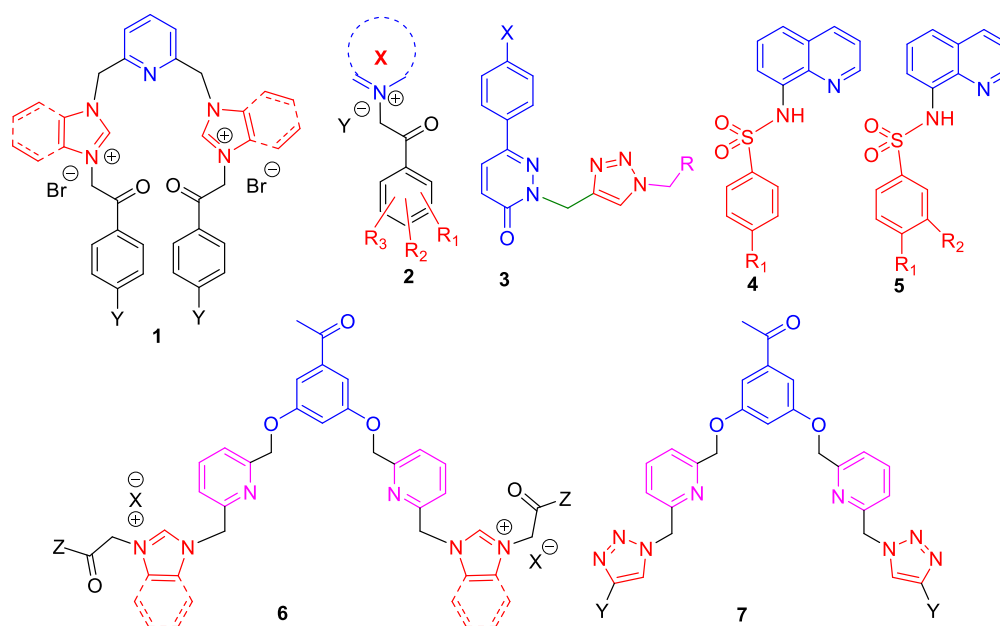
Mel-Temp apparatus was used to measure the melting points of compounds and are uncorrected. Elemental analyses were done using a FlashSmart CHNS/O Elemental Analyzer with MVC. The microanalyses were in satisfactory agreement with the calculated values: C, ± 0.15 ; H, ± 0.10 ; N, ± 0.30 . Infrared (IR) data were recorded with an FTIR Cary 630 spectrophotometer coupled to a ZnSe ATR module for measuring solid samples. The ¹H and ¹³C NMR spectra were recorded on a Bruker Avance III 500 MHz spectrometer operating at 500 MHz for ¹H and 125 MHz for ¹³C. HR-MS experiments were recorded on a HESI-Orbitrap Exploris 120 Mass Spectrometer in positive mode. Full details about the synthesis and spectral characterization of our hybrid and chimeric compounds could be founded in our previously published papers [8-12].

3. Results and discussion

In order to obtain hybrid and chimeric azaheterocycles compounds, initially, we designed them by using the MTD approach [1]. The CD were obtained by merging two different chemical entities in a single molecule (using an appropriate core and preserving the pharmacophores of the two initial drugs), while the HD were obtained by connecting two or more drug pharmacophores (with different biological activities) *via* a flexible linker. As starting materials, we used the following azaheterocycles: azine (pyridine, quinoline, isoquinoline, phthenatroline, bypyridine), diazine (pyridazine, phthalazine, pyrimidine), (di)azol (imidazole, benzimidazole, pyrrole), triazole and tetrazole. Both hybrid and chimeric compounds usually were synthesized using straightforward and efficient pathways, in two to four steps. A typical procedure to obtain hybrid azaheterocycles derivatives involves reactions of N-alkylation, N-acylation and click reactions. Thus, we obtained a large variety of hybrid compounds such us: pyrido- imidazole/benzimidazole salts 1, azaheterocycles – acetophenone salts 2, pyridazino – triazole 3, quinoline – sulfonamide 4 and 5,

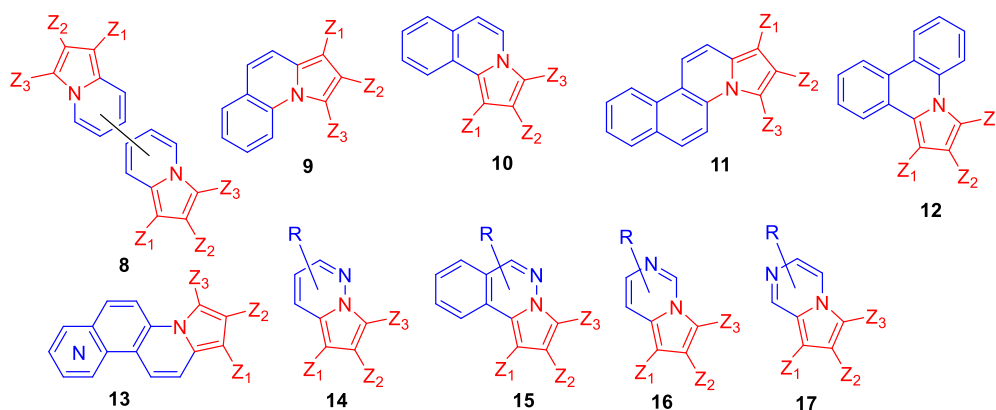


acetophenone – pyridine – imidazole / benzimidazole salts 6, acetophenone – pyridine – triazole
7, etc. (Scheme 1).



Scheme 1. Hybrid azaheterocycles 1-7.

A typical procedure to obtain chimeric azaheterocycles derivatives involve mainly 3+n dipolar cycloaddition reactions of cycloimmonium ylides to different dipolarophiles. Thus, we obtained a large variety of chimeric compounds such us: pyrrolo-bipyridine 8, pyrrolo-quinolines 9, pyrrolo-isoquinolines 10, pyrrolo-benzoquinoline 11 and 12, pyrrolo-phenatoline 13, pyrrolo-pyrdazine 14, pyrrolo-phthalazine 15, pyrrolo-pyrimidines 16, pyrrolo-pyrazines 17, etc. (Scheme 2).



Scheme 2. Chimeric azaheterocycles 8-17.

The obtained hybrid and chimeric compounds type 1 - 17 were tested for their *in vitro* anticancer activity according to the NCI 60 protocol on 60 distinct human tumor cell lines, these include leukemia, melanoma, and tumors of the lung, colon, brain, ovary, breast, prostate, and kidney. The *in vitro* antimicrobial activity was determined against bacterial strains (Gram positive and Gram negative), fungal strains (human and plant), and *Mycobacterium tuberculosis* (*Mtb*) strains (replicating and non-replicating form, drug-resistant strains). For anticancer activity point of view, the most active compounds (in the range of nano-molar) were the hybrid quinoline – sulfonamide 4 and 5 [against 3 types of leukemia (CCRF-CEM, MOLT-4 and SR), 1 type of non-small cell lung cancer (HOP-62) and 1 type of breast cancer (MDA-MB-468)] and the chimeric derivatives pyrrolo-bipyridine 8 (against melanoma MDA-MB-435, colon cancer HT-29, ovarian cancer

OVCAR-3), and pyrrolo-pyridazine 14 (against melanoma MDA-MB-435). Concerning antituberculosis activity, the hybrid acetophenone – pyridine – imidazole / benzimidazole salts 6, have an excellent activity against both replicating and non-replicating *Mtb*, a bactericidal mechanism of action, and excellent activity against drug-resistant strains. For antibacterial and antifungal activity, the most active compounds were the hybrid pyrido- imidazole/benzimidazole salts 1, having a quasi-nonselective activity against the tested human and plant pathogenic fungi, in some cases closely or superior to control drugs.

4. Conclusions

We present herein a thoroughly study concerning the synthesis, structure and biological activity of a large variety of hybrid and chimeric azaheterocycles with potential anticancer and antimicrobial activity. Some of the hybrid and chimeric azaheterocycles have excellent anticancer and antimicrobial activity, no toxicity, excellent solubility in microbiological medium, good ADME properties, and could be considered as good lead candidates for future drug development.

References

- [1]. Diaconu D, Savu M, Ciobanu C, Mangalagiu V, Mangalagiu II. Current strategies in design and synthesis of antifungals hybrid and chimeric diazine derivatives. *Bioorg. Med. Chem.* 119, 118069, 2025.
- [2]. Balaes T, Marandis C, Mangalagiu V, Glod M, Mangalagiu II. New insides into chimeric and hybrid azines derivatives with antifungal activity. *Future Med. Chem.* 16, 1163–1180, 2024.
- [3]. Bansal Y, Silakari O. Multifunctional compounds: smart molecules for multifactorial diseases. *Eur. J. Med. Chem.* 76, 31–42, 2014.
- [4]. Ivasiv V, Albertini C, Goncalves E, Rossi M, Bolognesi ML. Molecular hybridization as a tool for designing multitarget drug candidates for complex diseases. *Curr. Top. Med. Chem.* 19, 1694–1711, 2019.
- [5]. Raghavendra N, Pingili D, Kadasi S, Mettu A, Prasad S. Dual or multi-targeting inhibitors: the next generation anticancer agents. *Eur. J. Med. Chem.* 143, 1277–1300, 2018.
- [6]. Morphy R, Kay C, Rankovic Z. From magic bullets to designed multiple ligands. *Drug Discov. Today* 9, 641–651, 2004.
- [7]. Karoli T, Mamidyala S, Zuegg Z, Fry S, Bradford T, Madala P, Huang J, Ramu S, Butler M, Cooper MA. Structure aided design of chimeric antibiotics. *Bioorg. Med. Chem. Lett.* 22, 2428–2433, 2012.
- [8]. Balaes T, Mangalagiu V, Antoci V, Amariuca-Mantu D, Diaconu D, Mangalagiu II. hybrid bis-(imidazole/benzimidazole)-pyridine derivatives with antifungal activity of potential interest in medicine and agriculture via improved efficiency methods. *Pharmaceuticals* 18, 495, 2025.
- [9]. Moldoveanu C, Mangalagiu I, Zbancioc G, Danac R, Tataringa G, Zbancioc AM. Anticancer potential of azatetracyclic derivatives: in vitro screening and selective cytotoxicity of azide and monobrominated compounds. *Molecules* 30, 702, 2025.
- [10]. Oniciuc L, Amariuca-Mantu D, Diaconu D, Mangalagiu V, Danac R, Antoci V, Mangalagiu II. Benzoquinoline derivatives: an attractive approach to newly small molecules with anticancer activity. *Int. J. Mol. Sci.* 24, 8124, 2023.
- [11]. Diaconu D, Mangalagiu V, Dunca S, Amariuca-Mantu D, Antoci V, Roman T, Mangalagiu II. Ultrasound assisted synthesis of hybrid quinoline anchored with 4-R-benzenesulfonamide moiety with potential antimicrobial activity. *Heliyon* 9, e21518, 2023.
- [12]. Amarandi R, Al-Matarnah M, Popovici L, Ciobanu CI, Neamtu A, Mangalagiu I, Danac R. Exploring pyrrolo-fused heterocycles as promising anticancer agents: an integrated synthetic, biological, and computational approach. *Pharmaceuticals* 16, 865, 2023.



INACCURACIES IN INTERPRETING THERMORHEOLOGICAL BEHAVIOR OF SOME POLYMERS: TO WHAT EXTENT THEY INFLUENCE THE CONCLUSIONS

Daniela Ionita, Mariana Cristea,* Costel Gaina

Petru Poni Institute of Macromolecular Chemistry, Romanian Academy, Iasi, Romania

**mcristea@icmpp.ro*

1. Introduction

Lately, polymer characterization has acquired new dimensions and this happened not only because of the progress in instrument development, but also due to the significance of some specific values that are critical for immediate decisions. A present-day meaningful example belongs to the area of recycled plastics [1]. L. Yu et al. made use of dynamic mechanical analysis (DMA) and thermogravimetric analysis (TGA) to compare long-term viscoelastic parameters and thermal stability of virgin and recycled polysulfone plastics [2]. Also, series of biodegradable polymers were evaluated from the point of view of the onset and maximum degradation temperature (T_{onset} and T_{max}), calorimetric (DSC – differential scanning calorimetry) and DMA evaluation, before and after recycling processes up to seven cycles [3]. Likewise, a DSC-based study was employed to establish the quality of polyethylene terephthalate (PET): virgin PET, degraded PET, modified composition PET, PET suitable for recycling [4]. It is evident that any error or artifact associated with the evaluation of the thermorheological results conduct to incorrect conclusions. With this reflection in mind, we will present a very short survey of the most often possible misinterpretation encountered in polymer evaluation.

2. Experimental

The thermogravimetric analyses of the samples were performed on a Discovery TGA 5500 (TA Instruments, New Castle, DE, USA). The tests were conducted by using three heating rate algorithms: constant heating rate (20 °C/min), dynamic heating rate (HiRes TGA and modulated approach-MTGA), from ambient temperature to 700 °C. The HiRes TGA experiments were performed at resolution (R) 4 and sensitivity (S) 1, using the constant heating rate of 20 °C/min. The MTGA experiments were performed with 2 °C/min, a modulation amplitude of ± 5 °C and a period of 200 s.

Differential scanning calorimetry (conventional – DSC and modulated – MDSC) was performed with a Discovery DSC 250 (TA Instruments, New Castle, DE, USA) under nitrogen atmosphere (50 mL/min). The heating-cooling-heating program with a heating rate of 20 °C/min was employed. The MDSC analysis was carried out with 3 °C/min heating rate, modulation amplitude ± 1 °C and modulation period 60 s.

Dynamic mechanical analysis (DMA) tests were performed on a RSA G2 (TA Instruments, New Castle, DE, USA), in bending (three point bending clamp) and tension modes. The isochronal experiments (1 Hz) were run with the heating rate of 2 °C/min, from -100 °C up to the temperature at which the sample is not any more load-bearing. The deformation was kept within the limits of the linear viscoelastic range, which was established in a preliminary oscillation amplitude test. The isochronal variation of the viscoelastic properties (E' – storage modulus, E'' – loss modulus, $\tan \delta$ - loss factor) with temperature was recorded.

3. Results and discussion

Figures 1a and 1b include the results of the conventional TGA and modulated TGA (MTGA) for a polyurethane derived from poly(tetramethylene ether glycol), hexamethylene diisocyanate and 3,6-dithia-1,8-octanediol. The degradation temperature (T_{deg}) evaluated from the evolution of the sample mass vs.



temperature, associated with 5% mass loss (T_5), interferes with the loss of the solvent. The detail of the derivative weight curve (MTGA) presented in Figure 1b brings out the impact of the traces of solvent. Therefore, the values T_5 (TGA) and T_5 (MTGA) (262.3 °C and 220.4 °C) are out of the margin of admitted errors.

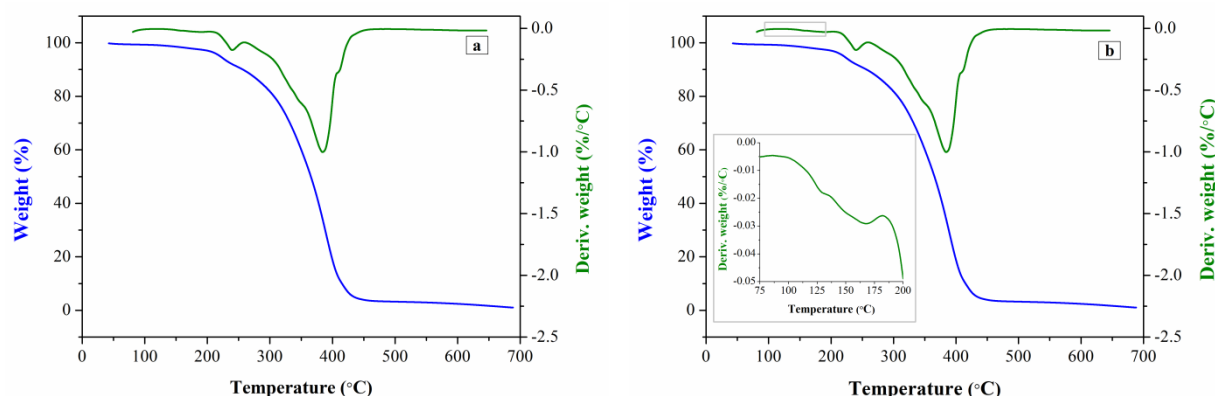


Figure 1. The thermal degradation curves for the investigated polyurethane, obtained by (a) TGA and (b) MTGA.

Briefly, the degradation of this polyurethane material is split in two main stages: the decomposition of the urethane groups (up to around 350 °C) and of the polyols that continue up to around 450 °C. It is clear from Figures 1 that the resolution of the MTGA is improved to a greater degree and allows to differentiate these steps.

The misinterpretation in DSC and DMA is mostly the result of overlapping phenomena. As a consequence of processing conditions, the glass transition region determined by conventional DSC intersects with the stress relaxation, i.e., the heat capacity step is disrupted by an endothermic peak. This fact questions the correctness of T_g identifying as the middle point of the transition. It is usual to differentiate the two events in a MDSC test. This procedure applied to a polyester resin derived from diglycidyl ether of bisphenol A (DGEBA) and 5-maleimidoisophthalic acid (MIPA) in a study dedicated to evidence the retro Diels-Alder reaction associated with the maleimide-anthracene adduct [5]. Commonly, for sensitivity reasons a conventional DSC is performed with a quite high heating rate (20 °C/min). In contrast, MDSC is performed with low heating rate (3 °C/min). The result of the two approaches (DSC and MDSC) gives different T_g for the DGEBA-MIPA polyester resin: 70.1 °C for conventional DSC (evaluated as the onset of the glass transition range) and 53.9 °C in MDSC, evaluated as the middle point of the heat flow step on the reversing curve. Importantly, the outcomes need to be comprehended much more in phenomenological terms than focusing on very specific values of temperature, which are less representative for the purpose of a certain study.

In the publications dedicated to polymers the glass transition region is usually reported as a single value of temperature, usually included in a table. In the same time, it is generally accepted that the accurate approach would be to replace this temperature with an interval. For scientists very familiar with thermorheological investigations of polymers, DMA reveals much more due to the fact that the variation of three parameters is taking in consideration (E' , E'' , $\tan \delta$). Figures 2a and 2b display the variation of $\tan \delta$ with temperature for a well-behaved polymer (2a) and for a polymer that undergoes a morphological transformation during the experiment (2b). Figure 2a reveals that once the coordinated motions of long chains advances during the glass transition, the value of $\tan \delta$ increases, reaches a maximum and returns to initial value, which is usually lower than 0.1.

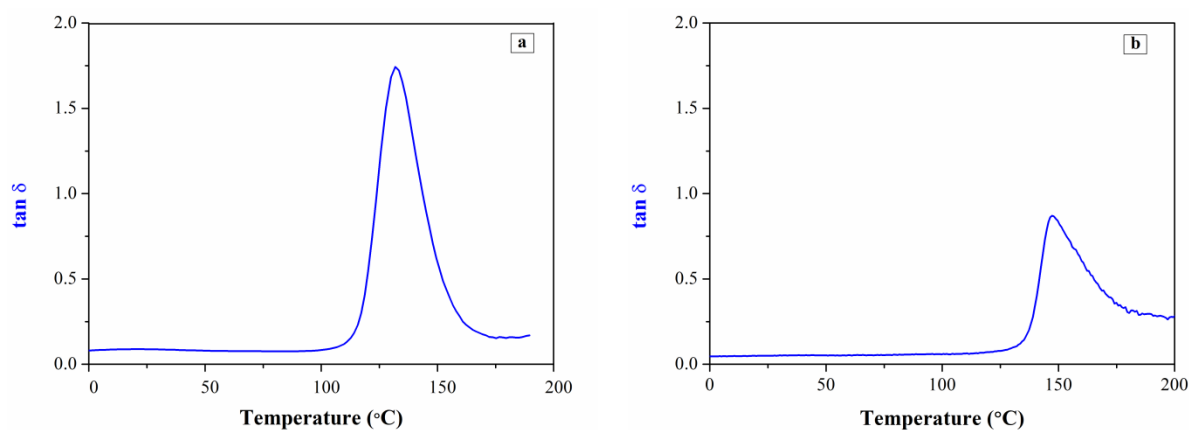


Figure 2. The variation $\tan \delta$ vs. T during for two circumstances: (a) a typical amorphous polymer and (b) a polymer with a change of morphology during the glass transition.

A close look at the increase of $\tan \delta$ with temperature shows at least three aspects (Figure 2b). First, the abrupt increase of $\tan \delta$ is suddenly interrupted and it switches to descending. Second, the descending side is less abrupt, which the occurrence of two super-imposed phenomena. Finally, the $\tan \delta$ value at the end of the glass transition is higher than the pre-transition value. Therefore, the glass transition temperature reported as the $\tan \delta$ peak value does not represent the correct point, it is just the value of temperature where the secondary phenomenon takes over the glass transition. Under these circumstances, T_g reported as the onset of E' would be more appropriate.

4. Conclusions

As long as the ascertainment of recycling quality by thermorheological approach became a routine, it is very relevant to pay attention to all the details of the outcome. Also, the application of advanced techniques such modulated or sample-controlled procedures are very relevant.

References

- [1]. Merrington A, Recycling of plastics. In: Myer Kutz, editor. *Plastics Design Library, Applied Plastics Engineering Handbook*. 2nd ed. Chadds Ford, PA: William Andrew Publishing; 2017. pp. 167–189.
- [2]. Yu L, Zhao D, Wang W. Mechanical properties and long-term durability of recycled polysulfone plastic. *Waste Manag.* 84, 402–412, 2019.
- [3]. Nomadolo N, Mtibe A, Ofosu O, Mekoa C, Letwaba J, Muniyasamy S. The effect of mechanical recycling on the thermal, mechanical and chemical properties of poly(butylene adipate-co-terephthalate) (PBAT), poly(butylene succinate) (PBS), poly(lactic acid) (PLA), PBAT-PBS blend and PBAT-TPS biocomposite. *J. Polym. Environ.* 32, 2644–2650, 2024.
- [4]. Šudomová L, Doležalová Weissmannová H, Steinmetz Z, Řezáčová V, Kučerik J. A differential scanning calorimetry (DSC) approach for assessing the quality of polyethylene terephthalate (PET) waste for physical recycling: a proof-of-concept study. *J. Therm. Anal. Calorim.* 148, 10843–10855, 2023.
- [5]. Ionita D, Cristea M, Gaina C, Silion M, Simionescu BC. Evidence through thermal analysis of retro Diels-Alder reaction in model networks based on anthracene modified polyester resins. *Polymers* 15, 4028, 2023.



SORPTION PERFORMANCE OF ZWITTERIONIC RESINS FOR HEAVY METAL
DECONTAMINATION OF POLLUTED WATERS

**Marius-Mihai Zaharia,^{1*} Alina-Petronela Moraru,¹ Ramona Ciobanu,²
Florin Bucatariu,¹ Marcela Mihai¹**

¹*Petru Poni Institute of Macromolecular Chemistry, Romanian Academy, Iasi, Romania*

²*Department of Environmental Engineering and Management,*

*Cristofor Simionescu Faculty of Chemical Engineering and Environmental Protection,
Gheorghe Asachi Technical University of Iasi, Romania*

**zaharia.marius@icmpp.ro*

1. Introduction

The contamination of waters with different heavy metal ions (HMIs) represents one of the most serious and severe problems nowadays, numerous studies being developed in order to solve it [1]. This study focusses on the Tarnița closed mine area because it is very polluted with heavy metal ions and the ecological disaster is pronounced, being necessary a rapid area recovery. Pollution of surface and underground waters with heavy metal ions around the closed mine in Tarnița continues to present a high risk to public health [2]. In this context, collected water from Tarnița contaminated area were qualitatively and quantitative analyzed for identification of principal contaminants (heavy metal ions) by atomic absorbance spectroscopy (AAS), significant amounts of heavy metal ions (Me^{2+}) (iron 154.59 mg/L, copper 19.91 mg/L and manganese 1.95 mg/L) being detected in the surface water.

The search for an effective and economical method of removing toxic metal ions requires the consideration of materials and processes that might have potential in this field. Some polymeric substances have the ability of metal ions complexation; the ion exchange resins (IExRs) representing an important category of synthetic polymers with wide applicability in removing HMIs from contaminated waters. The principal characteristics of chelating crosslinked acrylic polymers are the flexibility in optimization of pore size and the type of donor atoms from functional groups [3]. Among the functional chelating groups, the amino/imino ($-\text{NH}_2/-\text{NH}-$), carboxyl ($-\text{COOH}$) and amide ($-\text{NH}-\text{CO}-$) groups could selectively retained Lewis's acids (metal cations). Even if the literature presents distinct informations on the IExRs and their sorption capacity, this study represents a comprehensive study on the synthesis and characterization of some ion exchange resins based on acrylic copolymers with 8% crosslinking, and their applications as sorbents for heavy metal ions.

2. Experimental

The IExRs were obtained by copolymerizing ethyl acrylate, acrylonitrile and 8% divinylbenzene cross-linker, following a previous published method [4]. Ethylenediamine (EDA) or triethylenetetramine (TETA) were used to functionalize the copolymer bears by adding amino groups, creating thus weak cationic/anionic resins, while hydrazine hydrate (HA) was used to obtain weak anionic resins with hydrazide groups. Zwitterionic resins (Zw) were prepared by reacting these resins with sodium chloroacetate (Figure 1). The structure and surface of the resins were confirmed using FTIR-ATR and SEM.

Sorption tests were done by mixing 1 mL of resin with 20 mL of 1 mM metal ion solutions (Cu^{2+} , Fe^{2+} , Mn^{2+}) for 24 hours at room temperature, in batch experiments. The AAS method was used to determine the amount of heavy metal ions (Cu^{2+} , Fe^{2+} , Mn^{2+}) remained in the solutions after being in contact to IExRs, in tests using simulated waters (mono- and multicomponent HMIs) and water collected from Tarnița area. Also, batch sorption experiments using simulated aqueous solutions of mixtures of these four HMIs were performed to investigate the isotherms, kinetics and thermodynamics of the sorption process.



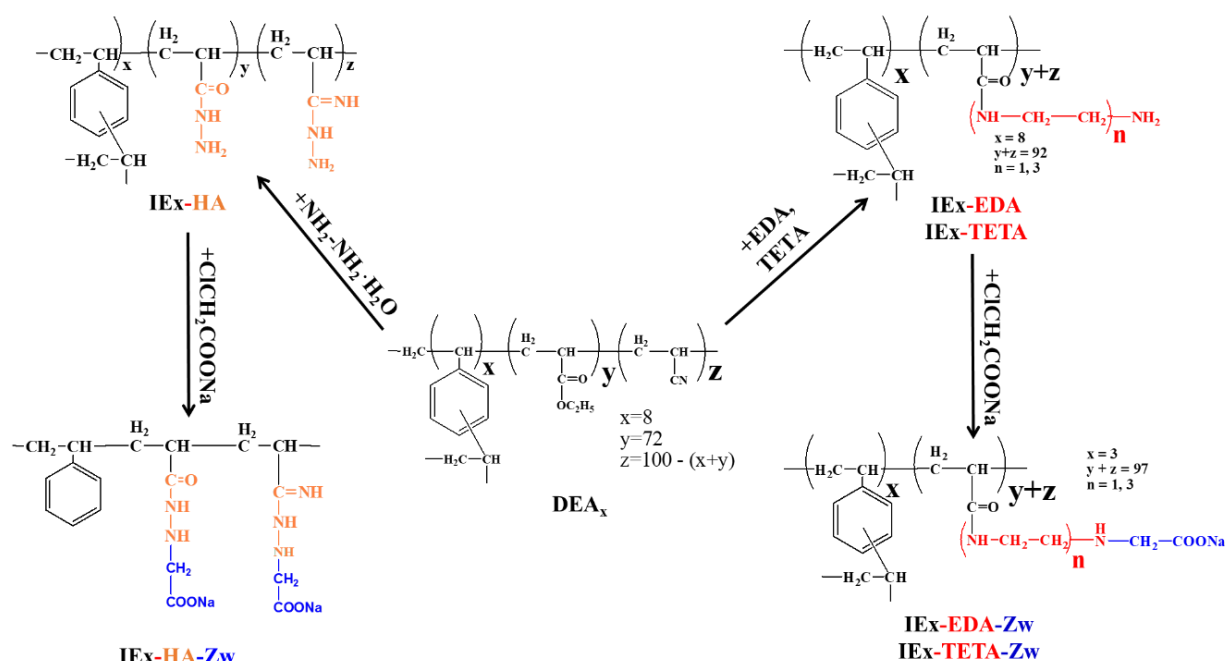


Figure 1. Synthesis scheme of the ion exchangers.

3. Results and discussion

Figure 2 shows that the removal effectiveness has significant differences, based on the type of functionalization of IExRs and the heavy metal ion present in the solutions.

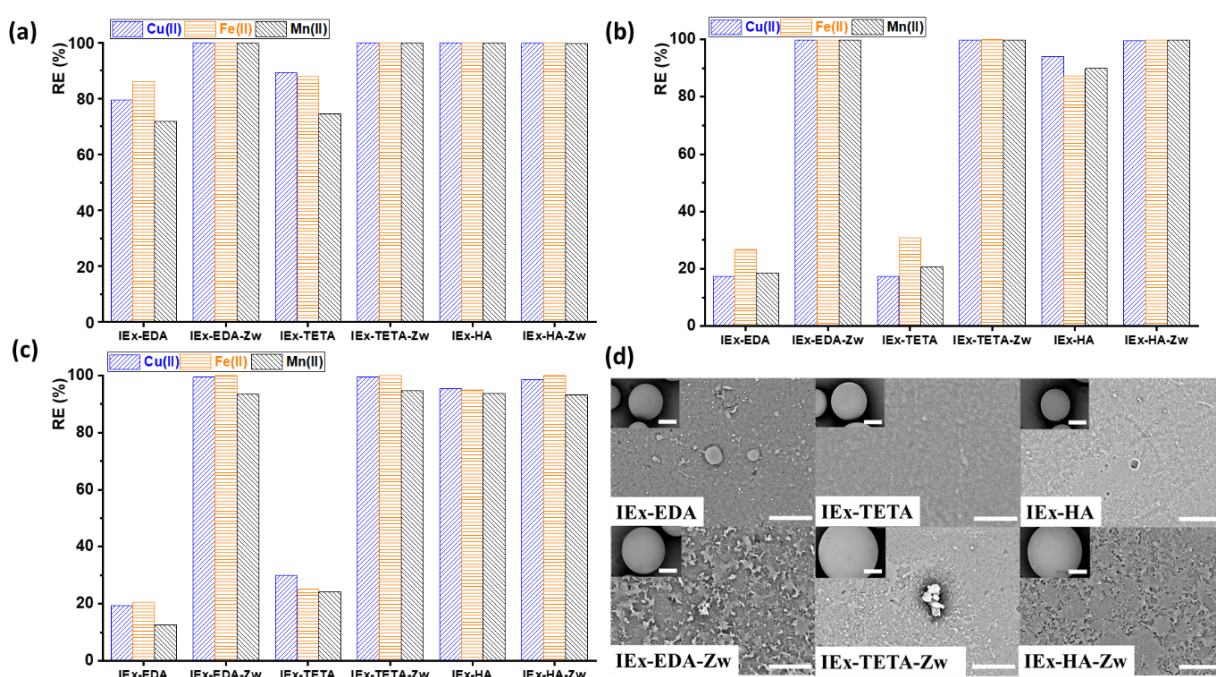


Figure 2. Removal efficiency of HMIs by IExRs from (a) monocomponent and (b) multicomponent synthetic polluted waters, and (c) Tarnita water; (d) SEM micrographs of tested IExRs (300 μm scale bar); insets (5 μm scale bar).

The removal efficiency of the parent resins such as $IEx-EDA$ and $IEx-TETA$ was consistently low, particularly in Figure 2(b) and (c), where the removal percentages is below 30% in most cases. Nevertheless, the functionalization with amphoteric group of both weak cationic resins, namely the samples $IEx-EDA-Zw$ and $IEx-TETA-Zw$, and both the weak anionic resins, $IEx-HA$, and its corresponding amphoteric derivative, $IEx-HA-Zw$, conducted to an increase on the HMIs sorption capacity and reaching

or exceeded 90–100% in specific cases. This enhancement on their sorption capacity is due to the increased density of active binding sites and the increased chemical affinity of functional groups (e.g., carboxyl, hydroxyl, amine) for divalent cations, which allows the formation of coordination complexes with metal ions. Additionally, the modified resins showed excellent selectivity and removal efficiency, especially for Cu^{2+} and Fe^{2+} ions.

The SEM images compare the surface morphologies before and after functionalization with amphoteric group of all the IExRs samples used in this study (Figure 2 (d)). Thus, the weak cationic and anionic IExR shows smooth surfaces (IEx-EDA, IEx-TETA, IEx-HA), while the amphoteric resin (IEx-EDA-Zw, IEx-TETA-Zw, IEx-HA-Zw) reveals rougher textures, which improves their ability to retain HMIs. Also, after functionalization, the microspheres maintain their structural integrity (inset micrograph), making them suitable for use in water filtering applications.

4. Conclusions

The tested zwitterionic resins and IEx-HA demonstrated effective removal of HMIs (Fe, Cu, Mn) from synthetic and Tarnița polluted water, reducing their content up to 90-100%. The zwitterionic resins maintained their high sorption performance over six regeneration cycles, highlighting their potential as reusable, efficient solutions for heavy metal remediation in contaminated real water.

Acknowledgements

This work was financially supported by a grant of the Ministry of Research, Innovation and Digitization, CNCS-UEFISCDI, project number PN-IV-P1-PCE-2023-0738, within PNCDI IV.

References

- [1]. Jagaba AH, Lawal IM, Birniwa AH, Affam AC, Usman AK, Soja UB, Saleh D, Hussaini A, Noor A, Yaro NSA. Sources of water contamination by heavy metals. In: Membrane technologies for heavy metal removal from water. Boca Raton: CRC Press; 2024. pp. 3–27.
- [2]. Zaharia M, Butnariu A, Zamfirache MM, Surleva A, Ciobanu CI, Pintilie O, Drochioiu G. Heavy metals and arsenic in an abandoned barite mining area: ecological risk assessment using biomarkers. *Environ. Forensics* 24, 1–12, 2023.
- [3]. Mita C, Bunea I, Roman T, Humelnicu D. Cross-linked and functionalized acrylic polymers: efficient and reusable sorbents for Zn (II) ions in solution. *J. Polym. Environ.*, 29, 2261–2281, 2021.
- [4]. Zaharia MM, Vasiliu AL, Trofin MA, Pamfil D, Bucatariu F, Racovita S, Mihai M. Design of multifunctional composite materials based on acrylic ion exchangers and CaCO_3 as sorbents for small organic molecules. *React. Funct. Polym.* 166, 104997, 2021.



SENSING COATINGS BASED ON A HARD-SOFT COPOLYIMIDE FOR TOLUENE DETECTION

**Irina Butnaru,* Adriana-Petronela Chiriac, Loredana Vacareanu,
Mariana-Dana Damaceanu**

Petru Poni Institute of Macromolecular Chemistry, Romanian Academy, Iasi, Romania

**butnaru.irina@icmpp.ro*

1. Introduction

Nowadays, air pollution is one of the most important issues which is determined by the particulate matter and gaseous components (NO_2 and NO , O_3 , SO_2 , CO , and volatile organic compounds (VOCs)). Although the life expectancy has increased significantly due to high living standards, air pollution by toxic gases and VOCs is still an unsolved problem in large cities, especially in countries with low- and middle-incomes. The long-term exposure to toxic gases and VOCs accelerates the global warming and climate changes, and in the short-term, can be hazardous to human health. World Health Organization claims that air pollution in cities is one of the important causes of global mortality, being responsible for almost 800 000 premature deaths each year. Despite the ability of the human olfactory system to detect odorous gases (such as H_2S , NH_3 , and most VOCs), in some cases, the gas or VOC concentration is below the limit of detection of the human nose. Moreover, when the air contains a mixture of gases, the human nose can't discriminate between different gases and VOCs. Therefore, the development of devices for the early detection of toxic gases and VOCs is essential.

Benzene, as part of the volatile organic compounds (VOC), is designated as a group 1 carcinogen by the International Agency for Research on Cancer [1]. Benzene may be found in the air emissions from burning coal and oil, gasoline service stations, and motor vehicle exhaust. Therefore, the human short-term inhalation exposure to benzene may cause drowsiness, dizziness, headaches, as well as eye, skin, and respiratory tract irritation. The long-term exposure has caused various disorders in the blood such as reduced numbers of red blood cells and aplastic anemia, adverse effects on the developing fetus, leukemia [2]. Despite its serious harmfulness, benzene is ubiquitous in our daily lives being found in adhesives, carpets, furniture e wax, is emitted with cigarette smoke and burning objects. However, it is impossible for non-scientific community to verify ambient benzene concentrations due to scarce cost-effective detectors capable of real-time benzene monitoring. Therefore, the need for the development of benzene sensors represents an urgent demand for society health [3].

Only several sensitive sensors for benzene/toluene/ethyl-benzene/xylene (BTEX) detection have been reported until now, including quartz crystal microbalance (QCM)-based sensors, fluorescent sensors, resonant-gravimetric gas sensors, microelectromechanical gas sensors, resistive-based gas sensors, etc. The performance of such sensors in terms of responses of is relatively low, while the selective detection of a single gas among the BTEX group is challenging because of the similar nature and chemical structure of the analytes to be detected. New sensing materials are necessary to be developed and tested in different sensor technology to enlarge the detection limit of BTEX beyond several ppb. Moreover, a rational strategy to make sensing materials selective to benzene with repressed cross-responses to other volatile organic compounds from BTEX is still challenging.

Polyimides, as part of high-performance polymers, are known for their excellent combination of chemical, physical and mechanical properties which endow them characteristics suitable for a large range of applications. To overcome the major disadvantages of poor solubility and non-melting characteristics of classical aromatic polyimides, various strategies were undertaken, which mainly include the perturbation



of the macromolecular symmetry by the incorporation in the main chain of flexible or unsymmetrical moieties or of various kinked pendant groups [4]. Polyimide-based sensor materials are appealing for this domain owing to their facile preparation methods, low cost, chemical inertness, mechanical and thermal stability, ease of deposition onto various substrates and high biocompatibility, being used in many high-tech fields [5]. In this context, polyimides have been used in the development of humidity sensors as functional layers, temperature sensor arrays, gas sensors or biosensors, among others.

Herein, we report the synthesis of a semi aromatic copoly(ether-imide) with hard and soft segments for toluene detection. Such structural architecture is expected to allow swelling of the soft segment when the polymer is in contact with the analyte, while the hard segment will remain intact, ensuring the integrity and dimensional stability of the material.

2. Experimental

The copoly(ether-imide) (CoPEI) was obtained by the classical two-step polycondensation reaction by using an equimolecular mixture between the an aromatic dianhydride (3,3',4,4'-benzophenone tetracarboxylic dianhydride) and the two diamines (2,6-bis(3-aminophenoxy) benzonitrile and Jeffamine® ED-2003), the weight ratio between the two diamines being of 0.7 aromatic diamine: 0.3 aliphatic diamine. The reaction was performed in NMP, with a concentration of 20% in solids.

3. Results and discussion

The copoly(ether-imide) structural confirmation was made by ¹H-NMR and FTIR spectroscopies, as shown in Figure 1. The ¹H-NMR spectrum proved the formation of the designed structure by the disappearance of the intermediary polyamidic acid signals (from 14 and 10 ppm) and by the existence of the peaks associated with dianhydride (8.28 ÷ 7.97 ppm), aromatic diamine (7.60 and 6.67 ppm), and aliphatic diamine segments (4.58, 3.30, 1.46 and 1.00 ppm). FTIR spectroscopy also confirmed the CoPEI structure by the presence of the absorption bands characteristic for the imide cycle at: 1778 and 1715 cm⁻¹ (symmetrical and asymmetrical stretching vibrations of C=O), 1371 cm⁻¹ (C–N stretching), and 715 cm⁻¹ (imide ring deformation). The absorption peak at 1226 cm⁻¹ was attributed to the aromatic ether groups, while the presence of nitrile groups was observed at 2228 cm⁻¹. The ED-2003 fragments in the soft part of the copolymer were identified as wide absorption bands attributed: to the asymmetric and symmetrical methylene group at 2944-2869 cm⁻¹, to the aliphatic ether C–O–C bond at 1090 cm⁻¹, as well as C–O bending group at 859-853 cm⁻¹.

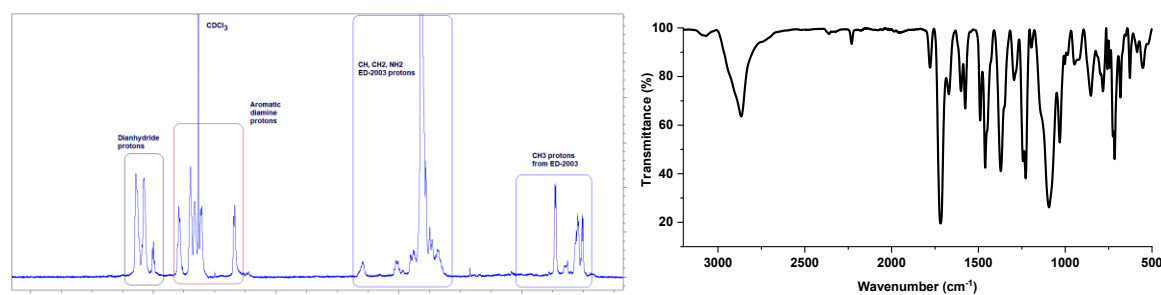


Figure 1. ¹H-NMR and FTIR spectra of CoPEI.

The copolymer had a good solubility in low boiling point solvents like CHCl₃ and THF, and in polar aprotic solvents like DMF, DMAc, DMSO and NMP. Due to the good film-forming ability of CoPEI in THF solution, it was used to prepare homogenous transparent coatings on different supports (Si, Si/SiO₂ and quartz), as can be seen in Figure 2. The thermal stability of the copolymer was high, with initial decomposition temperature of 399 °C and glass transition temperature of 104 °C.

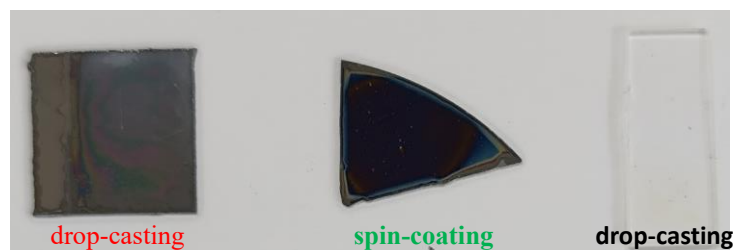


Figure 2. Images of CoPEI coatings on Si, Si/SiO₂ and quartz substrates.

The CoPEI coating on quartz was used afterwards in preliminary test for validation as sensitive coating material toward toluene (used for testing instead of carcinogen benzene) detection. After several exposure times to a saturated toluene vapours atmosphere, CoPEI film exhibited a decrease in the absorption bands of the UV-vis and PL spectra as compared to the initial sample. Contact angle measurements registered an increase, from 39 to 58°, indicating a decrease in wettability. QCM measurements indicated an important polyimide mass change triggered by toluene adsorption. The obtained data enabled the validation of CoPEI as suitable responsive material towards toluene detection, proving the interaction of the analyte with the copolymer matrix.

4. Conclusions

A semiaromatic copoly(ether-imide) was synthesized, characterized and preliminary tested as sensitive coating for toluene detection in a saturated vapours atmosphere. The data obtained from UV-vis, PL, QCM and contact angle measurements suggested a good sensitivity and selectivity of this coating towards toluene detection. Future work will involve measurements to establish the limit of detection in accordance to toxicological datasheet.

Acknowledgements

This work was financially supported by Horizon Europe, the European Union's Framework Programme for Research and Innovation (HEU 2021-2027) under grant agreement nr. 101135796 (COMPAS).

References

- [1]. IARC working group on the evaluation of carcinogenic risks to humans, chemical agents and related occupations, *IARC Monogr. Eval. Carcinog. Risks Hum.* 2012.
- [2]. Fenga C, Gangemi S, Costa C. Benzene exposure is associated with epigenetic changes, *Mol. Med. Rep.* 13, 3401–3405, 2016.
- [3]. Kim KB, Moon YK, Kim TH, Yu BH, Li HY, Kang YC, Yoon, JW. Highly selective and sensitive detection of carcinogenic benzene using a raisin bread-structured film comprising catalytic Pd-Co₃O₄ and gas-sensing SnO₂ hollow spheres. *Sens. Actuator B: Chem.* 386, 133750, 2023.
- [4]. Butnaru I, Sava I, Damaceanu MD. Exploring the impact of triphenylmethane incorporation on physical properties of polyimides with emphasis on optical and halochromic behaviour. *Polymer* 200, 122621, 2020.
- [5]. Chiriac AP, Butnaru I, Damaceanu M-D, Electrochemically active polyimides containing hydroxyl-functionalized triphenylmethane as molecular sensors for fluoride anion detection. *Electrochim. Acta* 353, 136602, 2020.



NANOMETRIC EM-VESICLES WITH ENHANCED BIOPHARMACEUTICAL ATTRIBUTES

Vera-Maria Platon,* Anda M. Craciun, Irina Rosca, Natalia Simionescu, Luminita Marin

Petru Poni Institute of Macromolecular Chemistry, Romanian Academy, Iasi, Romania

**platon.vera@icmpp.ro*

1. Introduction

Erythromycin (EM) is a broad-spectrum macrolide antibiotic used for the treatment of various infections, both internally and externally, as well as for other non-infectious pathologies, such as gastroparesis, due to its motilin receptor agonist properties [1,2]. In addition to its antibacterial activity, EM also possesses immunomodulatory properties that aid in managing inflammatory conditions, hence its wide-spread use in acne treatments [3]. However, limitations such as low solubility, instability in acidic environments and short half-life affect therapeutic efficiency and increase the risk of undesired effects [4,5]. The current study focused on designing a reproducible EM formulation by encapsulation of the drug into chitosan oligomer (CO)-coated vesicles, in order to achieve a nanometric drug-delivery system with enhanced properties and sustained release capacity, therefore addressing EM's limitations and difficulties in administration.

2. Experimental

The preparation of CO-coated liposomes loaded with EM (CE_{lip}) was conducted through an optimized method based on thin film hydration. The thin film was achieved through the dissolution of the drug and lipid (phosphatidylcholine, PC) in $CHCl_3$, followed by removal of the solvent through rotary evaporation. PBS 7.4 was used for the hydration of the previously obtained film, due to its isotonic and isohydric composition, similar to physiological fluids. A temperature above the lipid's phase transition temperature (37 °C) was ensured during the hydration process in order to support the rearrangement and self-organization of the vesicles under intense stirring. The optimal hydration time, determined by visual evaluation of the suspension's turbidity, was found to be 60 hours. Once the hydration was completed, the liposomes were subjected to extrusion through polycarbonate membranes, in order to reduce particle size and attain narrow polydispersity. The coating process was performed by the drop-wise addition of the liposomal suspension to a 0.5% CO solution in 0.5% acetic acid, thus promoting a greater stability of the formulation. Finally, a sucrose solution was added as a cryoprotectant, in an equivalent volume to that of the sample/coating solution. The final product was purified through dialysis in order to eliminate residual acetic acid and free EM. Both plain coated liposomes (C_{lip}) and plain liposomes encapsulating EM (E_{lip}) were obtained.

3. Results and discussion

The structural characterization through FTIR and NMR spectroscopy demonstrated the presence of all components of the liposomal formulation, as well as the physical interactions between them, confirming the effective encapsulation of EM and coating with CO. XRD and POM analysis of the formulation highlighted that EM was distributed amorphously in the lipid bilayer, and that the sample exhibited moderately birefringent domains. By using coupled heating/cooling cycles with POM microscopy, it was found that the CO coating significantly improved the thermal stability of the liposomes.

The STEM and AFM images confirmed the spherical morphology, uniform dimensions (average diameter measured ~97 nm), and structural stability of the coated liposomes, highlighting the efficiency of the CO coating in maintaining integrity and preventing aggregation (Figure 1).



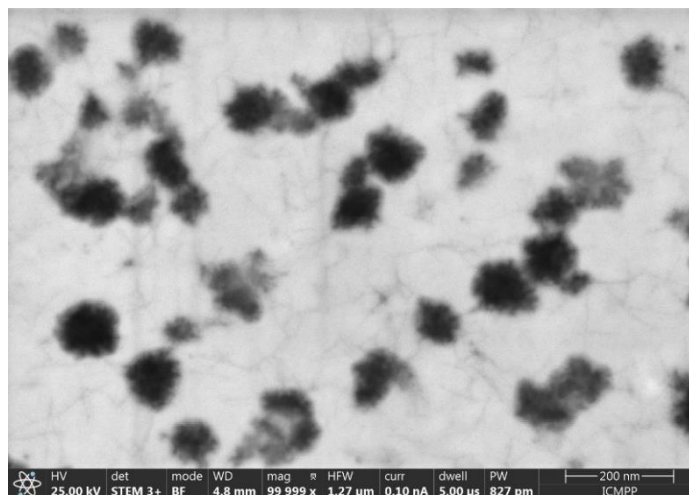


Figure 1. STEM images of CE_{lip} liposomes, with visible coating (scale: 200 nm).

DLS evaluations confirmed the nanoscale size of the tested liposomes (~97 nm), as well as their uniform size distribution (PDI~0.1), positive surface charge (~9 mV), and good colloidal stability, validating the STEM results. The optimized formulation remained stable for at least 6 weeks, particularly at 25 °C, making it suitable for safe and reproducible pharmaceutical applications.

The quantitative determination by UV-Vis of EM showed that the liposomal formulation had a satisfactory encapsulation efficiency (~63%). The study of the release kinetics revealed a sustained release of up to ~75% in 10 hours, highlighting the role of chitosan coating in protecting and controlling drug release under physiologically similar conditions.

Evaluation of the antioxidant activity confirmed a cumulative effect of the components, with values of ~80% for the CE_{lip} formulation (Figure 2). These results were mainly attributed to the presence of CO, although both PC and EM demonstrated radical scavenging capability, supporting the applicability of the formulation in treatments involving the combat of oxidative stress.

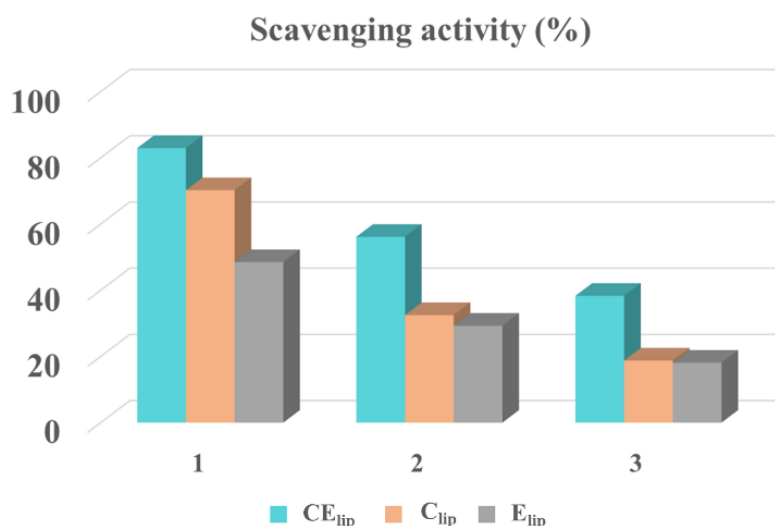


Figure 2. Graphical representation of the tested samples' scavenging activity, undiluted (1), 1:1 v/v dillution (2) and 1:3 v/v dillution (3).

The mucoadhesive properties of the investigated samples were determined through turbidity measurements, when turbidity changes upon contact with mucin. The samples demonstrated impressive mucoadhesion, confirmed by a significant decrease in transparency in the presence of mucin (from 41.57% to 3.19%), supporting their potential for prolonged release of EM at mucosal sites.



The liposomal formulations exhibited rapid and effective antibacterial activity, particularly against *Enterococcus faecalis*, surpassing the performance of the free antibiotic and highlighting their potential for infection and bacterial resistance prophylaxis.

Following the cytotoxicity tests on gingival fibroblasts, it was concluded that the liposomes exhibited good cytocompatibility, meeting ISO standards and indicating an appropriate safety profile for biomedical applications, with a possible protective role of EM towards the cells.

4. Conclusions

The current study presents the successful preparation and characterization of CO-coated EM liposomes, as an advanced drug-delivery system specifically designed for the sustained release of erythromycin. The vesicles displayed nanometric-scale dimensions with low polydispersity, indicating the quality of the formulation. Furthermore, the liposomes demonstrated good encapsulation efficiency, ensuring an optimal erythromycin amount within the carrier system. *In vitro* release studies confirmed a sustained release profile, controlled predominantly by both diffusion and matrix erosion mechanisms. The liposomes exhibited pronounced antioxidant activity, enhanced mucoadhesive properties and superior antibacterial activity compared to non-encapsulated EM. Importantly, cytotoxicity assays confirmed the formulation's safety profile, highlighting its suitability for use in therapeutic applications. Collectively, these findings establish the CO-coated EM liposomes as a promising and versatile formulation for antimicrobial therapy.

Acknowledgements

The support from the Romanian National Recovery and Resilience Plan through the project PNRR-III-C9-2022 – 18, 760081/23.05.2023 is acknowledged.

References

- [1]. Heilman FR, Herrell WE, Wellman WE, Geraci JE. Some Laboratory and clinical observations on a new antibiotic, Erythromycin (Ilotycin). *Proc. Staff. Meet. Mayo Clin.* 27, 285–304, 1952.
- [2]. Szczupak M, Jankowska M, Jankowski B, Wierzchowska J, Kobak J, Szczupak P, Kosydar-Bochenek J, Krupa-Nurcek S. Prokinetic effect of erythromycin in the management of gastroparesis in critically ill patients—our experience and literature review. *Front Med.* 11, 1440992, 2024.
- [3]. Zimmermann P, Ziesenitz VC, Curtis N, Ritz N. The immunomodulatory effects of macrolides - a systematic review of the underlying mechanisms. *Front. Immunol.* 9, 302, 2018.
- [4]. Platon VM, Dragoi B, Marin L. Erythromycin formulations - a journey to advanced drug delivery. *Pharmaceutics* 14(10), 2180, 2022.
- [5]. Haight TH, Finland M. Resistance of bacteria to erythromycin. *PSEBM.* 81(1), 183–188, 1952.



OLD COMPOUNDS, NEW PURPOSE: IODINE-SUBSTITUTED PYRROL-2-ONES FOR TARGETED ANTITUMOR THERAPY

**Cristina M. Al-Matarneh,^{1*} Natalia Simionescu,¹ Ashraf Al-Matarneh,^{1,2}
Ionel I. Mangalagiu²**

¹*Petru Poni Institute of Macromolecular Chemistry, Romanian Academy, Iasi, Romania*

²*Alexandru Ioan Cuza University of Iasi, Faculty of Chemistry, Iasi, Romania*

**almatarneh.cristina@icmpp.ro*

1. Introduction

Cancer remains a major global health challenge, responsible for approximately 1 in every 6 deaths and affecting nearly every household. In 2022, around 20 million people were diagnosed with cancer, with about 9.7 million deaths attributed to the disease. This burden is expected to rise by 77% by 2050, placing immense pressure on healthcare systems and communities [1]. The disease affects not only individuals' health and well-being but also carries profound social and economic consequences, particularly as it often strikes individuals during their prime working years. This leads to reduced workforce productivity and increased healthcare costs, thereby hampering sustainable development. Among the most prevalent cancers globally are breast, lung, colon and rectal, and prostate cancers. Lung cancer led to the highest number of cancer-related deaths in 2020, while breast cancer was the most frequently diagnosed. Despite advancements in treatment, current therapies are often limited by side effects and drug resistance, emphasizing the need for continued research into safer and more effective anticancer drugs [2].

A promising area of such research lies in the development of N-heterocyclic compounds, which contain nitrogen and often other heteroatoms like sulfur and oxygen, facilitating stronger interactions with DNA. These compounds are prevalent in pharmaceuticals, natural products, and biologically active molecules due to their diverse therapeutic effects [3]. Particular interest has been directed toward heteroaromatic compounds such as benzimidazoles, benzothiazoles, indoles, and quinolines for their anticancer properties, which include the inhibition of cell proliferation and induction of apoptosis. Notably, pyrrole and its derivatives stand out for their wide-ranging biological activities, including anticancer [4], antibacterial, antioxidant, and anti-inflammatory effects [5]. They also show potential as tyrosinase and carbonic anhydrase inhibitors, and in disrupting protein interactions critical to cancer progression. Given their multifunctional potential, designing new pyrrole-based molecules that can target multiple cellular pathways is a powerful strategy in modern drug discovery.

2. Experimental

Our aim was to repurpose hybrid molecules that have two iodine atoms on their sides and a core constituted of a small and active heterocycle, pyrrolo-2-one, respectively. Thus, we resynthesized the compounds starting from iodoaniline (1), aromatic substituted benzaldehyde (2, 6 or 8), pyruvic acid and a catalytic amount of trifluoroacetic acid in ethanol media (Figure 1) to obtain the desired derivatives. Despite employing conditions typically associated with the Doebner reaction—a well-established method for synthesizing quinolines—the electron-withdrawing nature of the substituted aniline directed the reaction pathway toward the formation of 1H-pyrrol-2(5H)-one derivatives (3a–n) rather than carboxyquinolines. [6].



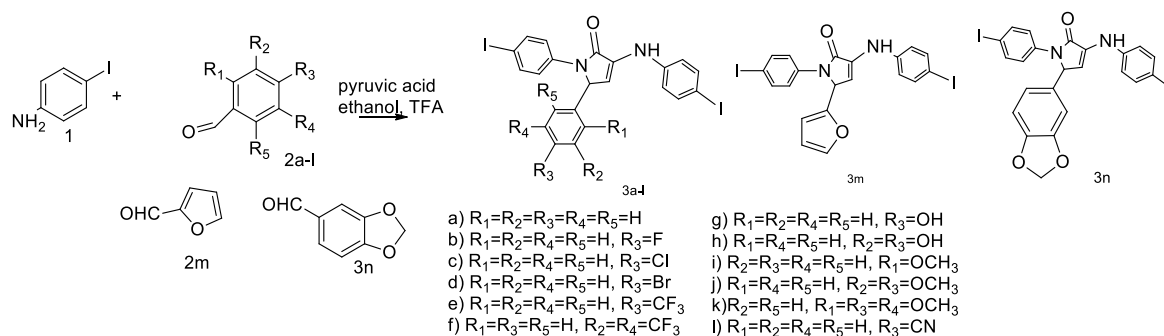


Figure 1. Reaction pathway to compounds 3a–n.

3. Results and discussion

The ADME profile of compounds 3a–n provides essential insights into their pharmacokinetic behavior and overall potential for drug development. By evaluating parameters such as gastrointestinal absorption, blood–brain barrier (BBB) permeability, metabolic stability, and potential interactions with cytochrome P450 enzymes, we can predict *in vivo* performance. High gastrointestinal absorption suggests good oral bioavailability, while limited BBB permeability may help minimize central nervous system side effects. Assessing CYP enzyme interactions further enables early identification of possible metabolic liabilities and drug–drug interactions. Our compounds demonstrated favorable gastrointestinal absorption and BBB permeability, though low water solubility remains a significant limitation that may affect bioavailability and formulation.

To complement these evaluations, we employed the CLC-Pred (Cell Line Cytotoxicity Predictor), a computational tool that predicts compound cytotoxicity across various human cancer cell lines based on machine learning models trained on large-scale experimental datasets. CLC-Pred assists in prioritizing candidates with the highest predicted efficacy, helping to streamline early-stage drug discovery and reduce reliance on costly *in vitro* testing. Particularly useful when exploring novel chemical scaffolds, this approach guided our compound selection prior to biological evaluation. Following the computational screening, we proceeded with *in vitro* testing.

The cytotoxic potential of the compounds was assessed in two stages. First, biocompatibility was evaluated on normal human gingival fibroblasts (HGF). At a concentration of 10 μ M, all compounds exhibited high biocompatibility, with cell viability exceeding 80%. At 50 μ M, compound 3h showed clear cytotoxicity, while compounds 3g, 3k, and 3l demonstrated moderate biocompatibility reductions, with viability values of 76%, 64%, and 77%, respectively.

In the next phase, all compounds were submitted to the National Cancer Institute (NCI) for single-dose (10^{-5} M) screening against the NCI-60 panel, which includes 60 human tumor cell lines representing leukemia, melanoma, and cancers of the lung, colon, central nervous system, ovary, kidney, prostate, and breast. Among the series, compounds containing trifluoromethyl or cyan substituents showed broad and potent growth inhibition across most cell lines, as reflected by low average growth percent (GP) values. Based on predetermined inhibition thresholds, compounds 3e, 3h, and 3l were selected for five-dose testing to determine GI₅₀, TGI, and LC₅₀ values, confirming their strong antiproliferative activity.

Despite osteosarcoma being the most prevalent primary bone malignancy in children and adolescents, it is notably absent from the NCI-60 panel. This omission presents a significant limitation, especially considering the tumor's aggressive nature and poor outcomes in advanced stages. Current treatments are largely confined to chemotherapy and surgery, with little therapeutic innovation in recent decades. One contributing factor is the lack of high-throughput drug screening models that incorporate osteosarcoma cell lines. Given the distinct genetic and resistance characteristics of osteosarcoma compared to other tumor

types, relying solely on surrogate models from the NCI-60 panel is scientifically inadequate.

To address this gap, we included two osteosarcoma cell lines, HOS and MG-63, in our *in vitro* evaluation. Encouragingly, the results from these tests demonstrated promising anticancer activity for several compounds, supporting their potential as leads for further development in osteosarcoma-specific therapies.

4. Conclusions

In this study, we successfully repurposed fourteen novel iodine-substituted pyrrol-2-one compounds as potential anticancer agents. The compounds were initially assessed through theoretical predictions, focusing on their antiproliferative potential and biocompatibility profiles. Experimental validation was conducted through the NCI-60 human tumor cell line screening, where all compounds were evaluated using standard internal protocols. Three compounds advanced to the second stage of testing, with their GI₅₀, TGI, and LC₅₀ values determined, indicating notable anticancer activity. Furthermore, all compounds were tested on osteosarcoma cell lines HOS and MG-63, addressing a critical gap not covered by the NCI-60 panel. The experimental results showed a strong correlation with the *in silico* predictions, reinforcing the reliability of the computational approach and supporting the potential of these compounds for further development as anticancer agents.

Acknowledgements

This work was supported by a grant of the Ministry of Research, Innovation and Digitization, CNCS/CCCDI-UEFISCDI, project number PN-IV-P8-8.1-PRE-HE-ORG-2023-0048, within PNCDI IV

References

- [1]. <https://www.iarc.who.int/>. Available at <https://www.iarc.who.int/> (Accessed on 15 August).
- [2]. Sung H, Ferlay J, Siegel RL, Laversanne M, Soerjomataram I, Jemal A, Bray F. Global cancer statistics 2020: GLOBOCAN estimates of incidence and mortality worldwide for 36 cancers in 185 countries. *CA Cancer J. Clin.* 71, 209–249, 2021.
- [3]. Akhtar J, Khan AA, Ali Z, Haider Z, Shahar Yar M. Structure-activity relationship (SAR) study and design strategies of nitrogen-containing heterocyclic moieties for their anticancer activities. *Eur. J. Med. Chem.* 125, 143–189, 2017.
- [4]. Geng Y, Wang X, Yang L, Sun H, Wang Y, Zhao Y. Antitumor activity of a 5-hydroxy-1H-pyrrol-2-(5 H)-one-based synthetic small molecule in vitro and in vivo. *PLoS One* 10, 1–15, 2015.
- [5]. Kabir A, Muth A. Polypharmacology: the science of multi-targeting molecules. *Pharmacol. Res.* 176, 106055, 2022.
- [6]. Al-Matarneh CM, Nicolescu A, Marinas IC, Chifiriuc MC, Shova S, Silion M, Pinteala M. Novel antimicrobial iodo-dihydro-pyrrole-2-one compounds. *Future Med. Chem.* 15, 1369–1391, 2023.



THE EFFECT OF MICELLIZATION ON THE EPR SPECTRA OF NITRONYL
NITROXIDES WITH ALKYL CHAINS RADICALS

**Alexandru Gabriel Bucur,^{1*} Alexandru V. F. Neculae,¹ Mihaela Lavinia Ciutu,¹
Georgiana Alexandra Sanda,^{1,2} Sevasti Matsia,¹ Gabriela Ionita¹**

¹*Ilie Murgulescu Institute of Physical Chemistry, Romanian Academy, Bucharest, Romania*

²*University of Bucharest, Faculty of Chemistry, Bucharest, Romania*

*abucur@icf.ro

1. Introduction

A series of nitronyl nitroxide radicals bearing alkyl chains with variable lengths from 2 to 9 C atoms was prepared and used to investigate their electron paramagnetic resonance (EPR) spectra in water and micellar solutions of sodium dodecyl sulphate. The analysis of the EPR spectra reveal that the nitronyl nitroxides with a long alkyl chain are more sensitive to the micelle formation.

2. Experimental

Materials: N,N'-(2,3-dimethylbutane-2,3-diyl)bis(hydroxylamine) synthesized in the laboratory following procedure described in literature [1]. Propanal, butanal, hexanal, octanal, nonanal, decanal, triethylamine, potassium periodate (KIO₄), sodium nitrite (NaNO₂) were purchased from Sigma Aldrich. The following solvents used for synthesis and purification were purchased from CHIMREACTIV.

Synthesis: In the first step, to a solution of N,N'-(2,3-dimethylbutane-2,3-diyl)bis(hydroxylamine) in methanol (MeOH) was added aliphatic aldehyde dissolved in a volume of 10 mL MeOH were added. The synthesis was carried out at reflux, equipped with a continuous stirring system, for 8 hours and monitored by thin layer chromatography (TLC). The nitronyl-nitroxide radicals were obtained as follows: the crude reaction mixture was cooled, diluted with 10 mL of distilled water, and treated with a saturated aqueous solution of NaHCO₃ to induce precipitation. Subsequently, the mixture was treated with a saturated KIO₄ solution to obtain the nitronyl-nitroxide radical. To purify each compound, extraction with DCM was used, followed by drying with anhydrous Na₂SO₄ and separation on a semi-preparative chromatographic plate.

EPR spectra: The EPR spectra of nitronyl nitroxides (2×10^{-4} M), in water and SDS 10^{-2} M water solutions were collected using Jeol FA-100 X-band spectrometer. The EPR parameters set for these measurements were: microwave power 1 mW, frequency 100 kHz, sweep field 100 G, center field 3217 G, sweep time 240 s, modulation width 1 G.

3. Results and discussion

A series of six nitronyl-nitroxides was obtained following a procedure described in Figure 1.

The eluents used for separation and the retention factor values, R_f, are specified in Table 1. Structural confirmation was obtained using electrospray ionization mass spectrometry.

The EPR spectra of nitronyl nitroxides in water and in 10^{-2} M SDS solution are shown in Figure 2. The EPR spectra of nitronyl-nitroxides usually show five lines due to the coupling of the unpaired electron with the two nitrogen atoms in their structures. In the case of nitroxides with an aliphatic chain shown in Figure 1, additional equally spaced lines appear due to coupling with the hydrogen atoms from the carbon atom adjacent to the heterocycle.

The spectra of each nitronyl nitroxide were simulated using the Winsim program to obtain the values of the



hyperfine splitting constants: a_{N1} , a_{N2} , and a_H . The values obtained are presented in Table 2. The spectral parameters of the six nitronyl nitroxides are not influenced by the length of the alkyl chain. It can be observed that in the case of radicals with a short alkyl chain, the value of a_H decreases in the SDS micellar solution. On the other hand, as the alkyl chain length increases, the a_N values decrease, which proves that the paramagnetic group penetrates deeper into the micelles.

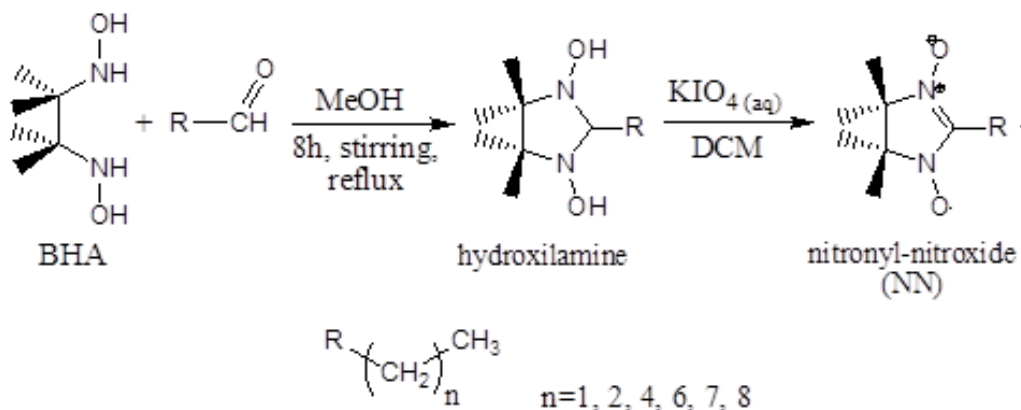


Figure 1. Synthesis scheme of nitronyl-nitroxide radicals with linear alkyl chain.

Table 1. Mixture of eluents, retention factor values, and m/z values corresponding to synthesized nitronyl nitroxides

Nitronyl-nitroxide	Eluent	R_f
NN-propanal	DCM:EA (3:7)	0.52
NN-butanal	DCM:EA (3:7)	0.48
NN-hexanal	DCM:EA (3:7)	0.43
NN-octanal	DCM:C5 (7:3)	0.40
NN-nonanal	DCM:EA:C5 (3:5:2)	0.54
NN-decanal	DCM:EA:C5 (3:4:3)	0.47

Table 2. The hyperfine coupling constants of NN in water and SDS 10^{-2} M.

Nitronyl-nitroxide	water			SDS		
	a_{N1}	a_{N2}	a_H	a_{N1}	a_{N2}	a_H
NN-propanal	8.2	8.2	2.2	8.2	8.2	1.9
NN-butanal	8.2	8.2	1.9	8.2	8.2	1.9
NN-hexanal	8.2	8.2	1.9	8.1	8.1	1.52
NN-octanal	8.2	8.2	1.9	8.15	8.15	1.92
NN-nonanal	8.2	8.2	1.9	7.9	7.9	1.9
NN-decanal	8.2	8.2	1.9	7.75	7.75	1.8

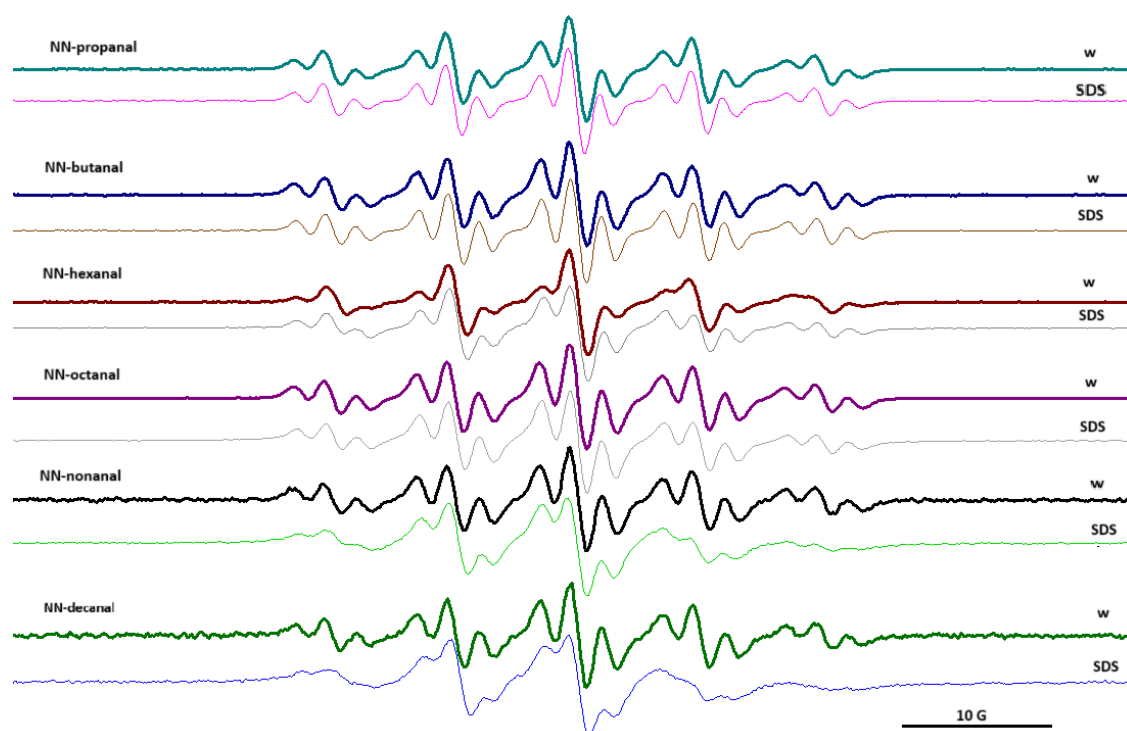


Figure 2. The EPR spectra of nitronyl-nitroxides (NN) in water and in SDS 10^{-2} M.

4. Conclusions

The experimental data obtained demonstrate that nitronyl-nitroxide spin probes with alkyl chains can be used to explore self-assembly processes in ionic surfactant solutions.

Acknowledgements

We gratefully acknowledge the financial support from project PNRR-III-C9-2023-I8 “Chemical host–guest molecular systems for health applications (OMRI for identification of inflammatory pathologies)”, contract no. 760283/27.03.2024, Romanian National Authority for Research, funded by European Union – NextGenerationEU.

References

- [1]. Constantinescu T, Ionita P, Chiorescu I, Ionita G. Hydrazyl, nitronyl-, and imino-nitroxides: synthesis, properties and reaction with nitric oxide and nitrogen dioxide. *Cent. Eur. J. Chem.* 4, 465–476, 2003.
- [2]. Hirel C, Vostrikova KE, Pecaut J, Ovcharenko VI, Rey P. Nitronyl and imino nitroxides: improvement of Ullman's procedure and report on a new efficient synthetic route. *Chem. Eur. J.*, 7, 2007–2014, 2001.
- [3]. Ulrich G, Zissel R. Synthesis of stable free radicals, *Tetrahedron Lett.*, 35, 1211–1214, 1994.

LIGNIN CARBON-BASED STRUCTURES: SYNTHESIS ROUTE AND PHYSICOCHEMICAL FEATURES

Irina Apostol,* Narcis Anghel

Petru Poni Institute of Macromolecular Chemistry, Romanian Academy, Iasi, Romania

**apostol.irina@icmpp.ro*

1. Introduction

Lignin is an aromatic biopolymer and by-product of the papermaking and biorefinery industries. Given its rich aromatic composition, lignin is a suitable material for the synthesis of carbon-based structures with interesting properties such as fluorescence, making it a promising compound for advanced functional applications [1]. Considering the above context, organosolv lignin, extracted from birch wood (OL) and Ecobinder lignin, extracted from flax (EL) were used as precursors to synthesize fluorescent carbon-based structures *via* a hydrothermal method.

2. Experimental

OL and EL were initially treated with HNO₃ at 90 °C under stirring for 4 hours, then cooled, washed and dried. After solvent addition, the sonicated mixtures underwent a thermal treatment (Table 1). The obtained suspensions were filtered, dialyzed 4 days, and dried at 60 °C, resulting in the lignin carbon-based structures coded as in Table 1.

Table 1. Conditions for the obtainment of carbon-based structures.

Sample cod	Solvent	Thermal treatment
OL-ac	Acetone	Autoclave (95 °C, 50 mbar, 8 h)
OL-et	Ethanol	
EL-ac	Acetone	
EL-et	Ethanol	

FTIR spectra of the obtained structures were recorded using a Vertex 70 FTIR spectrometer from Brüker. A Malvern Panalytical Zeta-sizer Advance Pro Red instrument (Malvern Panalytical Ltd., Malvern, UK) was used to analyze the particle size distribution and the zeta potential. Steady-state fluorescence and fluorescence lifetime decay were measured using a Horiba Fluoromax 4 spectrofluorometer (Horiba Ltd., Kyoto, Japan).

3. Results and discussion

FTIR spectra of lignins and the obtained structures are presented in Figure 1. Both lignin spectra present aromatic skeletal vibration related bands occurred at wavelengths between 1598 – 1420 cm⁻¹. At around 2900 cm⁻¹ are the signals attributed to stretching vibration of the –CH₃ and –CH₂– groups. Lignin-specific –CH₂– and tertiary C–H groups presented symmetric stretching vibrations at 2845 cm⁻¹. At around 3420 cm⁻¹ stretching vibration peaks of –OH are observed. In carbon-based structures spectra, the band at 1634 cm⁻¹ indicates sp²-hybridized carbon atoms with oxygen-containing groups, while the 1720 cm⁻¹ peak corresponds to non-conjugated C=O stretching due to HNO₃ treatment. These features suggest that the obtained compounds present the aromatic structure of lignins and have enhanced π -conjugation, explaining their fluorescence.



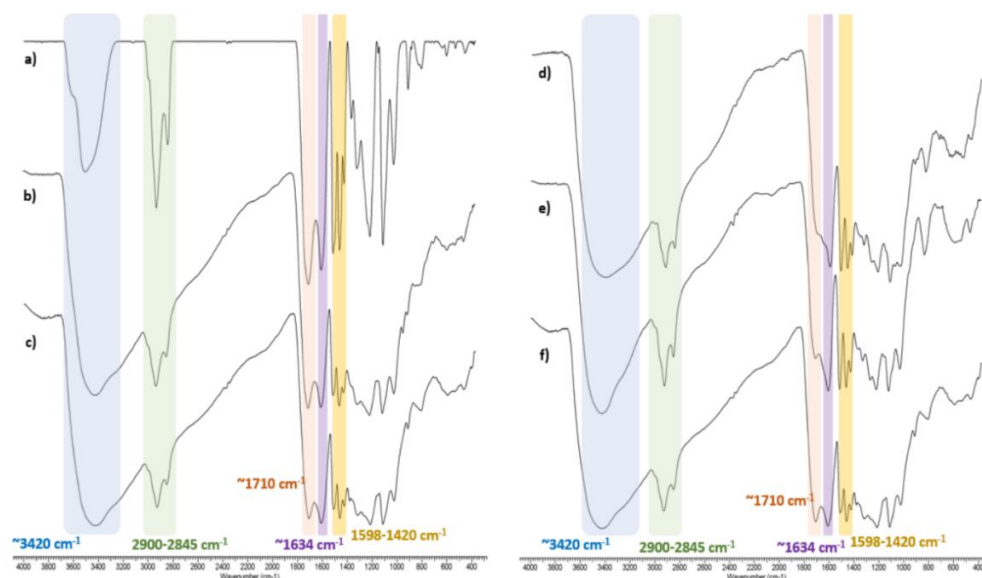


Figure 1. FTIR spectra of: (a) OL; (b) OL-ac; (c) OL-et; (d) EL; (e) EL-ac and (f) EL-et.

The fluorescence emission properties of the synthesized carbon-based structures revealed emissions in the blue-green region. As shown in Figure 2, increasing the excitation wavelength from 300 nm to 360 nm caused a gradual shifting in the direction of the long wavelength. The observed shift indicates the presence of multiple emissive states, likely arising from heterogeneous surface functional groups [2]. The fluorescence intensity of carbon structures derived from lignin is strongly influenced by its structural features/chemical composition. For example, Lignoboost lignin led to structures with higher fluorescence intensity [3] as compared to OL or EL. This enhancement could be attributed to its richer content of oxygen-containing functional groups which are known to improve photoluminescent properties.

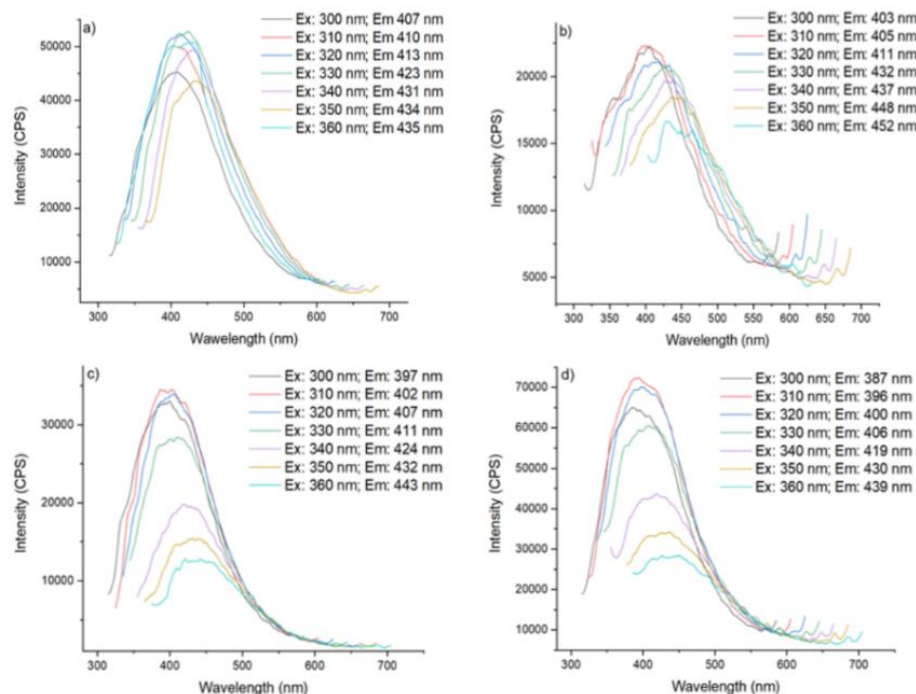


Figure 2. Fluorescence emission spectra of: (a) OL-ac; (b) OL-et; (c) EL-ac and (d) EL-et dispersed in water at 1 mg/mL concentration under different excitation wavelengths.

The time-resolved emission spectra of the carbon-based structures solutions, fitted with a multi-exponential decay model, revealed an average lifetime ($\langle\tau\rangle$, ns), between 5.01 and 5.95 ns (Table 2). Surface functional



groups influence structures fluorescence lifetime. Therefore, OL and FL-based carbon structures presented the lowest $\langle\tau\rangle$ as compared with Lignoboost derived structures [3].

Table 2. Fluorescence lifetime decay curve fitting parameters of the obtained carbon-based structures.

Sample	τ_1 (ns)	a_1	f_1	τ_2 (ns)	a_2	f_2	τ_3 (ns)	a_3	f_3	χ^2	$\langle\tau\rangle$ (ns)
OL-ac (Em=423 nm)	1.36	0.18	0.06	2.72	0.12	0.07	5.44	0.70	0.87	0.90	5.01
OL-et (Em=432 nm)	0.12	0.71	0.07	1.78	0.18	0.26	7.33	0.11	0.67	1.11	5.38
EL-ac (Em=402 nm)	1.53	0.05	0.01	3.06	0.06	0.03	6.12	0.89	0.95	0.92	5.95
EL-et (Em=396 nm)	2.17	0.16	0.51	8.94	0.02	0.30	0.16	0.81	0.19	0.77	5.81

DLS analysis revealed that obtained structures with acetone as solvent have a smaller hydrodynamic diameter as compared to those obtained with ethanol (Table 3). Moreover, their low zeta potential values suggest improved colloidal stability as compared with structures obtained using ethanol. Similar behavior was observed for Lignoboost-derived carbon-based structures, their particle size and zeta potential being influenced by the solvent used during the thermal treatment [3].

Table 3. Hydrodynamic diameter and zeta potential for the obtained carbon-based structures.

Sample	Hydrodynamic diameter	Zeta potential
OL-ac	395.6 ± 26.12	-32.41 ± 0.54
OL-et	613.8 ± 81.8	-31.72 ± 0.67
EL-ac	466.5 ± 127.9	-26.47 ± 1.34
EL-et	484.9 ± 44.99	-17.95 ± 1.32

4. Conclusions

Lignin carbon-based structures were obtained by HNO₃ assisted hydrothermal method, followed by thermal treatment. The negative values of zeta potential suggested a good stability of the particle in water. Also, they demonstrated excitation-dependent fluorescence emission behavior. The fluorescence data supported the heterogeneous composition of the carbon-based structures due to the complex structure of lignin, as evidenced by FTIR analysis. This study offers approaches for transforming biomass-derived lignin waste into high-value products with a reduced carbon footprint.

Acknowledgments

The authors are thankful for the financial support from the grant of the Romanian National Authority for Research, project no. PNRR-III-C9-2022-I8-291, contract no. 760081/23.05.2023, within the National Recovery and Resilience Plan.

References

- [1]. Yao M., Bi X., Wang Z., Yu P., Dufresne A., Jiang C. Recent advances in lignin-based carbon materials and their applications: A review. *Int. J. Biol. Macromol.* 223, 980–1014, 2022.
- [2]. Chen ML, Zhai JC, An YL, Li Y, Zheng YW, Tian H, Shi R, He XH, Liu C, Lin X. Solvent-free pyrolysis strategy for the preparation of biomass carbon bots for the selective detection of Fe³⁺ ions. *Front. Chem.* 10, 940398, 2022.
- [3]. Coroaba A, Apostol I, Dascalu IA, Bele A, Marangoci NL, Doroftei F, Uritu CM, Spiridon I. Exploring the characteristics of carbon structures obtained from LignoBoost lignin. *Polymers.* 17(9), 1221, 2025.



SUSTAINABLE PET RECYCLING THROUGH DESIGN THINKING: CIRCULAR CHEMISTRY SOLUTIONS

**Andra-Cristina Enache,* Petrisor Samoila, Corneliu Cojocaru,
Ionela Grecu, Valeria Harabagiu**

Petru Poni Institute of Macromolecular Chemistry, Romanian Academy, Iasi, Romania

**enache.andra@icmpp.ro*

1. Introduction

Plastic pollution has become one of the most pressing environmental challenges of our time. Global plastic production has surged dramatically, increasing from just 2 million metric tons in 1950 to over 400 million metric tons by 2022. Among various types of plastics, polyethylene terephthalate (PET) plays a dominant role, particularly in the packaging sector, which alone accounts for nearly 44% of total plastic consumption. Alarmingly, more than 90% of the approximately one million PET bottles sold every minute are not properly recycled; instead, they end up in landfills or the natural environment—where they can persist for centuries and contribute to long-term pollution [1]. The urgent need to develop sustainable solutions for plastic waste management has led to increased research efforts focused on circular economy principles.

In this context, the Plan-C project — Moving PLastics and mACHine iNDustry towards CirculariTy — unites 14 partners from across the Danube Region to drive circular economy transformations specifically in the plastics industry. The project offers a holistic and forward-looking framework to rethink the entire plastics value chain by fostering transnational collaboration based on the design thinking methodology. Its main goals are to co-create innovative circular plastic solutions, develop practical prototypes and guidelines tailored for SMEs, and align regional action plans with EU policies to support systemic and sustainable change [2].

Within Plan-C, the design thinking approach — an iterative five-phase process (empathize, define, ideate, prototype, test) — is especially effective in addressing the complex challenges of circularity in the plastics sector. This methodology enables stakeholder-driven solutions that balance technical feasibility with economic and environmental sustainability. Consequently, design thinking was applied to reimagine the PET recycling process from a systemic perspective, identifying key areas for improvement.

Chemical recycling, in particular, offers a promising pathway to recover valuable monomers from PET waste, potentially closing the material loop and reducing dependence on fossil resources. Thus, chemical recycling of PET waste, including both transparent and colored bottles, was performed via catalytic glycolysis using newly developed spinel ferrite catalysts. While this process efficiently produces BHET (bis(2-hydroxyethyl) terephthalate), a valuable monomer, an important and often overlooked challenge arises with colored PET waste. The embedded coloring agents persist in the liquid phase generated during depolymerization, resulting in distinctly colored residual solution. This issue raises significant environmental concerns, which are frequently neglected in PET recycling process. Effective management and removal of these dyes from the glycolysis medium is necessary to enable truly sustainable chemical recycling. Therefore, developing novel sorbents capable of selectively adsorbing these colorants is essential to reduce environmental impact and close the loop in circular PET recycling.

2. Results and discussion

Catalytic glycolysis for PET depolymerization

Catalytic glycolysis was employed to chemically recycle PET waste from two sources: transparent and colored water bottles. This process involves depolymerizing PET using ethylene glycol (EG) under



moderate temperatures, using a newly developed spinel ferrite-based catalyst. The catalyst accelerates reaction rates and enables a cleaner, potentially scalable process. As shown in Figure 1, the main product of this reaction is bis(2-hydroxyethyl) terephthalate (BHET), a valuable monomer that can be reused to produce new, recycled PET (r-PET).

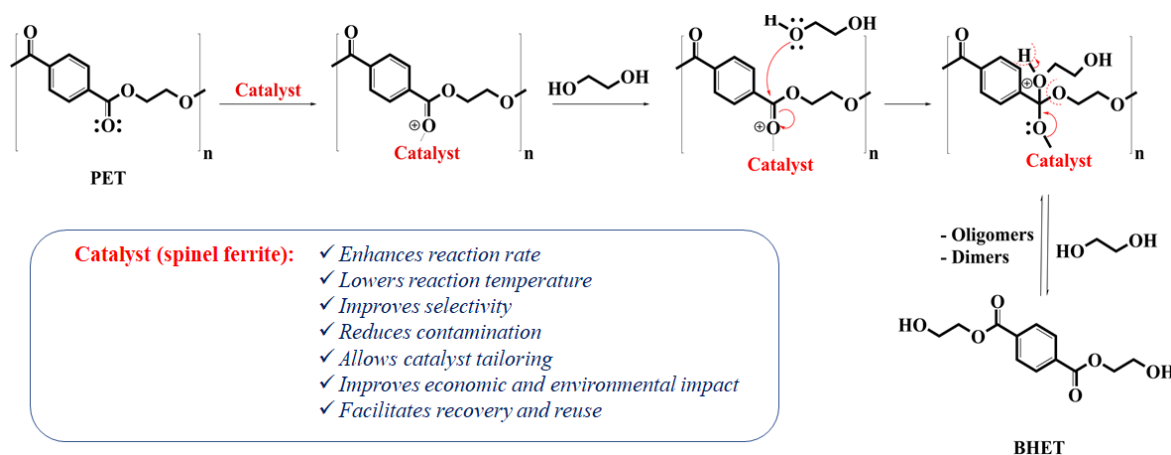


Figure 1. Possible catalytic glycolysis mechanism and role of the spinel ferrite-based catalyst [1].

The process demonstrates high efficiency, delivering over 90% monomer yield in less than one hour. It is designed for rapid operation and facile catalyst recovery, showing strong potential for industrial application, particularly in the manufacture of high-performance r-PET.

While the process yields high-purity BHET from both transparent and colored PET, a notable challenge emerges from the liquid phase generated during the glycolysis of colored PET. This phase retains intense coloration due to residual dye compounds embedded within the polymer matrix, which persist through depolymerization. The presence of this colored residue poses environmental concerns, representing a significant yet often overlooked challenge in the chemical recycling of colored PET. Addressing this issue is essential to achieve a sustainable recycling.

Biopolymeric magnetic composite beads for dye adsorption

To address dye removal from the residual phase of PET glycolysis, bio-based composite beads—previously developed from sodium carboxymethyl cellulose (CMC) ionically crosslinked with iron cations to form stabilized ionotropic hydrogels in beads form—were proposed as effective adsorbents [3]. Spinel ferrite nanoparticles, synthesized via sol-gel auto-combustion, were incorporated within the cellulose hydrogel matrix to facilitate magnetic separation of the beads from aqueous solutions.

The beads were thoroughly characterized structurally, morphologically, and magnetically. Initial adsorption tests were conducted using methylene blue, a common model dye for persistent colorants. Kinetic studies revealed that dye adsorption follows a pseudo-first-order (PFO) model, while equilibrium data fit well to the Langmuir isotherm, indicating monolayer adsorption on a homogeneous surface. The maximum adsorption capacity was 234 mg/g for methylene blue at 300 K. Thermodynamic analysis showed the adsorption process to be spontaneous (negative ΔG) and exothermic (negative ΔH), confirming the beads' efficiency under mild conditions. Molecular docking studies suggested that the primary interaction mechanism between methylene blue and CMC involves electrostatic Coulomb forces between the negatively charged carboxylate ($-\text{COO}^-$) groups of CMC and the positively charged amino groups of the dye.

Circular principles: recover, regenerate, reuse

The developed sorbent demonstrated excellent reusability, achieving up to 93% desorption efficiency following acetone immersion, while maintaining adsorption capacity across multiple cycles and with various persistent dyes. These desorption assays confirmed that the magnetic beads can be efficiently

recovered, regenerated, and reused without significant performance loss, underscoring their potential for integration into circular wastewater treatment systems.

Moreover, heat treatment of spent beads at 700 °C can enable recovery of the spinel ferrite nanoparticles from the composite beads. This recovery process highlights an important step in material reuse. This closed-loop approach exemplifies the principles of circular chemistry by enabling recovery, regeneration, and reuse of key materials in the recycling process.

4. Conclusions

This study proposes a practical and integrated solution to improve PET recycling, combining principles of circular chemistry and design thinking. The newly developed spinel ferrite catalysts effectively break down both transparent and colored PET into valuable BHET monomers, offering a scalable and environmentally friendly chemical recycling method. To address the issue of the liquid phase generated during glycolysis of colored PET, bio-based magnetic composite beads were introduced as efficient dye adsorbents. These beads show high adsorption capacity, spontaneous and exothermic dye uptake, and can be easily recovered, regenerated, and reused.

A key advantage of the spinel ferrites is their dual role: they serve both as catalysts for PET depolymerization and as magnetic components in the adsorbent beads. This allows for recovery and reuse of materials, helping to close the loop and support circular economy practices.

Overall, this combined catalytic and adsorption systems contributes to more sustainable PET recycling by lowering environmental impact, improving process efficiency, and supporting the development of circular plastic value chains in line with EU policy goals. Future work will focus on optimizing the adsorption system for the colored residual solutions from PET glycolysis.

Acknowledgements

The project Moving PLastics and mAchine iNdustry towards Circularity — acronym Plan-C (ID: DRP0200194), supported by the Interreg Danube Region Programme co-funded by the European Union, is kindly acknowledged.

References

- [1]. Enache AC, Grecu I, Samoilă P. Polyethylene Terephthalate (PET) recycled by catalytic glycolysis: a bridge toward circular economy principles. *Materials*. 17, 2991, 2024.
- [2]. Plan-C Design Thinking. <https://interreg-danube.eu/projects/plan-c/library>. Accessed 1 Aug 2025.
- [3]. Enache AC, Grecu I, Samoilă P, Cojocaru C, Harabagiu V. magnetic ionotropic hydrogels based on carboxymethyl cellulose for aqueous pollution mitigation. *Gels*. 9, 358, 2023.



MODULATED TEMPERATURE DSC: FROM THEORY TO APPLICATIONS IN POLYMER CHARACTERIZATION

Paul Lazar

Laboratorium SRL Bucharest, Romania

paul.lazar@laboratorium.ro

1. Introduction

The principle of DSC as thermal analysis technique is presented together with the different types of instruments that are commonly used (power-compensation and heat-flux). In the conventional DSC experiment, we measure heat flow versus temperature and time. Processes like glass transition, crystallization, or melting, are measured by detecting differences in heat flow to a sample and reference material by heating or cooling at a constant rate. AC calorimetry is a technique that measures the specific heat capacity of a sample by measuring the heat flux generated when the sample temperature is periodically oscillated; it has been used extensively as a method for measuring specific heat capacity.

2. Results and discussion

Modulated Temperature DSC (MT-DSC) is a technique that combines periodic temperature control performed by AC calorimetry and constant rate temperature control performed by standard DSC measurement. A comparison of DSC and MT-DSC techniques is presented: DSC uses a single linear heating rate vs. MT-DSC which uses two simultaneous heating rates, linear and sinusoidal. The linear heating rate in MT-DSC provides the same total heat flow as standard DSC. The sinusoidal heating rate in MT-DSC permits separation of the total heat flow signal of DSC into two components: one called reversing heat flow which includes heat capacity, changes in heat capacity and most melting, while the second component, (called non-reversing / kinetic component) contains time-dependent transitions:

$$dH/dt_{(total)} = C_p dT/dt_{(rev)} + f(T,t)_{(non-rev)}$$

First term of the above equation corresponds to heat capacity, glass transition and most melting processes; the second term can be attributed to processes like enthalpic recovery, evaporation, crystallization, thermoset cure, protein denaturation, starch gelatinization, decomposition and some melting. The raw data in MT-DSC experiment are the time-dependent temperature of the sample (the two components combined) and its corresponding oscillating heat flux. The total heat flow is obtained by performing contour integration of the oscillating heat flow. Next, the heat capacity component is obtained by performing amplitude ratio calculations of the heat flow signal and temperature signal using Fourier transform same as in AC calorimetry. The kinetic component then is obtained by subtracting the heat capacity component from the total heat flow.

Advantages of DSC (MT-DSC limitations): relatively fast, 20 °C/min average heating rate vs. MT-DSC with an average heating rate of 3°C/min, relatively simple, provides single signal and requires only a few experimental parameters vs. MT-DSC which uses three signals (but more than ten available) and requires two additional experimental parameters: modulation period and modulation amplitude of the temperature.

Advantages of MT-DSC (DSC limitations): MT-DSC has two independent heating rates. The average heating rates can be as low as necessary to achieve desired resolution, while the modulated rate can be kept high to maintain sensitivity (with a single heating rate of DSC it is not possible to optimize sensitivity and resolution in a single experiment). MT-DSC provides an almost perfect heat capacity baseline due to the way the signal is calculated (real sensitivity to small transitions is limited by the straightness of the



baseline). MT-DSC greatly improves interpretation of the results because overlapping transitions can be separated into different signals (DSC data is often difficult to interpret because multiple transitions can occur in the same temperature range).

MT-DSC significantly improves the accuracy of the measurement of the initial crystallinity in semi-crystalline samples. The DSC calculation of crystallinity is often wrong (too high) because DSC fails to detect ongoing crystallization as the sample is heated. MT-DSC continuously measures heat capacity as well as heat flow. This makes possible to measure how the heat capacity of a material is changing during a reaction such as thermoset cure, crystallization, protein denaturation, starch gelatinization. It is recommended that new samples to be first analyzed by DSC then switch to MT-DSC when you need any of its advantages.

Results obtained using current MT-DSC are strongly dependent on modulation period and heating rate: long periods and low heating rates are necessary. Tzero (TM) technology developed by TA Instruments greatly reduces period and heating rate dependence. Tzero DSC gives independent sample and reference heat flows:

$$q_s = \Delta T_0/R_s - C_s dT_s/dt$$

$$q_r = (\Delta T_0 - \Delta T)/R_r - C_r (dT_s/dt - d\Delta T/dt)$$

The two signals are deconvoluted separately. The reference reversing and non-reversing heat flows are subtracted from sample corresponding signals.

Most common applications of MT-DSC are presented: the heat capacity of a material is the result of molecular motion within the material. If the heat capacity increases during a transition, the transition results in an increase in molecular mobility. Since heat capacity (J/g) is a function of sample weight, a decrease in weight should cause a decrease in Cp. By being able to measure heat capacity and heat flow at the same time, MT-DSC provides significantly more information than DSC, which can only measure heat flow. Examples: the molecular mobility (heat capacity) of epoxy resins decreases as the result of crosslinking but in the case of corn starch gelatinization (1st heat), the same parameter increases.

Regarding the reversibility of the transitions: MT-DSC separates the total DSC flow into two parts that does and does not respond to a change in heating rate; MT-DSC applies two heating rates; the linear heating rate provides the equivalent to DSC while the modulated (changing) heating rate permits the simultaneous measurement of the heat capacity component of the total heat flow. In general, only heat capacity and melting respond to the changing heating rate. Although heat capacity is a reversible thermodynamic property, the change in heat capacity during a transition is almost never reversible. The reversing and non-reversing signals of MT-DSC should never be interpreted as the measurement of reversible and non-reversible properties.

The frequency effect of MT-DSC: the frequency of its inverse, the modulation period, is an experimental parameter that controls the frequency of the experiment. The glass transition is the result of macromolecular (large scale) motion in a material. This is a co-operative motion between the molecules and therefore takes time (seconds). Because of the time required for macromolecular motion, the glass transition shifts to higher temperatures as the frequency of the experiment increases. The total signal of MT-DSC is calculated from the average value of the modulated heat flow signal which is only function of the average heating rate. Therefore, the heat flow value of the total signal does not change with frequency and the glass transition temperature does not change with the modulation period.

The reversing signal is calculated from the amplitude of the modulated heat flow signal, the glass transition seen in the reversing signal is frequency dependent and shifts to higher temperatures as the modulation period is shortened.



The non-reversing signal of MT-DSC is calculated by subtracting the reversing signal from the total signal, therefore in the region of glass transition, the non-reversing signal shows any enthalpic recovery in the sample and additional heat flow which is only the result of different response of the total and reversing signals to the modulation period. In order to calculate an accurate value for enthalpic recovery, it is necessary to correct for the frequency effect.

This is done in two ways: a) quench cool to at least 50 °C below T_g and run the sample under the same conditions as the original (aged) sample; subtract the area of the peak in the quenched-cooled sample from the area of the peak in the aged sample, b) cool the sample from a temperature above T_g and measure the area of the peak in the non-reversing signal; subtract this area from the area on heating of the aged sample.

References

- [1]. T_{zero} (TM) DSC Technology, T_{zero} (TM) MDSC(R), Robert L. Danley, TA Instruments presentation.
- [2]. DSC and MDSC: Ideal Techniques for Resins and Thermoset Polymer Characterization, TA Instruments presentation.



Laboratorium



PLASMA-ACTIVATED POLYMERS AND FORMULATIONS FOR
CANCER TREATMENT

Camelia Miron,^{1*} Luminita Marin,² Taishi Yamakawa,¹ Koki Ono,¹ Ryo Wakatsukasa,¹ Manuela Iftime,² Kenji Ishikawa,¹ Shinya Toyokuni,³ Masaru Hori,¹ Hiromasa Tanaka¹

¹Center for Low-temperature Plasma Sciences, Nagoya University, Nagoya, Japan.

²Petru Poni Institute of Macromolecular Chemistry, Romanian Academy, Iasi, Romania

³Department of Pathology and Biological Responses, Nagoya University,
Graduate School of Medicine, Nagoya, Japan.

*miron.camelia.s8@f.mail.nagoya-u.ac.jp

1. Introduction

Cancer is the second leading cause of death globally, exerting tremendous physical, emotional, and financial strain on individuals and families. Despite ongoing improvements in cancer therapy, the number of people affected by this devastating disease is increasing. Due to the unsatisfactory clinical results, new therapeutic approaches are urgently needed.

Cold atmospheric plasma (CAP) holds a promising perspective of becoming a new type of oncological therapy. CAP is used to treat a liquid that is transferred after irradiation to the treatment target, such as cancer cells or tissues [1-3]. The newly generated chemically active species in plasma induce a selective cytotoxic effect on cancer cells. Therefore, the plasma-activated liquids (PAL), as well as the development of drug delivery systems using these liquids to improve the bioavailability, provide a foundation for clinical applications to enhance selectivity during therapy, offering patients a more effective and less harmful option.

Cyclodextrins, nontoxic cyclic oligosaccharides with a lipophilic cavity and a hydrophilic outer surface, have aroused great interest because of their ability to interact with a large variety of guest molecules to form noncovalent inclusion complexes [4].

In this study, we present a method for structural modification of (2-hydroxypropyl)- β -cyclodextrin (HP β CD) by plasma for a selective cytotoxic effect on cancer cells. The antitumor effect of cold atmospheric plasma-activated HP β CD solution (PA-HP β CD) on breast cancer cell lines (MCF-7) and its selectivity in killing these cells, compared to non-tumorigenic epithelial cell lines (MCF-10A), was investigated. The structural characterization of the PA-HP β CD, as well as the formation of chemical compounds in plasma and reaction pathways, was analyzed.

2. Experimental

Plasma was ignited between stainless steel electrodes using a 60 Hz pulse power supply (Fuji Co., Ltd., Aichi, Japan) in argon gas. A quartz dish was used to irradiate 8 mL of a solution of 2-hydroxypropyl)- β -cyclodextrin solution (HP β CD) (24 mM). The plasma irradiated samples were investigated by LC-MS/MS and HPLC-RI, while the effect on the normal (MCF-10A) and cancer cells (MCF7) was tested by MTS assay. The analysis methods are presented in detail elsewhere [2]. Particle size and zeta-potential were investigated using an Otsuka Electronics particle size & zeta-potential analyzer.

3. Results and discussion

Cell viability was tested on the non-tumorigenic epithelial cell line (MCF-10A) and breast cancer cell line (MCF-7) by MTS assay. The plasma-treated solutions (T) were up to 16 times diluted in medium DMEM (-). The control sample (Ctrl) was incubated with the DMEM (-). The cells were also incubated with the untreated HP β CD (U). The MTS assay results showed that both types of cells were entirely killed when



incubated with untreated, plasma-treated, 1-fold, and 2-fold diluted samples when Ar gas was used in the discharge (Figure 1). A good selectivity was obtained for the 4-fold diluted samples, the MCF-7 being almost entirely killed (viability of $\sim 12.42 \pm 3.3$), while the MCF-10A cells were unharmed. The mechanism responsible for this selectivity may involve the reactive species (RONS) formation in plasma, but also some other chemical compounds derived from the chitosan precursor under plasma irradiation, further investigated by LC-MS/MS.

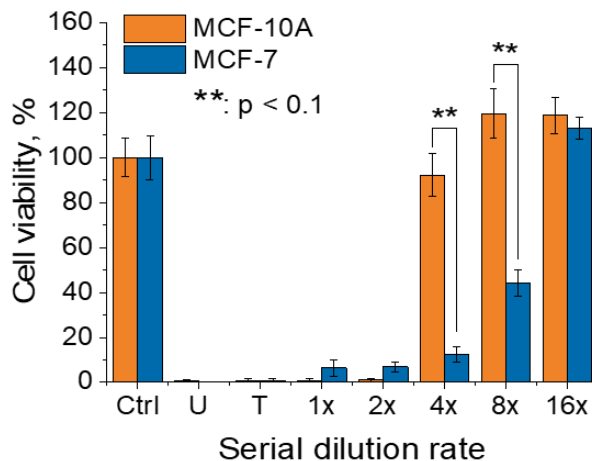


Figure 1. MTS assay of MCF-10A and MCF-7 cell lines incubated with untreated (U) and argon plasma-activated HPbCD undiluted (T) and diluted up to 16-fold in DMEM (-).

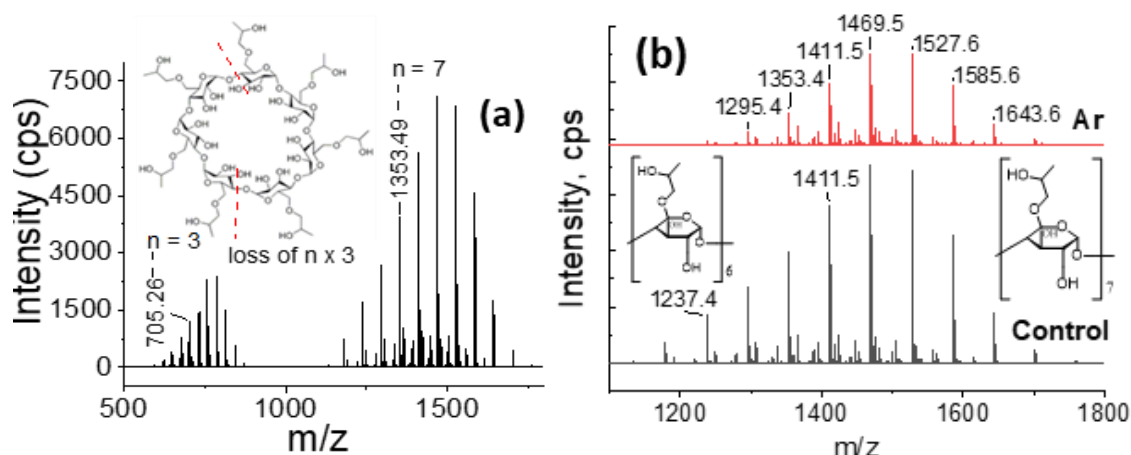


Figure 2. Mass spectra of (a) control HPbCD and (b) enlarged region of mass spectra for the control and argon plasma-activated HPbCD (1100 Da - 1800 Da).

The IDA TOF-MS ion scan mode for the control and plasma-treated solutions gave precursor molecular ions representing HPbCD $[\text{C}_{54}\text{H}_{102}\text{O}_{39} - \text{H}]^+$, m/z 1353.49 Da, and fragments formed in the ESI process in the range of 600 Da – 900 Da (Figure 2a and b). The mass spectra of control sample shows that fragmentation led to neutral loss of 46 Da (COOH) and 58.04 Da ($\text{C}_3\text{H}_6\text{O}$), and 17 Da (OH) (Figure 2a). The typical fragmentation of cyclodextrins proceeds through scission of the 1,4-glycosidic bonds between glycoside units to yield linear fragments with 162 Da (the mass of one glycoside unit) sequence [5]. The mass spectra of the plasma-treated samples look almost same; however, it can be clearly seen that one unit from the HPbCD structure (m/z 1179.37) could not be identified (Figure 2b). This implies that the precursor compound was modified in plasma and several other chemical structures were formed. The concentration of HPbCD samples decreased after plasma irradiation (Table 1). New compounds, such as beta-cyclodextrins ($[\text{C}_{42}\text{H}_{69}\text{O}_{35} - \text{H}]^+$, m/z 1133.58 g/mol), 2,3 dihydroxy-beta-cyclodextrin (m/z 1391.6), 2,3,4-trimethyllevoglucosan ($[\text{C}_9\text{H}_{16}\text{O}_5 - \text{H}]^+$, m/z 204.09), glucose ($[\text{C}_6\text{H}_{12}\text{O}_6 - \text{H}]^+$, m/z 179.04), alpha-keto-glutaric acid ($[\text{C}_5\text{H}_6\text{O}_5 - 2\text{H}]^+$, m/z 142.89), were identified in the mass spectra, and may be responsible for

the selective cytotoxic effect on cancer cells. The zeta-potential measurements showed positive values after the plasma treatment (Table 1), indicating an increased dispersion stability of the particles formed in plasma. Superficial groups formation with positive charges on the particles that tend to repel each other, leading to greater stability of the dispersion.

Table 1. Concentration and zeta-potential of control and plasma-activated HPbCD.

Sample	Concentration [mM]	Zeta potential [mV]
Control	24.01	-1.5
Ar	20.42	11.65

4. Conclusions

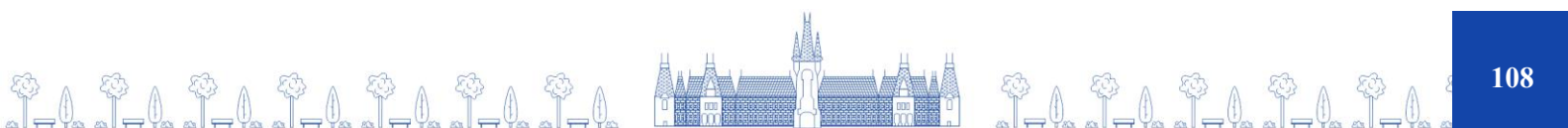
The selective antitumor effect of argon plasma-treated 2-hydroxypropyl-beta-cyclodextrin was present for MCF-7 cancer cells, leaving the normal MCF-10A cells unharmed, as a consequence of chemically active species formation in the discharge. Therefore, the plasma-activated liquids provide a foundation for clinical applications of combinatorial chemistry to enhance selectivity during therapy, offering patients a more effective and less harmful option.

Acknowledgements

This study was partly supported by JSPS-KAKENHI nos. 19H05462, 17H02805, 20H00142, 21H04451.

References

- [1]. Tanaka H, Hosoi Y, Ishikawa K, Yoshitake J, Shibata T, Uchida K, Hashizume H, Mizuno M, Okazaki Y, Toyokuni S, Nakamura K, Kajiyama H, Kikkawa F, Hori M. Low temperature plasma irradiation products of sodium lactate that induce cell death on U251SP glioblastoma cells were identified, *Sci. Rep.* 11 (1), 18488, 2021.
- [2]. Miron C, Andreica B, Iftime MM, Fifere A, Yamakawa T, Toyokuni S, Mizuno M, Tartau LM, Bejan A, Motooka Y, Kondo T, Sava I, Harabagiu V, Kumagai J, Tanaka A, Tanaka H, Marin L, Hori M. Cold plasma irradiation of chitosan: a straight pathway to selective antitumor therapy, *Int. J. Biol. Macromol.* 281, 136513, 2024.
- [3]. Sato K, Yang M, Nakamura K, Tanaka H, Hori M, Nishio M, Suzuki A, Hibi H, Toyokuni S. Ferroptosis induced by plasma-activated Ringer's lactate solution prevents oral cancer progression, *Oral Dis.* 30, 3912–3924, 2024.
- [4]. Poulson BG, Alsulami QA, Sharfalddin A, El Agammy EF, Mouffouk F, Emwas AH, Jaremko L, Jaremko M. Cyclodextrins: structural, chemical, and physical properties, and applications, *Polysaccharides* 3, 1–31, 2022.
- [5]. Blaj DA, Kowalczyk M, Peptu C. Mass Spectrometry of Esterified Cyclodextrins, *Macromolecules* 28, 1–34, 2023.



SUPRAMOLECULAR GOLD AGGREGATES WITH ENHANCED VISIBLE-LIGHT ABSORPTION FOR PHOTOTHERMAL APPLICATIONS

Elena-Laura Ursu

Petru Poni Institute of Macromolecular Chemistry, Romanian Academy, Iasi, Romania

ursu.laura@icmpp.ro

1. Introduction

Materials with broadband light absorption have gained significant interest due to their capability to effectively absorb light through a wide spectral range. Their remarkable physical and chemical properties make them promising candidates for various applications, including biotechnology [1,2]. While an ideal blackbody is an broadband photoabsorber that theoretically absorbs all incident light regardless of wavelength and polarization, real materials exhibit an absorption behavior determined by their composition and structure [3]. Attaining such an ideal blackbody absorber remains a challenge, although recent advances in the design of gold nanoparticle assemblies that closely mimic this behavior have brought closer to this goal. These black gold nanostructures utilize collective plasmonic effects to overcome the inherently narrowband response of individual nanoparticles, providing a promising route toward highly efficient optical absorbers.

Numerous synthesis strategies have been developed to produce black plasmonic gold nanostructures. One such method, described by *Kwon et al.*, involves a one-step, high temperature process to obtain black Au colloidal superstructures [4]. During synthesis, Au "superparticles" are formed by self-assembly of individual Au nanoparticles formed *in situ*, driven by solvophobic interactions between nanoparticles and solvent. Alternatively, *Dhiman et al.* reported an approach for fabricating black Au plasmonic colloidosomes by depositing individual Au nanoparticles onto dendritic fibrous nanosilica. The spacing between the particles within the resulting structure was precisely controlled by a cycle-by-cycle growth method [5]. This assembly exhibits broadband absorption in the entire visible and near-infrared range, due to the interparticle plasmonic coupling – through the formation of "hot spots" – and the heterogeneous size distribution of the Au nanoparticles. However, whether template-based, high-temperature, or electrochemical, these methods often involve complex, multi-step processes or specialized equipment, which limit scalability and reproducibility.

Although black gold nanostructures have been successfully demonstrated in various studies, achieving a straightforward, one-step synthesis of colloidal plasmonic black gold remains a considerable challenge

2. Experimental

For the obtaining of black aggregates of Au nanoparticles, a matrix, composed of guanosine, benzene-1,4-diboronic acid (BDDBA), lithium hydroxide (LiOH) and dextran, was prepared using adapted protocols [6,7]. Next, in the previously prepared solutions different volumes ranging from 100 μ L to 400 μ L of chloroauric acid (HAuCl₄) (1%) were added and the final reaction volume was adjusted at 2 mL with ultrapure water. Then, 25 μ L of NaOH (1M) were added, followed by stirring and heating the mixture at a temperature of 100 °C until a black suspension forms (about 5 minutes). Finally, the gold nanoparticles were washed twice with ultrapure water and separated by centrifugation (10000 rpm, 30 min). Nanoparticles used in subsequent experiments were redispersed in 500 μ L of ultrapure water. Various analysis techniques, such as UV-Vis spectroscopy, transmission electronic microscopy and FTIR spectroscopy, were applied to investigate the structural and chemical properties of the obtained Au aggregates solutions. Photothermal performance was evaluated under NIR-II excitation (1064 nm, 0.8 W cm⁻²) for gold assemblies. The cytotoxicity was evaluated by exposing melanoma cells (MeWo) to different concentrations of gold assemblies for 48 hours.



SERS (Surface Enhanced Raman Scattering) measurements were performed using methylene blue as model analyte.

3. Results and discussion

The present study describes a straightforward synthetic strategy involving the formation of Au-guanosine supramolecular structures that lead to the formation of gold nanoaggregates, with an intense and uniform absorption in a wide visible-NIR spectral range (Figure 1a) and high photothermal conversion efficiency (Figure 1b). The process implies the use of dextran-guanosine-BDBA matrix that at temperatures of 100 °C allows obtaining compact monodispersed Au aggregates with dimensions of about 50 nm.

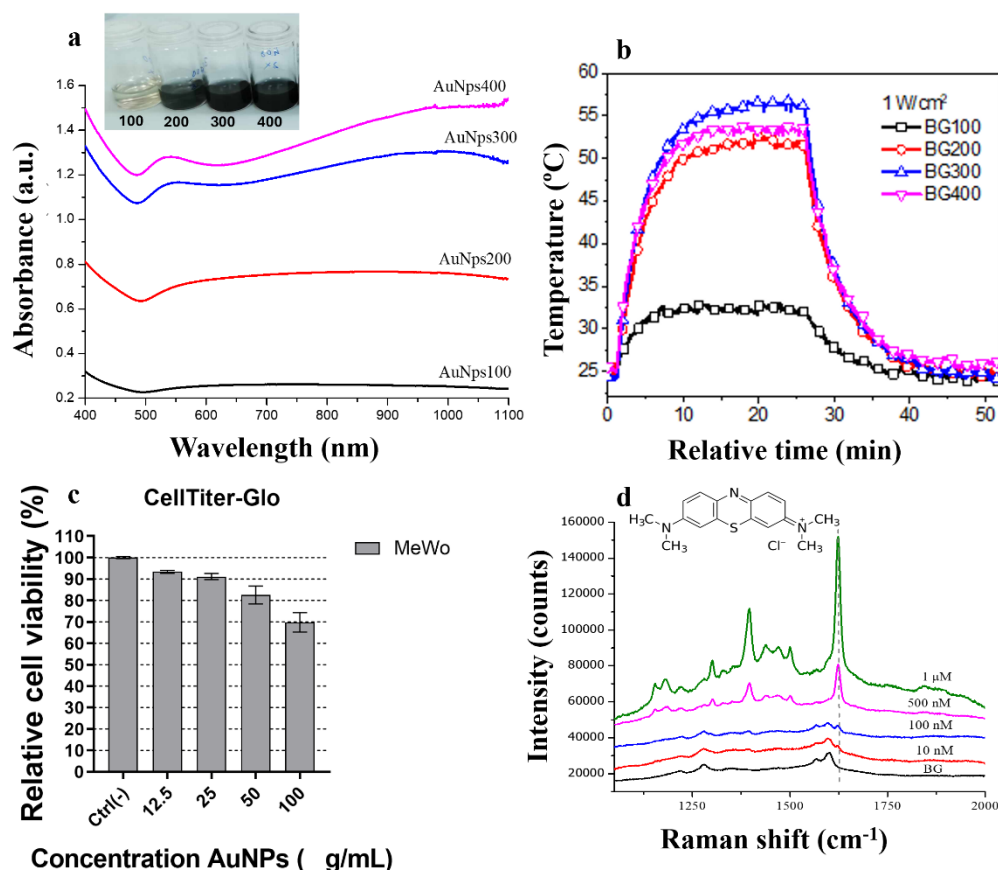


Figure 1. a) UV-Vis absorbance spectra of Au aggregates at different concentrations of HAuCl₄ (100–400 μL); b) Photothermal heating curves of Au assemblies at 1064 nm laser irradiation (1 W cm⁻²); c) Luminescence-based viability of MeWo cells after 48-hour exposure to Au solutions (12.5–100 μg/mL); d) SERS spectra of the methylen blue molecule, using λ=633 nm.

Evaluation of the photothermal conversion performance and aqueous dispersion photostability of the obtained supramolecular Au assemblies reveals an increase of 30 °C compared to the ambient temperature for a power density of the incident laser radiation of 1 W/cm² and a stable, reversible temperature response without significant loss of heating capacity.

To evaluate the cytotoxicity of Au assemblies, melanoma cells (MeWo) were exposed to varying concentrations for 48 hours. Cell viability was evaluated using the CellTiter-Glo assay, which quantifies cellular ATP levels through luminescence. Cell viability remained above 80% at 50 μg/mL but decreased to ~70% at the highest tested concentration (100 μg/mL), indicating a cytotoxic effect at higher doses.

The Au assemblies are a promising candidate for SERS detection because a large number of “hot spots” could be generated between adjacent close-packed individual gold nanoparticles. Herein, methylen blue was selected as the probe molecule to characterize the SERS performance of Au assemblies. Figure 1d

shows the SERS spectra of methylen blue solutions with different concentrations (10^{-6} to 10^{-8} M) measured in the presence of Au assemblies. Even for 10^{-8} M methylen blue solution, the characteristic peak at 1623 cm^{-1} can be clearly distinguished on obtained SERS spectrum, indicating that Au assemblies exhibits high sensitivity as a SERS substrate.

4. Conclusions

The proposed approach enables the preparation of black plasmonic gold assemblies using a guanosine–BDDBA–dextran template, yielding nanostructures with strong and uniform absorption in a wide visible–NIR spectral range, along with enhanced photothermal performance. Cytotoxicity evaluations confirmed the biocompatibility of the obtained nanostructures. The rapid and straightforward synthesized nanostructure with high photoconversion efficiency could be exploited in various photothermal applications and constitutes an important step towards the advancement of alternative methods of developing new materials and technologies, particularly where controlled light-induced effects are needed.

Acknowledgements

This work was financially supported by the Romanian National Authority for Research, project no. PNRR-III-C9-2023-I8-161, contract no. 760285/27.03.2024, within the National Recovery and Resilience Plan.

References

- [1]. Zhou J, Jiang Y, Hou S, Upputuri P K, Wu D, Li J, Wang P, Zhen X, Pramanik M, Pu K, Duan H. Compact plasmonic blackbody for cancer theranosis in the near-infrared II window. *ACS Nano*. 12, 2643–2651, 2018.
- [2]. Yu R, Wang J, Han M, Zhang M, Zeng P, Dang W, Liu J, Yang Z, Hu J, Tian Z. Overcurrent electrodeposition of fractal plasmonic black gold with broad-band absorption properties for excitation-immune SERS. *ACS Omega* 5, 8293–8298, 2020.
- [3]. Liu D, Zhou F, Li C, Zhang T, Zhang H, Cai W, Li Y. Black gold: plasmonic colloidosomes with broadband absorption self-assembled from monodispersed gold nanospheres by using a reverse emulsion system. *Angew. Chem. Int. Edit.* 54, 9596–9600, 2015.
- [4]. Kwon N, Oh H, Kim R, Sinha A, Kim J, Shin J, Chon J W M, Lim B. Direct chemical synthesis of plasmonic black colloidal gold superparticles with broadband absorption properties. *Nano Lett.* 18, 5927–3592, 2018.
- [5]. Dhiman M, Maity A, Das A, Belgamwar R, Chalke B, Lee Y, Sim K, Nam J-M, Polshettiwar V. Plasmonic colloidosomes of black gold for solar energy harvesting and hotspots directed catalysis for CO_2 to fuel conversion. *Chem. Sci.* 10, 6594–6603, 2019.
- [6]. Rotaru A, Pricope G, Plank T N, Clima L, Ursu E L, Pinteala M, Davis J T, Barboiu M. G-Quartet hydrogels for effective cell growth applications. *Chem. Commun.* 53 12668–12671, 2017.
- [7]. Sardaru M-C, Morariu S, Carp O-E, Ursu E-L, Rotaru A, Barboiu M. Dynameric G-quadruplex-dextran hydrogels for cell growth applications *Chem. Commun.* 59, 3134–3137, 2023.



ENHANCEMENT OF AUTOPHAGY-INDUCING COMPOUNDS BY NITROGEN
REACTIVE SPECIES FROM ATMOSPHERIC PRESSURE PLASMA

**Taishi Yamakawa,^{1*} Ayako Tanaka,² Miron Camelia,² Kenji Ishikawa,²
Masaru Hori,² Hiromasa Tanaka²**

¹*Department of Electronics, Graduate School of Engineering, Nagoya University, Nagoya, Japan*

²*Center for Low-temperature Plasma Sciences, Nagoya University, Nagoya, Japan*

**yamakawa.taishi.m3@s.mail.nagoya-u.ac.jp*

1. Introduction

Plasma-activated Ringer's lactate (PAL) solution, produced by plasma irradiation of Ringer's lactate solution has shown the potential to provide novel cancer therapeutic applications, alongside conventional therapies. Plasma generated in a gaseous mixture at an atmospheric pressure is easily and abundantly producing highly reactive species such as reactive nitrogen and oxygen species as well as plasma-activated organic species. It is well known that this kind of species has a significant effect for biomolecules including induction of the cell death or cell proliferation. Among various applications, PAL has selective anti-tumour effects compared to normal cells. To date, the effort of elucidating the mechanism including identifying selective anti-tumour agents and analysis of a biomolecule reaction is ongoing. As one of these efforts, it was reported that autophagy is induced by PAL on the cell death pathways [1]. The autophagy is one of the proliferation systems for cancer cells induced by the degradation of components in cells such as damaged organelles and proteins. It is expected that anti-tumour effects using PAL improve if the autophagy is suppressed in cancer cells. In this study, investigations of the autophagy induction condition were conducted, and the generation of an autophagy-inducing compound was discussed.

2. Experimental

Preparation of PAL solution

The PAL solution was prepared by irradiating Ringer's lactate solution (Otsuka Pharmaceutical Co., Ltd., Tokyo, Japan) with atmospheric pressure plasma. The plasma source used in this study was the same as that developed in our previous work [2]. Plasma irradiation was conducted within a metal chamber (FUJI Corporation, Aichi, Japan) equipped with a controllable gas composition system.

Cytotoxicity evaluation by MTS assay

MCF-7 human breast cancer cells were cultured in DMEM with 10% FBS and 1% penicillin/streptomycin under 5% CO₂ at 37 °C. To assess the effect of PAL solution on cell viability, 5000 cells were seeded and treated with PAL for 2 hours. After a total of 24 hours of culture, viability was measured using the Aqueous One Solution assay. Six replicate wells were used per PAL dilution for statistical analysis via Welch's t-test.

Protein expression analysis

LC3B (Cat. #3868; Cell Signaling Technology, Massachusetts, USA) expression was tested at 6 h after start of PAL treatment as an autophagy expression marker. The primary antibodies used for immunoblotting were against AKT (Cat. #4691; Cell Signaling Technology, Massachusetts, USA) and phosphorylated Akt (p-AKT) (Ser473) (Cat. #4060; Cell Signaling Technology, Massachusetts, USA). Antibodies against Actin (Cat. #ab179467; Abcam) were used as protein-loading controls.



Components analysis

LC–MS/MS was performed using a SCIEX X500 QTOF with an ESI source in negative-ion mode. Separation used a 150 mm × 2.1 mm, 5 μm column at 40 °C with a flow rate of 0.20 mL/min and a 10 min run time. Data were acquired in IDA mode, automatically conducting MS/MS at two energy levels to identify unknown compounds based on mass and fragmentation. H₂O₂ concentration in PAL was measured using a digital pack test device and a chemical probe for hydrogen peroxide (WAK-H₂O₂(C), KYORITSU CHEMICAL-CHECK Laboratory Corp., Kanagawa, Japan).

3. Results and discussion

To evaluate MCF-7 cells cytotoxicity by PAL solution, an MTS assay was conducted as shown in Figure 1(a). The cell viability was decreased under the conditions up to 1/64x dilution. To examine autophagy induction, expression of LC3B, which is a membrane component of autophagy-related protein, was investigated as shown in Figure 1(b). Even if LC3B was strongly expressed under higher concentration conditions, its expression was also observed under the lowest concentration condition. In addition, p-AKT was expressed for the 1/64x and lower diluted samples, although its expression was reduced at 1/32x, as shown in Figure 1(c). The trend of p-AKT expression corresponds to the cell viability results. Furthermore, co-expression of LC3B and p-AKT was observed even though they are known to be inversely correlated [3]. These results suggest that PAL can induce autophagy-related protein expression even under non-cytotoxic conditions, supporting cell survival through co-expression of LC3B and p-AKT.

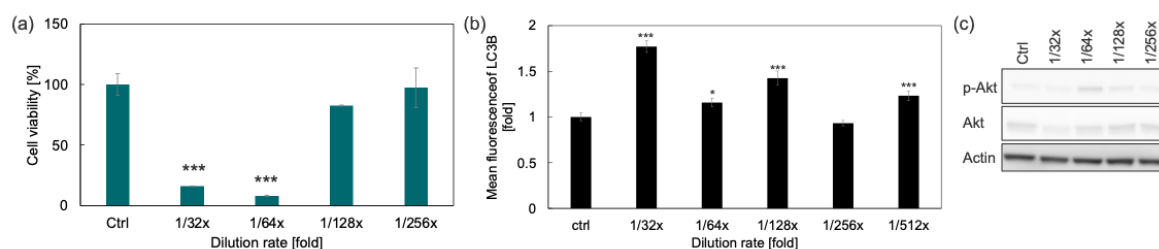


Figure 1. Cell response analysis. (a) cell viability at 24 h after start of PAL treatment; (b) the intensity from LC3B at 6 h, and (c) the expression of p-AKT and AKT at 6 h.

To explore the molecular basis of this effect, identification of autophagy inducers is ongoing. One such candidate is 2,3-dimethyltartrate which has the potential to induce cell death and autophagy [2]. It is important to generate this component at levels exceeding the threshold for inducing cell death. Fig. 2(a) and (b) showed extracted ion chromatograms of 2,3-dimethyltartrate identified in PAL solution under Ar/O₂ and Ar/N₂/O₂ gas conditions, respectively. The concentration was 6.9 μM and 9.0 μM, respectively. It is suggested that N₂-related active species play a role of enhancing the generation of 2,3-dimethyltartrate. Oxidation process by \cdot OH and H₂O₂ is needed on the generation pathway of 2,3-dimethyltartrate [4]. Nitrogen atom can induce \cdot OH [5], and it is possible that the \cdot OH derived from nitrogen atoms enhance the formation of H₂O₂ (Figure 2(c)). Although nitrogen-related reactive species do not directly participate in the formation of 2,3-dimethyltartrate, they have been shown to contribute to its increased production by promoting the generation of \cdot OH, which are essential for the reaction pathway.

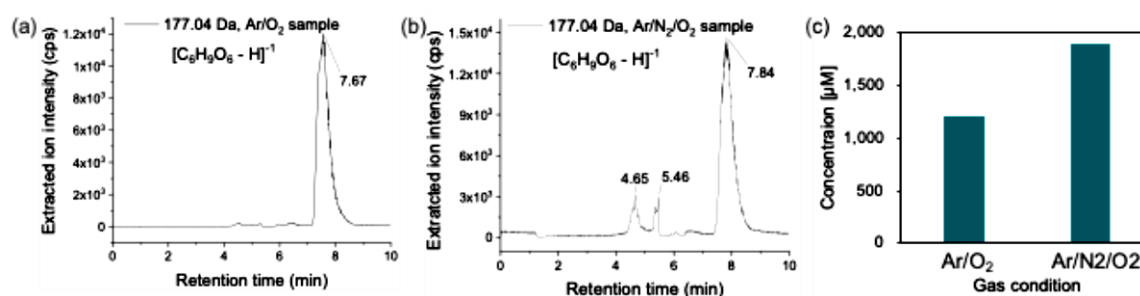


Figure 2. Synthesis of autophagy inducers under different gas conditions was evaluated; extracted ion chromatograms of 2,3-dimethyltartrate formed in (a) Ar/O₂ and (b) Ar/N₂/O₂ plasma; (c) H₂O₂ concentrations measured in PAL.

4. Conclusions

PAL was shown to induce autophagy-related proteins even under non-cytotoxic conditions, suggesting its involvement in cancer cell survival and treatment resistance. In addition, 2,3-dimethyltartrate was identified as a potential inducer, and nitrogen-related reactive species were found to promote its formation through \cdot OH generation.

Acknowledgements

This work was partly supported by a Grant-in-Aid for Specially Promoted Research (No. 19H05462), a Grant-in-Aid for Scientific Research (B) (No. 21H01072) and a Grant-in-Aid for Scientific Research (A) (No. 24H00202) from the Ministry of Education, Culture, Sports, Science and Technology of Japan.

References

- [1]. Jiang L, Zheng H, Lyu Q, Hayashi S, Sato K, Sekido Y, Nakamura K, Tanaka H, Ishikawa K, Kajiyama H, Mizuno M, Hori M, Toyokuni S. Lysosomal nitric oxide determines transition from autophagy to ferroptosis after exposure to plasma-activated Ringer's lactate. *Redox Biol.* 43, 101989, 2021.
- [2]. Yamakawa T, Tanaka A, Miron C, Nakamura K, Kajiyama H, Toyokuni S, Mizuno M, Hori M, Tanaka H. Effects of autophagy on the selective death of human breast cancer cells exposed to plasma-activated Ringer's lactate solution. *Free Radic. Res.* 3, 58, 758–769, 2024.
- [3]. Kaminsky VO, Zhivotovsky B. Free radicals in cross talk between autophagy and apoptosis. *Antioxid. Redox Signal.* 21(1), 86–102, 2014.
- [4]. Liu Y, Ishikawa K, Tanaka H, Miron C, Kondo T, Nakamura K, Mizuno M, Kajiyama H, Toyokuni S, Hori M. Organic decomposition and synthesis reactions in lactated solution exposed to nonequilibrium atmospheric pressure plasma. *Plasma Processes Polym.* 20(5), 1–14, 2023.
- [5]. Takamatsu T, Uehara K, Sasaki Y, Miyahara H, Matsumura Y, Iwasawa A, Ito N, Azuma T, Kohno M, Okinmo A. Investigation of reactive species using various gas plasmas. *RSC Adv.* 4(75), 39901–39905, 2014.



MULTIFUNCTIONALITY OF XANTHAN-BASED CRYOGELS ENRICHED WITH ANTHOCYANINS

Ioana-Victoria Platon, Irina Elena Raschip, Nicusor Fifere, Maria Valentina Dinu*

Petru Poni Institute of Macromolecular Chemistry, Romanian Academy, Iasi, Romania

**dinu.valentina@icmpp.ro*

1. Introduction

Food packaging significantly contributes to plastic pollution due to its slow decomposition rate [1]. Furthermore, conventional food labeling leads to avoidable waste, as products often remain safe beyond expiration dates [2]. Another significant concern is that packaging materials are typically inert, indicating that they do not impede microbial growth or prevent oxidative spoilage [3]. Traditional spoilage detection methods are time-consuming and can't be used for real-time monitoring [4]. In this context, colorimetric pH indicators offer a straightforward way to assess food spoilage and are typically composed of a biopolymeric matrix, a pH-sensitive dye and a cross-linker or immobilizing agent [5]. Recent research favors natural, food-grade pigments like anthocyanins over synthetic dyes due to toxicity concerns [6].

Polysaccharides act as effective matrices for anthocyanin immobilization, but solvent casting, a common fabrication method used for producing films can degrade anthocyanins and result in inconsistent performance of the material and pigment leaching [7]. In this regard, polysaccharide-based hydrogel systems offer enhanced versatility due to their high swelling, biodegradability, and good barrier properties [8]. Cryogels, a subtype of hydrogels created through freeze-thawing, exhibit higher porosity, improved mechanical strength and excellent elasticity [9]. The encapsulation of natural compounds such as anthocyanins into polysaccharide-based cryogels afford multifunctional characteristics, including super-absorbency, enhanced mechanical strength, improved antioxidant and antimicrobial properties and pH-responsiveness.

This study explores the development of xanthan gum (Xn)-based cryogels incorporating anthocyanin-rich bilberry (BLB) extract for real-time monitoring of Prussian carp (*Carassius gibelio*) spoilage [10].

2. Results and discussion

The first stage of the study aimed to obtain and characterize polyphenolic extracts from three berry species known for their high anthocyanin content: bilberries (*Vaccinium myrtillus* L., BLB), blackcurrants (*Ribes nigrum* L., BKC) and blackberries (*Rubus fruticosus* L., BBB and BBS) [11]. Chemical and chromatographic methods, as well as *in vitro* antioxidant activity assays were used. The stability of the extracts was also evaluated over time and across different pH levels. The phytochemical analysis showed that the BLB extract exhibited the highest polyphenolic content, featuring a rich profile of flavonoid glycosides (e.g., rutoside, hyperoside, etc.), phenolic acids (e.g., chlorogenic acid), and anthocyanins (e.g., cyanidin-3-glucoside, C3G). The *in vitro* antioxidant activity of BLB extract demonstrated its strong scavenging ability, achieving over 80% inhibition of 2,2-diphenyl-picryl-hydrazil (DPPH) after 5 minutes. Given the limited stability of the BLB extract in aqueous solutions—varying from 2 to 12 days depending on pH—encapsulation within polymeric matrices was considered essential to preserve its bioactive properties.

Therefore, the second part of the experimental work focused on the development and characterization of hybrid systems based on Xn and the BLB extract [11]. To assess the impact of formulation strategy and composition on the properties of the resulting biomaterials, Xn/poly(vinyl alcohol) (PVA) cryogels were obtained by freeze-thaw cycles. Chemically cross-linked Xn-based cryogels with 1,4-butanediol-diglycidyl



ether (1,4-BDGE), dried either by freeze-drying or in the oven were also prepared.

The successful incorporation of the BLB extract was confirmed by FTIR analysis. SEM analysis revealed a porous morphology in the case of freeze-dried cryogels whereas oven-dried samples showed a continuous structure, indicating that oven drying led to the collapse of the pores formed by cryogelation. The average pore sizes and pore wall thicknesses were dependent on material composition. Increasing the extract content resulted in more compact pore walls and a significant decrease in the average pore size. These changes are directly linked to the increased density of physical interactions determined by the polyphenolic compounds present in the BLB extract. Increasing the amount of the BLB extract in the biomaterial formulation influenced their mechanical properties. In freeze-dried cryogels, this resulted in network stiffening, and enhanced compressive strength. The double-cross-linked matrices exhibited even higher compressive strength values due to the additional reinforcement provided by chemical cross-linking. Furthermore, the incorporation of the extract increased the hydrophobic character of the cryogels, as reflected by the rise in contact angle values, and reduced the swelling ratio.

The Xn-based biomaterials were able to preserve the antioxidant activity of the BLB extract. Additionally, the presence of the extract significantly enhanced the antibacterial activity of the materials, achieving 100% inhibition against standard strains of *Salmonella typhimurium*, *Escherichia coli*, and *Listeria monocytogenes*. Another key finding was the improved stability of the extract following its incorporation into Xn-based biomaterials. This was evidenced by the relatively constant values of the colorimetric parameters observed over 42 days under acidic or alkaline pH conditions, and up to 50 days under ambient conditions.

The chemically cross-linked cryogel showed a rapid colorimetric response (within < 1 h) and a detectable color change ($\Delta E > 5$) upon exposure to ammonia concentrations ranging from 50 to 200 ppm (Figure 1A) demonstrating its potential as a freshness indicator for protein-rich foods.

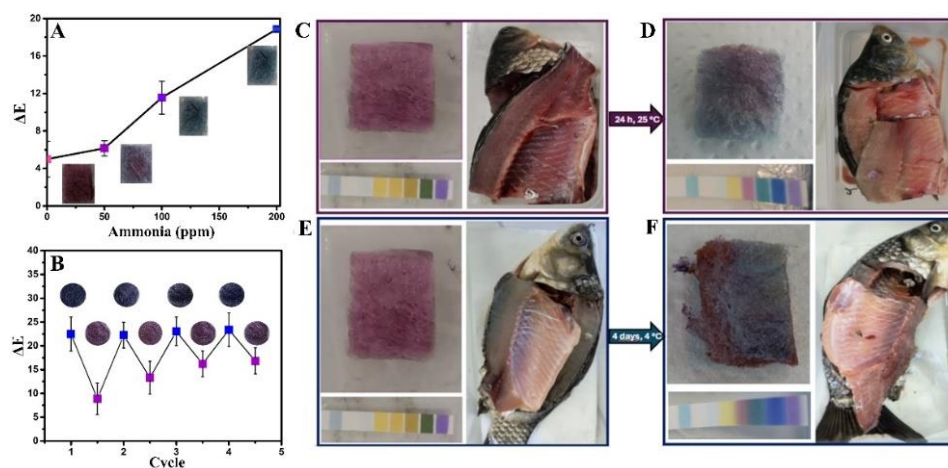


Figure 1. (A) Color difference (ΔE) after one hour of exposure to ammonia vapors of various concentrations; (B) color reversibility of the cryogel under alternating exposure to alkaline and acidic vapors; visual appearance of cryogel, pH indicator paper, and *Carassius gibelio* before (C, E) and after storage: 24 h at 25 °C (D) and 4 days at 4 °C (F). Adapted from ref. [11]

Additionally, the tested cryogel displayed reversible color changes: from pink to blue upon exposure to ammonia vapors, and back to pink when exposed to acetic acid vapors (Figure 1B). This reversible behavior was maintained even after four consecutive exposure cycles to acidic and alkaline conditions, confirming its recyclability and chromogenic stability. When the cryogel was placed in contact with two *Carassius gibelio* (Prussian carp) specimens — stored either for 24 h at 25 °C or for 4 days at 4 °C, a visible color change from pink to blue was observed attributed to the pH change of environment due to the diffusion of volatile amines released by the decaying meat (Figure 1C-F).

4. Conclusions

In summary, the bilberry extract was effectively entrapped within physically or double cross-linked Xn-based biomaterials. These hybrid biomaterials demonstrate a combination of mechanical strength, structural integrity, and multifunctional properties—antioxidant, antimicrobial, and chromogenic—underscoring their potential as pH-sensitive sensors for advanced food packaging solutions.

Acknowledgements

The authors are grateful for the financial support from projects PN-III-P1-1.1-TE-2021-1683 (TE6/2022) and PN-IV-P1-PCE-2023-1968 (4PCE/2025).

References

- [1]. Phelan A, Meissner K, Humphrey J, Ross H. Plastic pollution and packaging: Corporate commitments and actions from the food and beverage sector. *J. Clean. Prod.* 331, 331, 2022.
- [2]. Yu Z, Boyarkina V, Liao Z, Lin M, Zeng W, Lu X. Boosting food system sustainability through intelligent packaging: Application of biodegradable freshness indicators. *ACS Food Sci. Technol.* 3, 199–212, 2023.
- [3]. Yanat M, Schroen K. Bio-nanocomposites as future food packaging materials: A multi-faceted comparison. *React. Funct. Polym.*, 209, 1061842025.
- [4]. Khan S, Monteiro JK, Prasad A, Filipe CDM, Li Y, Didar TF. Material breakthroughs in smart food monitoring: Intelligent packaging and on-site testing technologies for spoilage and contamination detection. *Adv. Mat.* 36, 1, 2023.
- [5]. Pirayesh H, Park BD, Khanjanzadeh H, Park HJ, Cho YJ. Nanocellulose-based ammonia sensitive smart colorimetric hydrogels integrated with anthocyanins to monitor pork freshness. *Food Control.* 147, 109595, 2023.
- [6]. Zhai X, Sun Y, Cen S, Wang X, Zhang J, Yang Z, Li Y, Wang X, Zhou C, Arslan M, Li Z, Shi J, Huang X, Zou X, Gong Y, Holmes M, Povey M. Anthocyanins-encapsulated 3D-printable bigels: A colorimetric and leaching-resistant volatile amines sensor for intelligent food packaging. *Food Hydrocoll.* 133, 107989, 2022.
- [7]. Becerril R, Nerin C, Silva F. Bring some colour to your package: Freshness indicators based on anthocyanin extracts. *Trends Food Sci. Technol.* 111, 495–505, 2021.
- [8]. Ghiorghita CA, Platon IV, Lazar MM, Dinu MV, Aprotosoia AC. Trends in polysaccharide-based hydrogels and their role in enhancing the bioavailability and bioactivity of phytochemicals. *Carbohydr. Polym.* 334, 122033–122033, 2024.
- [9]. Dinu MV, Gradinaru AC, Lazar MM, Dinu IA, Raschip IE, Ciocarlan N., Aprotosoia AC. Physically cross-linked chitosan/dextrin cryogels entrapping *Thymus vulgaris* essential oil with enhanced mechanical, antioxidant and antifungal properties. *Int. J. Biol. Macromol.* 184, 898–908, 2021.
- [10]. Raschip IE, Platon IV, Fifere N, Darie-Nita RN, Aprotosoia AC, Dinu MV. Stabilization of anthocyanins in xanthan-based systems for synergistic cryogels with enhanced physicochemical and biological properties for visual freshness monitoring of Prussian carp (*Carassius gibelio*). *Food Hydrocoll.* 168, 111566–111566, 2025.



INTERACTION STUDIES OF CHITOSAN-*g*-PNIPAM MULTIRESPONSIVE CHAINS
WITH A MODEL PROTEIN

**Florin Bucatariu,^{1*} Marius-Mihai Zaharia,¹ Larisa-Maria Petrila,¹
Marcela Mihai,¹ Stergios Pispas^{1,2}**

¹*Petru Poni Institute of Macromolecular Chemistry, Romanian Academy, Iasi, Romania*

²*Theoretical and Physical Chemistry Institute,
National Hellenic Research Foundation, Athens, Greece*

*fbucatariu@icmpp.ro

1. Introduction

Chitosan is among the most important polysaccharides due to its versatility based on functional groups, which attract great interest in material science, medicine, pharmacy, engineering, etc. [1]. Chitosan complexation with proteins, is a process that gets significant attention in the research field due to its potential application as drug delivery systems with release controlled by medium stimuli (pH, ionic strength, temperature, etc.) [2,3]. This study presents the interaction of a model protein, human serum albumin (HSA) and grafted chitosan (Chit) with a RAFT polymerized poly(*N*-isopropylacrylamide) (PNIPAM). The main goal of the study was the understanding of the assembly process under various conditions, such as mixing order and molar ratio of the components, as well as the behaviour of the obtained Chit-*g*-PNIPAM/HSA complexes under modification of temperature.

2. Results and discussion

The effect of Chit-*g*-PNIPAM concentration, pH, temperature and ionic strength of the medium on the turbidity and rheological properties (viscosity) of solutions has been studied below and above copolymer lower critical solution temperature (LCST) [3] (Figure 1).

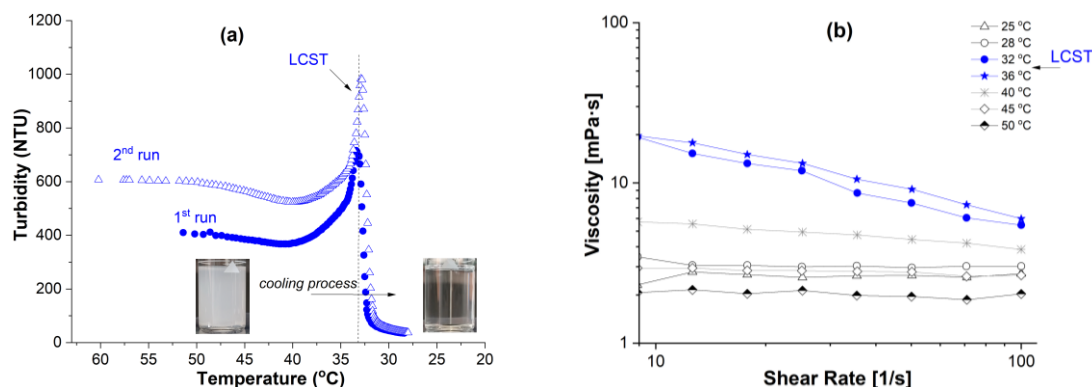
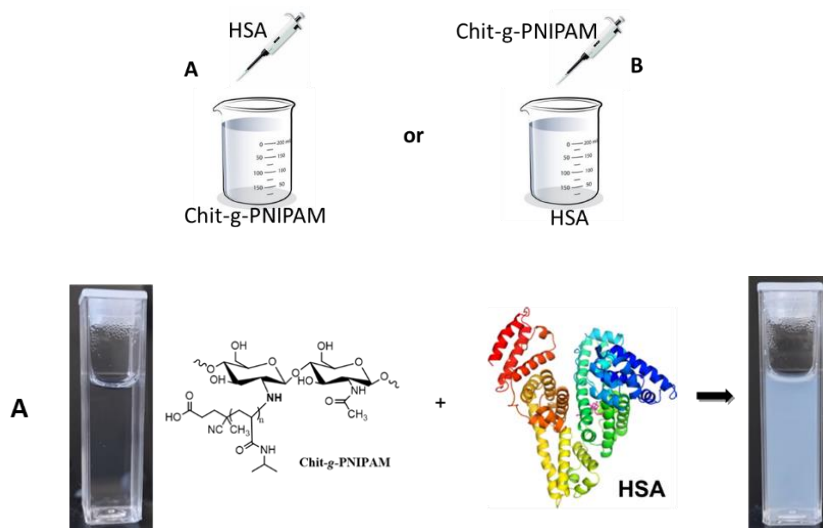


Figure 1. The turbidity (a) and viscosity (b) measurements of Chit-*g*-PNIPAM solution as a function of temperature.

The change in turbidity was measured as a function of temperature changes (Figure 1a), followed by a repeated cooling sequence, the Chit-*g*-PNIPAM concentration being kept constant (3.2 mg/mL). The initial turbidity has been generated by the collapsed chains, followed by a relative plateau region during cooling until 40 °C. Around LCST, the copolymer suspension presented an increase in turbidity, this fact being attributed to the swelling process of the previously formed Chit-*g*-PNIPAM nanoparticles. The fast solubilization process of the polymeric chains took place immediately after the spike. The shear viscosity was registered at high shear rate (10 – 100 1/s) as a function of temperature (25 – 50 °C). It was observed that the viscosity increased at temperatures situated around LCST, followed by a decrease with further

increase of temperature (Figure 1b). Therefore, LCST transition (changing of chains conformation due to the increase of hydrophobic interactions between the PNIPAM isopropyl groups) could be considered a transition between Newtonian and non-Newtonian (shear-thinning) behavior. Two series of complexes, $[\text{Chit-g-PNIPAM}]_5/[\text{HSA}]_x$ and $[\text{HSA}]_{100}/[\text{Chit-g-PNIPAM}]_x$ have been prepared by the dropwise addition of the titrant at different molar ratios between components (5:x and 100:x) calculated based on their average molar masses ($M_{\text{HSA}} = 66,000$ g/mol and $M_{\text{Chit-g-PNIPAM}} = 204,700$ g/mol) (Scheme 1).



Scheme 1. Hybrid nanostructures obtained by mixing Chit-g-PNIPAM with HSA (A) and HSA with Chit-g-PNIPAM (B).

In the first series of experiments (Scheme 1A), the Chit-g-PNIPAM/HSA complexes were formed by progressive immobilization of HSA protein molecules by Chit-g-PNIPAM chains, the complexes size increasing with HSA content. At the molar ratio $[\text{Chit-g-PNIPAM}]:[\text{HSA}] = 5:15$, the formed complexes are stable in time with a size of around 200-500 nm (Figure 2).

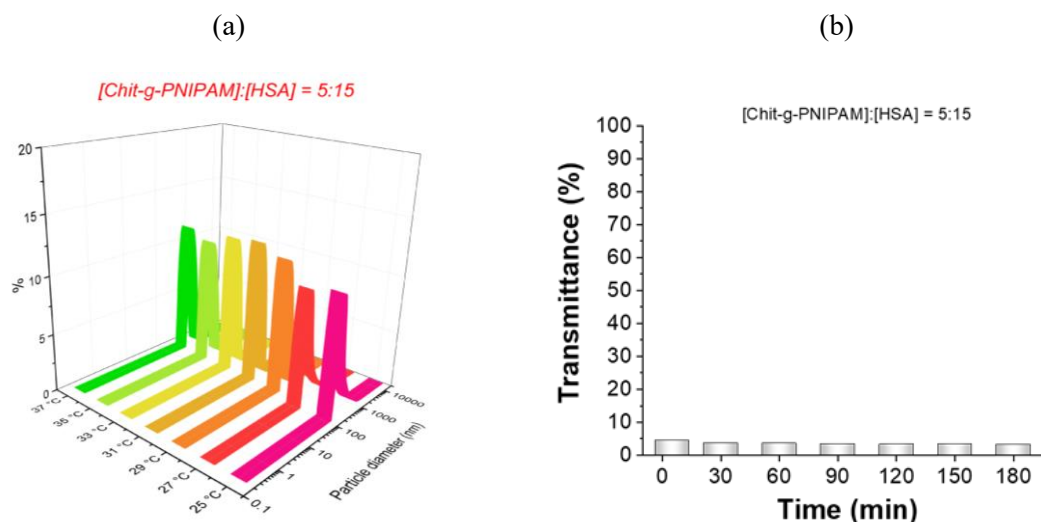


Figure 2. Particle size distribution as a function of temperature (a) and stability in time (b).

In the second series (Scheme 1B), the HSA/Chit-g-PNIPAM complexes agglomerated in large size aggregates (~600 nm) at a very low content of copolymer (100:2), this fact being attributed to the larger size of Chit-g-PNIPAM compared with protein macromolecules (Figure 3).

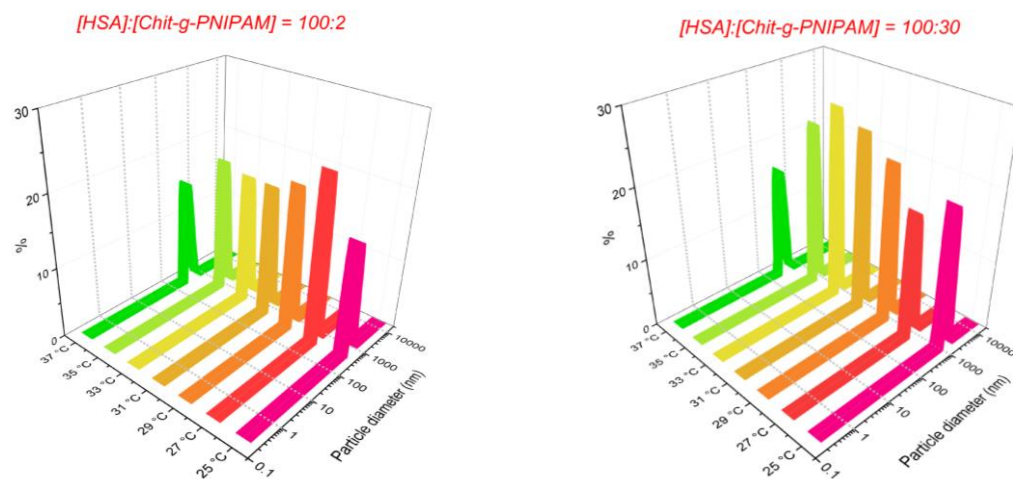


Figure 3. Particle size number distribution (%) as function of temperature (25 – 37 °C) at two molar ratios of components.

During further increase of Chit-g-PNIPAM concentration in the aqueous system ($[HSA]:[Chit-g-PNIPAM] = 100:30$), the newly introduced Chit-g-PNIPAM chains act like a macromolecular cross-linker, with the already formed HSA/Chit-g-PNIPAM complexes, producing flocs at micrometer size. The suspension stability was very low, with a large amount of sediments/coacervates being observed.

3. Conclusions

The Chit-g-PNIPAM chains and HSA macromolecules have been used to obtain protein/copolymer complexes. The aqueous solutions of the Chit-g-PNIPAM solution exhibited thermo-responsiveness, due to the PNIPAM side chains, with a LCST value at around 31–33 °C. The rheological parameters were influenced by the copolymer LCST value, with viscosity increases and decreases, before and after the LCST value, respectively. The order of component addition and the molar ratio influenced the size of the formed complexes.

Acknowledgements

This work was financially supported by the Romanian National Authority for Research, with project number PNRR-III-C9-2022-I8-201, within the National Recovery and Resilience Plan.

References

- [1]. Gao S, Holkar S, Srivastava S. Protein-polyelectrolyte complexes and micellar assemblies. *Polymers* 11, 1097, 2019.
- [2]. Turgeon SL, Schmitt C, Sanchez C. Protein-polysaccharide complexes and coacervates. *Curr. Opinion Colloid Interface Sci.* 12, 166–178, 2007.
- [3]. Zaharia MM, Bucatariu F, Karayianni M, Lotos ED, Mihai M, Pispas S. Synthesis of thermoresponsive chitosan-graft-poly(*N*-isopropylacrylamide) hybrid copolymer and its complexation with DNA. *Polymers* 16, 1315, 2024.



EVALUATION OF *BACCAUREA* PLANT FOR THEIR USE AS ANTIOXIDANT COMPOUNDS IN POLYMERIC MATERIALS

**Daniela Pamfil,^{1*} Elena Butnaru,¹ Benedict Samling,² Sim Siong Fong,²
Shafri Bin Semawi,² Mihai Brebu,¹ Elena Stoleru¹**

¹*Petru Poni Institute of Macromolecular Chemistry, Romanian Academy, Iasi, Romania*

²*University Malaysia Sarawak, Faculty of Resource Science & Technology, Sarawak, Malaysia*

**pamfil.daniela@icmpp.ro*

1. Introduction

Native to Malaysia's tropical rainforests, *Baccaurea* species are wild fruit trees widely recognized as traditional healing plants. In the last years, these species have gain interest due to their rich composition in a diverse type of bioactive compounds such us tannins, terpenoids, glycosides, phenols, flavonoids, alkaloids, volatile and fixed oils, carotenoids *etc.* [1]. While these compounds possess various therapeutic and healing properties, their stability and bioavailability in biological/physiological media are in general limited due to their susceptibility to oxidative degradation and their intrinsic hydrophobic nature [2]. Moreover, the extraction procedures of these bioactive compounds have a hindered feasibility since the process presents low product yield, e.g. for essential oils the extraction yield is approximately 0.35 % [3]. Considering these limitations, the incorporation of *Baccaurea* biomass as bioactive filler into aqueous polymeric systems represents a valuable approach [4]. It is well known that the vegetal biomass has a complex composition, therefore very difficult to accurately determine the exact bioactive compounds. *Baccaurea* biomass is also reach in volatile bioactive compounds, contributing to the overall bioactivity of the material. Hence, determination of the volatiles composition by pyrolysis-gas chromatography–mass spectrometry (Py-GC-MS) analysis can be successfully applied to obtain information about the bioactive compounds found in the biomass material. One of the targeted properties of the biomaterials is in general the antioxidant activity, alongside to the antimicrobial one. *Baccaurea* plants powders were incorporated into polymeric matrices based on chitosan and gelatin (CS/G) to exploit the potential of plants in their raw state and to improve their bioavailability and stability.




The current work presents the determination of volatile composition by Py-GC-MS and preparation of the biocomposite hydrogels based on chitosan/gelatin loaded with *Baccaurea* biomass powders. Three different species of *Baccaurea* trees, namely yellow *B. macrocarpa* (Bmy), white *B. macrocarpa* (Bmw) and *B. angulata* (Ba) were examined in this study. The main focus was on the evaluation of the antioxidant activity and the selection of the most bioactive biocomposite system.

2. Experimental

Fruits and leaves of Bmy, Bmw and Ba species were collected from Sarawak, Malaysia's forests, rinsed, air-dried, grinded, and stored in dark for further analysis. Sample codes are given in Table 1. The antioxidant capacity of bioactive compounds from Bmw, Bmy and Ba powders was evaluated using the DPPH assay. The experimental protocol was performed in two manners. One approach involved the direct contact of the plant powders with DPPH solution and the other one the preparation of an extract of the plant powders and its reaction with the DPPH solution. To validate the DPPH results, the ABTS test was also performed for the *Baccaurea* methanolic extracts. The release of light volatile compounds was determined by Py-GC-MS under the temperature program of 80 °C for 10 minutes. The polymeric matrix used as support for plant powders consisted in a hydrogel composite based on chitosan, gelatin and bentonite.



Table 1. *Baccaurea* plant species and their sample codes

<i>B. macrocarpa</i> white	<i>B. macrocarpa</i> yellow	<i>B. angulata</i>
		
Bmw	Bmy	Ba

3. Results and discussion

The antioxidant activity was tested by solvent extraction and direct contact with DPPH. The impact of different solvents (methanol, ethanol, PBS) on the *in vitro* antioxidant activities of *Baccaurea* extracts was evaluated. Figure 1 represents the UV-Vis spectra showing the antioxidant activity against DPPH of *Baccaurea* powder extracts in three different solvents. The methanolic extract of powders was identified as having the highest antioxidant activity, followed by the ethanolic and PBS extract. Comparing the antioxidant activity of the three *Baccaurea* plant powder (fruits and leaves), fruits powder of white *B. macrocarpa* (Bmw F) has registered the most increased values.

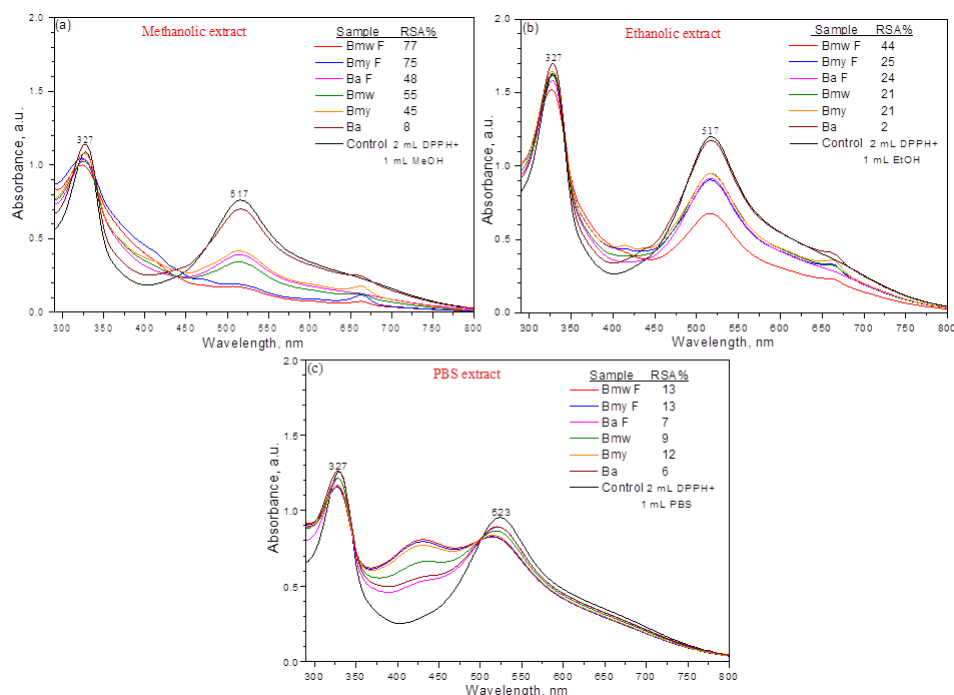


Figure 1. UV-Vis spectra of *Baccaurea* plant extract in methanol (a), ethanol (b), and PBS (c) in reaction with DPPH solution.

A similar trend was observed in the ABTS assay for the methanolic extracts, noticing also that ABTS values were considerably lower than their corresponding DPPH results. The DPPH assay that involves the direct contact of plant powder with the DPPH solution exhibited the highest antioxidant activity expressed as percentage radical scavenging activity (RSA %). The extract from *B. angulata* leaves seemed to behave differently from the fruit of the same species, showing values comparable to those of *B. macrocarpa* fruits.

Powder loaded xerogel materials could be used in various applications involving the release of bioactive compounds. To evaluate the retention of bioactive compounds by the polymeric matrix, the antioxidant activity was evaluated in methanolic extraction medium. Was observed that *Baccaurea* plant powders impart antioxidant activity to the CS/G polymeric matrix, although less active than the biomass powders.

This behavior could be due to the strong entrapment of *Baccaurea* powder in the xerogel matrix. The methanolic extract of xerogel loaded with BmwF powder exhibited the highest antioxidant activity among the tested *Baccaurea* extracts. The radical scavenging activity of *B. macrocarpa* fruits and leaves powders determined in direct contact with the DPPH solution was lower when comparing with the loaded CS/G xerogels. These enhanced values might be attributed to the presence of the clay component within CS/G xerogels which has the ability to preserve the antioxidant activity of the system acting as a protective stabiliser [5].

4. Conclusions

The antioxidant activity was tested on powders and loaded xerogels by solvent extraction (methanol, ethanol and PBS for powders and methanol for xerogels) and by direct contact assays. Fruits of *B. macrocarpa* displayed the strongest antioxidant activity *in vitro*, while the leaves of *B. angulata* showed the lowest antioxidant activity. Incorporation of *Baccaurea* powders into the CS/G xerogels led to materials with good antioxidant properties. Determining the most efficient extraction solvent in this study, could be useful for both food and pharmaceutical industries in preparing bioactive compounds extracts from *Baccaurea* powders. Volatile compounds, as terpenes and terpenoids, were identified into the *Baccaurea* powders. The antioxidant activity results were well correlated with the pyrolysis–gas chromatography–mass spectrometry data. This suggests that Py-GC-MS method can be useful as prescreening analytical technique in facilitating biomass selection with high-value bioactive potential for targeted applications in pharmaceuticals, nutraceuticals, and bioenergy applications.

Acknowledgements

This research was funded by the grant from the Ministry of Research, Innovation and Digitization, CNCS/CCCDI–UEFISCDI, project code PN-IV-P2-2_1-TE-2023-1725, HydroFib-ACT. We also thank the financial support provided by the European Union’s Horizon Europe research and innovation program under the Marie Skłodowska-Curie grant (HORIZON-MSCA-2021-SE-01-01: 101086360 VOLATEVS).

References

- [1]. Chamkouri H, Chamkouri M. A review of hydrogels, their properties and applications in medicine. *Am. J. Biomed. Sci. & Res.* 11(6), 2021.
- [2]. Yildiz AY, Öztekin S, Anaya K. Effects of plant-derived antioxidants to the oxidative stability of edible oils under thermal and storage conditions: Benefits, challenges and sustainable solutions. *Food. Chem.* 479, 143752, 2025.
- [3]. Samling BA, Assim Z, Tong WY, Leong CR, Rashid SA, Syazni Nik NN, Kamal M, Muhamad M, Tan WN. *Cynometra cauliflora* L.: An indigenous tropical fruit tree in Malaysia bearing essential oils and their biological activities. *Arab. J. Chem.* 14(9), 103302, 2021.
- [4]. Brebu M, Dumitriu RP, Pamfil D, Butnaru E, Stoleru E. Riboflavin mediated UV crosslinking of chitosan-gelatin cryogels for loading of hydrophobic bioactive compounds. *Carbohydr. Polym.* 324, 121521, 2024.
- [5]. Mansilla AY, Lanfranconi M, Alvarez VA, Casalengué CA. Development and characterization of bentonite/wGLP systems. *App. Clay Sci.* 166, 159–165, 2018.



SYNTHESIS OF AN INDOLOBENZAZOCINE DERIVATIVE FOR
INHIBITION OF TUBULIN POLYMERIZATION

**Marin-Aurel Trofin,* Irina Kuznetcova, Ioana-Antonia Iftimie, Mihaela Balan-Porcarasu,
Mihaela Dascalu, Gheorghe Roman, Maria Cazacu, Vladimir Arion**

Petru Poni Institute of Macromolecular Chemistry, Romanian Academy, Iasi, Romania

**marin.trofin@icmpp.ro*

1. Introduction

Cancer is a leading death cause worldwide, as well as an important impediment toward increasing life expectancy [1]. Even though cancer treatment has greatly improved in the last decades, this disease is still a major health, social and economic problem. From a physiopathological point of view, cancer is a failure of the regulatory mechanisms that control cell proliferation and differentiation. Since mitosis, the fifth phase of cell division cycle, is dependent on the cell's ability to polymerize tubulin into microtubules and to synthesize new DNA chains, emerging therapeutic strategies aiming to disrupt the processes involving tubulin and R2 ribonucleotide reductase (R2 RNR) have been considered in the last decades.

Latonduines (Figure 1a) belong to a group of alkaloids isolated from marine sponge *Stylissa carteri* that have been shown to exhibit anti-proliferative activity. The presence of an indole ring system fused to other heterocyclic rings and further expansion of the saturated ring to an eighth-membered heterocycle as in indolo[2,3-*e*]benzazocines (Figure 1b) resulted in high cytotoxicity, while homologous indolo[2,3-*f*]benzazonines (Figure 1c) also show anti-proliferative activity [2].

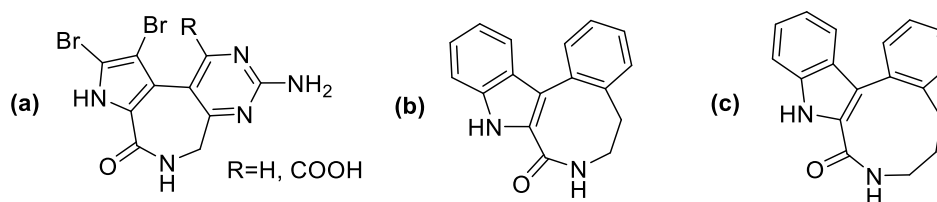


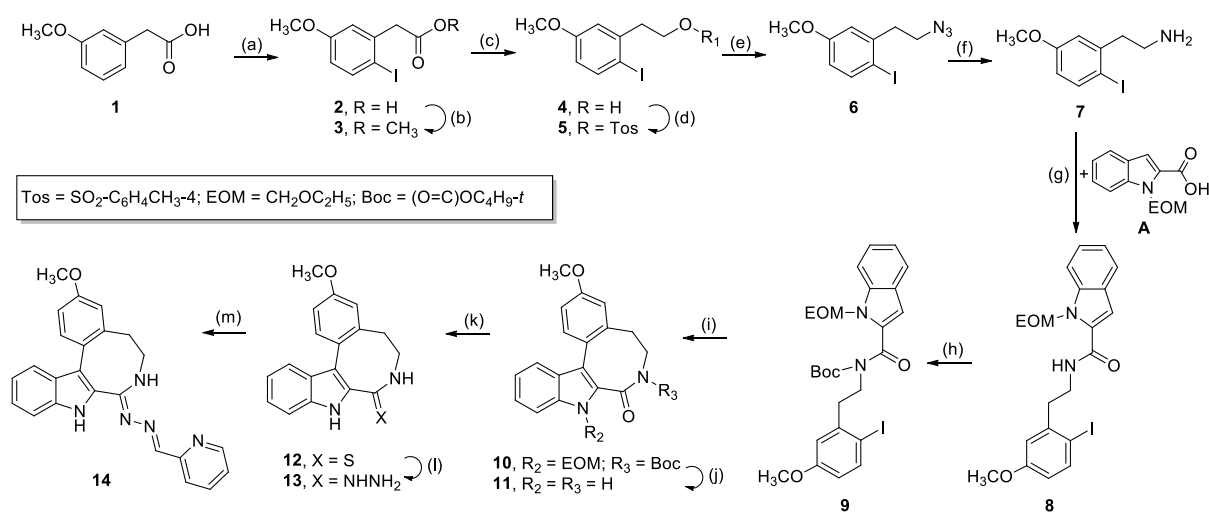
Figure 1. Structures of latonduines (a), indolo[2,3-*e*]benzazocine (b), indolo[2,3-*f*]benzazonine (c).

Aiming to further broaden the library of synthetic analogues of latonduines, design of new indolobenzazocines suitably substituted to act as ligands in metal complexes was undertaken. An initial computer modeling study examined the effect of several carefully selected substituents at different positions on the tetracyclic ring system on their binding ability to colchicine binding site of tubulin for both the ligand and its copper(II) complex. Careful inspection of the information gleaned from this study suggested that a methoxy substituent in benzene ring directly connected to the benzazocine fragment would be favorable, and could improve both the activity and the affinity toward colchicine binding site. The present study details the preparation of this new indolobenzazocine useful as a potential ligand for coordination to transition metal ions.

2. Results and discussion

The synthetic approach toward this novel ligand generally followed the strategy reported in the literature for the unsubstituted indolo[2,3-*e*]benzazocine [2]. A retrosynthetic analysis showed that the assembly of the novel methoxy-substituted ligand requires 2-(2-iodo-5-methoxyphenyl) ethylamine as one of the starting materials. Because the aforementioned amine is not commercially available, its synthesis started with the iodination with *N*-iodosuccinimide of commercial 3-methoxyphenylacetic acid (**1**) (Scheme 1), which is activated for aromatic electrophilic substitution by the presence of a methoxy group. Under the

conditions employed, iodination was directed primarily *para* to methoxy to afford compound **2**, while small amounts of an isomer having the iodo substituent in the less sterically hindered *ortho* position to the methoxy group has also been produced. Product **2** was purified by recrystallization and further converted into the corresponding methyl ester **3** that was sufficiently pure to be used in subsequent transformations. The steps that follow aimed at creating the aminoethyl side chain in the structure of compound **7**. Although reduction of esters to primary alcohols usually employs anhydrous solvents and LiAlH_4 as the source of hydrogen, phenylacetic ester **3** could be converted into ethanol derivative **4** in the presence of methanol by NaBH_4 as a less expensive and easier to handle reducing agent. In the next step, the hydroxyl group in alcohol **4** was converted into the easily leaving tosyloxy moiety in intermediate **5**. The isolation of pure tosylate **5** required chromatographic separation to remove excess tosyl chloride and by-product *N,N*-diethyltoluenesulfonamide. Replacement of the tosyloxy moiety with an azide function through nucleophilic substitution occurred easily, affording azide **6** with good yields and satisfactory purity, as evidenced by NMR spectroscopy. In the last step of the synthesis of 2-(2-iodo-5-methoxyphenyl)ethylamine (**7**), the Staudinger reaction was successfully employed to generate the desired compound, which was easily separated from the by-products using a simple extraction in an acidic aqueous phase. Despite numerous steps in this first stage, only one chromatographic separation was required to ensure low-cost access to amine **7** in batches up to 6–7 grams with a satisfactory total yield of 60%.



Scheme 1. Reaction sequence for the synthesis of novel indolobenzazocine-based ligand **14**. Reaction conditions: (a) *N*-iodosuccinimide, acetonitrile, trifluoroacetic acid, rt, 20 h; (b) SOCl_2 , methanol, rt, 2 h; (c) NaBH_4 , methanol, tetrahydrofuran, reflux, 6 h; (d) 4-toluenesulfonyl chloride, triethylamine, dichloromethane (DCM), 20 h, rt; (e) NaN_3 , NaI, *N,N*-dimethylformamide (DMF), 80 °C, overnight; (f) triphenylphosphine, diethyl ether, 0 °C, 3 h, then water, rt, overnight; (g) 1-ethyl-3-(3-dimethylaminopropyl)carbodiimide hydrochloride, DCM, 0 °C, 4 h, then rt, overnight; (h) di-*tert*-butyl dicarbonate, 4-(dimethylamino)pyridine, dry acetonitrile, rt, overnight; (i) palladium(II) acetate, triphenylphosphine, Ag_2CO_3 , K_2CO_3 , dry DMF, 110 °C, 2 h; (j) 1M HCl, 1,4-dioxane, 70 °C, 1 h; (k) silica- P_4S_{10} , toluene, reflux, 2 h; (l) hydrazine monohydrate, chloroform, reflux, 3 h; (m) pyridine-2-carboxaldehyde, ethanol, reflux, overnight.

The second stage of the synthesis of the ligand comprised the construction of the tetracyclic core structure and its functionalization. The reaction sequence started with the condensation of amine **7** with acid **A**, which was obtained as described in the literature [2] by *N*-alkylation of ethyl indole-2-carboxylate with ethoxymethyl chloride followed by hydrolysis of the ester group. Amide **8** was conveniently recrystallized to afford a pure material that was next subjected to protection of the nitrogen amide with a *tert*-butoxycarbonyl group prior to the ring closure reaction. Open-chain protected amide **9** was then involved in an intramolecular Heck-type palladium-catalyzed cyclization that generated the benzazocine eight-membered ring in lactam **10**. A molar excess of silver(I) carbonate was initially used in the process, as this

reagent works both as iodine binder and as a base. High costs associated with this reagent and the difficult removal of the resulting colloidal silver prompted us to examine its partial replacement with anhydrous K_2CO_3 as a base. As a result, the processing of the reaction mixture becomes more facile, and the yield of the ring closure reaction was significantly improved. Besides NMR, single-crystal X-ray diffraction confirmed the formation of the tetracyclic core in lactam 10 protected at both nitrogen atoms. Deprotection of intermediate 10 through simultaneous removal of ethoxymethyl and *tert*-butoxycarbonyl groups using reaction conditions employed for analogous compounds has resulted in modest yields of lactam 11, along with copious amounts of by-products that presumably arise from the opening of the benzazocine ring. Modification of the reaction conditions by slightly lowering the reaction temperature to 70 °C and shortening of the reaction time to 1 h led to good yields of the desired lactam at the expense of the formation of by-products. To enable the reaction with hydrazine hydrate, lactam 11 was first converted into thiolactam 12. While the use of Lawesson's reagent according to a previously published procedure [2] afforded compound 12 with modest yields after chromatographic separation, silica-supported P_4S_{10} proved to be a better thionation agent for substrate 11. Condensation of thiolactam 12 with excess hydrazine hydrate produced pure hydrazone 13 with high yield, and subsequent condensation with pyridine-2-carboxaldehyde gave the potentially tridentate Schiff base 14 with a total yield of the second stage of 31%. Synthesis of a second tridentate ligand, homologous to compound 14, through condensation of hydrazone 13 with 1-(pyridin-2-yl)ethanone is anticipated. Then, both these ligands will be used for the synthesis of Cu(II), Ni(II), Co(II), Fe(III) and Ru(III) complexes, and their anti-proliferative activity against a series of cancer cell lines and effect on inhibition of tubulin polymerization and R2 RNR inhibition will be investigated.

3. Conclusions

The Schiff base ligand derived from indolobenzazocine and identified by *in silico* screening as being capable of binding to the colchicine site in tubulin was successfully synthesized through a general sequence of 13 reaction steps.

Acknowledgements

This work was financially supported by a grant from the Romanian National Authority for Research, project no. PNRR-III-C9-2023-I8-99 within the National Recovery and Resilience Plan.

References

- [1]. Sung H, Ferlay J, Siegel R, Laversanne M, Soerjomataram I, Jemal A, Bray F. Global cancer statistics 2020: GLOBOCAN estimates of incidence and mortality worldwide for 36 cancers in 185 countries. *CA Cancer J. Clin.* 71, 209–249, 2021.
- [2]. Wittmann C, Dömötör O, Kuznetcova I, Spengler G, Reynisson J, Holder L, Miller G, Enyedy E, Bai R, Hamel E, Arion V. Indolo[2,3-*e*]benzazocines and indolo[2,3-*f*] benzazonines and their copper(II) complexes as microtubule destabilizing agents. *Dalton Trans.* 52, 9964–9982, 2023.



MULTIFUNCTIONAL PULLULAN–POLYVINYL ALCOHOL HYDROGELS WITH MULTIPLE CROSSLINKING STRATEGIES

Ioana-Sabina Trifan,* Gabriela Biliuta, Raluca Baron, Sergiu Coseri

Petru Poni Institute of Macromolecular Chemistry, Romanian Academy, Iasi, Romania

**trifan.sabina@icmpp.ro*

1. Introduction

Although polysaccharides represent a meticulously studied class of biopolymers since their discovery in the 19th century, they continue to be an attractive topic for researchers due to their impressive traits, including biocompatibility, biodegradability and the lack of toxicity. Pullulan is one of the polysaccharide representatives noted for its exceptional solubility in water, an aspect that is not characteristic of the other polysaccharides, as well as for its capacity to form film layers and the multiple hydroxyl groups per repetitive unit of maltotriose that can be easily involved in functionalization reactions to form derivatives with superior properties, mainly oxidation reactions with the most commonly used selective oxidizing agents in the scientific literature – TEMPO radical (in the presence of sodium hypochlorite and sodium bromide) and sodium periodate (NaIO₄). Using the TEMPO radical/NaBr/NaClO system for the oxidation, the primary hydroxyl groups are turned into carboxyl groups, while NaIO₄-oxidation manifests its influences only on the secondary hydroxyl groups which are converted to aldehyde groups, with the destruction of the bonds between the carbon atoms on which the hydroxyl groups are attached to [1].

The aim of this study was to obtain multi-crosslinked hydrogels endowed with properties suited for environmental and biomedical applications. To design these types of hydrogels, we used two pullulan derivatives and polyvinyl alcohol (PVA). Carboxypullulan and dialdehyde pullulan, obtained by the pullulan oxidation following the two oxidation protocols previously mentioned, either were used in coupling reactions with 3-aminophenylboronic acid (3-BA) and subsequently mixed with the PVA or were directly mixed with PVA. Following the syntheses, the chemical structures of each component compound and the composition of the hydrogel were thoroughly investigated by FTIR and NMR spectroscopy, while the crystallinity of the hydrogel was determined by XRD spectroscopy. Hydrogels' major properties were evaluated by SEM analysis, swelling studies and porosity and density determination studies [1-3].

2. Experimental

To synthesize the hydrogels based on pullulan, polyvinyl alcohol and 3-aminophenylboronic acid and the component compounds, the following chemical compounds, reagents and solvents were used: pullulan (P), $M_n \sim 3 \times 10^5$ g/mol determined by SEC (steric exclusion chromatography), PVA, 2,2,6,6-tetramethyl piperidin-1-oxyl radical (TEMPO), analytical purity 99%, sodium periodate (NaIO₄), 99%, 3-aminoboronic acid, analytical purity $\geq 98\%$, sodium bromide (NaBr), analytical purity 99%; sodium hypochlorite (NaClO), 3% chlorine; *N*-hydroxysuccinimide (NHS), analytical purity 96%; 1-ethyl-3-(3-dimethylaminopropyl)-carbodiimide hydrochloride (EDC HCl), distilled water; millipore water; ethanol (EtOH), analytical purity 99% and sodium hydroxide solution (NaOH), 2M purchased from Sigma Aldrich, Fluka and Merk, as received, without further purification.

3. Designing pullulan and PVA based-hydrogels

The multi-crosslinked hydrogels were classified as P and T series according to the used oxidation protocol and were suggestively named after the precursors and oxidizing agents. The gravimetric ratios between the hydrogels' components are indicated in Table 1.



Table 1. The gravimetric ratio between the hydrogel components of the P series (in which the pullulan derivative is dialdehyde pullulan) and T series (in which the pullulan derivative is carboxypullulan).

T series			
T ₁ = P-OT-PVA		T ₂ = P-OT-BA-PVA	
P-OT	PVA	P-OT-BA	PVA
25	75	25	75
50	50	50	50
75	25	75	25

P series			
P ₁ = P-OT-PVA		P ₂ = P-OT-BA-PVA	
P-OP	PVA	P-OP-BA	PVA
25	75	25	75
50	50	50	50
75	25	75	25

T SERIES: P-OT=TEMPO-oxidized pullulan derivative (carboxypullulan); P-OT-PVA=hydrogel based on P-OT and PVA; P-OT-BA = pullulan derivative obtained by coupling reaction of P-OT and 3-BA; P-OT-BA-PVA = hydrogel based on P-OT-BA and PVA.

P SERIES: P-OP=NaIO₄-oxidized pullulan; P-OP-PVA=hydrogel based on P-OP and PVA; P-OP-BA= pullulan derivative obtained by coupling reaction of P-OP and 3-BA; P-OP-BA-PVA= hydrogel based on P-OP-BA and PVA

The existing crosslinks in the P and T series hydrogels are of physical and chemical nature. Figure 1a presents the chemical structures of the precursors of the P series hydrogels, the synthesis methods of P1 and P2 hydrogels, as well as the crosslinking types formed between the functional groups of the dialdehyde derivative and PVA. In the P1 series, hydrogen bonds and (semi)acetal bonds may appear between the alcoholic groups in PVA and the aldehyde groups in P-OP. The existence of these types of bonds is less likely in the case of the P2 series because the grafted 3-BA residues are bulky and prevent their formation, instead, new ester chemical bonds can appear between PVA and the 3-BA sequences in P-OP (the pullulan derivative is a Schiff base compound offered to the grafted 3-BA sequences through imine bonds).

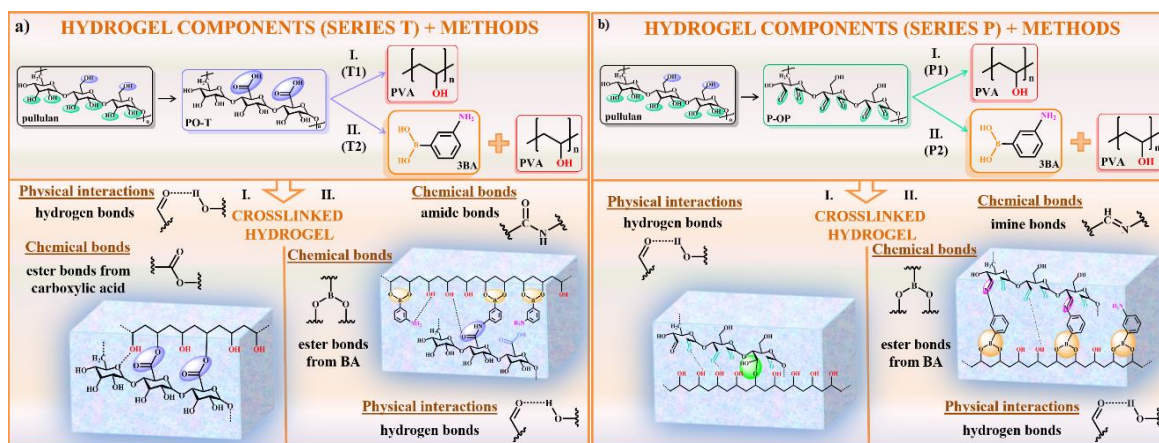


Figure 1. Schematic representation of the hydrogel components of P series (a) and T series (b).

Similar to P1 and P2 hydrogels, T-series hydrogels (Figure 1b) contain physical interactions. Between the PVA chains and the carboxylic groups formed in pullulan by oxidation reactions, chemical crosslinks are formed – ester bonds originating from carboxylic acids. The T2 series also contains ester bonds, but these originate from 3-BA, although there could also be bonds formed between the unreacted carboxylic groups (which could not form amide bonds with 3-BA) and PVA.

4. Results and discussion

Spectral techniques demonstrated the success of the pullulan oxidation reactions, the coupling reactions with 3-aminophenylboronic acid and the formation of hydrogels from PVA and the pullulan derivatives.

SEM analysis allowed the investigation of the morphology presented by each hydrogel. These hydrogels are porous materials, with pore sizes in the order of micrometers. The porosity determination tests were carried out in order to complete the interpretations of the results provided by SEM analysis. The main investigated characteristic was the liquid absorption capacity, the swelling degrees of the hydrogels being calculated. Analyzing the obtained values, it was found that, although the ratio of pullulan with 3-BA sequences varies from hydrogel to hydrogel, 3-BA determines a strong liquid absorption, followed by the collapse of the materials. Therefore, it can be concluded that hydrogels without 3-BA sequences are more stable when in a wet state. In conclusion, the preliminary studies conducted on T and P series hydrogels open the possibility of a more rigorous investigation for the proposed applications.

4. Conclusions

Undeniably, in recent years, the research in macromolecular chemistry has entailed the development of polymeric materials within the scope of "green chemistry" (compounds of provenance and solvents, chosen to be manipulated in experiments, which must not present toxicity), with impressive and vast properties, allowing their use in more applications. Starting from this aspect, the experiments carried out within the framework of this study focused on valorizing the polysaccharide properties by obtaining hydrogels, characterized by high porosity. These types of hydrogels have the potential to be used for applications that involve the synthesis of metallic nanoparticles or as bioadsorbent materials for organic and inorganic pollutants found in wastewater. Such studies are already found in the specialized literature, but the novelty of these hydrogels refers to the ester bonds originating from 3-BA, characterized by a dynamic character (reversible bonds), giving the materials good mechanical and chemical properties, as well as another possible application – use in the controlled release of drugs.

Acknowledgements

This work was supported by a grant of the Ministry of Research, Innovation and Digitization, CNCS-UEFISCDI, project number PN-IV-P1-PCE-2023-0558, within PNCDI IV.

References

- [1]. Biliuta G, Coseri S. Cellulose: a ubiquitous platform for ecofriendly metal nanoparticles preparation. *Coord. Chem. Rev.* 383, 155–173, 2019.
- [2]. Coseri S, Spatareanu A, Sacarescu L, Rimbu C, Suteu D, Spirk S, Harabagiu V. Green synthesis of the silver nanoparticles mediated by pullulan. *Carbohydr. Polym.* 116, 9–17, 2015.
- [3]. Baron RI, Duceac IA., Morariu S, Bostanaru-Iliescu AC, Coseri S. Hemostatic cryogels based on oxidized pullulan/dopamine with potential use as wound dressings. *Gels* 8, 726, 2022.



DUAL FUNCTIONAL PHENOXAZINE-BASED POLYMERS: BRIDGING NIR ELECTROCHROMIC AND ENERGY STORAGE APPLICATIONS

Catalin-Paul Constantin,* Andra-Elena Bejan, Chiriac Adriana-Petronela

Petru Poni Institute of Macromolecular Chemistry, Romanian Academy, Iasi, Romania

**constantin.catalin@icmpp.ro*

1. Introduction

In response to rising energy demands, electrochromic (EC) devices have emerged as key technologies for energy-efficient smart windows and optoelectronic applications. Polymers are especially prominent in this domain because their electrochemical and optical properties can be readily tuned. Among the various active materials, triphenylamine (TPA) is well-established. In contrast, phenoxazine (POZ), a less studied electroactive unit in electrochromic applications, features an electron-rich core and a non-planar structure, which imparts promising electrochromic properties and stability [1]. However, polymer systems based on POZ remain largely unexplored for electrochromic energy storage (EES). This study introduces a novel POZ–diphenylamine diamine, which has been incorporated into polyimide, polyazomethine, and polyamide matrices. The most effective material was subsequently tested in prototype near-infrared (NIR) EES devices.

2. Results and discussion

We synthesized a POZ–DPA-based diamine through a multi-step process. This new diamine integrates two oxidation centers for NIR electrochromism. This synthetic route was deliberately designed to yield a diamine with a low oxidation potential, enhanced electrochemical stability, superior electrochromic performance, energy storage characteristics and higher polymer solubility. The structure of the new diamine was confirmed using NMR spectroscopy. Proton chemical shift assignments were determined using two-dimensional (2D) NMR techniques.

Three new polymeric materials (a polyimide, a polyazomethine, and a polyamide) were obtained through a polycondensation reaction involving the POZ–DPA-derived diamine. This synthetic approach sought to embed a common electroactive unit into various polymer backbones to enhance electrochromic and energy storage performance. Structural confirmation was achieved using NMR and FTIR spectroscopy, while thermal behavior (TGA/DSC) revealed decomposition and glass transition temperatures in the expected range. The polymers demonstrated favorable solubility, facilitating straightforward solution-based processing. Gel permeation chromatography revealed moderate to high molar masses. Uniform, defect-free thin films (~210 nm) were consistently fabricated, confirming their suitability for use in NIR electrochromic and energy storage technologies.

A comprehensive investigation using cyclic voltammetry (CV) and differential pulse voltammetry (DPV) refined the redox characteristics and durability of POZ–DPA-derived polymers. Through the application of ITO substrates and different electrolyte systems, two distinct and reversible oxidation processes were observed (Figure 1), with MeCN/LiClO₄ determined as the most effective medium. Electrochemical impedance spectroscopy (EIS) highlighted efficient ion mobility and improved interfacial charge transport, especially for the polyamide-based sample (PA).



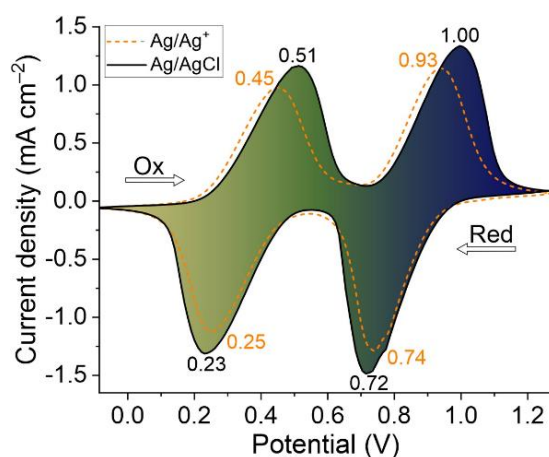


Figure 1. CV profiles of polyamide PA.

The electrochromic performance of the POZ–DPA polymer series was assessed via spectroelectrochemistry (SEC) in MeCN/LiClO₄. Thin films exhibited visible chromatic shifts corresponding to two oxidation states (0.45–0.6 V and up to 0.85–1 V), with transmittance modulation ($\Delta\%T$) reaching as high as 80.6% for PA (Figure 2). Coloration efficiencies (CE) were measured between 160–180 cm²/C for the first oxidation and 133–275 cm²/C for the second oxidation process. Among the polymers, PA demonstrated superior durability, maintaining electrochromic efficiency with minimal CE and ΔOD decay after 1000 redox cycles.

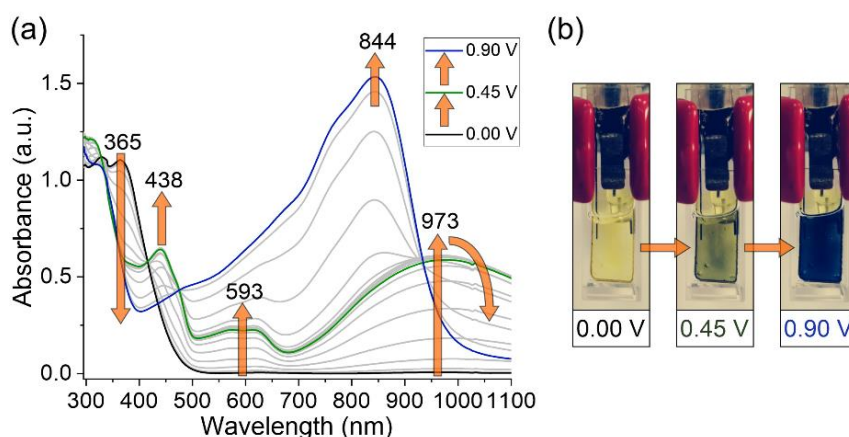


Figure 2. SEC profiles of polyamide PA.

Given that polyamide PA demonstrated the most promising electrochemical properties, the subsequent objective was to assess its functional potential. This was achieved by fabricating small-scale prototype devices, as illustrated in the schematic shown in Figure 3.

Under fully oxidized conditions, the polyamide-based systems exhibited the following electrochromic (EC) features: notable optical contrast, fast switching durations for coloration and bleaching, and high coloration efficiency, with moderate declines in both optical density and EC performance. On the other hand, their energy storage performance revealed substantial capacitance values through CV and GCD measurements, high Coulombic efficiency, minimal capacity fading over repeated cycling, and stable voltage retention across a two-hour window. Assembled in a miniaturized configuration with a 1 cm² active area, two EES devices wired in series were capable of powering a 3 V LED for approximately 30 seconds, confirming the dual electrochromic and storage functionality of the material.

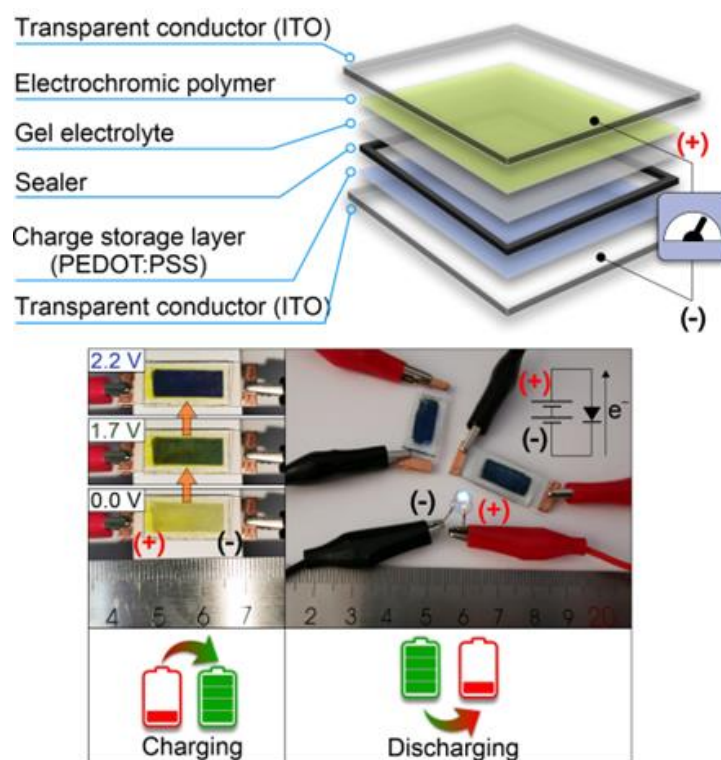


Figure 3. The structure of the EES prototype devices based on polyamide PA.

3. Conclusions

In this work, novel phenoxazine–diphenylamine (POZ–DPA)-based diamine was synthesized and integrated into three polymeric platforms: polyimide (PI), polyazomethine (PAz), and polyamide (PA), aiming at NIR electrochromic energy storage (EES) applications. Structural confirmation was achieved by FTIR, ¹H NMR, and GPC. The polymers exhibited good solubility and thermal stability (T_{onset} of 387–408 °C, T_g of 189–285 °C), enabling film fabrication via wet processing. UV–Vis analysis revealed high optical transparency for PI and PA, while PAz showed potential as a light-filtering material. Electrochemical studies (CV/DPV) confirmed two reversible redox events for all polymers below 1 V. PA demonstrated excellent stability and electrochromic performance: high contrast (up to 62.15%), fast switching (1.02–9.24 s), and strong efficiency (up to 280 cm²/C). In EES prototype devices, PA retained 1.7 V after 2 h, with ~19% capacitance loss after 500 cycles. Two devices connected in series powered a 3 V LED for 30 s. Future studies will focus on tuning the POZ core to further optimize performance.

Acknowledgements

This work was supported by a grant of the Ministry of Research, Innovation and Digitization, CNCS-UEFISCDI, project number PN-IV-P2-2.1-TE-2023-0213 (contract number 36TE / 08.01.2025) within PNCDI IV.

References

- [1]. Constantin CP, Damaceanu MD. A refreshing perspective on electrochromic materials: phenoxazine as an opportune moiety towards stable and efficient electrochromic polyimides. *Chem. Eng. J.* 465, 142883, 2023.

NOVEL BIOCATALYSTS AS LACCASE/POLYSACCHARIDE NANOASSEMBLIES

**Larisa-Maria Petrila,^{1*} Maria Karayianni,¹ Tudor Vasiliu,¹
Stergios Pispas,^{1,2} Marcela Mihai¹**

¹*Petru Poni Institute of Macromolecular Chemistry, Romanian Academy, Iasi, Romania*

²*Theoretical and Physical Chemistry Institute,*

National Hellenic Research Foundation, Athens, Greece

**larisa.petrila@icmpp.ro*

1. Introduction

Laccase (LAC) is a multi-copper oxido-reductase enzyme, highly recognized for its catalytic activity, manifested on various substrates, directly or in the presence of redox mediators [1]. Due to its high redox potential and good catalytic properties, LAC is utilised in various processes, including polymerisation and depolymerisation reactions, the delignification and bleaching of wood, and the degradation of environmental pollutants such as phenol, dyes, and pharmaceutical compounds [1,2]. However, its use in large-scale processes is limited by its reduced stability at extreme temperatures, pH or in the presence of organic solvents.

An important solution to mitigate these disadvantages is the immobilisation of LAC on solid supports or its embedding in polymeric matrices. While the immobilisation of enzymes on solid supports typically leads to a reduction in the catalytic activity of the enzyme due to conformational changes or diffusional limitations, the embedment of enzymes on polymeric matrices has a lower effect on the catalytic properties of the enzyme and, in some conditions, can even lead to increases in the catalytic properties [2]. The embedment of enzymes in polymeric matrices typically occurs through the formation of weak interactions between the functional groups of the polymer and the amino acid residues of the enzyme. The formation of such interactions leads to self-assembly in solution, with the formation of enzyme/polymer nanoassemblies. The current study investigates the formation of nanoassemblies based on *Trametes versicolor* LAC and chitosan (CHI) or CHI grafted with poly(N-isopropylacrylamide) chains (CHI-g-PNIPAM).

2. Experimental

The used materials were *Trametes versicolor* LAC (Sigma Aldrich, Germany) and CHI ($M_w = 162$ Kg/mol, 88.2% deacetylation degree, Shandong AK Biotech Co., Ltd., China) or CHI-g-PNIPAM ($M_w = 206.8$ Kg/mol, 88.06% deacetylation degree, obtained by the grafting of PNIPAM side chains on CHI, according to the method proposed by Zaharia et al. [3]). The formation of the nanoassemblies was studied by mixing the LAC solution (0.5 mg/mL, pH = 4.5) with various volumes of the CHI or CHI-g-PNIPAM (1 mg/mL, pH = 4.5). The mixing of the components leads to the formation of interpolyelectrolyte complexes under various mass ratios (MR= 2, 1, 0.5 or 0.25), which were further coded (LAC/CHI)_{MR} or (LAC/CHI-g-PNIPAM)_{MR}.

The obtained nanoassemblies were characterised by dynamic and electrophoretic light scattering (DLS/ELS) using the Litesizer 500 equipment (Anton Paar, Austria), by scanning transmission electron microscopy (STEM), with the Verios G4 UC scanning electron microscope (Thermo Fisher Scientific, USA) and by fluorescence spectroscopy, employing the FLS5 photoluminescence spectrometer (Edinburgh Instruments, UK). Moreover, the interaction mechanism between LAC and the two polysaccharides was confirmed by performing molecular dynamics simulations. The preservation of the catalytic activity of LAC upon CHI or CHI-g-PNIPAM interaction was assessed using 2,2'-azino-bis(3-ethylbenzothiazoline-6-sulfonic acid) (ABTS, Sigma Aldrich, Germany) as substrate. The effect of pH, temperature incubation or long-term storage of the nanoassemblies on the catalytic activity was additionally assessed. Moreover,



the potential use of the obtained nanoassemblies as catalysts was followed on the enzymatic degradation of indigo carmine (IC, VWR Chemicals), in the presence of syringaldehyde (Alfa Aesar) as redox mediator.

3. Results and discussion

In a first attempt to understand the interaction mechanism between LAC and CHI or CHI-g-PNIPAM, molecular dynamics simulations were performed. The simulated systems emphasised the fast interaction between the enzyme and the two polysaccharides, with the formation of surface interactions such as electrostatic interactions, hydrogen bonds and hydrophobic forces, with the surface of the enzyme being partially cover by the CHI or CHI-g-PNIPAM chains, leading to the formation of positively charged nanoassemblies as confirmed by the zeta potential measurements (Figure 1). Moreover, the prepared nanoassemblies presented lower zeta potential values as compared to the initial solutions of CHI or CHI-g-PNIPAM, confirming the important role of charge neutralisation due to electrostatic interactions in the formation and stabilisation of the nanoassemblies. Furthermore, the obtained nanoassemblies exhibited rather uniform morphologies, with average sizes increasing as the amount of CHI or CHI-g-PNIPAM used increases.

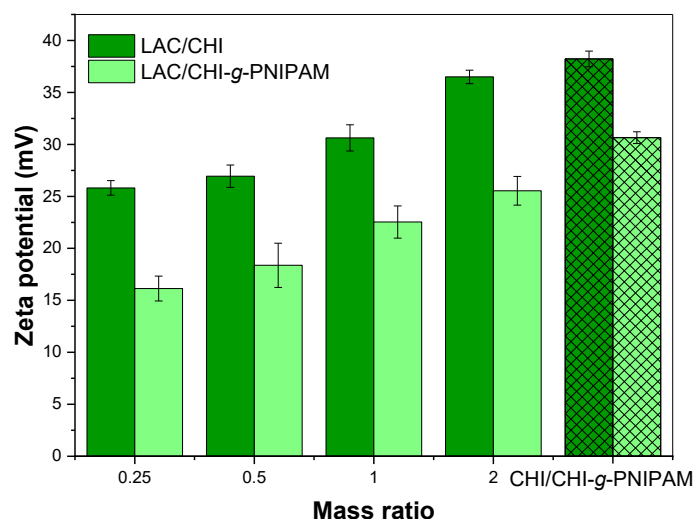


Figure 1. Zeta potential values of the obtained LAC/CHI and LAC/CHI-g-PNIPAM nanoassemblies (full colour) and of the initial CHI and CHI-g-PNIPAM solutions (textured)

As concerns the catalytic properties of the prepared nanoassemblies, an enhancement in the catalytic activity was observed upon the interaction of LAC with either CHI or CHI-g-PNIPAM, with a 1-10% increase for the (LAC/CHI)_{MR} nanoassemblies and 3-17% for the (LAC/CHI-g-PNIPAM)_{MR} nanoassemblies (Figure 2). The positive effect of CHI and CHI-g-PNIPAM complexation on the catalytic properties of LAC was additionally observed upon variations in the pH of the media or upon temperature incubation of the samples. It is hypothesised that the observed positive effect is the result of the surface covering of the enzyme by the polysaccharide chains, which protects the enzyme from solvent/temperature exposure. Additionally, CHI and CHI-g-PNIPAM may stabilise the conformation of the enzyme while also enhancing the affinity between the enzyme and the substrate or improving the microenvironment of the enzyme, thus facilitating the catalytic reactions.



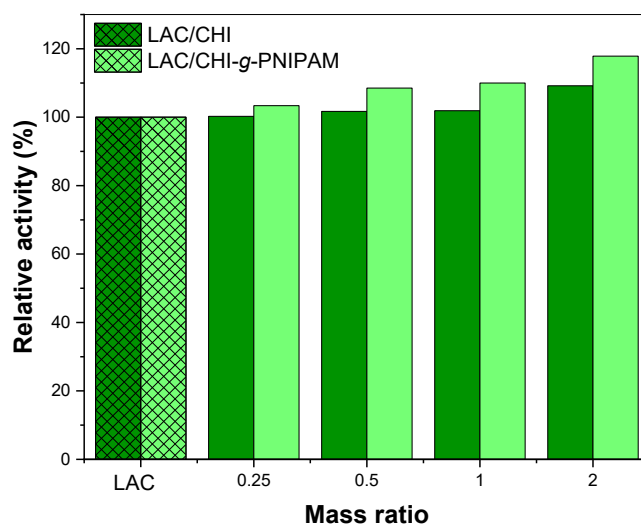


Figure 2. Catalytic activity of the obtained LAC/CHI and LAC/CHI-g-PNIPAM nanoassemblies (full colour) in relation to the initial LAC solutions (textured)

The catalytic activity of the obtained nanoassemblies was additionally tested on a model reaction targeting the degradation of IC. Both types of obtained nanoassemblies (LAC/CHI and LAC/CHI-g-PNIPAM) were able to catalyse the full degradation of the IC sample under the assay conditions, while a diffusion-controlled degradation process was observed. A higher efficiency (lower degradation time) was observed for the LAC/CHI-g-PNIPAM nanoassemblies, which was correlated with their increased catalytic activity and a better accessibility of the catalytic center of the enzyme upon complexation with CHI-g-PNIPAM. Nonetheless, the obtained results demonstrate the potential of the LAC/CHI and LAC/CHI-g-PNIPAM nanoassemblies to act as catalysts in more complex reaction media.

4. Conclusions

The presented study proposes a comparative study on the formation of nanoassemblies between LAC and CHI or CHI-g-PNIPAM. With an increase in catalytic activity following polysaccharide binding and an improvement in the stability of the embedded enzyme at pH modification, temperature incubation, or storage, the data demonstrated the successful preparation of the nanoassemblies. Moreover, the nanoassemblies exhibited a satisfactory catalytic activity on the degradation of IC, proving their potential as novel catalysts for the degradation of water pollutants.

Acknowledgements

This work was financially supported by the Romanian National Authority for Research, with project number PNRR-III-C9-2022-I8-201, within the National Recovery and Resilience.

References

- [1]. Petrilă LM. A green approach combining polyelectrolyte-based core-shell microparticles and laccase for indigo carmine degradation. *J. Environ. Chem. Eng.* 13, 115631, 2025.
- [2]. Chapman J, Ismail AE, Dinu CZ. Industrial applications of enzymes: Recent advances, techniques, and outlooks. *Catalysts* 8, 238, 2018.
- [3]. Zaharia MM, Bucatariu F, Karayianni M, Lotos ED, Mihai M, Pispas S. Synthesis of Thermoresponsive Chitosan-graft-Poly(N-isopropylacrylamide) Hybrid Copolymer and Its Complexation with DNA. *Polymers* 16, 1315, 2024.



CHITOSAN-*g*-POLY(*N*-ISOPROPYLACRYLAMIDE) POLYPLEXES WITH DNA MOLECULES OF DIFFERENT LENGTHS

Maria Karayianni,^{1*} Elena-Daniela Lotos,¹ Marcela Mihai,¹ Stergios Pispas^{1,2}

¹*Petru Poni Institute of Macromolecular Chemistry, Romanian Academy, Iasi, Romania*

²*Theoretical and Physical Chemistry Institute,
National Hellenic Research Foundation, Athens, Greece*

**m.karayianni@icmpp.ro*

1. Introduction

Non-viral drug and gene delivery systems utilizing polymers, liposomes, and nanoparticles have gained scientific interest due to their lower immunogenicity, increased safety, low cost, and ease of manufacture [1]. Natural polysaccharides like chitosan are promising non-viral vectors due to their biocompatibility, biodegradability, low toxicity, and cationic charge. Chitosan's positive charge allows binding of negatively charged genetic material, while also facilitating cellular uptake and transport. Its chemical modification with amino and hydroxyl functional groups enhances carrier performance [2]. Grafting with natural or synthetic polymers improves adhesive properties, water solubility, and therapeutic applications. Temperature-responsive poly(*N*-isopropylacrylamide) (PNIPAM) is a notable example of grafted polymers that offer additional functionalities and responsiveness to external stimuli [3].

2. Experimental

This study focuses on the co-assembly of a chitosan-*graft*-poly(*N*-isopropylacrylamide) (Chit-*g*-PNIPAM) copolymer with DNA molecules of different lengths (i.e., 50 or 2000 bp) to create polyplexes that could be used as gene delivery systems [4]. The chitosan's amino groups facilitate electrostatic interactions with the negatively charged phosphate groups of DNA molecules, while the PNIPAM side chains provide thermoresponsive properties to the assembly. Various N/P (amino to phosphate groups) mixing ratios were tested to form stable polyplexes. The mass, size, size distribution, and effective charge of the resulting nanoassemblies were analyzed using dynamic and electrophoretic light scattering (DLS and ELS), and their morphology was examined through electron microscopy (STEM). The polyplexes' response to environmental changes, such as temperature and ionic strength, and their stability in biological media were also assessed. The DNA binding affinity of the graft copolymer was evaluated using fluorescence spectroscopy and EtBr quenching assays, while the structure of the complexed DNA chains was investigated by infrared spectroscopy.

For the preparation of the polyplex solutions, appropriate volumes of a 1.4 mg/mL DNA50 or 2000 solution were added to 1 mL of a 1 mg/mL Chit-*g*-PNIPAM solution, and the final volume was adjusted to 5 mL. This way, the concentration of the graft copolymer is kept constant throughout the series of samples, while the N/P ratio ranges from 0.5 to 4. In some cases, partial precipitation was observed, and the corresponding measurements were performed on the supernatant.

3. Results and discussion

As seen in Figure 1, for both DNAs, an increase in mass (proportional to scattered intensity) and charge neutralization was observed as the concentration of DNA increases (or equivalently, the N/P ratio decreases). This denotes an increased interaction or aggregation, eventually leading to precipitation at low N/P values. For N/P above one, soluble or stable polyplexes with lower mass and increased positive charge are formed, apparently due to the contribution of the Chit-*g*-PNIPAM copolymer. Regarding the effect of DNA length, the polyplexes formed with the long DNA have greater mass or density and less charge,



indicating a stronger interaction with the graft copolymer. Regarding the corresponding sizes (DLS size distributions), the Chit-g-PNIPAM copolymer exhibits two peaks, with the larger one ranging from 300 to 600 nm, which suggests some degree of self-aggregation in solution. For the short DNA sample, at high N/P values, two peaks are observed, attributed to polyplexes formed with the corresponding species of the grafted chitosan, while at N/P equal to 1, only one peak is discerned, indicating denser or more compact structures. For the long DNA, only one peak at about 75 nm is observed in all cases, which implies the formation of more compact structures, also denoting increased interaction between the two components.

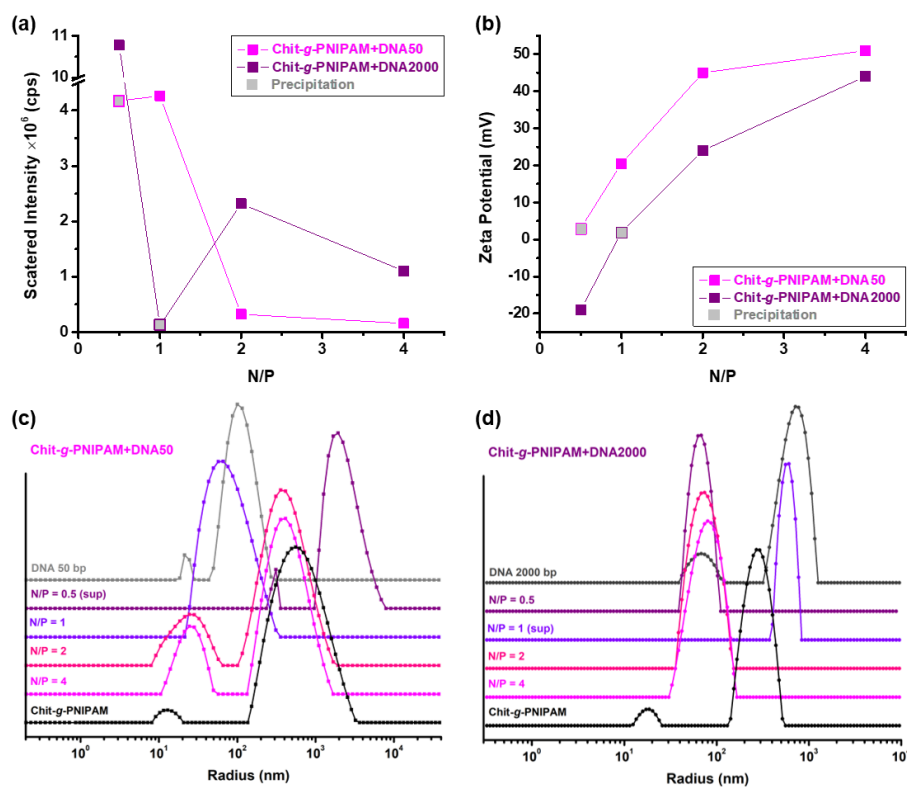


Figure 1. DLS and ELS results regarding: (a) scattered intensity; (b) zeta potential; (c, d) size distributions, for the polyplexes of the two Chit-g-PNIPAM+DNA systems. Adapted from [4].

The morphology of the polyplexes was visualized by STEM, with the obtained images for both DNAs shown in Figure 2 indicating the existence of spherical, homogeneous nanostructures of various sizes and relatively loose conformation. The size of the nanostructures for the long DNA sample is smaller than that for the short one, verifying once more the formation of more compact structures.

The polyplexes exhibited thermoresponsiveness above 35 °C as thermally triggered aggregation takes place, due to the presence of PNIPAM. This is evidenced by a significant increase in intensity, which is more intense in the case of the short DNA sample. From the corresponding changes in the size distributions (Figure 3), the formation of more compact structures (due to hydrophobic interactions) is observed for the short DNA sample. For the long DNA, no significant change in size occurred, most probably because of the already increased initial compactness of these polyplexes. Nevertheless, the transitions are fully reversible upon cooling back to 25 °C.

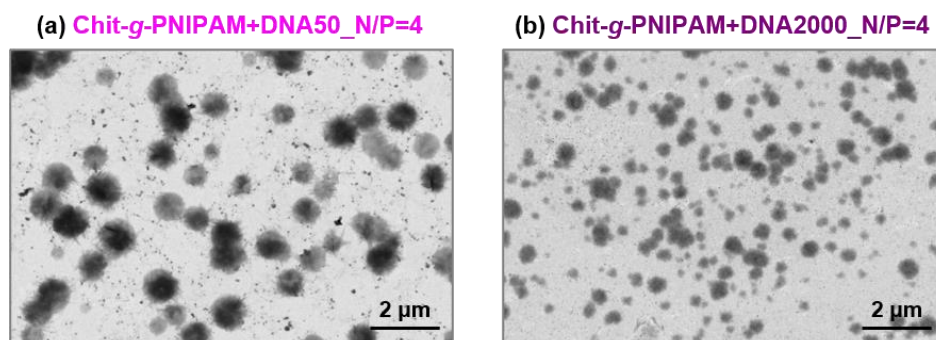


Figure 2. STEM images for representative polyplexes of the two Chit-g-PNIPAM+DNA systems. Adapted from [4].

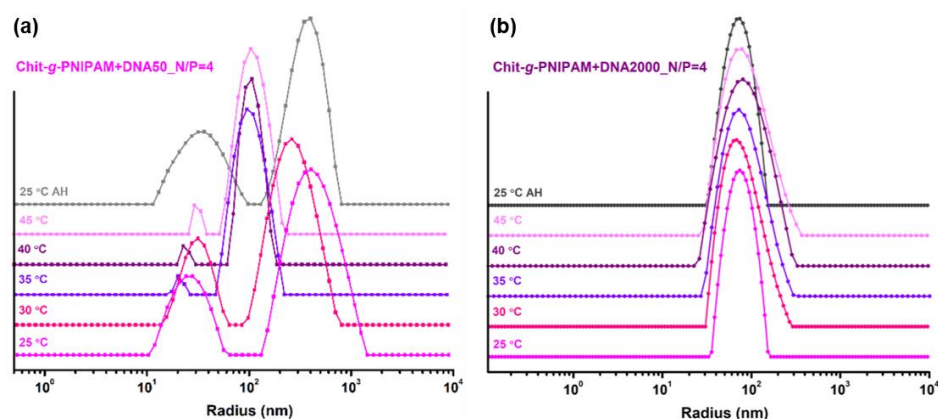


Figure 3. DLS size distributions at different temperatures for representative polyplexes of the two Chit-g-PNIPAM+DNA systems. Adapted from [4].

4. Conclusions

The Chit-g-PNIPAM copolymer interacts electrostatically with both DNAs, forming stable and thermoresponsive polyplexes, whose physicochemical properties depend on the intrinsic conformation of the graft copolymer, the length of the DNA molecule, and the mixing ratio of the two components.

Acknowledgements

This work was financially supported by a grant of the Romanian National Authority for Research, project “Polysaccharide based (bio)hybrid nanostructures (HYBSAC)”, project no. PNRR-III-C9-2022-I8-201, within the National Recovery and Resilience Plan.

References

- [1]. Ren S, Wang M, Wang C, Wang Y, Sun C, Zeng Z, Cui H, Zhao X. Application of non-viral vectors in drug delivery and gene therapy. *Polymers* 13, 3307, 2021.
- [2]. Iqbal Y, Ahmed I, Irfan MF, Chatha SAS, Zubair M, Ullah A. Recent advances in chitosan-based materials; the synthesis, modifications and biomedical applications. *Carbohydr. Polym.* 321, 121318, 2023.
- [3]. Lanzalaco S, Armelin E. Poly(*N*-isopropylacrylamide) and copolymers: a review on recent progresses in biomedical applications. *Gels* 3, 36, 2017.
- [4]. Karayianni M, Lotos E-D, Mihai M, Pispas S. Coassembly of a hybrid synthetic–biological chitosan-g-poly(*N*-isopropylacrylamide) copolymer with DNAs of different lengths. *Polymers* 16, 3101, 2024.



GREEN SYNTHESIS OF GOLD NANOPARTICLES STABILIZED BY AMYLOPECTIN-*g*-POLY(ACRYLIC ACID) COPOLYMER

Melinda-Maria Bazarghideanu,^{1*} Marius-Mihai Zaharia,¹

Alina-Petronela Moraru,¹ Florin Bucatariu,¹ Stergios Pispas,^{1,2} Marcela Mihai¹

¹*Petru Poni Institute of Macromolecular Chemistry, Romanian Academy, Iasi, Romania.*

²*Theoretical and Physical Chemistry Institute,*

National Hellenic Research Foundation, Athens, Greece

**melinda.bazarghideanu@icmpp.ro*

1. Introduction

Gold nanoparticles (AuNPs) are submicrometer-sized gold particles suspended in different fluids (water or organic solvents) that exhibit localized surface plasmon resonance properties and possess exceptional optical and electronic characteristics. AuNPs are inert, non-toxic, and do not react with the body's internal environment making them ideal for medical applications, including drug delivery, photomedicine, biosensing, antimicrobial and anticancer agents. Due to their high surface energy, AuNPs have a tendency to aggregate, making necessary the use of stabilizers or capping agents to ensure their high performance. In the last years, polymers have attracted considerable attention, being used as reducing and stabilizing agents, in order to avoid aggregates during AuNPs synthesis and leading to a better distribution and orientation of the metal particles [1].

Amylopectin (AMP) is a natural polymer with a higher molecular weight, known as the major component found in starch granules (75–85%). AMP, has highly branched structure and is composed of α -D-glucopyranose units linked together by α -(1,4) and α -(1,6)-glycosidic bonds. Among the abundant content in nature, high biocompatibility and biodegradability, AMP containing numerous free hydroxyl groups that may facilitate the synthesis of AuNPs by reduction of Au^{3+} ions to Au^0 and immobilization of Au ions into its network. Moreover, numerous hydroxyl groups facilitate its chemical modification with different synthetic polymers to create hybrid molecules with adapted functionalities [2]. Poly(acrylic acid) (PAA) is a pH responsive anionic synthetic polymer with high water absorption capacity. Due to its outstanding properties, high biocompatibility, nontoxicity, and recyclability, PAA is widely used with polysaccharides for the development of materials suitable for biomedical applications [3]. In this context, the use of hybrid macromolecular materials based on polysaccharides and stimuli-responsive polymers, as stabilizing and coating agents for AuNPs, is identified as a promising approach for the development of smart/responsive hybrid nanomaterials that integrate their functionalities and properties.

2. Experimental

The overall objective of this study was the synthesis and characterization of a new hybrid copolymer based on AMP and PAA, followed by the synthesis of gold nanoparticles mediated by AMP-*g*-PAA.

PAA was synthesized in our laboratory via reversible addition-fragmentation chain transfer (RAFT) polymerization of acrylic acid (AA) following a previously published methodology [4, 5], where AIBN was used as the polymerization initiator and 4-cyano-4-[(dodecylsulfanylthiocarbonyl) sulfanyl] pentanoic acid as the chain transfer agent. Then, the hybrid copolymer AMP-*g*-PAA was synthesized by anchoring of PAA homopolymer chains to the backbone of AMP via a covalent coupling reaction, following the "grafting to" technique, and using potassium persulfate as the radical initiator (Figure 1). After the reaction has occurred, the non-grafted homopolymer chains have been removed by dialysis, and the copolymer has been freeze-dried. ATR-FTIR and ¹H-NMR spectroscopy were performed to verify and confirm the structure of the obtained grafted copolymers.



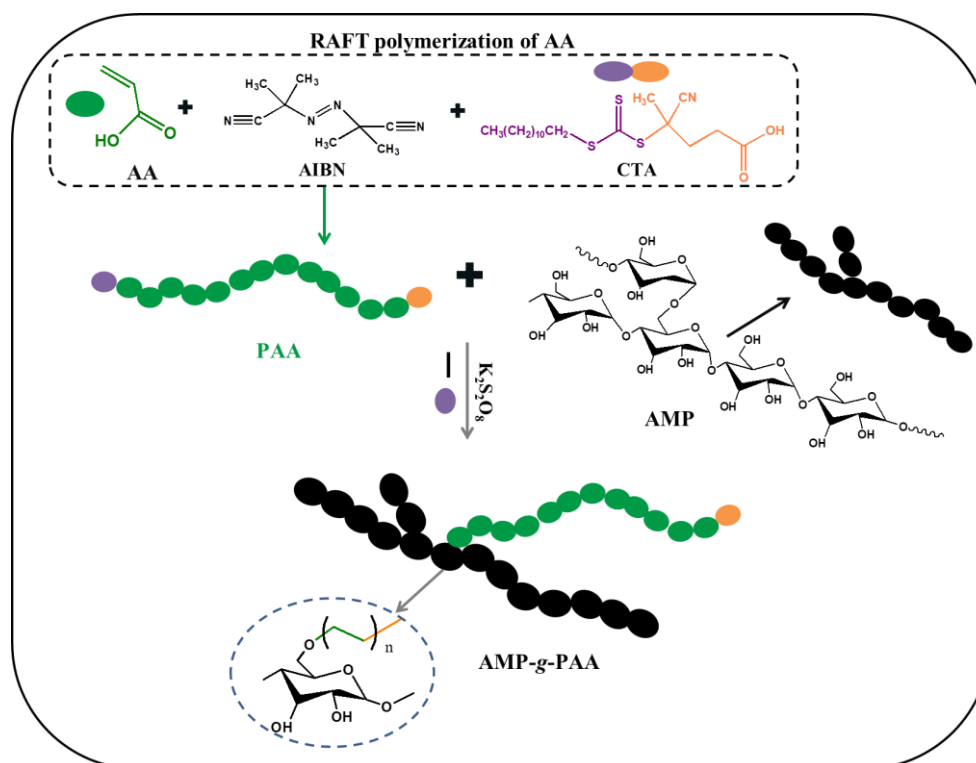


Figure 1. PAA synthesis by RAFT polymerization and “grafting to” synthesis of AMP-g-PAA copolymer.

The AMP-g-PAA/gold nanoparticles (AuNPs) hybrid composite have been synthesized through a green synthesis method using AMP-g-PAA as reducing and stabilizing agent. The AuNPs were formed in aqueous solution using chloroauric acid and AMP-g-PAA copolymer in different molar ratios $MR = [AMP-g-PAA]/[Au]$, without the use of any additional reducing agents. The samples were heated at different temperatures, in a water bath, and then the solutions were left at room temperature (25 °C). To investigate the kinetics of AMP-g-PAA/AuNPs hybrid nanostructures synthesis in relation to the reaction temperature and molar ratio, UV-Vis measurements, dynamic light scattering (DLS) and scanning transmission electron microscopy (STEM) were performed.

3. Results and discussion

The grafting of PAA chains onto the AMP backbone was confirmed by both ATR-FTIR and ¹H-NMR spectroscopies. The spectra obtained for AMP-g-PAA displayed the main characteristic signals of AMP and PAA structures. Moreover, from the second derivative of ATR-FTIR spectrum, an increase in the intensity of the alkyl ether bonds (–C–O–C–) stretch was observed in the copolymer spectrum, which suggests the formation of new aliphatic ether bonds by the reaction of –OH groups of AMP with the PAA homopolymer.

The formation of AuNPs in the presence of AMP-g-PAA was confirmed by registering the UV-Vis absorption spectra, following the presence of the peak located at 540 nm (Figure 2). After mixing the samples at specific MR and temperatures, the samples were kept at room temperature, and the UV-Vis measurements were carried out for 10 days, at different time intervals, in order to observe the formation of AuNPs and their stability over time. The UV-Vis absorption spectra revealed that the most efficient formation of AuNPs in aqueous solution occurred at 60 °C and with a $[AMP-g-PAA]/[Au]$ molar ratio of 2.05.

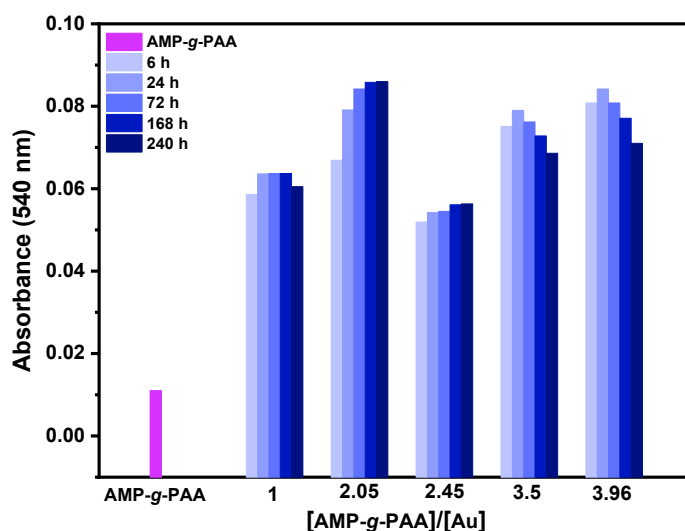


Figure 2. The formation of AuNPs in the presence of AMP-g-PAA at 60 °C and different molar ratios, evidenced by the intensity of the absorbance at 540 nm.

4. Conclusions

In this study, the new hybrid graft copolymer AMP-g-PAA was successfully obtained using the “grafting to” method. The formation of the AMP-g-PAA copolymer was confirmed by FTIR and ¹H-NMR spectroscopic methods. Furthermore, the formation of AuNPs in the presence of a AMP-g-PAA, which acts as reducing agent, has been correlated with the [AMP-g-PAA]/[Au] ratio, using DLS and UV-Vis absorption techniques.

Acknowledgements

This work was supported by the Romanian National Authority for Research, by project HYBSAC, project number PNRR-III-C9-2022-I8-201, within the National Recovery and Resilience Plan.

References

- [1]. Tepale N, Fernández-Escamilla VVA, González-Coronel VJ, Luna-Flores A, Aguilar J, Carreon-Alvarez C, Carreon-Alvarez A. Nanoengineering of gold nanoparticles: green synthesis, characterization, and applications. *Crystals*, 9, 612, 2019.
- [2]. Sarkar AK, Mandre NR, Pandac AB, Pal S. Amylopectin grafted with poly (acrylic acid): development and application of a high performance flocculant. *Carbohydr. Polym.* 95, 753–759, 2013.
- [3]. Dalei G, Das S. Polyacrylic acid-based drug delivery systems: a comprehensive review on the state-of-art. *J. Drug Deliv. Sci. Technol.* 78, 103988, 2022.
- [4]. Giaouzi D, Pispas S. PNIPAM-b-PDMAEA double stimuli responsive copolymers: effects of composition, end groups and chemical modification on solution self-assembly. *Eur. Polym. J.* 135, 109867, 2020.
- [5]. Zaharia M, Bucatariu F, Karayianni M, Lotos ED, Mihai M, Pispas S. Synthesis of thermoresponsive chitosan-graft-poly(N-isopropylacrylamide) hybrid copolymer and its complexation with DNA. *Polymers* 16(10), 1315, 2024.



NEW THERMORESPONSIVE COMPOSITES CONTAINING CHITOSAN-*g*-PNIPAM
AND *IN SITU* FORMED GOLD NANOPARTICLES

**Marius-Mihai Zaharia,^{1*} Melinda-Maria Bazarghideanu,¹ Alina-Petronela Moraru,¹
Florin Bucatariu,¹ Marcela Mihai,¹ Stergios Pispas^{1,2}**

¹*Petru Poni Institute of Macromolecular Chemistry, Romanian Academy, Iasi, Romania*

²*Theoretical and Physical Chemistry Institute,
National Hellenic Research Foundation, Athens, Greece*

*zaharia.marius@icmpp.ro

1. Introduction

Thermoresponsive polymer-coated AuNPs have recently been proven to be attractive materials for the colorimetric sensors since they are particularly sensitive to outside stimuli, including temperature, pH, and salts - all of which are critical indications for biological system monitoring [1,2]. Motivated by this demand, the goal of this research was to create novel AuNPs/smart polymer composite nanostructures with biological applications. This paper offers a novel method for generating AuNPs with diameters smaller than 100 nm utilizing an eco-friendly chitosan-*g*-poly(*N*-isopropylacrylamide) (Chit-*g*-PNIPAM) thermoresponsive copolymer. This study originality is the one-pot, *in situ* synthesis of AuNPs assisted by an aqueous Chit-*g*-PNIPAM copolymer solution, which requires no extra reducing agent. The Chit-*g*-PNIPAM copolymer was developed using the "grafting to" approach employing a radical-mediated coupling reaction between chitosan and PNIPAM obtained using RAFT polymerization [3]. The kinetics of Chit-*g*-PNIPAM/AuNPs composite structure synthesis were investigated using Scanning transmission electron microscopy (STEM), dynamic light scattering (DLS) and UV-Vis spectroscopy as a function of reaction temperature and amine group/gold ([N]/[Au]) molar ratio and also used to illustrate the thermoresponsive capabilities of the resulting smart nanoparticle colloids.

2. Results and discussion

The optical qualities of AuNPs are significantly influenced by the separation distance, facilitating the monitoring of aggregation using optical properties. Any color transitions from colorlessness to purple are regarded positively, indicating the AuNPs production. After eight days after mixing, the color shift was evaluated as a function of temperature and the [N]/[Au] molar ratio (Figure 1).

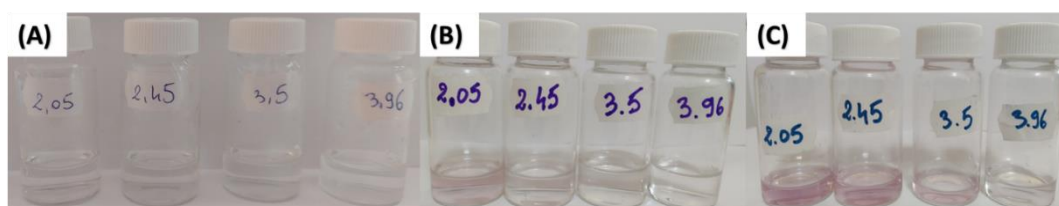


Figure 1. Color visualization of Chit-*g*-PNIPAM/AuNPs after heating at 40 °C (A), 50 °C (B) and 60 °C (C) and 8 days at room temperature.

Figure 1A indicates that the reaction conditions for the samples heated to 40 °C were unfavorable for the *in situ* formation of AuNPs since the color change did not occur, regardless of the [N]/[Au] molar ratio. However, samples exposed to 50 °C and 60 °C show color changes from colorless to various shades of purple after 8 days at room temperature (Figures 1B and 1C). Additionally, the color intensity decreases as the [N]/[Au] molar ratio increases from 2.05 to 3.96 and is dependent on the amount of Au supplied in the reaction media.



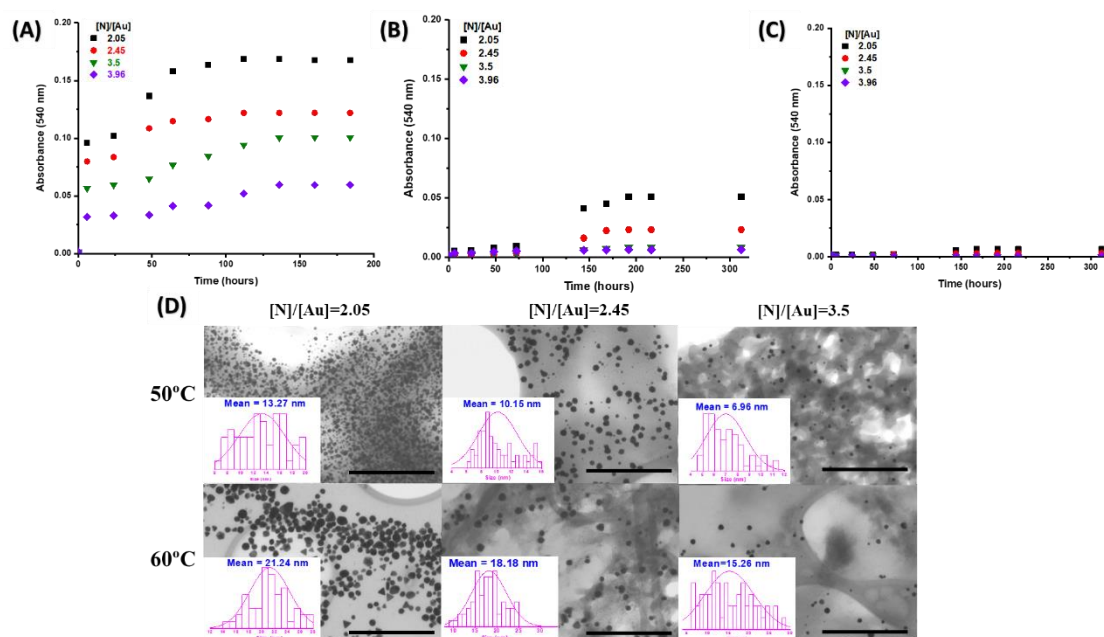


Figure 2. UV-Vis results vs time for [N]/[Au] of 2.05, 2.45, 3.5, and 3.96, heated at 40 (A), 50 (B), and 60 °C (C), and STEM micrographs at 100 nm scale bar (D).

The production of AuNPs may be monitored by localized surface plasmon resonance (SPR), which involves the excitation of free electrons in the conduction band of Au with an absorption peak at approximately 540 nm. The variation of absorbance versus time was used to track the formation of AuNPs (Figure 2). The results indicate that the SPR values at 540 nm varied with temperature and with the [N]/[Au] molar ratio. From STEM images varied mean sizes and mixed geometries (spheres, rhomboids, hexagons, triangles) of AuNPs were found dispersed on the macromolecular matrix, influenced by the preparation conditions. Thus, the reaction temperature and component molar ratio are crucial factors for the synthesis of composite structures in the presence of Chit-g-PNIPAM, ruling the size and shape of the in-situ synthesized AuNPs. Additionally, the Chit-g-PNIPAM copolymer chains may have dual functions, both as a stabilizer and as a nucleation controller.

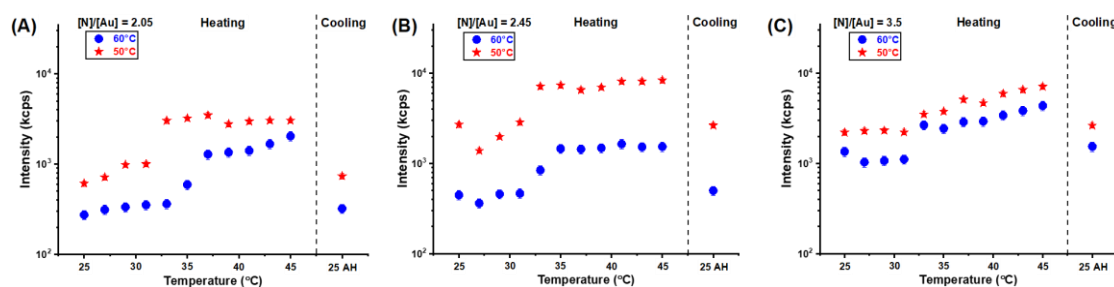


Figure 3. Influence of temperature on the scattered intensity from DLS for Chit-g-PNIPAM/AuNPs obtained at 50 °C and 60 °C and [N]/[Au] of 2.05, 2.45 and 3.5.

Figure 3 illustrates the intensity of the scattered light for Chit-g-PNIPAM/AuNPs at different temperatures and [N]/[Au] molar ratio. At temperatures below 35 °C, the low scattered intensity of the Chit-g-PNIPAM/AuNPs solution indicates that the majority of the hybrid copolymer chains are free in solution, with just a small proportion of the Chit-g-PNIPAM in the aggregates form. The increase in scattered intensity at about 35 °C indicates the formation of aggregated particles with a compact structure. As the temperature increases, the individual chains of the copolymer interact with one another, forming micelle-like aggregates. The intensity in the 35–45 °C temperature range remains constant at 2.05 and 2.45 [N]/[Au] molar ratios (at both reaction temperatures) (Figure 3A and B), indicating unusual stability at such high

temperatures. Above the LCST, the PNIPAM chains from Chit-g-PNIPAM/AuNPs tends to avoid water, resulting in the formation of a core-shell structure with a hydrophobic PNIPAM core and a hydrophilic corona. The corona is constructed from Chit-g-PNIPAM copolymer which can stabilize the whole structure, proved by low scattering intensity, as compared to the intensity obtained for the Chit-g-PNIPAM copolymer [3]. The cationic component of the Chit-g-PNIPAM copolymer enables the polyelectrolyte properties, the electrostatic repulsions expanding the temperature range at which the particles are stable. Consequently, there is a competition between the repulsive forces and the associative tendency of the PNIPAM chains. Furthermore, when the [N]/[Au] molar ratio is increased, the intensity starts to rise slowly in the 35-45 °C range, reaching values of about 10^4 kcps at 45 °C (Figure 3C). As a result, the stability of these polymer/Au structures in aqueous conditions is still impacted, and a new aggregation process is occurring. The difference in intensity between the samples obtained at 50 °C and 60 °C are lower as compared to the previously described [N]/[Au] molar ratio. This fact confirms that the stability of Chit-g-PNIPAM/AuNPs hybrid system is correlated with the Au concentration in the mixture. Furthermore, the hydrophobic/hydrophilic behavior and aggregation of Chit-g-PNIPAM/AuNPs through the LCST appear to be reversible for all the investigated samples.

3. Conclusions

The Chit-g-PNIPAM copolymer has been effectively used for the *in-situ* production of AuNPs with varying sizes and thermoresponsive characteristics. The formation of Chit-g-PNIPAM/AuNPs composite nanostructures was conducted without an external reducing agent, since the copolymer served as both reducing and protective agent in aqueous solutions. The kinetics and dimension of the AuNPs were associated with the [N]/[Au] molar ratios (2.05; 2.45, 3.5, and 3.96) and reaction temperatures (40, 50, and 60 °C), employing STEM, DLS and UV-Vis methods. Measurements of particle size by DLS were conducted to evaluate the thermoresponsive characteristics of Chit-g-PNIPAM/AuNPs nanostructures in aqueous solution, attributed to the presence of PNIPAM chains, with a lower critical solution temperature (LCST) transition occurring at approximately 35°C, near physiological temperature, signifying composite particle aggregation at elevated temperatures. Thus, the synthesized thermoresponsive Chit-g-PNIPAM/AuNPs composites may serve as materials in photothermal treatment. Despite the significant promise demonstrated by Chit-g-PNIPAM/AuNPs nanostructures, more study is needed to translate them into medicinal applications.

Acknowledgements

This work was financially supported by the Romanian National Authority for Research, with project number PNRR-III-C9-2022-I8-201, within the National Recovery and Resilience Plan.

References

- [1]. Altammar KA. A review on nanoparticles: characteristics, synthesis, applications, and challenges. *Front. Microbiol.* 14, 1155622, 2023.
- [2]. Gupta MN. Smart Systems in Biotechnology, Boca Raton: CRC Press; 2024.
- [3]. Zaharia MM, Bucatariu F, Karayianni M, Lotos ED, Mihai M, Pispas S. Synthesis of thermoresponsive chitosan-graft-poly(N-isopropylacrylamide) hybrid copolymer and its complexation with DNA. *Polymers* 16, 1315, 2024.



SYNTHESIS AND CHARACTERIZATION OF pH-RESPONSIVE GRAFT COPOLYMER BASED ON POTATO STARCH AND POLY(ACRYLIC ACID)

Diana Felicia Loghin,^{1*} Stefania Racovita,¹ Silvia Vasiliu,¹ Mihaela Iuliana Avadanei,¹ Ana-Maria Macsim,¹ Melinda-Maria Bazarghideanu,¹ Stergios Pispas,^{1,2} Marcela Mihai¹

¹*Petru Poni Institute of Macromolecular Chemistry, Romanian Academy, Iasi, Romania*

²*Theoretical and Physical Chemistry Institute,
National Hellenic Research Foundation, Athens, Greece*

**diana.loghin@icmpp.ro*

1. Introduction

Grafting approach is one of the most attractive methods to develop polymeric materials with improved properties, high performance and sensitivity to stimuli [1]. This study is dedicated to the synthesis of new grafted copolymer based on potato starch (PS) and a poly(acrylic acid) (PAA) obtained by RAFT polymerization, as well as to the structure validation of the grafted copolymer by various methods. PAA is a water-soluble polymer widely used in various fields of applications [2]. Starch is well known for its biocompatibility, biodegradability, low cost and nontoxicity [3].

2. Results and discussion

The synthesis of the new grafted copolymer based on potato starch backbone and poly(acrylic acid) side chains took place in two stages and presented in Figure 1. First, the PAA homopolymer was prepared by RAFT polymerization of acrylic acid (AA) in presence of 4-cyano-4[(dodecylsulfanylthiocarbonyl)sulfanyl]pentanoic acid (CTA) and 2,2'-azobis(2-methyl propionitrile) (AIBN) (Figure 1A). In the second stage, the copolymer PS-g-PAA was synthesized by the “grafting to” approach (Figure 1B) using potassium persulfate (KPS) as initiator.

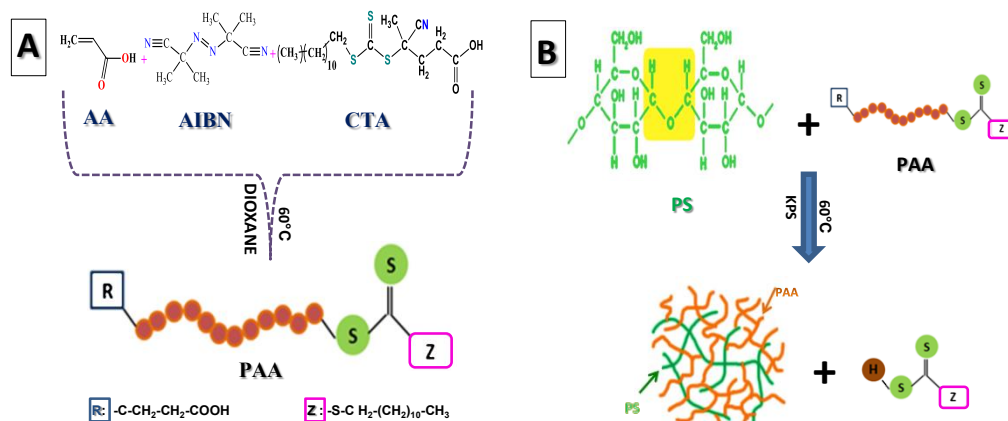


Figure 1. Schematic representation of: (A) RAFT polymerization of AA; (B) grafting reaction of PAA to potato starch.

To certify that PAA side chains were successfully grafted onto PS backbone, the grafted copolymer was characterized by FTIR-ATR and ¹H NMR spectroscopies. The FTIR-ATR spectrum of grafted copolymer (Figure 2A) was compared with the spectra of PS and PAA and it can be observed that in the PS-g-PAA spectrum the vibration bands corresponding to both starting polymers are present, the strong band at 1718 cm⁻¹ being attributed to the –C=O stretching vibration of the carboxyl group in the PAA structure [4]. ¹H NMR spectroscopy gives additional information about the structure of the PS-g-PAA (Figure 2D) compared with those of PAA (Figure 2C) and PS (Figure 2B). Thus, from the spectrum of the PS-g-PAA it can be

observed the signals (1.3-1.8 ppm and 12.8 ppm) characteristic of PAA, and a decrease of the intensity and shift of the signals characteristic for PS, respectively [5]. These features are indicative for successful PAA grafting onto PS backbone.

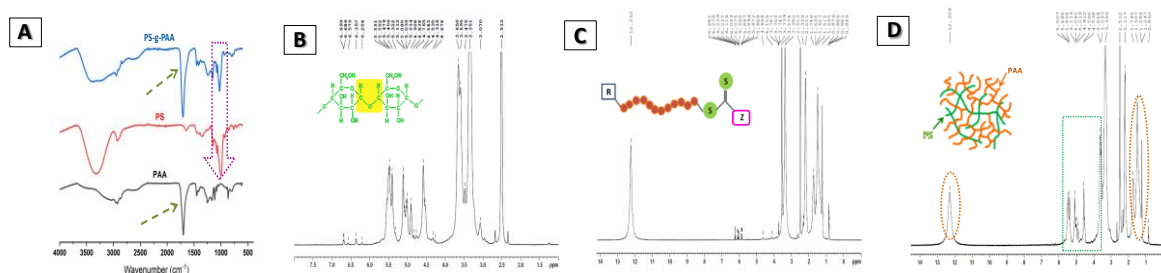


Figure 2. FTIR-ATR (A) and ¹H NMR (B-D) spectra of PS, PAA and PS-g-PAA.

The behavior of the polymers in aqueous solution can be influenced by various factors, such as polymer structure, molecular weight, pH, concentration or temperature, being very important for various applications such as, drug delivery or wastewater treatment. In this context, the pH-responsive behavior of PS-g-PAA in aqueous solution was studied using the viscometry method (Figure 3).

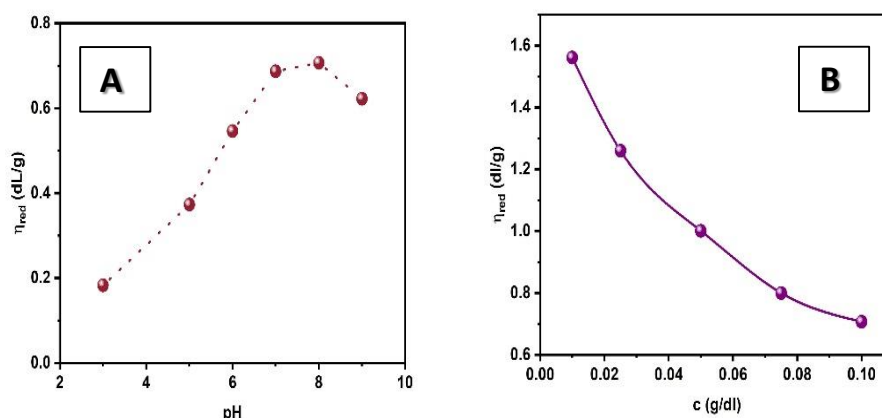


Figure 3. (A) The reduced viscosity vs pH values of PS-g-PAA aqueous solutions ($c=0.1$ g/dL) at 25 °C; (B) The reduced viscosity vs concentration of PS-g-PAA aqueous solutions at 25 °C and pH=8.

The reduced viscosity increases with the increase of pH up to pH = 8 (Figure 3A), after which the value of the reduced viscosity decreases, this behavior being explained by the conformational change of the macromolecular chain. The plots of the reduced viscosity as a function of the PS-g-PAA concentration in water (Figure 3B) show a nonlinear shape, which is a typical behavior for polyelectrolyte solutions, i.e., a continuous increase in the reduced viscosity with dilution.

The values of the intrinsic viscosity were estimated by Rao (1) and Fuoss-Strauss (2) equations:

$$\frac{1}{2(\eta_r^2 - 1)} = \frac{1}{c[\eta]_R} - \frac{a - 1}{2.5} \quad (1)$$

$$\frac{1}{\eta_{red}} = \frac{1}{[\eta]_F} + c^{1/2} \quad (2)$$

where: $[\eta]_R$ and $[\eta]_F$ is the intrinsic viscosity determined by the Rao [6] and Fuoss [7] method, respectively, η_r represents the relative viscosity, a is a constant defined as reciprocal of the maximum volume fraction to which particles can pack, η_{red} is the reduced viscosity and c is the concentration of PS-g-PAA solution.

The values of the intrinsic viscosity, $[\eta]$, for the PS-g-PAA aqueous solution at 25 °C and pH = 8 are listed in Table 1.

Table 1. Intrinsic viscosity values of PS-g-PAA obtained by Rao and Fuoss-Strauss equations.

Sample	$[\eta]_R$	R^2_{Rao}	$[\eta]_F$	R^2_{Fuoss}
PS-g-PAA	1.813±0.006	0.996	4.050±0.0489	0.986

Table 1 shows that there are differences between the $[\eta]$ values calculated using the Rao and Fuoss equations. These differences may be assigned to the approximations used to calculate the parameters of the equations. Also, the higher values for R^2_{Rao} confirm that the Rao method used for the determination of $[\eta]$ for the copolymer PS-g-PAA solution in water was correctly chosen and shows high reliability.

3. Conclusions

In this study, a two-step process is presented: the first step involves the RAFT polymerization of PAA and the second step is represented by the grafting of PAA onto the PS chain. The chemical structure of PS-g-PAA was demonstrated by FTR-ATR and ¹H NMR. The viscometric studies provide information about the conformational change of the grafted copolymer macromolecular chains as well as about the pH-sensitive behavior.

Acknowledgements

This work was funded by the Romanian National Authority for Research, with project number PNRR-III-C9-2022-18-201, within the National Recovery and Resilience Plan.

References

- [1]. Puroit P, Bhatt A, Nittal RK, Abdellattif MH, Farghaly TA. Polymer grafting and its chemical reactions. *Front. Bioeng. Biotechnol.* 10, 1044927, 2022.
- [2]. Llauro MF, Loiseau J, Boisson F, Delolme F, Ladaviere C, Claverie J. Unexpected end-groups of poly(acrylic acid) prepared by RAFT polymerization. *J. Polym. Sci.: Part A: Polym. Chem.*, 42, 5439–5462, 2004.
- [3]. Fang JM, Fowler PA, Tomkinson J, Hill CAS, The preparation and characterization of a series of chemically modified potato starches, *Carbohydr. Polym.*, 47 920020, 245–252.
- [4]. Marta H, Cahyana Y, Bintang S, Soeherman GP, Djali M. Physicochemical and pasting properties of corn starch as affected by hydrothermal modification by various methods. *Int. J. Food Prop.*, 2, 792–812, 2022.
- [5]. Dragunski DC, Pawlicka A. Preparation and characterization of starch grafted with toluene poly (propylene oxide) diisocyanate. *Mater.Res.*, 4, 77–81, 2001.
- [6]. Rao MSV. Viscosity of dilute to moderately concentrated polymer solutions. *Polymer*, 34, 592–596, 1993.
- [7]. Fuoss RM, Strauss UP. Polyelectrolytes. II. Poly-4-vinylpyridonium chloride and poly-4-vinyl-N-n-butylpyridonium bromide. *J. Polym. Sci.*, 3, 246–263, 1948.



NEW POLYSACCHARIDE GRAFTING METHOD PAIRING CHITOSAN WITH
PNIPAM BEARING CARBOXYL END GROUP**Elena-Daniela Lotos,^{1*} Maria Karayianni,¹ Marcela Mihai,¹ Stergios Pispas^{1,2}**¹*Petru Poni Institute of Macromolecular Chemistry, Iasi, Romania*²*Theoretical and Physical Chemistry Institute,
National Hellenic Research Foundation, Athens, Greece***daniela.lotos@icmpp.ro***1. Introduction**

Due to its remarkable biological properties, such as biocompatibility, biodegradability, hemostatic, bacteriostatic, and anticarcinogenic activity, chitosan has become an important component in the preparation of biomaterials and is still being thoroughly studied for use in drug delivery systems [1]. However, its use can be hindered by the limited surface activity/amphiphilicity and heat resistance as well as its poor solubility in basic and neutral solvents, therefore, its physical or chemical modification is very important in order to overcome these disadvantages [2]. Stimuli-responsive polymers are commonly used to impart additional properties to chitosan, such as the ability to react to a range of stimuli, including temperature, pH, mechanical force, electric and magnetic fields etc. Temperature response is by far the most extensively investigated and well-understood. Many polymers exhibit a lower critical solution temperature (LCST), which is the lowest temperature at which phase separation occurs due to a temperature change [3]. Poly(*N*-isopropylacrylamide) (PNIPAM), one of the most widely studied temperature-responsive polymers, exhibits a lower critical solution temperature (LCST) around 32 °C—close to human physiological temperature [4]. In this study, we examine the electrostatic complexation between chitosan (Chit) and the homopolymer PNIPAM that has a chargeable carboxyl end group. We also examined the complexes' temperature responsiveness and evaluated their potential as drug delivery carriers using curcumin (CRC) as the third component of the systems.

2. Experimental

We investigated the formation of polyelectrolyte complexes between chitosan and PNIPAM at different volume ratios (4/1, 4/2, 4/4), while maintaining a constant polysaccharide concentration. Dynamic and electrophoretic light scattering (DLS and ELS) techniques were employed to assess the structural properties of the obtained complexes, focusing on their mass, size and zeta potential. Additionally, changes in mass and size were monitored using DLS to investigate the complexes' thermoresponsive behavior in solution. Lastly, the drug delivery potential of a representative Chit/PNIPAM complex was evaluated by loading curcumin as a model hydrophobic drug at varying concentrations (2.5, 5, and 10% w/w) and analyzing the properties of the resulting drug-loaded complexes.

3. Results and discussion

The scattered intensity and the zeta potential were assessed by DLS and ELS measurements and the results are shown in Figure 1. As it can be seen in Figure 1a, the scattered intensity increases significantly with the rising concentration of PNIPAM in the formed complexes. The observed increase provides clear evidence of complexation between the two polymers, given that the scattered intensity is proportional to the mass of the complexes in solution. Figure 1b shows no significant differences in the zeta potential values of the formed complexes, regardless of the PNIPAM concentration. However, a decrease in the effective charge compared to the neat chitosan solution is observed, confirming the interaction between the components.



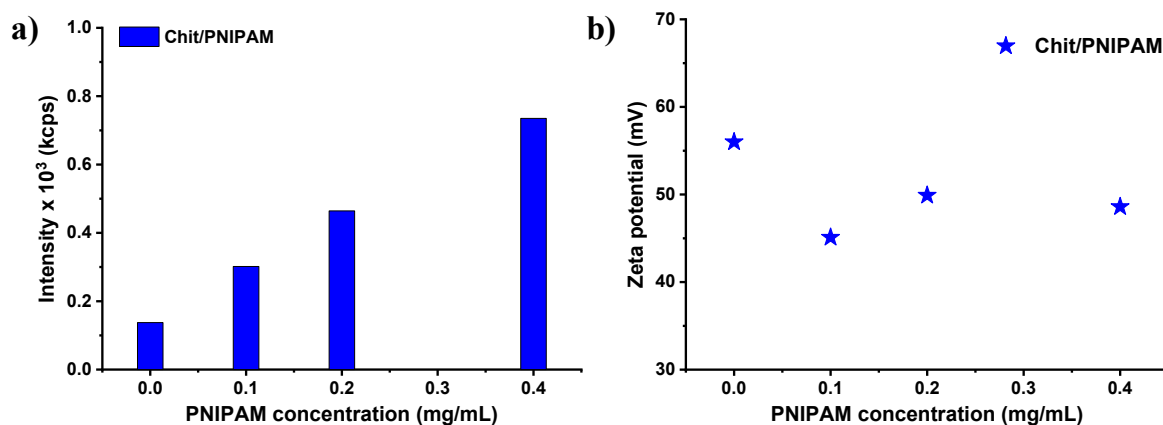


Figure 1. (a) Scattered intensity and (b) zeta potential for the Chit/PNIPAM complexes.

DLS measurements were performed between 25 and 45 °C, with 5 °C increments, to investigate the thermal response of PNIPAM and Chit/PNIPAM 4/1 complex. The effect of temperature on the scattered intensity was examined for the representative Chi/PNIPAM complex at a 4/1 volume ratio and compared with the PNIPAM samples (Figure 2). A distinct increase in turbidity, along a sharp rise in scattered intensity, was observed at 35 °C - above the LCST of PNIPAM. This characteristic reflects the thermoresponsive nature of PNIPAM and is attributed to increased hydrophobic interactions that lead to aggregation between polymer chains. The similar trend observed in both the free PNIPAM and the complex suggests that the thermal phase transition of PNIPAM is preserved upon complexation with chitosan. Importantly, upon cooling to 25 °C, the scattering intensity returns to its original values, indicating that the thermal transition is fully reversible.

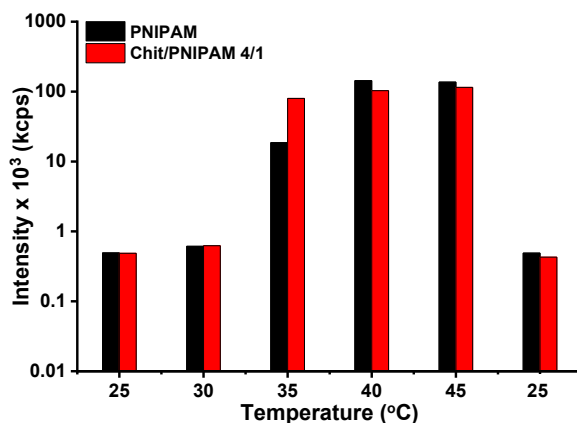


Figure 2. Temperature effect on the scattered intensity for PNIPAM and Chit/PNIPAM 4/1 samples.

The potential application of the obtained Chit/PNIPAM polyelectrolyte complexes as drug delivery systems was investigated by evaluating their encapsulation efficiency of curcumin, a hydrophobic drug. DLS measurements were employed to characterize the physicochemical properties of the CRC-loaded Chit/PNIPAM 4/4 samples. Figure 3 presents the measured scattered intensity values alongside the corresponding average particle sizes. As shown, the DLS results indicate that the CRC-loaded complexes exhibit a significant increase in scattered intensity compared to the unloaded samples (Figure 3a). This increase reflects a higher mass and potentially greater aggregation or complex formation within the nanostructures due to the encapsulation of CRC. Additionally, an increase in the average particle size of the loaded systems is observed (Figure 3b) with increasing curcumin concentration. This increase in size further supports the possibility of aggregation or clustering between the components, likely induced by curcumin incorporation. These variations in scattered intensity and average size indicate an effective drug loading, which changes the hybrid nanostructures' physicochemical characteristics.

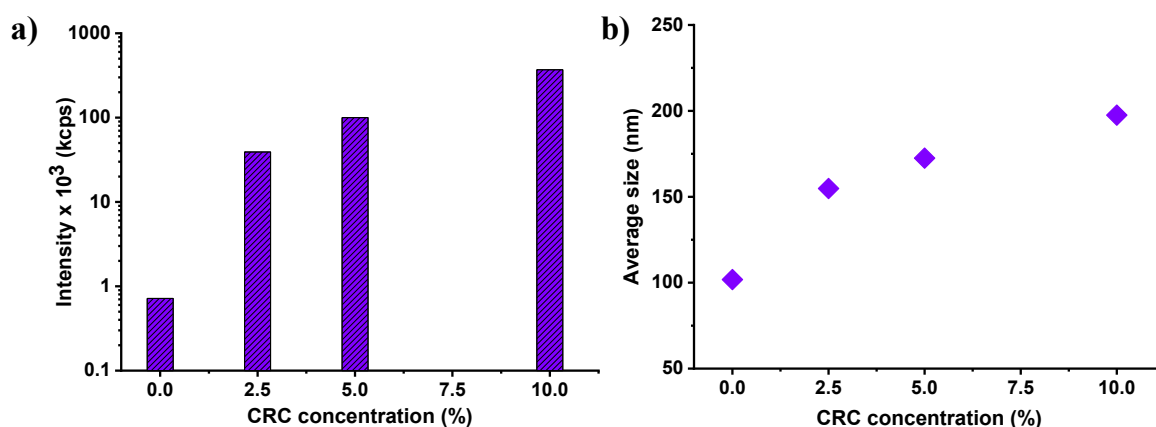


Figure 3. (a) Scattered intensity and (b) average hydrodynamic diameter for the complex Chit/PNIPAM 4/4 loaded with curcumin.

4. Conclusions

Hybrid nanostructures were obtained successfully through complexation method between chitosan and the thermoresponsive homopolymer PNIPAM. The properties in solution for the prepared Chit/PNIPAM systems, regarding the zeta potential, average size and scattering intensity, were assessed by light scattering methods. The temperature response of the Chit/PNIPAM complexes was also evaluated due to PNIPAM's thermoresponsive nature and it was demonstrated that they show similar temperature-dependent behavior above 35 °C. Lastly, the potential use of the obtained nanostructures as drug delivery systems was confirmed through the encapsulation of curcumin, facilitated by the hydrophobic interactions between PNIPAM and the drug.

Acknowledgements

This work was financially supported by a grant of the National Research Authority, project “Polysaccharide based (bio)hybrid nanostructures (HYBSAC)”, project no. PNRR-III-C9-2022-I8-201, within the National Recovery and Resilience Plan.

References

- [1]. Ali A, Ahmed S. A review on chitosan and its nanocomposites in drug delivery. *Int. J. Biol. Macromol.* 109, 273–286, 2018.
- [2]. Lingait D, Rahagude R, Gaharwar SS, Das RS, Verma MG, Srivastava N, Kumar A, Mandavgane S. A review on versatile applications of biomaterial/polycationic chitosan: An insight into the structure-property relationship. *Int. J. Biol. Macromol.* 257, 128676, 2024.
- [3]. Wei M, Gao Y, Li X, Serpe MJ. Stimuli-responsive polymers and their applications. *Polym. Chem.* 8(1), 127–143, 2017.
- [4]. Alsuraifi A, Curtis A, Lamprou DA, Hoskins C. Stimuli responsive polymeric systems for cancer therapy. *Pharmaceutics.* 10(3), 136, 2018.



FLUORESCENCE PROPERTIES OF CARBON DOTS SYNTHESIZED VIA HYDROTHERMAL TREATMENT OF TRYPTOPHAN/N- HYDROXYPHTHALIMIDE PRECURSORS WITH MANGANESE DOPING: AN EXCITATION-EMISSION MATRIX STUDY

Adina Coroaba,* Ioan-Andrei Dascalu, Oana-Elena Carp, Narcisa-Laura Marangoci
Petru Poni Institute of Macromolecular Chemistry, Romanian Academy, Iasi, Romania
*adina.coroaba@icmpp.ro

1. Introduction

In the last several years, bifunctional nanomaterials with magnetic and fluorescence characteristics have drawn a lot of attention due to their applications in magnetic resonance (MR) and fluorescence imaging [1]. When MR and fluorescence imaging are merged, a powerful combination of complementary approaches is created. MR imaging provides great spatial resolution and excellent tissue penetration in microscopic tissue evaluation, whereas fluorescence imaging delivers high sensitivity and ease of observation. As a result, a lot of work has gone into developing different magnetofluorescent (MF) nanomaterials for MR and fluorescence imaging [1,2].

Dual-modality contrast agents that are MF have recently emerged as effective and useful probes in biomedical research. Iron-oxide nanoparticles ($\text{Fe}_2\text{O}_3/\text{Fe}_3\text{O}_4$), MnO , Gd_2O_3 , and Dy_2O_3 were the most commonly used metal-oxide nanoparticles [2]. These nanoparticles, however, displayed drawbacks such as rapid renal elimination ($\text{Fe}_2\text{O}_3/\text{Fe}_3\text{O}_4$), severe cytotoxicity (Gd_2O_3), poor biocompatibility at a shorter exposure time, reduced functionalization, lower magnetic center payload, and chelate etching [2]. Additionally, transition metals with conjugated polymeric nanoparticles also have significant downsides, such as large hydrodynamic diameters (ranging from 50 to 700 nm), time-consuming and expensive synthesis techniques, and systemic toxicity at higher concentrations [3]. In this context, carbon dots (CDs) could be considered to be the next generation of fluorescent nanomaterials used for MR and fluorescence imaging, due to their exceptional fluorescence efficiency, high biocompatibility, durable chemical inertness, improved water solubility, and ease of surface modification [4].

CDs are a new class of materials that have triggered a lot of interest in the scientific community because of their unique architecture, which consists of a graphitic core with less than 10 nm in size, which is comprised of carbon atoms in sp^2 hybridization decorated on surface with various functional groups (e.g. $-\text{COOH}$, $-\text{OH}$, $-\text{CHO}$, $-\text{NH}_2$ etc.) [4]. In addition to their unique tunable PL and other outstanding physicochemical characteristics, Cdots have remarkable and outstanding characteristics such as excitation-dependent photoluminescent emission, high quantum emission yields, physico-chemical stability, biocompatibility, photostability, and versatility [4].

Amino acids like tryptophan (TRP) are attractive as precursors due to their intrinsic fluorescence and abundance of functional groups, which can promote both carbonization and efficient surface passivation during synthesis [5]. Co-precursors such as N-hydroxyphthalimide (NHF) offer additional chemical complexity, potentially modifying the CDs' surface states and emission profiles. Furthermore, incorporating transition metals like manganese (Mn) can generate defect sites and electron traps, enabling further modification of the photophysical properties.

Excitation-Emission Matrix (EEM) fluorescence spectroscopy provides multidimensional spectral data by mapping fluorescence intensity against both excitation and emission wavelengths. This technique surpasses traditional single-wavelength fluorescence by revealing heterogeneity in fluorophore populations and enabling comprehensive insight into the evolution of fluorescence during synthesis and doping.



2. Experimental

CDs were prepared by hydrothermal treatment of aqueous solutions containing TRP, NHF, or their equimolar mixtures, with selective manganese chloride doping. The solutions were sealed in Teflon-lined autoclaves and heated at 170 °C for 20 hours. After reaction, samples were cooled and purified through centrifugation followed by filtration using 0.2 µm filters to remove residual precursors and impurities. The EEM fluorescence spectra were recorded on precursor solutions (TRP, NHF) and the hydrothermally produced samples (TRP-HT, TRP-Mn-HT, TRP-NHF-HT, TRP-NHF-Mn-HT) using a FluoroMax-4 spectrofluorometer (Horiba, Japan). Excitation wavelengths ranged from 320 to 450 nm, with emission being collected between 350 and 540 nm. The resulting EEM maps were analyzed for changes in fluorescence intensity, wavelength shifts, and spectral broadening as indicators of carbonization and doping effects.

3. Results and discussion

This study reports the synthesis of carbon dots (CDs) derived from L-tryptophan using a hydrothermal method. N-hydroxyphthalimide (NHF) was included as a co-precursor, and manganese chloride (MnCl₂) was added as a metal dopant.

The EEM map for TRP (Figure 1a) displayed a sharp, intense fluorescence peak at around 280 nm excitation and 350 nm emission, characteristic of tryptophan's indole ring [5]. In contrast, NHF (Figure 1b) showed weaker intrinsic fluorescence features.

Hydrothermal treatment significantly altered fluorescence patterns. The fluorescence profile of TRP-HT (Figure 1c) changes dramatically compared to the precursor, with a broad, intense emission region spanning 430-500 nm upon excitation between 340-380 nm. Such broad bands are typical fingerprints of CDs, reflecting heterogeneous surface states and nanoscale carbon cores. The observed red-shift and broadening suggest new emissive traps and functional groups formed during carbonization.

Manganese doping, TRP-Mn-HT (Figure 1d) and TRP-NHF-Mn-HT (Figure 1f), further influenced the fluorescence spectra. EEM maps of doped samples showed additional peak broadening and subtle shifts in emission maxima, along with changes in intensity, indicating that Mn introduces new surface defects or trap states. The samples synthesized with both TRP and NHF, TRP-NHF-HT (Figure 1e), exhibited more complex fluorescence patterns, with broader emission profiles and increased heterogeneity across excitation and emission spectra. This complexity likely arises from diversified surface chemistry and formation environments driven by NHF's oxidative or coordination effects.

Collectively, the EEM data illustrates a clear transition from discrete molecular fluorophores to complex carbon dot emission profiles with excitation-dependent fluorescence. The disappearance of native main peaks from TRP and NHF confirms successful carbon dot formation with modified emissive properties. Both Mn doping and NHF co-precursor effectively tailor surface states and defects.



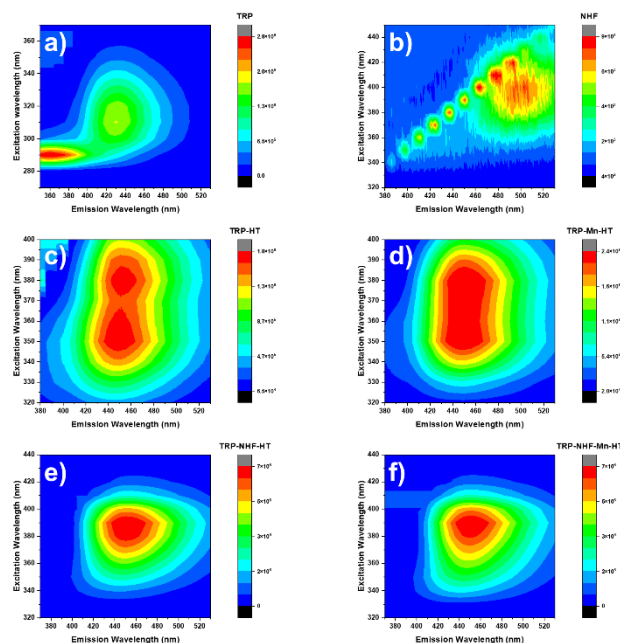


Figure 1. EEM maps of: (a) TRP; (b) NHF; (c) TRP-HT; (d) TRP-Mn-HT; (e) TRP-NHF-HT; (f) TRP-NHF-Mn-HT.

4. Conclusions

Hydrothermal synthesis of carbon dots from L-tryptophan and *N*-hydroxyphthalimide yields fluorescent nanomaterials with tunable optical properties. Manganese doping and co-precursor effects significantly influence fluorescence, broadening and shifting emission bands by introducing new surface or defect states. EEM fluorescence spectroscopy effectively captures these emission changes, providing detailed fingerprints of carbon dot formation and modification processes. This study highlights the power of compositional and synthetic parameter control to engineer photophysical behavior in carbon dots, enhancing their versatility for advanced fluorescent applications.

Acknowledgements

The authors are thankful for the financial support of the grant of the Romanian National Authority for Research, project no. PNRR-III-C9-2022-I8-291, contract no. 760081/23.05.2023, within the National Recovery and Resilience Plan.

References

- [1]. Kunjachan S, Ehling J, Storm G, Kiessling F, Lammers T. Noninvasive imaging of nanomedicines and nanotheranostics: principles, progress, and prospects. *Chem. Rev.* 115, 10907–10937, 2015.
- [2]. Lee DE, Koo H, Sun IC, Ryu JH, Kim K, Kwon IC. Multifunctional nanoparticles for multimodal imaging and theragnosis. *Chem. Soc. Rev.* 41, 2656–2672, 2012.
- [3]. Howes P, Green M, Bowers A, Parker D, Varma G, Kallumadil M, Hughes M, Warley A, Brain A, Botnar R. Magnetic conjugated polymer nanoparticles as bimodal imaging agents. *J. Am. Chem. Soc.* 132, 9833–9842 2010.
- [4]. Coroaba A, Ignat M, Carp OE, Stan CS, Filipciuc SI, Uritu CM, Simionescu N, Marangoci NL, Pinteala M, Ania CO. Antioxidant activity and in vitro fluorescence imaging application of N-, O- functionalized carbon dots. *Sci. Rep.* 15, 25834, 2025.
- [5]. Noureena MM, Puhazhendhi A, Sivalingam S, Anu AS, Vinod Kumar N, Rithesh Raj D. L-tryptophan carbon dots as a fluorescent probe for malachite green detection. *Spectrochim. Acta A* 329, 125625, 2025.

NORFLOXACIN LOADED BIODEGRADABLE CHITOSAN/QUATERNIZED CHITOSAN NANOFIBERS FUNCTIONALIZED WITH AN ANTIFUNGAL ALDEHYDE AS WOUND DRESSINGS

**Vera-Maria Platon,^{1*} Sandu Cibotaru,¹ Alexandru Anisie,¹ Irina Rosca,¹
Isabela-Andreea Sandu,¹ Corneliu-George Coman,^{2,3} Liliana Mititelu-Tartau,²
Bianca-Iustina Andreica,¹ Luminita Marin¹**

¹*Petru Poni Institute of Macromolecular Chemistry, Romanian Academy, Iasi, Romania*

²*Pharmacology, Clinical Pharmacology and Algesiology Department, Faculty of Medicine, Grigore T. Popa University of Medicine and Pharmacy, Iasi, Romania*

³*Université de Mons, Faculté de Médecine, Pharmacie et Sciences Biomédicales, Mons, Belgium*

**platon.vera@icmpp.ro*

1. Introduction

Driven by the current need for prophylactic and therapeutic wound-healing formulations, including those for burn injuries [1], this study focuses on the development of advanced dressings based on chitosan (CS) and quaternized chitosan (TMC) nanofibers, functionalized with 2-formylphenylboronic acid (A) in order to achieve enhanced properties. The dressings were designed as a formulation for norfloxacin (NFX), a second generation fluoroquinolone antibiotic, with a wide antibacterial spectrum [2].

The selected composition combines the inherent advantages of chitosan and its quaternized derivative, including high biocompatibility, biodegradability, and potent antimicrobial properties [3,4]. The fibers were thoroughly characterized, regarding their structural, thermal, morphological and supramolecular properties, as well as their biological activity and general toxicity both *in vitro* and *in vivo*.

2. Experimental

The preparation method of the binary chitosan/quaternized chitosan nanofibers (CT), implied electrospinning a mixture of CS:TMC:PEO with a mass ratio of 7:1:2, in 75% acetic acid using a Inovenso NanoSpinner apparatus. The resulting non-woven mats were subjected to washing through immersion in previously dried ethanol, in order to remove the PEO, which acts as both a co-spinning agent and a sacrificial matrix. Subsequently, the previously attained fibers were first subjected to loading with norfloxacin (NFX) by the adsorption method, which implies immersion of the nanofibers into an ethanolic solution of the drug (0.1%), followed by a 24 hour incubation and further drying under atmospheric conditions in an enclosed space, giving CTN samples.

The second preparation stage involved functionalization of both CT and CTN fibers with an antifungal aldehyde (A) by spraying a solution of the A (0.2% in ethanol) on the surface of the fibers, on both sides, giving CTA and CTNA samples. A 10:1 molar ratio between the glucosamine units of CS/TMC and the aldehyde units of A was chosen and calculated in order to determine the amount of aldehyde used for the imination process. A schematic representation of the nanofiber preparation can be seen in Figure 1.

Results and discussion

FTIR and NMR spectroscopy confirmed the presence of all components and the formation of imine-type bonds, while ATG thermograms indicated the efficient removal of PEO from the fibers. The encapsulation efficiency of NFX in the nanofibers was adequate and relatively homogenous (~3.5%), suggesting that the drug is predominantly distributed within the fibers.

Morphological and supramolecular analysis through POM, SEM, and XRD revealed that the nanofibers



maintain a stable morphology over time, with a constant average diameter (~150 nm) and a compact structure, while the imine formation and encapsulation process induced a consolidated supramolecular organization, supported by intermolecular interactions between components.

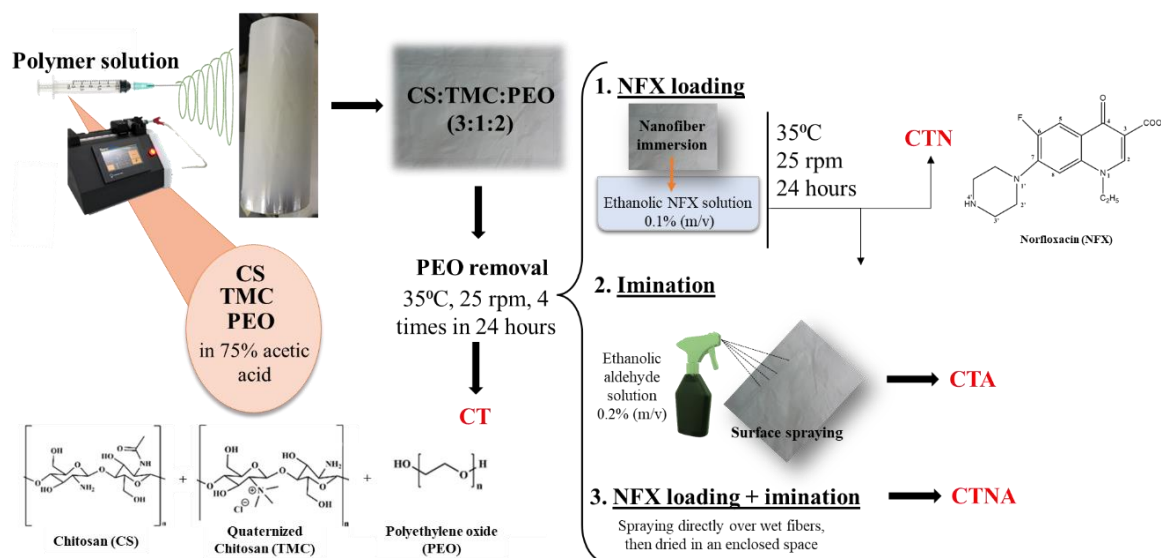


Figure 1. Schematic representation of the nanofiber preparation.

The composite nanofibers exhibited improved mechanical properties, with elastic modulus values of up to 1250 MPa, a high swelling capacity, with a moisture retention of 10 g/g in the first 5 minutes, highlighting their increased potential as modern dressings for healing exudate-abundant wounds. CTNA fibers demonstrated superior antioxidant activity (~70%), suggesting their ability to contribute to supporting the wound healing process by controlling oxidative stress. Bioadhesivity testing on model tissue (chicken skin) revealed adequate adhesive properties (0.9 N) similar to those of other chitosan-based materials, indicating their capacity to effectively adhere to tissues and remain stable during administration.

The investigation of the nanofibers enzymatic biodegradation revealed a degradation behaviour adaptable to the local wound environment, progressively degrading according to evolution of pH values over the healing period, while maintaining their structural integrity. Complete degradation in acidic media confirmed their bioresorbability, providing an essential advantage in avoiding traumatic debridement and supporting tissue regeneration. The study of *in vitro* release kinetics of NFX showed a rapid and consistent release of the drug from the nanofibers, regardless of pH, supporting the formulation's performance in infection prevention during the early phases of wound healing.

The antimicrobial properties of the samples were tested on both Gram-positive and Gram-negative bacterial strains, as well as one fungal strain, revealing good capacity to inhibit microbial growth. The results are presented in Figure 2.

Cytocompatibility tests confirmed that all investigated nanofibers are safe for contact with human cells, showing cell viability within the limits set by ISO standards for biomedical devices, supporting their potential for therapeutic applications. Nanofibers have demonstrated strong and long-lasting antimicrobial and antifungal activity, enhanced by the presence of NFX and aldehyde, highlighting the effectiveness of these materials as active dressings with long-term stability for infection prevention. The *in vivo* toxicity assessment of subcutaneously implanted nanofibers revealed excellent biocompatibility, with no signs of systemic toxicity or inflammatory reactions.

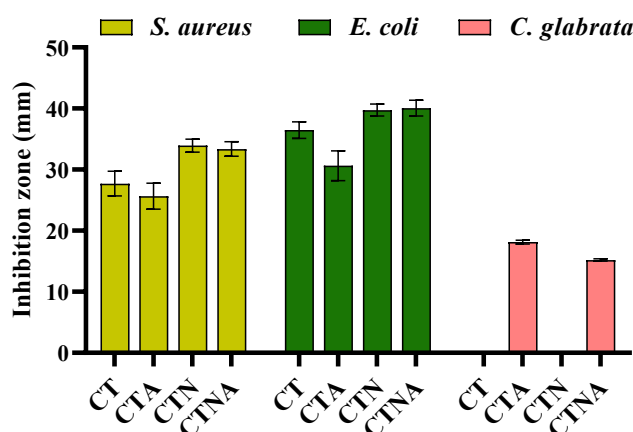


Figure 2. Graphical representation of inhibition zones reached by tested samples against *Staphylococcus aureus*, *Escherichia coli* and *Candida glabrata*.

4. Conclusions

The present study managed to effectively obtain a complex formulation of imino-CS/TMC-based nanofibers for the encapsulation of NFX as promising wound dressings. The composition and contents were successfully confirmed through NMR, FTIR spectroscopy and TGA analysis. SEM micrographs indicated appropriate morphology, expected for nanofibers, with nanometric mean diameters (approx. 150 nm), while DVS studies revealed mesopore dimensions of 3 nm. The non-woven mats exhibited advanced mechanical strength (1250 MP), good swelling capacity (up to 6 g/g MES values), enhanced antioxidant activity (up to 70%), as well as good antimicrobial activity over a series of bacterial and fungal strains. The biodegradation experiments carried out in isotonic-isohydric solution revealed gradual decomposition, thus strongly indicating the nanofibers bioresorbability, minimizing the risk of traumatic debridement. The toxicity studies, both *in vitro* and *in vivo*, showed good biocompatibility and therefore lack of toxicity, making the obtained formulation suitable for biomedical applications.

Acknowledgements

The support from the European Commission through the project H2020-MSCA-RISE-2019, SWORD-DIV-873123 is acknowledged.

References

- [1]. Joshi S, Maan M, Barman P, Sharely I, Verma K, Preet S, Saini A. Advances in biomaterials for wound care management: insights from recent developments. *Adv Coll Int Sci*. 103563, 2025.
- [2]. Newsom SWB, The antimicrobial spectrum of Norfloxacin. *JAC*. 13, 25–31, 1984.
- [3]. Nair LS, Laurencin CT. Biodegradable polymers as biomaterials. *Prog Polym Sci*, 32, 762–798, 2007.
- [4]. Xu T, Xin M, Li M, Huang H, Zhou S. Synthesis, characteristic and antibacterial activity of *N,N,N*-trimethyl chitosan and its carboxymethyl derivatives. *Carbohydr Polym*. 81, 931–936, 2010.



DEVELOPMENT AND CHARACTERIZATION OF A MULTIFUNCTIONAL BIOACTIVE COMPLEX AS A REGULATOR FOR MELANOGENESIS

**Alexandra Vieru,^{1*} Alina Gabriela Rusu,¹ Alina Ghilan,¹ Liliana Mititelu-Tartau,²
Alexandru Serban,¹ Loredana Elena Nita¹**

¹*Natural Polymers, Bioactive and Biocompatible Materials Laboratory, Petru Poni Institute of
Macromolecular Chemistry, Romanian Academy, Iasi, Romania*

²*Pharmacology, Clinical Pharmacology and Algesiolog Department, Faculty of Medicine, Grigore T.
Popa University of Medicine and Pharmacy, Iasi, Romania*

**croitoriu.alexandra@icmpp.ro*

1. Introduction

Melanogenesis is a complex biochemical process responsible for the production of melanin. The biosynthesis of melanin begins in melanocytes when the tyrosinase enzyme (TYR) catalyzes L-tyrosine into the melanin precursors L-3,4-dihydroxyphenylalanine (L-DOPA) and dopaquinone (DQ) [1]. Excessive TYR production leads to skin hyperpigmentation diseases, including pigment spots, melasma, solar lentigines, and even melanoma. Treatments for hyperpigmentation disorders or melanoma are directly related to TYR activity, involving compounds that block the enzyme's active site or chelate copper ions.

Hence, different compounds with effects on anti-melanogenesis, low toxicity, and reduced skin irritability were sought. Kojic acid (KA) and arbutin (Ar) are natural inhibitors with antioxidant, antifungal, and anti-melanogenic properties [2]. Besides these benefits, the compounds have limited efficiency due to poor penetration. Several studies revealed that amino acids and short peptides enhance absorption efficiency [3], serving as a strong substitute for chemical skin-lightening agents by inhibiting the TYR enzyme.

In this context, the present study aimed to develop an eco-friendly approach for preparing a new multifunctional bioactive system (MBS) starting from a supramolecular gel based on lysine and glycyl-glycyl-glycine, modified at the N-terminal with a fluorenylmethyloxycarbonyl (Fmoc) protecting group, and enhanced with a glycoside-pyrone-based complex (Ar-KA). This complex system will present a synergistic effect to inhibit peroxidase, an enzyme similar to tyrosinase, and implicitly control melanin production.

2. Experimental

The MBS was prepared at room temperature in two steps. Initially, 0.8% w/v Fmoc-Lys(Fmoc)-OH and 0.1% w/v Fmoc-Gly-Gly-Gly-OH solutions were prepared, forming the SG matrix through a co-assembly process [4]. Subsequently, a co-drug mixture containing 1% w/v KA and 1% w/v Ar was prepared. The final step involves mixing the SG matrix with the co-drug, thus obtaining the MBS gel.

In the MBS development process, two distinct formulations (F₁, consisting of SG and Ar, and F₂, consisting of SG and KA) were obtained to investigate the synergistic efficacy of the co-drug mixture. The MBS and F₁, F₂ formulations were left at room temperature for 24 hours.

3. Results and discussion

The MBS gel was obtained by adding the bioactive mixture to a supramolecular system, which served as a matrix. Figure 1 illustrates the structure of the MBS, which was formed through hydrogen bonds between the -NH, -C=O, and -OH groups of the supramolecular compounds and the glycoside-pyrone-based complex. Therefore, the supramolecular gel provides consistency and enhances absorption efficiency, while the bioactive compounds provide synergistic benefits, having effects against skin disorders.



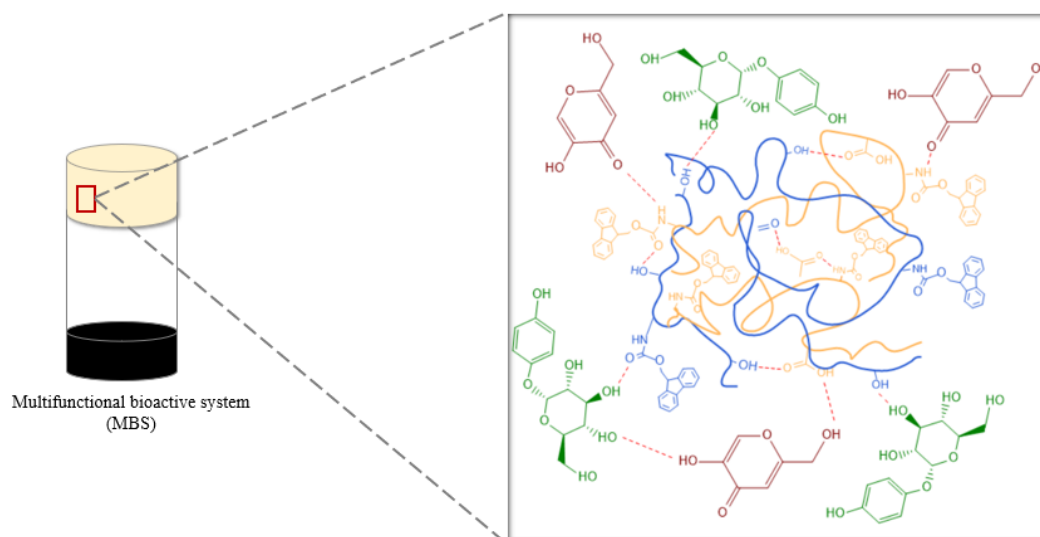


Figure 1. Schematic representation of the MBS structure.

The MBS stability was evaluated over 84 days at different temperatures (4 °C, 25 °C). The bioactive gel was also tested every 7 days to assess its pH and conductivity. As can be seen in Figure 2a, at the initial time point (T_0), freshly prepared MBS exhibited a pH of 6.16. Throughout 12 weeks, the pH of MBS stored at 4 °C decreased to 5.1, similar to skin pH. Evident changes were observed for MBS stored at 25 °C, with a decrease in pH to 3.4 indicating acidification due to compound degradation. Conductivity, an important parameter in assessing the durability of a topical bioactive substance, was initially 2.08 μS . After 12 weeks, conductivity at 4 °C increased slightly to 3.98 μS , while at 25 °C, it rose from 2.08 to 6.3 μS , reflecting increased ion mobility and molecule dissociation with temperature, linked to compound degradation.

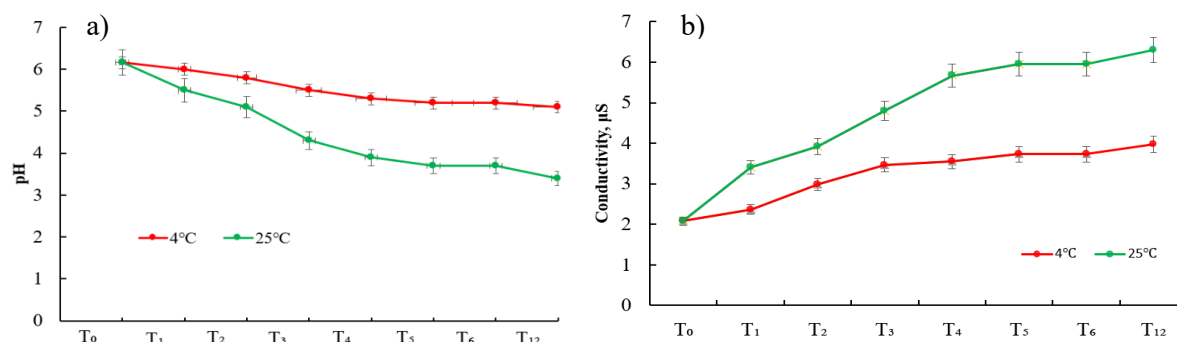


Figure 2. a) pH and b) conductivity values of MBS at 4 °C and 25 °C storage conditions.

The anti-melanogenesis effect and the inhibition mode of the prepared gels were determined by using horseradish peroxidase. The MBS bioactive gel presents a higher peroxidase inhibitory activity than F_1 or F_2 , its inhibition being composition-dependent.

Table 1. The Lineweaver-Burk parameters for Ar, KA, and MBS inhibitors.

Inhibitor	K_m (M)	V_{max} (M/s)	K_{cat} s ⁻¹
Ar	2.482	0.0019	0.191
KA	0.039	0.0002	0.0267
MBS	0.044	0.0002	0.0289
No inhibitor	0.0651	0.0014	0.1447

* K_m - Michaelis constant; V_{max} - maximum velocity; K_{cat} - catalytic constant;

Table 1 shows the Lineweaver-Burk parameters for the Ar, KA and MBS inhibitors, indicating the type of inhibition (competitive, uncompetitive, non-competitive or mixed) characteristic of each inhibitor. In the absence of the inhibitor, a low value of the K_m suggests efficient enzymatic activity. An increase in the K_m value shows that the inhibitor Ar causes competitive inhibition, competing with the substrate for the active site. In the case of KA and MBS inhibitors, the low values of the K_m and V_{max} parameters show that they are uncompetitive inhibitors, binding reversibly to the enzyme-substrate complexes.

4. Conclusions

In conclusion, a multifunctional bioactive system was prepared via physical interactions between amino acid/peptide motifs-based and an arbutin-kojic acid bioactive complex. The study evaluates MBS's potential as an anti-melanogenesis agent. The stability over twelve weeks was assessed by analyzing pH and conductivity, showing better stability at 4 °C than at 25 °C. MBS strongly inhibited peroxidase activity through uncompetitive inhibition, binding only to the enzyme-substrate complex. Overall, the results suggest that MBS is a suitable skin product against hyperpigmentation, with anti-melanogenic effects.

Acknowledgements

This work was supported by a grant of the Ministry of Research, Innovation and Digitalization, CCCDI-UEFISCDI, project number PN-IV-P7-7.1-PED-2024-1788, within PNCDI IV.

References

- [1]. Song W. Melanin: insights into structure, analysis, and biological activities for future development. *J. Mater. Chem. B* 11, 32, 7528–7543, 2023.
- [2]. Phasha V, Senabe J, Ndzotoyi P, Okole B, Fouche G, Chuturgoon A. Review on the use of kojic acid - a skin-lightening ingredient. *Cosmetics* 9, 3, 64, 2022.
- [3]. Venkatesan J, Anil S, Kim SK, Shim M. Marine fish proteins and peptides for cosmeceuticals: a review. *Mar. Drugs*, 15, 5, 143, 2017.
- [4]. Croitoriu A, Chiriac AP, Rusu AG, Ghilan A, Ciolacu DE, Stoica I, Nita L. Morphological evaluation of supramolecular soft materials obtained through co-assembly processes. *Gels* 9, 11, 886, 2023.
- [5]. Santis VD, Chen XL, Laakso I, Hirata A. An equivalent skin conductivity model for low-frequency magnetic field dosimetry. *Biomed. Phys. Eng. Express* 1, 015201, 2015.



NEXT-GENERATION ANTIBACTERIAL MATERIALS:
TAILORED DESIGN AND SYNTHESIS OF PULLULAN DERIVATIVES

Gabriela Biliuta,* Raluca Ioana Baron, Sergiu Coseri

Petru Poni Institute of Macromolecular Chemistry, Romanian Academy, Iasi, Romania

*biliuta.gabriela@icmpp.ro

1. Introduction

The overuse of antibiotics has led to the emergence of multi-drug resistant bacterial strains, posing a significant challenge in the management of wound infections. The primary pathogens associated with such infections include *Staphylococcus aureus* (79.4%), *Pseudomonas aeruginosa* (40.2%), *Proteus mirabilis* (11.2%), and *Staphylococcus haemolyticus* (4.4%), along with other clinically relevant species such as *Klebsiella pneumoniae*, *Enterococcus faecalis*, and *Acinetobacter baumannii*. In the early stages of wound colonization, Gram-positive bacteria—particularly *S. aureus*—are the most prevalent [1]. Natural polysaccharides are widely employed in wound dressing formulations due to their inherent biocompatibility, non-immunogenic nature, and antimicrobial properties. With their diverse chemical and physical characteristics, polysaccharides represent a valuable class of biomaterials for biomedical applications. Many of these polymers exhibit antioxidant and antibacterial activity against both Gram-positive and Gram-negative bacteria, along with notable anti-inflammatory effects—an essential attribute in the treatment of chronic wounds [2]. Previous studies on polysaccharide-based scaffolds for chronic wound healing often highlight the need for chemical crosslinkers or combinations of multiple polysaccharides to achieve desired therapeutic effects. To overcome these limitations, we propose to explore the tunable properties of the natural polysaccharide pullulan by chemically modifying it into a therapeutically active, antibacterial form. Pullulan is a commercially available polysaccharide and biological macromolecule predominantly produced by the yeast-like fungus *Aureobasidium pullulans* [3]. It consists of maltotriose units connected by α -1,4 and α -1,6 glycosidic linkages. Due to its unique physicochemical properties, pullulan and its derivatives have been widely explored for various biomedical applications, including targeted drug and gene delivery, tissue engineering, and vaccine development [4]. Although pullulan is well known for its adhesiveness, biocompatibility, anticoagulant, antithrombotic, and anti-inflammatory properties, it inherently lacks bactericidal activity. To enhance its antimicrobial potential, we hypothesized that the introduction of functional groups through chemical modification—specifically oxidation—could improve its effectiveness against pathogenic bacteria. This study aims to evaluate the impact of pullulan oxidation on its antibacterial activity against bacteria commonly associated with wound infections. Owing to its biocompatibility and biodegradability, oxidized pullulan (PO) holds promise as a multifunctional biomaterial for antibacterial and therapeutic applications.

2. Experimental

Materials and reagents: Pullulan (TCI Europe, Belgium, $M_n \sim 3 \times 10^5$ g/mol by SEC), *N*-hydroxyphthalimide (NHPI), sodium bromide (NaBr), 10% (wt) sodium hypochlorite (NaClO), and other chemicals and solvents were of pure grade (Sigma Aldrich) and used as received without further purification.

Oxidation of pullulan: Pullulan (1 g) was added to 200 mL of deionized water/acetonitrile solution (5:1 vol) containing NHPI (0.5 mM/g pullulan) and NaBr (8 mM/g pullulan) using a magnetic stirrer. The pH was adjusted to 10, and a 10% NaClO solution (10 mM/g pullulan for PO-10 and 25 mM/g pullulan for PO-25) was added to the mixture and kept at room temperature for 5 h under vigorous stirring. The pH was



carefully monitored and kept at pH = 10 during the reaction by using a 0.5 M NaOH solution (to compensate for the decrease in pH due to the formation of carboxyl groups).

Characterization: The NMR spectra were obtained on a Bruker Avance DRX 400 MHz Spectrometer, equipped with a 5 mm QNP direct detection probe and z-gradients. Infrared absorption spectra of samples were acquired using an IRAffinity-1S spectrometer (manufactured by Shimadzu Corp., Kyoto, Japan). The antimicrobial activity was studied using Gram-positive bacteria (*S. aureus* ATCC 25923, *S. lutea* ATCC 9341), Gram-negative bacteria (*E. coli* ATCC 25922, *Pseudomonas aeruginosa* ATCC 27853), and pathogenic yeasts (*C. albicans* ATCC 10231, *C. glabrata* ATCC MYA 2950, *C. parapsilosis* ATCC 22019). Antimicrobial tests were carried out using a disc-diffusion method (CLSI, 2016). A small amount of each microbial culture was diluted in sterile 0.9% NaCl until the turbidity was equivalent to McFarland standard no. 0.5 (106 CFU/mL). The suspensions were further diluted 1:10 in Mueller Hinton agar for bacteria and Sabouraud agar for yeasts and then spread on sterile Petri plates (25 mL/Petri plate). Sterile stainless steel cylinders (5 mm internal diameter; 10 mm height) were applied on the agar surface in Petri plates. Then, 0.1 mL of each compound was added to the cylinders. Commercially available discs containing ampicillin (10 µg/disc), ciprofloxacin (5 µg/disc), and nystatin (100 µg/disc) were used as positive controls. The plates were incubated at 37 °C for 24 h (bacteria) and at 24 °C for 48 h (yeasts). After incubation, the diameters of inhibition zones were measured in mm, including disc size.

3. Results and discussion

Pullulan was selectively oxidized through a NHPI-mediated reaction to introduce carboxylic groups along the polymer backbone. Notably, NHPI alone is insufficient to drive the oxidation; the process critically depends on the formation of the phthalimide-*N*-oxyl (PINO) radical, generated from the hydroxylated NHPI precursor. This PINO radical acts as the key initiator of the catalytic cycle. To enable and enhance this transformation, a combination of NaClO and NaBr is employed (Figure 1a).

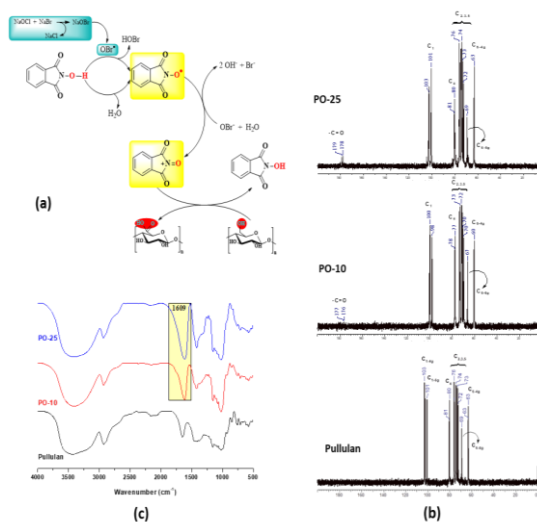


Figure 1. (a) PINO-mediated cycle for the oxidation of the primary OH groups of pullulan in the presence of NaClO/NaBr; (b) NMR spectra of the pullulan and oxidized pullulan; (c) FTIR spectra of the pullulan and its PINO-oxidized correspondents.

This system serves two essential functions: (i) it promotes the conversion of NHPI into the reactive PINO radical, and (ii) it further oxidizes PINO into the nitrosonium cation, which serves as the actual oxidant targeting the primary hydroxyl groups of pullulan. The oxidation of the pullulan was confirmed by NMR spectroscopy, with the ¹³C-NMR spectra indicating the presence of a new signal that was well-defined at 176 ppm, specific to the carboxylic groups (Figure 1b). Also, from the FTIR spectra of the pullulan and oxidized pullulan samples, the formation of carboxylic groups (COO⁻) can be easily observed by the

presence of an absorption band centered at 1609 cm⁻¹ (Figure 1c). The oxidized pullulan samples were employed to test their antimicrobial activity against Gram-positive and Gram-negative bacteria. Both test organisms have multiresistant strains (MRSA, VREC), which often cause problems in the course of medical interventions. The diameters of the inhibition zones (in mm) corresponding to the tested substances are shown in Table 1. All assays were carried out in triplicate. Results are expressed as means ± SD.

Table 1. Antibacterial and antifungal activities of the tested compounds

Sample	Diameter of inhibition zones (mm)						
	<i>S. aureus</i>	<i>S. lutea</i>	<i>E. coli</i>	<i>Pseudomonas aeruginosa</i>	<i>C. albicans</i>	<i>C. glabrata</i>	<i>C. parapsilosis</i>
PO-10	15±0.57	15±0.00	0	0	0	0	0
PO-24	12±0.07	20±0.07	0	0	0	0	0
Ampicillin (10 µg/disc)	29±0.07	34±0.07	21±0.57	NT	*NT	*NT	*NT
Ciprofloxacin (5 µg/disc)	23±0.07	34±0.57	30±0.07	20±0.57	*NT	*NT	*NT
Nystatin (100 µg/disc)	NT*	NT*	NT*	NT*	20±0.00	18±0.57	18±0.57

4. Conclusions

This study demonstrates that oxidized pullulan (PO), synthesized via a single-step selective oxidation process, exhibits notable antibacterial activity against Gram-positive bacteria, specifically *Staphylococcus aureus* and *Sarcina lutea*. In contrast, PO shows no efficacy against Gram-negative bacterial strains and lacks antifungal activity. These findings highlight the selective antimicrobial potential of PO and suggest its applicability may be limited to targeting Gram-positive pathogens.

Acknowledgements

This work was supported by a grant of the Ministry of Research, Innovation and Digitization, CNCS-UEFISCDI, project number PN-IV-P2-2.1-TE-2023-1005, within PNCDI IV.

References

- [1]. Glik J, Kawecki M, Gaździk T, Nowak T. The impact of the types of microorganisms isolated from blood and wounds on the results of treatment in burn patients with sepsis. *Pol. J. Surg.* 84(1), 6–16, 2012.
- [2]. Zhang W, Zhang X, Zou K, Xie J, Zhao S, Liu J, Liu H, Wang J, Wang Y. Seabuckthorn berry polysaccharide protects against carbon tetrachloride-induced hepatotoxicity in mice via anti-oxidative and anti-inflammatory activities. *Food Funct.* 8(9), 3130–38, 2017.
- [3]. Cheng KC, Demirci A, Catchmark JM, Pullulan: biosynthesis, production, and applications. *Appl. Microbiol. Biotechnol.* 92, 29–44, 2011.
- [4]. Singh RS, Kaur N, Kennedy JF. Pullulan and pullulan derivatives as promising biomolecules for drug and gene targeting. *Carbohydr. Polym.* 123, 190–207, 2015.



IDENTIFICATION OF FLUORESCENCE ORIGIN IN
CARBON DOT SYNTHESIS – A CASE STUDY

Ioan-Andrei Dascalu,* Maurusa Ignat, Adina Coroaba, Narcisa-Laura Marangoci

Petru Poni Institute of Macromolecular Chemistry, Romanian Academy, Iasi, Romania

*idascalu@icmpp.ro

1. Introduction

Carbon dots (CDs) are carbon nanomaterials (<10 nm), with a considerable potential for biological applications owing to their extremely low cytotoxicity, excellent water solubility, and unique photoluminescence (PL) properties [1]. Typical preparation methods consist in solvothermal, hydrothermal, or microwave-assisted treatment of natural polymers or small molecular weight compounds. The reaction conditions induce precursor degradation, recombination, and condensation reactions to afford condensed carbon particles, which are considered as stacked graphene sheets with various degrees of ordering. The presence of heteroatoms and surface functional groups are considered to be of significant influence to the photoluminescent behavior of CDs, the selection of precursors is therefore of critical importance [2].

2. Results and discussion

This report describes an attempt to prepare carbon dots through the hydrothermal or solvothermal treatment of *N*-hydroxyphthalimide (NHF) and *o*-phenylenediamine (OPD) (Figure 1). *N*-hydroxyphthalimide was used as the carbon source and for the potential marginal carbonyl and hydroxyl groups that could potentially enhance the fluorescence emission and ensure the water solubility of the resulting CDs. The aromatic diamine was used as a nitrogen source due to its reactivity in condensation or polymerization reactions, which could allow the formation of N-heterocyclic domains within the CDs core. The hydrothermal or solvothermal reactions of a NHF:OPD 3:1 mixture afforded the isolation of dispersion that presented PL emission under UV light (Figure 1).

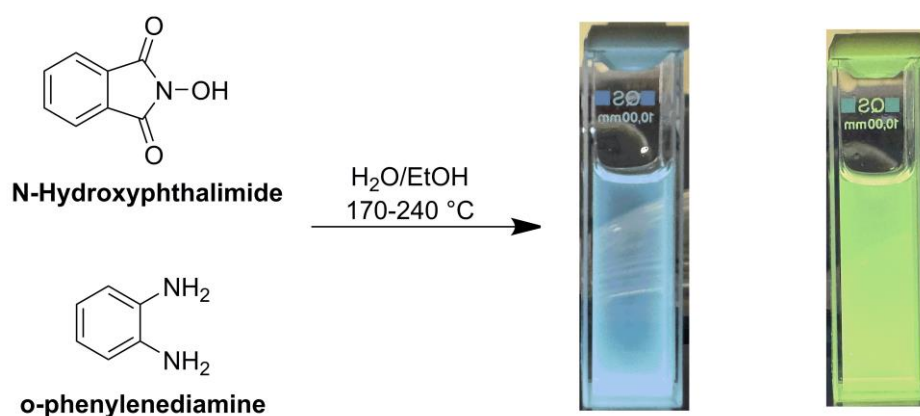


Figure 1. The reagents and reaction conditions used for the hydro- or solvothermal treatment and the resulting dispersion under different wavelengths of UV light.

To further investigate the emission behavior the PL emission spectra of the ethanol dispersion were recorded for excitation wavelengths between 270 and 500 nm (Figure 2). The analysis revealed two broad emission bands: one in the blue region (approx. 440 nm) and one in the green region (approx. 530 nm), depending on the excitation wavelength. The maximum intensity of the green emission band was observed



for $\lambda_{\text{ex}} = 380$ nm. Similar results were obtained for aqueous dispersions isolated from hydrothermal reactions.

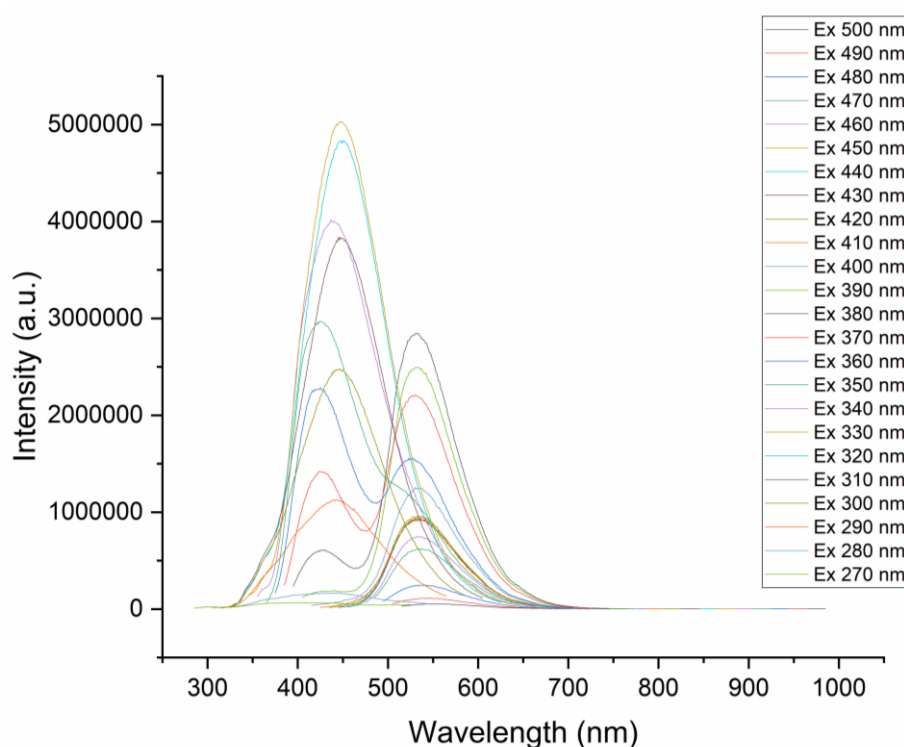


Figure 2. PL emission spectra of the ethanol dispersion isolated from the solvothermal reaction at different excitation wavelengths.

To investigate whether increasing the amount of OPD in the reaction mixture shifts the fluorescence emission maxima of the resulting dispersion to longer wavelengths, additional synthesis experiments were performed using NHF:OPD molar ratios of 2:1, 1:1, and 1:2 under the same reaction conditions. The resulting dispersions displayed emission profiles similar to those observed in the initial synthesis. Due to an increase in the OPD quantity in the reaction mixtures while maintaining the ethanol volume constant, small crystals were isolated in the resulting dispersions following cooling to room temperature.

Single crystal X-ray diffraction analysis (Figure 3) of the crystals revealed the presence of a heterocyclic organic compound. The structure of the isolated bis-benzimidazole compound suggests that in the reaction conditions, the heterocyclic part of NHF is opened and further participates in condensation reactions with OPD to facilitate the formation of two benzimidazole units.

Further investigation of the compound revealed that it can exhibit fluorescence emission. The close proximity of the two benzimidazole units allows the formation of intramolecular hydrogen bonds, which alters the fluorescence emission behaviour of the compound. When intramolecular hydrogen (H) bonds are formed, the observed emission is in the blue region of the spectra, whereas in the absence of the H bonds, the observed fluorescence is in the green region [3]. The emission profile of the organic molecular compound is in this case consistent with that of the dispersions obtained from the hydrothermal or solvothermal treatment of NHF and OPD. In this context it is safe to assume that the photoluminescent properties are imparted mainly by the isolated compound and to a lesser extent by the carbon nanomaterials.



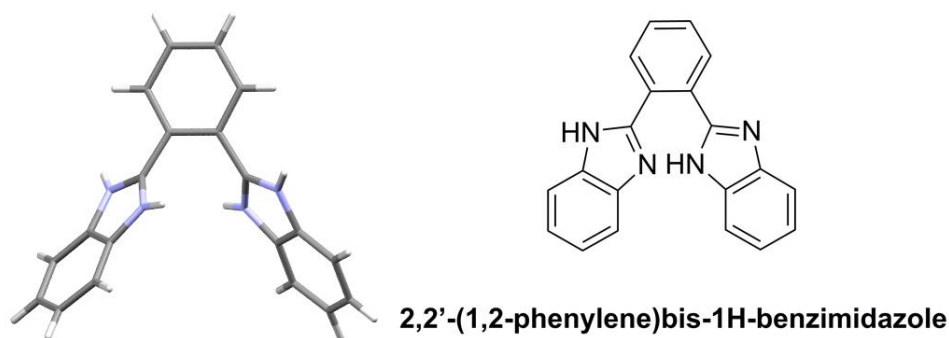


Figure 3. Single crystal X-ray structure and chemical structure of the crystalized compound isolated from the solvothermal treatment of NHF and OPD.

3. Conclusions

In this study, the preparation of carbon dots by the hydrothermal or solvothermal treatment of NHF and ODP was investigated. The photoluminescence profile of the resulting dispersions suggested that the formation of carbon dots had occurred. Additional synthesis experiments performed in the attempt to optimize the optical properties of the carbon nanostructures revealed the presence of an organic molecular compound with the help of X-ray diffraction. Additional investigations concluded that the photoluminescent properties of the dispersions were in fact imparted by the organic compound. The results indicate that the choice of reagents or reaction conditions does not lead to the formation of carbon dots but to a stable organic compound. Additionally, X-ray diffraction is an essential technique for screening organic compounds during the investigation of carbon dots.

Acknowledgements

The authors are thankful for the financial support of the grant of the Romanian National Authority for Research, project no. PNRR-III-C9-2022-I8-291, contract no. 760081/23.05.2023, within the National Recovery and Resilience Plan.

References

- [1]. Coroaba A, Ignat M, Carp OE, Stan CS, Filipiuc SI, Uritu CM, Simionescu N, Marangoci NL, Pinteala M, Ania CO. Antioxidant activity and in vitro fluorescence imaging application of N-, O- functionalized carbon dots. *Sci. Rep.* 15, 25834, 2025.
- [2]. Stan CS, Coroaba A, Simionescu N, Uritu CM, Bejan D, Ursu LE, Dascalu AI, Doroftei F, Dobromir M, Albu C, Ania CO. Mn-doped carbon dots as contrast agents for magnetic resonance and fluorescence imaging. *Int. J. Mol. Sci.* 26(13), 6293, 2025.
- [3]. Jena B, Manoharan SS. Blue to green shifted fluorescence in inter- and intramolecular hydrogen bonded di(benzimidazol-2-yl)benzene. *Chem. Commun.*, 4426-4428, 2009.



INVESTIGATION OF AMINE-RESPONSIVE PROPERTIES OF FUNCTIONALIZED
AZULENES FOR POTENTIAL SENSING APPLICATIONS**Mihaela Homocianu,^{1*} Dragos Lucian Isac,¹ Anton Airinei,¹ Mihaela Cristea²**¹*Petru Poni Institute of Macromolecular Chemistry, Romanian Academy, Iasi, Romania*²*Costin D. Nenitescu Institute of Organic and Supramolecular Chemistry,
Romanian Academy, Bucharest, Romania***mlupu@icmpp.ro***1. Introduction**

Organic amines pose health and environmental risks due to their toxicity [1,2]. Consequently, the development of efficient and reliable sensing systems for their detection is crucial. Azulenes, with their unique donor-acceptor electronic structure, cost-effectiveness, and stability, show considerable promise as sensors for amine and metal ions. This study explores the optical properties of a series of functionalized azulenes for detecting n-butylamine (NBA), ethylenediamine (EDA), and triethylamine (TEA) in methanol. The proposed sensing mechanism involves hydrogen bonding between amine lone pairs and azulene carbonyl groups, altering electronic configurations and optical responses of the amine treated azulenes.

2. Experimental

Azulenes O1-O5 were synthesized as previously reported [3]. UV-Vis titrations were performed by incrementally adding amine stock solutions (0.1 N in H₂O) to methanolic azulene solutions. UV-Vis spectra were recorded using an Analytik Jena 210+ spectrophotometer (200–1100 nm) with a 10 mm quartz cuvette. Binding constants (K_a) were calculated using the Benesi-Hildebrand equation [4]. Limit of detection (LOD) was determined as $LOD = 3\sigma/m$, where σ is the standard deviation of blank measurements, and m is the slope from absorbance versus amine concentration plots. The Gibbs free energy (ΔG) was estimated from $\Delta G = -2.303RT \log K$. The molecular structures of the azulene derivatives taking into consideration for amine interplay have been built and therefore minimized for energetically point. To predict the validity of the optimized geometries, the Hessian matrix has been computed, and no imaginary frequency was obtained. The electronic configuration and interactions were computed with CAM-B3LYP/Def2TZVP method [5,6]. The experimental conditions such as theoretical UV-Vis spectra were mimicked by computational protocol using the polarizable continuum model (PCM) [7] and the integral equation formalism variant (IEFPCM) [8]. Moreover, the UV-Vis spectra were estimated with the time-dependent density functional theory (TD-DFT). The chemical reaction between amine and azulene was described following two pathways. The first step includes an analysis of electron density to localize the active center that can directly participate in the interaction. The second step of computational stage includes the direct interaction between amine and the azulene derivative. The chemistry interaction between azulene derivatives and amine has been calculated with our in-laboratory developed methodology.

3. Results and discussion

The azulene derivatives under study exhibited three characteristic absorption bands: Band I (250–330 nm), Band II (340–390 nm, $\pi \rightarrow \pi^*$ azulene transition), and intense Band III (400–650 nm, high-energy $\pi \rightarrow \pi^*$ transition). Functionalization induced bathochromic shifts in Band III (e.g., O1: 470 nm \rightarrow O5: 546 nm) due to extended π -conjugation (Figure 1a and Table 1).



Table 1. Key spectral responses of O1-O5 to amines.

Samples		Neutral	NBA	EDA	TEA
O1	λ_{\max} , nm	303, 352, 470	330, 400	330, 400	329, 400
O2	λ_{\max} , nm	318, 365, 513	337, 424	336, 424	337, 427
O3	λ_{\max} , nm	320, 365, 489	336, 426	339, 404	336, 407
O4	λ_{\max} , nm	260, 338, 524	334, 409	334, 407	336, 409
O5	λ_{\max} , nm	238, 337, 546	337, 427	336, 426	338, 428

All amines quenched Band III, while Bands I and II increased in intensity. Largest λ_{\max} shifts occurred in O5 ($\Delta\lambda \sim 100$ nm with NBA/TEA), indicating strong binding. Smallest shifts occurred in O3 with EDA. Titration revealed isosbestic points (e.g., 425 nm for O1), confirming complex formation (Figure 1b). Benesi-Hildebrand plots indicated 1:2 stoichiometry (Figure 1c). O5 showed highest K_a ($5.82 \times 10^5 \text{ M}^{-1}$ with NBA) and low LODs (e.g., $5.40 \times 10^{-5} \text{ M}$ for EDA), while unfunctionalized O1 exhibited weakest binding (Table 2).

Table 2. Thermodynamic parameters and detection limits.

Samples		K_a, M^{-1}	$\Delta G, \text{kJ mol}^{-1}$	LOD, M
O1	EDA	2.75×10^4	-25.33	1.04×10^{-4}
O5	NBA	5.82×10^5	-32.89	1.05×10^{-4}
O5	EDA	0.28×10^3	-13.87	5.40×10^{-5}

Negative ΔG values confirmed spontaneous complexation. Binding strength depended on azulene substituents (electron-donating groups enhanced affinity) and amine properties (NBA > TEA > EDA).

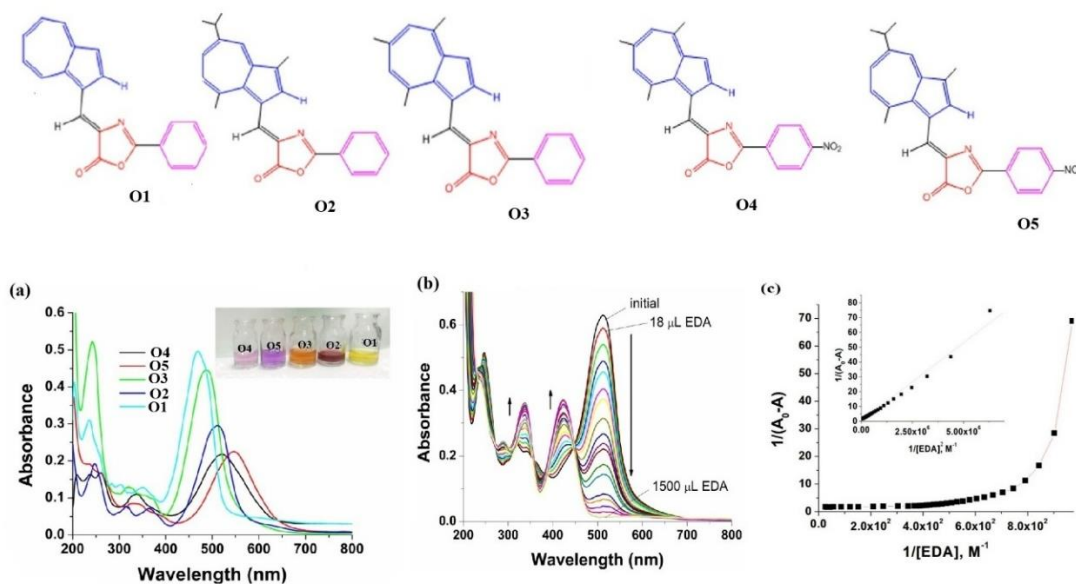


Figure 1. Structures of five azulenes (O1-O5) with UV-Vis absorption spectra in methanol (a); changes in UV-Vis spectra upon titration of O2 with varying amounts of EDA (b); and Benesi-Hildebrand plots to calculate the association constant of O2 towards EDA (c).

In particular, for theoretical calculations the first simulation scenario reveals the interaction between amine and azulene derivatives, and the results were shown in Figure 2a. In this case, the initial reactants were obtained, and the theoretical calculations proceeded with an investigation of the UV-Vis spectra. The study began with the theoretical absorption spectra of the unreacted azulene derivatives (labeled as 1), and continued by probing different amine treating sites, based on prior electron density analyses to identify the most reactive centers. Hence, treating amine azulene species were included in the geometry optimizations. In the second scenario, an explicit interaction between the amine and azulene derivatives was considered.

Theoretical results from this scenario indicate the possible formation of transient species (2-10) during the reaction pathway and the theoretical electronic spectra was depicted in Figure 2b. Both simulation scenarios show good agreement with the experimental data.

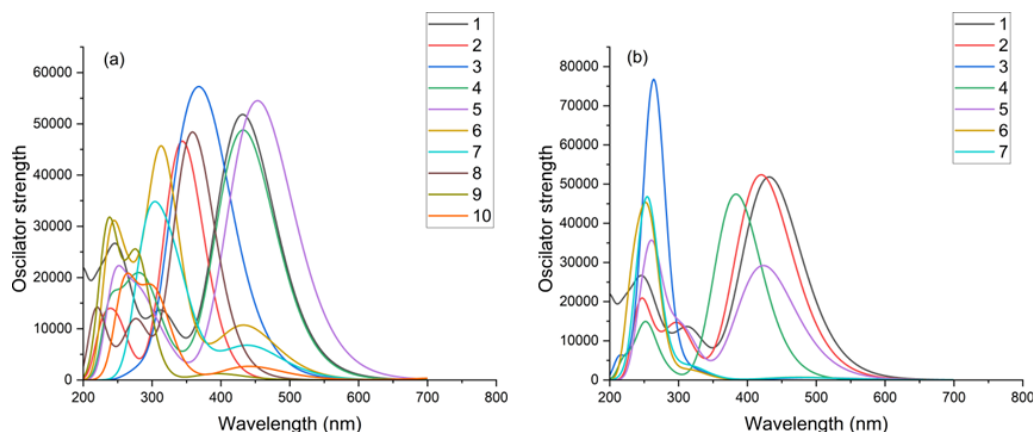


Figure 2. Graphical representation of the electronic absorption spectra of transient species identified through theoretical calculations using the CAM-B3LYP/Def2TZVP method.

4. Conclusions

Functionalized azulenenes (O2-O5) exhibit bathochromic shifts of the absorption maxima vs. unfunctionalized O1. Amine binding quenches Band III, while enhancing Bands I and II *via* electronic perturbations. All 1:2 azulenenes form complexes with amines spontaneously ($\Delta G < 0$). O5 (with push-pull substituents) shows highest sensitivity (K_a up to $5.82 \times 10^5 \text{ M}^{-1}$, LODs $\sim 10^{-5} \text{ M}$). Structure-activity relationships demonstrate tunable amine sensing *via* azulene functionalization. Theoretical results show that, during the reaction between amine and azulene derivatives, protonation is likely to occur at the azulene core, assisted by the formation of transient intermediate species.

References

- [1]. Gheni SA, Ali MM, Ta GC, Harbin HJ, Awad SA. Toxicity, hazards, and safe handling of primary aromatic amines. *ACS Chemical Health & Safety*. 31(1), 8–21, 2023.
- [2]. Zhou C, Liu Y, Liu Z, Qiu Z, Sun Z, Chen M, Xie B, Wen HM., Hu J. A highly sensitive MOF fluorescence probe for discriminative detection of aliphatic and aromatic amines. *J Mat Chem. C* 13, 5611–5616, 2025.
- [3]. Homocianu M, Airinei A, Matica OT, Cristea M, Ungureanu EM. Solvent effects and metal ion recognition in several azulenyl-vinyl-oxazolones. *Symmetry* 15, 327, 2023.
- [4]. Yang C, Liu L, Mu TW, Guo QX. The performance of the Benesi-Hildebrand method in measuring the binding constants of the cyclodextrin complexation. *Anal Sci*. 16, 537, 2000.
- [5]. Yanai T, Tew DP, Handay NC. A new hybrid exchange-correlation functional using the Coulomb-attenuating method (CAM-B3LYP). *Chem Phys Lett*. 393, 51–57, 2004.
- [6]. Weigend F, Ahlrichs R. Balanced basis sets of split valence, triple zeta valence and quadruple zeta valence quality for H to Rn: design and assessment of accuracy. *Phys Chem Chem Phys*. 7, 3297–305, 2005.
- [7]. Tomasi J, Mennucci B, Cammi R. Quantum mechanical continuum solvation models. *Chem Rev*. 105, 2999–3093, 2005.
- [8]. Scalmani G, Frisch MJ. Continuous surface charge polarizable continuum models of solvation. I. General formalism. *J Chem Phys*. 132, 114110, 2010.



POLY(VINYL ALCOHOL)/GELATIN/TANNIC ACID/LIGNIN NANOPARTICLES HYDROGELS FOR AGRICULTURE APPLICATION

Cosmina-Maria Bogza,* Maria-Cristina Popescu

Petru Poni Institute of Macromolecular Chemistry, Romanian Academy, Iasi, Romania

**bogza.cosmina@icmpp.ro*

1. Introduction

Natural and synthetic polymer-derived hydrogels are especially attractive for the agricultural domain. They can serve as planter materials, seedling guards, flower pots, water ponds, soil conditioners, and pesticide carriers [1]. PVA is a biodegradable polymer often employed as a component in hydrogel because of its capability of film forming, its biocompatibility, and biodegradability. Nevertheless, its mechanical properties and environmental response can be improved by the addition of bioactive components and natural cross-linking agents. It has been proved that a plant polyphenol, tannic acid (TA), crosslinks PVA effectively *via* oxidative and hydrogen bonds and thereby imparts high mechanical properties and functionality to the hydrogels [2]. Lignin nanoparticles, which have antibacterial properties, can further enhance the environmental adaptability and functional properties of these materials [3].

In this study, PVA-based hydrogels comprising lignin nanoparticles, gelatin, and tannic acid were developed and characterized.

2. Experimental

Preparation of hydrogels: Initially, a certain amount of tannic acid (TA) was dissolved in distilled water, followed by the addition of PVA to this solution and stirring at 90 °C for 4h. Over the PVA-TA solution, 10 wt% gelatin (GEL) from the total mass of PVA was added, resulting in the PVA-GEL-TA solution. Finally, the lignin nanoparticles solution was added in different concentrations to obtain PVA-GEL-TA-L2%, PVA-GEL-TA-L5% and PVA-GEL-TA-L10% solutions. To obtain the hydrogels the freeze-thawing method was used. The solution was kept for 20h at -20 °C and then for 4h at room temperature.

Chemical structure of hydrogels: PVA-GEL-TA and PVA-GEL-TA-L (2%, 5%, and 10%) hydrogels were structurally analyzed using Fourier transform infrared spectroscopy using an ALPHA Bruker spectrometer. The recording of the spectra was made in absorbance mode and between 4000 and 400 cm⁻¹ spectral regions.

The swelling characteristics and kinetics: Samples that had been previously dried and weighed were submerged in distilled water at room temperature, taken out at prearranged intervals, and weighed. The excess of water was removed with a filter paper. The swelling rate was calculated using the following equation and the data derived from the measurements:

$$\text{Swelling ratio (\%)} = \frac{\text{Weight of swollen gel} - \text{Weight of dry gel}}{\text{Weight of dry gel}} \times 100 \quad (1)$$

The diffusion of polymeric structures and the dynamics of swelling are explained by the Fick's equation.

$$F = S_t / S_e = k t^n \quad (2)$$

F - swelling fraction, S_e - the equilibrium swelling content of the hydrogel, n - the diffusion exponent of the solvent, k - the constant that changes according to the gel's network structure.



3. Results and discussion

Chemical structure of hydrogels

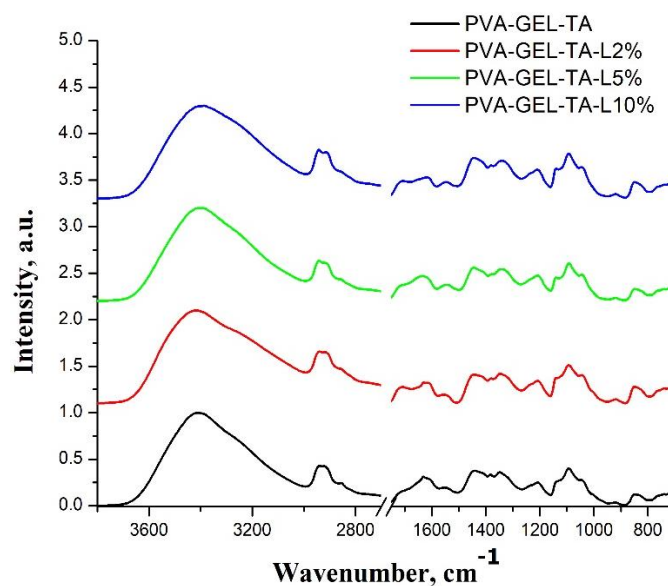


Figure 1. FT-IR spectra of the hydrogels.

The FT-IR results confirm that the lignin nanoparticles were successfully incorporated into the PVA–gelatin–tannic acid matrix. Key spectral changes include stronger O–H stretching signals (due to lignin’s phenolic groups), increased intensity in bands linked to aromatic structures (around 1600, 1510 and 850 cm^{-1}), and slight shifts or changes in the amide I and II protein bands (Figure 1). These suggest that lignin is interacting with gelatin and tannic acid, mainly through hydrogen bonding.

The swelling characteristics and kinetics

Table 1. Maximum sample absorption over cycles and at different temperatures.

Sample Cod	Cycles			Temperature		
	1 st	2 nd	3 rd	20 °C	37 °C	45 °C
PVA-GEL-TA	110.92	105.73	103.06	110.92	139.50	173.20
PVA-GEL-TA-L2%	114.97	108.26	108.26	114.97	145.70	169.38
PVA-GEL-TA-L5%	115.06	115.06	110.85	115.06	149.94	186.25
PVA-GEL-TA-L10%	112.45	112.45	108.24	112.45	141.85	162.74

One thing that affects the hydrogel's swelling capacity is the concentration of lignin nanoparticles. At low concentrations, the nanoparticles are well dispersed, promoting pore formation and establishing hydrogen bonds with the matrix. This results in a more porous network, which helps the hydrogel absorb more water, as seen for the samples with 2% and 5% lignin.

However, as the lignin concentration increases, the nanoparticles tend to agglomerate. This reduces their ability to interact with the polymer matrix, since there's less surface area available. In the 10% lignin sample this aggregation leads to a denser, less porous structure. As a result, the hydrogel absorbs less water, due to less available sorption sites and smaller pores (Table 1) [4].



Table 2. Kinetic parameter for the swelling process of hydrogels.

Sample Cod	Temperature		
	20 °C	37 °C	45 °C
	Diffusion exponential (n)		
PVA-GEL-TA	0.841	0.467	0.540
PVA-GEL-TA-L2%	0.897	0.458	0.558
PVA-GEL-TA-L5%	0.826	0.582	0.562
PVA-GEL-TA-L10%	0.861	0.570	0.544

As the temperature increases, the hydrogel matrix relaxation is higher, thus the water molecules have more freedom to move. This facilitates the penetration of water into the hydrogel matrix, while the network itself becomes more swollen, leading to the creation of more voids and larger pores into which water can penetrate. When the equilibrium between hydrophobic and hydrophilic components is established, the hydrogel structure remains open instead of being compacted, thus the interactions between water and hydrogel are stronger.

Additionally, the higher kinetic energy of water molecules at elevated temperatures speeds up diffusion and can even help the polymer network rearrange itself [5]. As shown in the Table 2, this change in behavior also shifts the diffusion mechanism from non-Fickian at 20 °C towards Fickian at higher temperatures.

4. Conclusion

In conclusion, hydrogels are obtained by combining biodegradable and biocompatible components, such as PVA, tannic acid, gelatin and lignin nanoparticles. These can offer a promising approach for sustainable agricultural applications as they have water-retaining properties and makes them suitable for nutrient delivery and soil enhancement.

References

- [1]. Guilherme MR, Aouada FA, Fajardo AR, Martins AF, Paulino AT, Davi MFT, Rubira AF, Muniz EC. Superabsorbent hydrogels based on polysaccharides for application in agriculture as soil conditioner and nutrient carrier: a review. *Eur. Polym. J.* 72, 365–385, 2015.
- [2]. Karakuş NR, Türk S, Guney Eskiler G, Syzdykbayev M, Appazov NO, Özacar M. Investigation of tannic acid crosslinked PVA/PEI-based hydrogels as potential wound dressings with self-healing and high antibacterial properties. *Gels*. 10(11), 682, 2024.
- [3]. Thakur VK, Thakur MK. Recent advances in green hydrogels from lignin: a review. *Int. J. Biol. Macromol.* 72, 834–847, 2015.
- [4]. Wu L, Huang S, Zheng J, Qiu Z, Lin X, Qin Y. Synthesis and characterization of biomass lignin-based PVA super-absorbent hydrogel. *Int. J. Biol. Macromol.* 140, 538–545, 2019.
- [5]. Lan Y, Xie Z, Wang T, Lu J, Li P, Jiang J. Characterization of cross-linking in guar gum hydrogels via the analysis of thermal decomposition behavior and water uptake kinetics. *Sustainability*. 15(12), 9778, 2023.



NEW NANOCOMPOSITE MATERIALS WITH MULTIPLE THERMOREGULATION MECHANISMS – MATNANOTHERM

George Theodor Stiubianu,¹ **Bianca-Iulia Ciubotaru**,^{1,2*} Alexandra Bargan,¹
Mihaela Dascalu,¹ Adrian Bele,¹ Cristian Ursu,¹ Roxana Solomon¹¹Petru Poni Institute of Macromolecular Chemistry, Romanian Academy, Iasi, Romania²Department of Biomedical Sciences, Faculty of Medical Bioengineering,
Grigore T. Popa University of Medicine and Pharmacy, Iasi, Romania

*ciubotaru.bianca@icmpp.ro

1. Introduction

Taking inspiration from the capabilities of the mirror comb-footed spider (*Thwaitesia sp.*) able to adjust very fast its shape, color, and light reflection, we aimed to develop an innovative biomimetic platform as thermoregulatory composite material (Figure 1). The advantages of passive strategies for thermal comfort (low cost, straightforward implementation, and energy efficiency) will be brought together with the fast on-demand control capabilities of active strategies for thermal comfort. The new nanocomposite will have the advantage of the flexibility of silicone chemistry as a cost-affordable approach to develop a laboratory technology for thermoregulatory clothing which can significantly expand the temperature range for a comfortable thermal envelope for the user. Approximately 14% of the energy use is directed for heating and cooling buildings. Novel thermoregulatory clothing which brings together the advantages of passive thermoregulation with the on-demand active control capabilities would reduce energy use. Inspired by light-reflecting capability of the mirror-spider skin, we developed nanocomposite materials with tunable thermal infrared properties. This material is two-sided, one side can keep the skin surface cool in warm environments and the other side can keep the skin warm in cold environments, and it can regulate a heat flux of $>50 \text{ W/m}^2$ for setpoint temperature ranges between 0–40 °C.

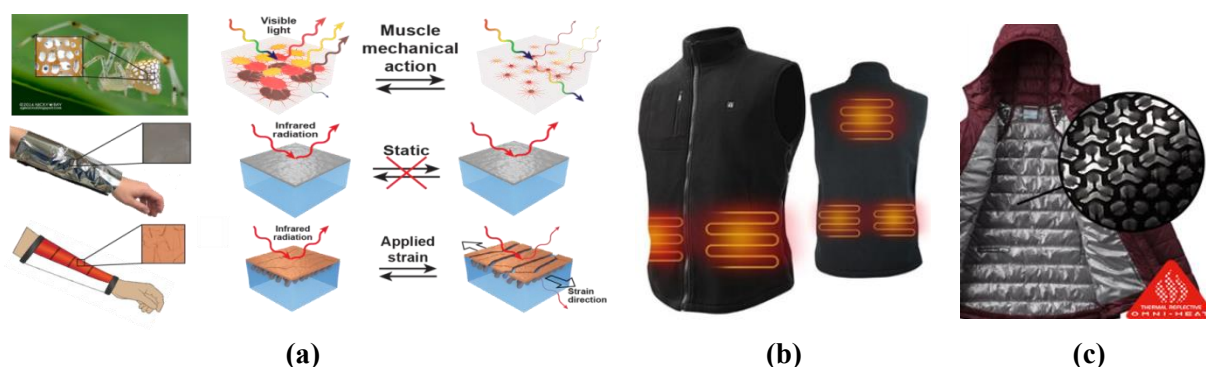


Figure 1. (a) Bioinspired dynamic polymer-based thermal comfort nanocomposites; (b) active clothing; (c) passive clothing.

2. Experimental

The air gap thickness t_a , and thermal comfort material thickness t_m , are \ll the size of human body - heat transfer can be modelled as 1D transport between parallel slabs. The air between the skin and thermal comfort material is stationary - convective heat transfer is negligible in this region. Air circulation through the thermal comfort material and between clothing and the skin surface is negligible. Internal scattering and internal self-absorption within the material are negligible. The absorption and emission are linear within the nanocomposite material. The skin temperature is $T_1=31\ldots35 \text{ }^\circ\text{C}$, the ambient temperature is $T_6=30 \text{ }^\circ\text{C}$ for cooling and $T_6=15 \text{ }^\circ\text{C}$ for heating (Figure 2). The body is in a sedentary state-uniform skin temperature and heat generation.

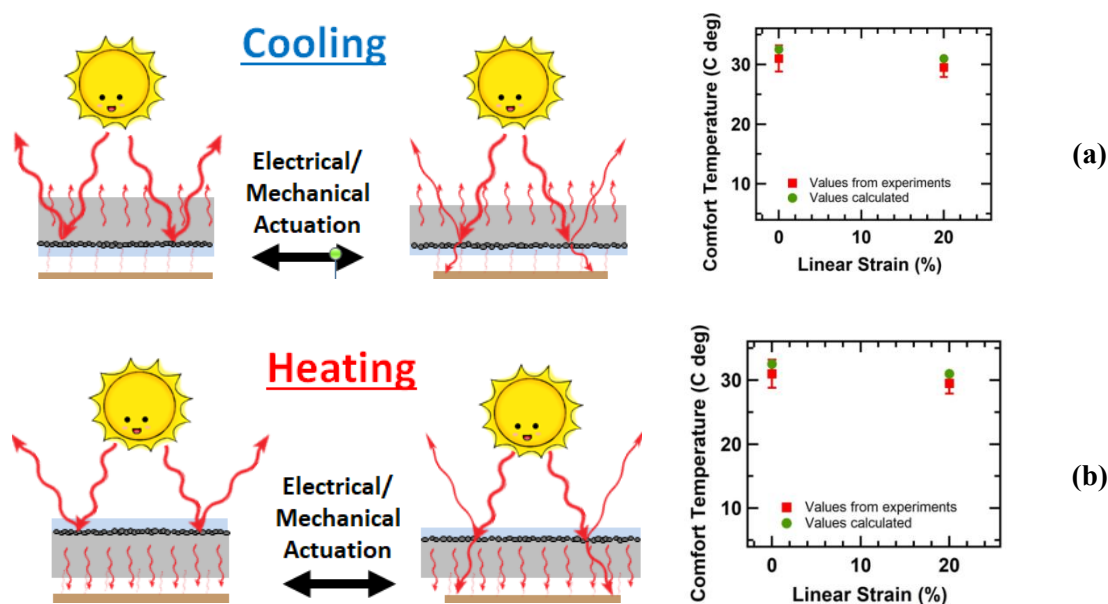


Figure 2. Expanded temperature range for different types of environments:
(a) hot and (b) cold environment.

3. Results and discussion

First, to prepare the base of reflective metal layer, 10-20 nm thick planar metal film (Cu, Al, Ni) was deposited onto a silicon wafer (University Wafer) by using an electron beam evaporation system. Next, to embed the nanosized layer within an IR-transparent elastomer, a 30 μm thick film of styrene block copolymer was spincoated directly on the metal-modified substrate. Lastly, the material was treated at 60-70 $^{\circ}\text{C}$, followed by delamination with a Mylar frame. The material was characterized in terms of physical, mechanical (Instron 3365 Universal Testing System), morphological (SEM), and IR (Perkin Elmer FTIR Spectrometer with a Pike Technologies Integrating Sphere) properties.

One of the main innovative aspects of the thermoregulating material and the integrated clothing with dynamic thermoregulating capability is the use of all four mechanisms of heat exchange to manage the heat exchange with the environment and to preserve the thermal comfort of the user. Thus, this platform for thermal regulation will use synthetic polymers, metal nanolayer, and textile fabric, as well as polymers with capacity for water transport (Figure 3.A). The heat exchange by radiation represents over 50% of heat exchange in sedentary environments, such as offices and can be tuned by the nanometer thick metal layer. The heat exchange by perspiration/evaporation constitutes is $\sim 50\%$ of heat exchange in highly active environments, such as sports activities and the use of polymer materials with sulfonic groups.

In order to lower the research costs and achieve the objective in the desired timeline, we used commercial polymers with proven capability for an unparalleled transport rate for moisture vapor when compared with classic textile materials (Figure 3.B), being instrumental in providing a sensation of thermal comfort in humid environments and during intense exercise. The heat exchange by convection constitutes $>50\%$ of heat exchange in extremely windy environments such as marine and polar environments. The heat exchange by conduction, due to contact between the thermoregulatory clothing and skin is another mechanism besides infrared radiation, for transfer of heat between skin and clothing.

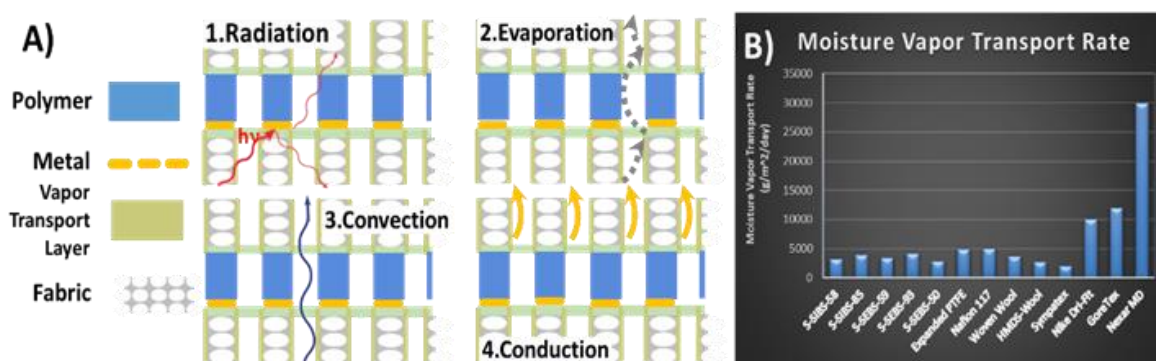


Figure 3. A) Mechanisms of heat exchange applied to the structure of the proposed thermoregulatory nanocomposite clothing, which consists of a metal or metal oxide film deposited on a patterned polymer support between two layers of textile cloth with dissimilar thermal properties: **1.** heat exchange by radiation. **2.** heat exchange by perspiration/evaporation. **3.** heat exchange by convection. **4.** heat exchange by conduction. b) comparison of moisture vapor transport rate for different textiles, shows the excellent value for polymer material with sulfonated groups such as Nexar MD, leading to unparalleled capability for heat exchange by perspiration/evaporation and preservation of dry non-sweat skin.

4. Conclusions

A dynamic thermo-regulatory platform based on flexible, stretchable and conformable polymer was developed. The polymer-based material displays a unique reversible mechanism of mechanically-actuated changes in surface nanosized structure of metal layer. The material adaptively alters the reflectance and transmittance within the thermal infrared region of the electromagnetic spectrum and, thus, changes its thermoregulatory properties to resemble those of various common wearable materials, such as the space blanket, fleece lining, wool, and cotton, as well as construction and insulation materials for buildings. It behaves like radiative thermal switch providing ease of actuation, reversibility and tunability without hysteresis, dynamic environmental setpoint temperature ranges resembling common clothing materials, and can precisely regulate local body temperature changes for wearers in real time. The manufacturing of such materials can be scaled up for commercial applications with low-cost commercial polymers in order to cover millions of square meters of surface area for buildings, clothing and electronics

Acknowledgements This work was supported by a grant of the Ministry of Education and Research – UEFISCDI, project number PN-IV-P7-7-1-PED-2024-2073, MatNanoTerm (Contract 50PED/2025).

References

- [1]. Choi JH, Yeom D. Development of the data-driven thermal satisfaction prediction model as a function of human physiological responses in a built environment. *Build. Environ.* 150, 206–218, 2019.
- [2]. Leung EM, Escobar MC, Stiubianu GT, Jim SR, Vyatskikh AL, Feng Z, Garner N, Patel P, Naughton KL, Follador M, Karshalev E, Trexler MD, Gorodetsky AA. A dynamic thermoregulatory material inspired by squid skin. *Nat. Commun.* 10, 1947, 2019.
- [3]. Xu C, Stiubianu GT, Gorodetsky AA. Adaptive infrared-reflecting systems inspired by cephalopods. *Science* 359, 1495–1500, 2018.

POLYIMIDE-BASED SENSING COATINGS FOR PHENOL VAPOURS DETECTION

Adriana-Petronela Chiriac,* Irina Butnaru, Mariana-Dana Damaceanu

Petru Poni Institute of Macromolecular Chemistry, Romanian Academy, Iasi, Romania

**chiriac.adriana@icmpp.ro*

1. Introduction

Phenol and phenolic compounds are important contaminants of food and environment, exhibiting significant toxicity with harmful effects on plants, animals and human health. As a chemical pollutant, phenol is produced by different industries such as pharmaceutical, dye, oil, detergent, and chemical synthesis, being easily absorbed by the skin, with carcinogenic effect on humans, whose determination and monitoring are of great importance. For this reason, the US Environmental Protection Agency and European Commission have placed phenol and phenolic compounds on the Priority Pollutants List to be monitored in the next years. Different techniques are used to determine phenolic derivatives, such as spectroscopy methods (Raman, infrared, colorimetry, fluorimetry), gas chromatography coupled with mass spectrometry, electrochemical methods (capacitive, voltametric), and capillary electrophoresis, which are time-consuming and require expensive equipment [1,2].

In the last years, versatile sensor technologies have been employed for air quality monitoring, each with specific advantages and limitations. Due to their strong adsorption capacity, excellent electrical conductivity and optical properties, graphene-based materials and conducting polymers-based materials are considered high-potential sensing layers in the development of sensors for phenolic compounds [3]. Among different sensors for phenol detection, spectrophotometric and fluorescence - based sensors which use optical fibers demonstrated fast and accurate response [2]. Electrochemical gas sensors are also very challenging due to their sensitivity, selectivity, and operation at room temperature. Thus, a voltammetric sensor based on sodium polyacrylate was successfully used as electrochemical sensor for phenol detection at room temperature [1].

Polyimides are high-performance polymers that possess excellent properties, such as high resistance to extreme temperatures, good dielectric and mechanical properties, chemical stability, strong processability, biocompatibility, ease of deposition onto various substrates, and flexibility, leading to applications in aerospace, medical, electronic devices, energy storage devices, or sensors (humidity, temperature and gas sensors) [4]. For this reason, polyimides were used as matrix in the development of numerous polymer composites. Hybrid materials show better characteristics than the aggregate of the inborn properties of the individual material and essentially have usefulness that is absent in either of the individual materials.

Recently, our group developed molecular sensors based on polyimides containing hydroxy group grafted on triphenylmethane core as receptor for the fluoride anion recognition [5]. Since phenols display good affinity for halogenated derivatives, using tetrabutylammonium bromide (TBAB) dispersed in a polymer matrix should enable the detection of the OH group from phenol by interaction with bromide anion from the TBAB salt. The interaction of bromide anion with the polar segments in the polyimide and/or with the carbonyl imide groups through dipole-ion bonds, may lead to film morphology and even hydrophobicity changes. This may enable the overall increase of sensing ability of the hybrid material towards phenol detection. Considering all these aspects, here we report the synthesis and characterization of a hybrid material based on TBAB-as inorganic filler and a polyimide as polymer matrix, to be used as sensing coating in interferometer sensors for phenol detection.



2. Experimental

The synthesis of the polyimide matrix incorporating isopropylidene and ether group was made by a two-step polycondensation reaction, starting from commercially monomers 4,4'-(4,4'-isopropylidenediphenyl-1,1'-diyl-dioxy)-dianiline and 4,4'-(4,4'-isopropylidene diphenoxy)-bis(phthalic anhydride) (BPADA), which were mixed in *N*-methylpyrrolidone (NMP) at a concentration of 15%. In the first step, the two monomers were mixed and stirred at room temperature for 16h to obtain the intermediary polyamic acid (PAA). In the second step, PAA was converted into the corresponding polyimide by cyclodehydration reaction at high temperature (180°C) for 6h, under a strong flow of nitrogen, also used to eliminate the water resulted from the process. Due to the presence of flexible ether and isopropylidene groups, the polyimide exhibited a very good solubility, in polar solvents such as NMP, DMAc, DMF or DMSO, and even in less polar solvent, such as CHCl₃ and THF. The increased processability in various solvents sustains the good film-forming ability and further development of homogeneous films. To obtain hybrid material, the polyimide was mixed with 10 w.t.% TBAB in CHCl₃, followed by stirring at room temperature. A salt-free polyimide solution was also prepared to be used as benchmark for the preliminary detection measurements. Both solutions were further processed into thin coatings by drop casting onto glass/quartz and SiO₂, followed by solvent evaporation at room temperature. The pathway to obtain the hybrid composite coating is presented in Figure 1.

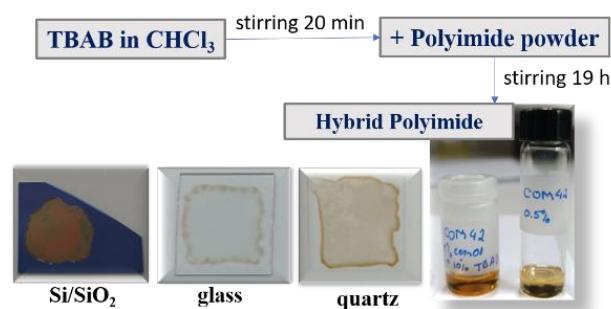


Figure 1. The schematic representation of the hybrid polyimide and photographs of the coatings obtained onto Si/SiO₂/glass/quartz/supports.

3. Results and discussion

The structural characterization of the polyimide matrix was performed by using ¹H-NMR and FTIR spectroscopies (Figure 2). Thus, in ¹H-NMR spectrum, the absence of the signal corresponding to the amide (~9.5–9 ppm) and carboxylic (~15–13 ppm) protons demonstrated the complete cyclodehydration reaction of the intermediary polyamic acid to the fully cyclized imide form. The aliphatic protons were identified in the range of 1.76–1.71 ppm, while the aromatic ones were found at 7.91–6.99 ppm. FTIR spectroscopy also evidenced the formation of the imide cycle by the absorption bands found at 1778 and 1722 cm⁻¹ (C=O symmetric and asymmetric stretching vibrations), at 1374 cm⁻¹ (C–N stretching) and at 744 cm⁻¹ (imide ring deformation). Other functional groups were found at 1237 cm⁻¹ (aromatic ether groups), 2968 and 2875 cm⁻¹ (C–H aromatic linkage).

The detection studies have been performed by using UV-Vis, fluorescence, FTIR and contact angle measurements, before and after exposure to phenol. The UV-Vis absorption spectra showed the appearance of new absorption bands (at 216 nm and 271 nm), which gradually increased after exposure to phenol. In the case of the polyimide benchmark, no specific bands associated with phenol adsorption were observed. The fluorescence spectroscopy evidenced a shift (from 400 nm to 382 nm) and a decrease in the emission band maximum after the sensitive coating interacted with phenol.

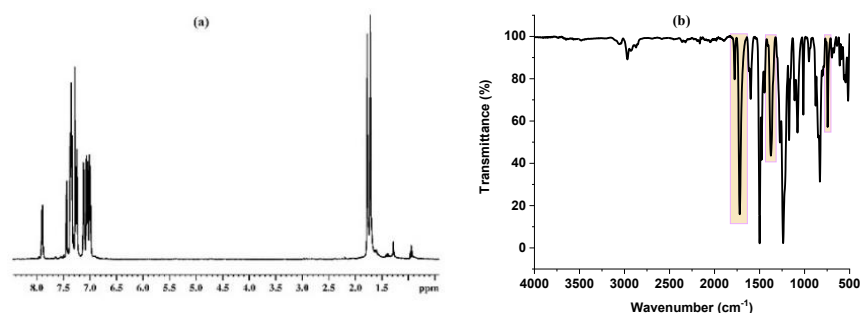


Figure 2. (a) ¹H-NMR spectrum, and (b) FTIR spectrum of polyimide matrix containing isopropylidene and ether units.

FTIR spectra revealed that after several minutes of exposure to phenol, a broad band appeared at about 3350 cm⁻¹ which was associated with the stretching vibration of the -OH group from phenol. Also, the formation of hydrogen bonds with the carbonyl group from the imide matrix, together with a slight shift and change in intensity of the C=O imide absorption band was observed, which confirmed the presence of adsorbed phenol in the hybrid material. Contact angle measurements showed a decrease in the value after exposure to phenol vapours from 43 to 29°, which indicates an increase of the coating wettability as a consequence of phenol adsorption.

4. Conclusions

A hybrid polyimide material was developed to be used as sensing coating material in phenol detection. The flexible structure of the polyimide matrix enabled mixing with 10 w.t.% TBAB in low boiling solvent, which further allowed generation of homogenous thin coatings on various substrates. The preliminary results showed changes in UV-Vis and FTIR spectra which indicate strong interactions of phenol with both polyimide and TBAB, most likely due to ion-dipole interactions between the -OH group of phenol and TBAB, but also hydrogen interactions of Phenolic OH with carbonyl imide group. Contact angle measurements supported the adsorption of phenol in the coating material, leading to an increased the hydrophilicity. Therefore, the obtained polyimide hybrid can be regarded as a potential candidate to be further tested as sensitive layer in sensors for phenol detection.

Acknowledgements

This work was financially supported by Horizon Europe, the European Union's Framework Programme for Research and Innovation (HEU 2021-2027) under grant agreement nr. 101135796 (COMPAS).

References

- [1]. Romih T, Menart E, Jovanovski V, Jerič A, Andrenšek S, Hocevar S. Sodium-polyacrylate-based electrochemical sensors for highly sensitive detection of gaseous phenol at room temperature. *ACS Sens.* 5, 2570–2577, 2020.
- [2]. Delfino I, Diano N, Lepore M. Advanced optical sensing of phenolic compounds for environmental applications. *Sensors* 21, 7563–7588, 2021.
- [3]. Hashim HS, Fen YW, Omar NAS, Fauzi NIM. Sensing methods for hazardous phenolic compounds based on graphene and conducting polymers-based materials. *Chemosensors* 9, 291–331, 2021.
- [4]. Lin J, Su J, Weng M, Xu W, Huang J, Fan T, Liu Y, Min Y. Applications of flexible polyimide: barrier material, sensor material, and functional material. *Soft Sci* 3, 1–53, 2023.
- [5]. Chiriac AP, Butnaru I, Damaceanu MD. Electrochemically active polyimides containing hydroxyl-functionalized triphenylmethane as molecular sensors for fluoride anion detection. *Electrochim. Acta* 353, 136602, 2020.



HYBRID THERMOREVERSIBLE POLYURETHANE-PEPTIDE HYDROGELS WITH SELF-HEALING PROPERTIES

Alexandra Lupu,^{1*} Luiza Madalina Gradinaru,¹ Vasile-Robert Gradinaru,² Maria Bercea,¹

¹*Petru Poni Institute of Macromolecular Chemistry, Romanian Academy, Iasi, Romania*

²*Alexandru Ioan Cuza University of Iasi, Faculty of Chemistry, Iasi, Romania*

*lupu.alexandra@icmpp.ro

1. Introduction

Self-healing hydrogels are smart three-dimensional chemical or physical reversible networks that are distinguished by the ability to recover their structure after the action of external forces and restore the original shape and functionality. Stimuli-responsive systems that exhibit self-healing characteristics have received attention for the development of various scaffolds used especially in the biomedical fields such as tissue engineering, wound dressings, drug carriers and so on [1-3].

In order to obtain new biocompatible hydrogels with antimicrobial and antioxidant characteristics, many researchers explored the specific interactions between polymer chains and peptides. By combining the amphiphilic polyurethane structures with self-assembly blocks with peptide sequences, novel gels could be designed as drug carriers for targeted delivery. Thus, different polyurethane-peptide systems have been formulated, to induce the bioactivity [4,5] or to control the degradation [6,7] of the material.

The aim of this study was to prepare novel thermoreversible amphiphilic polyurethane/peptide-based hydrogels that could function as a platform for sustained release of various drugs or biomolecules in physiological conditions.

2. Experimental

The amphiphilic polyurethane (APU) was synthesized by the classical polyaddition reaction, using one equivalent of Pluronic P123, as soft segment, and two equivalents of 1,6-hexamethylene diisocyanate (HDI) as hard segments. The composite polyurethane/peptide-based hydrogels were obtained by mixing an aqueous solution of 20% APU with DVCYYASR peptide (PEP) solutions in a mass ratio of APU: PEP = 1000:1; 500:1; 250:1 (denoted as S1, S2 and S3, respectively). All samples were analyzed in similar conditions with the polyurethane sample, denoted APU.

The thermostated gels at 37°C were investigated in different shear conditions. A thixotropy test was carried out in strain steps oscillatory mode for $\omega = 5$ rad/s and step strains successively varied every 300 s from low (1%) to high values (50%, 100%, 200%, 500%, and 1000%) and again the low step of strain (1%). The creep and recovery behaviors were analyzed by applying different constant shear stress values during the creep test (30 s), followed by the shear stress removal. The strain recovery was monitored in time.

3. Results and discussion

The self-healing ability of the hydrogels was analyzed by performing rheological tests to assess the structure recovery. The thixotropy of the hydrogel samples was analyzed in oscillatory shear conditions for $\omega = 5$ rad/s, when step strains were applied successively for 5 minutes. Firstly, a low amplitude strain ($\gamma = 1\%$, in the linear range of viscoelasticity) was applied, followed by a high amplitude deformation and again the low strain value was selected ($\gamma = 1\%$). The high strain values for the step 2 were selected in the nonlinear viscoelastic regime: 50%, 100%, 200%, 500%, and 1000%. During these experiments, the viscoelastic parameters G' , G'' and $\tan\delta$ were monitored as a function of time (Figure 1). Polyurethane sample (APU), which includes only polymer in its composition, presented very good recovery after the first three cycles



of deformation. The required time to recover the initial structure is higher as the strain increases, from 30 s after the first cycle, at $\gamma = 50\%$ to 200 s after the fourth cycle ($\gamma = 500\%$). For high values of deformation, the structure recovery is delayed and the initial values of the rheological parameters (corresponding to the rest state) are reached during more than 2000 s.

After shearing in various conditions of deformation, for the hybrid APU/peptide hydrogels the recovery of the network structure after every cycle of deformation is also a time-dependent process, but it is completed after 300 s. However, the structural integrity is less affected by the high strains applied in the case of peptide-containing systems compared to the pure polyurethane (sample APU). The hydrophobic interactions and hydrogen bonds responsible for the formation of network structure are reestablished relatively quickly, in about 300 s.

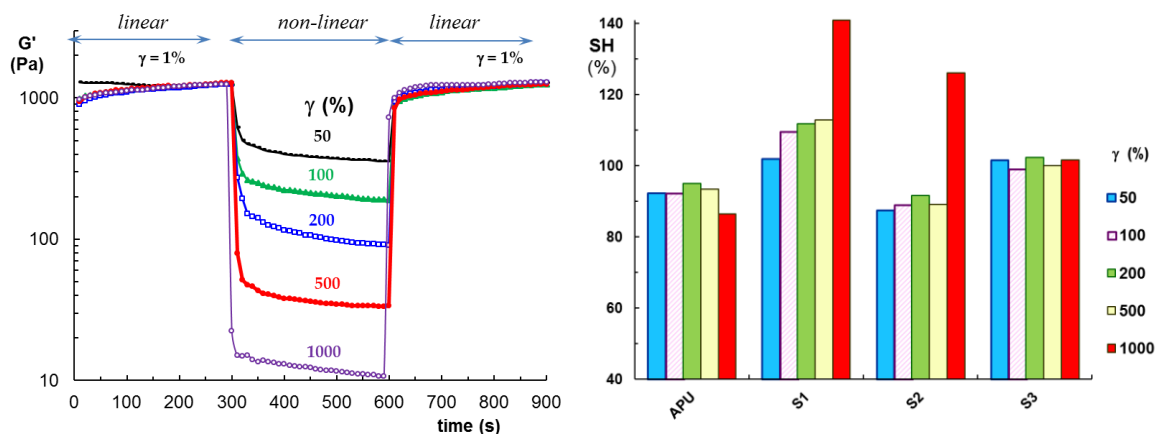


Figure 1. (a) The elastic modulus G' for sample S3 during the thixotropy experiments at successive low, high and low strain steps applied every 300 s; (b) self-healing efficiency (SH, %).

By considering the self-healing ability, the optimum behavior for the gels investigated in the present study is shown by formulation S3. In this case, the gelation starts at room temperature, the network strength is close to the S3 formulation, but the structure recovery occurs in 300 s after the sample was subjected to several cycles of large deformations (Figure 1).

The viscoelasticity of the hydrogels can also be revealed through the creep and recovery tests (Figure 2). The gels were submitted to constant shear stress (σ) for $t = 30$ s, and a time-dependent strain (t) is registered. During the creep test, $\gamma(t)$ is correlated with the creep compliance, $J(t)$ (Figure 2b). Then, after 30 s the shear stress is removed and the recovered strain is followed until the equilibrium state is attained (Figure 2a). A remarkable behavior was observed for the investigated hydrogels, they show only instantaneous elastic deformation and delayed elastic deformation [7], the viscous component being negligible.

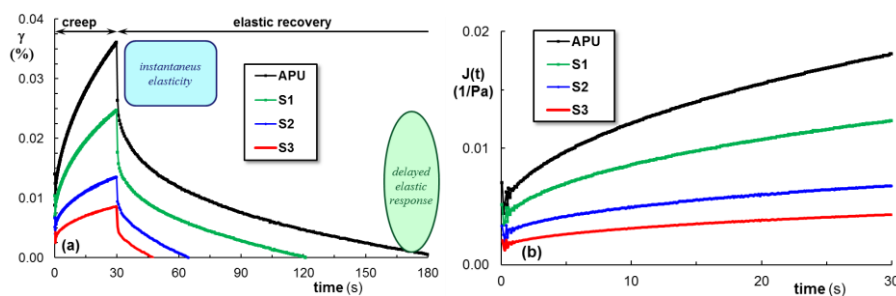


Figure 2. The behavior of hydrogel samples (APU, S1, S2 and S3) (a) creep and elastic recovery; (b) $J(t)$ variation during creep tests [7].

4. Conclusions

The self-healing ability of the thermoreversible polyurethane hydrogels was investigated by performing rheological tests in various shear conditions that offer information concerning the viscoelastic behavior and the structure recovery after applying high values of strain. The complete recovery of the rheological parameters corresponding to the rest state after removing the repetitive action of high strain demonstrates the stability and of network and reversible behavior of hybrid gels when it is submitted to external deformations. This excellent self-healing ability was attributed to the physical interactions established into the micellar network between the polyurethane functional groups and peptide molecules that enable the structural entities to quickly reorganize as a function of the deformation state.

The results demonstrated that the hybrid polymer/peptide hydrogels present a great potential as carriers for the targeted delivery of hydrophobic drugs or biologically active peptides. Therefore, the study provides a new method for the development of tailored medical devices by using minimally invasive procedures.

References

- [1]. Pathan N, Shende P. Strategic conceptualization and potential of self-healing polymers in biomedical field. *Mater. Sci. Eng. C*. 125, 112099, 2021.
- [2]. Rumon MMH, Akib AA, Sultana F, Moniruzzaman M, Niloy MS, Shakil MS, Roy CK. Self-healing hydrogels: development, biomedical applications, and challenges. *Polymers*. 14, 4539, 2022.
- [3]. Lupu A, Gradinaru LM, Rusu D, Bercea M. Self-healing of Pluronic® F127 hydrogels in the presence of various polysaccharides. *Gels*. 9, 719, 2023.
- [4]. Aluri R, Jayakannan M. Development of tyrosine-based enzyme-responsive amphiphilic poly(ester-urethane) nanocarriers for multiple drug delivery to cancer cells. *Biomacromolecules*. 18, 189–200, 2017.
- [5]. Ding X, Chin W, Lee CN, Hedrick JL, Yang YY. Peptide-functionalized polyurethane coatings prepared via grafting-to strategy to selectively promote endothelialization. *Adv. Healthc. Mater.* 7, 1700944, 2018.
- [6]. Benhardt H, Sears N, Touchet, T, Cosgriff-Hernandez E. Synthesis of collagenase-sensitive polyureas for ligament tissue engineering. *Macromol. Biosci.* 11, 1020–1030, 2011.
- [7]. Gradinaru LM, Bercea M, Lupu A, Gradinaru VR. Development of polyurethane/peptide-based carriers with self-healing properties. *Polymers*. 15, 1697, 2023.



POLY(2-OXAZOLINE)S CONJUGATED WITH CHELATORS FOR THE DESTRUCTION OF BACTERIAL CELL MEMBRANES

Marcelina Bochenek,¹ Barbara Mendrek,^{1*} Wojciech Walach,¹ Aleksander Foryś,¹
Jerzy Kubacki,² Łukasz Jałowicki,³ Jacek Borgulat,³ Grażyna Plaza,⁴
Agnieszka Klama-Baryła,⁵ Anna Sitkowska,⁵ Agnieszka Kowalczyk,¹
Natalia Oleszko-Torbus¹

¹Centre of Polymer and Carbon Materials, Polish Academy of Sciences, Zabrze, Poland

²A. Chelkowski Institute of Physics, University of Silesia in Katowice, Chorzów, Poland

³Institute for Ecology of Industrial Areas, Katowice, Poland

⁴Faculty of Organization and Management, Silesian University of Technology, Zabrze, Poland

⁵Dr. Stanisław Sakiel Center for Burn Treatment, Siemianowice Śląskie, Poland

*bmendrek@cmpw-pan.pl

1. Introduction

In the face of a recent epidemiological threat, researchers have expressed increasing interest in chemical compounds with disinfecting and antiseptic activities. Particularly interesting are antibacterial polymers, as they exhibit high stability, non-volatility, resistance to leaching and lack of permeability through the skin into the body.

The Gram-negative bacterial outer membrane (OM) is rich in phospholipids and predominantly composed of polyanionic molecules known as lipopolysaccharides (LPS). Within the OM, the repulsive forces arising from accumulation of the negative charges are screened and bridged by divalent cations (Ca^{2+} and Mg^{2+}), which is crucial to preserve the integrity of the membrane. The trapping of various ions (including calcium or magnesium) by low molecular weight chelates (e.g. EDTA, DTPA and others) disrupts membrane permeability, thus reducing the growth of bacteria.

The goal of these studies is to develop a new, stable and metal-free polymer with antibacterial activity. The work includes the synthesis of the 2-oxazoline copolymer and its conjugation with 1,4,7,10-tetraazacyclododecane- $\text{N},\text{N}',\text{N}'',\text{N}'''$ -tetraacetic acid (DOTA) chelating agent, detailed characterization of the conjugate, taking into account its behavior in aqueous solutions and its ability to capture calcium ions.

2. Results and discussion

The polymeric precursor (POx) with a random microstructure, consisting of 2-ethyl-2-oxazoline (EtOx) and 2-(3-butenyl)-2-oxazoline (ButEnOx), was obtained via cationic ring opening polymerization. The copolymer of the composition EtOx : ButEnOx = 73:27 mol% was obtained, which was consistent with the feed. A large excess of EtOx in the copolymer ensured its solubility in water, while through vinyl double bonds present in the ButEnOx substituent it was possible to modify the macromolecules by means of a “thio-click” reaction.

POx molar mass measured using SEC-MALLS was equal $M_n = 11\,700$ g/mol, $\bar{D} = 1.07$. POx was soluble in water, and its aqueous solution ($c = 5$ mg mL⁻¹) exhibited thermoresponsive behavior based on UV-Vis spectrometry measurements of the cloud point temperature ($T_{CP} = 38$ °C). POx was further modified via the radical addition of cysteamine onto vinyl double bonds of ButEnOx substituents (“thio-click”) (Figure 1). The macromolecule containing 14 mol% of units substituted with pendant primary amino groups was obtained (denoted as POx-NH₂). SEC-MALLS analysis revealed a monomodal and low dispersity of POx-NH₂ ($\bar{D} = 1.07$), suggesting that a well-defined copolymer with good control was obtained. POx-NH₂ was soluble in water and due to cysteamine incorporation its T_{CP} increased to 50 °C, compared to that of the



copolymer before modification.

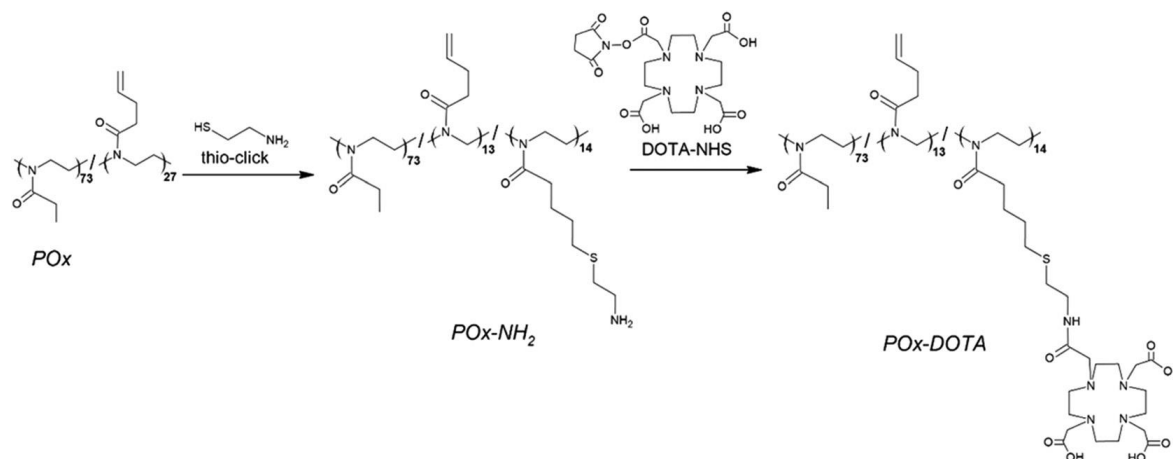


Figure 1. Scheme of POx modification.

In the final step, POx-NH₂ was modified with the monoactivated DOTA (DOTA-NHS) chelating agent (Figure 1). The conjugate POx-DOTA was obtained by amide bond formation between the N-hydroxysuccinimide ester of monoactivated DOTA and amino groups of the copolymer POx-NH₂. Attachment of DOTA to POx-NH₂ was confirmed by ¹³C NMR. A monomodal molar mass distribution with low dispersity ($\bar{D} = 1.18$) was observed for POx-DOTA, indicating that no side reactions took place during the modification (Figure 2).

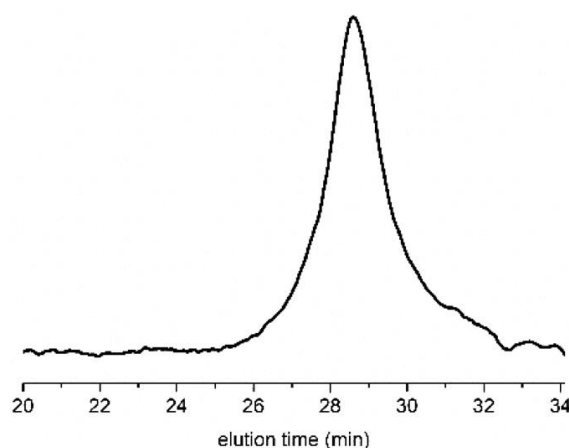


Figure 2. RI trace of POx-DOTA (SEC-MALLS, DMF, 1mL/min).

The conjugate was characterized in aqueous solutions. The POx-DOTA conjugate formed two populations of nanostructures in the aqueous solution, with hydrodynamic diameter (D_h) values of 6 nm and 160 nm, respectively (based on dynamic light scattering (DLS) studies). The smaller population of particles observed in DLS is most likely attributed to individual chains (unimers), while the bigger population consists of aggregated structures.

The obtained POx-DOTA was analyzed in terms of its ability to trap metal ions. The capacity of the conjugate to chelate model Ca^{2+} was determined, since these cations are involved in the stabilization of the bacterial OM, and their uptake would cause disintegration of the cell membrane. Complexometric titrations were used to quantify the chelating capacity of POx-DOTA. The POx-DOTA chelation efficiency was 49% (± 4). For comparison, the chelation efficiency of poly(2-ethyl-2-oxazoline) (PEtOx, a polymer without the chelating compounds) was 5% (± 4), while free DOTA entrapped over 90 mol% of Ca^{2+} . Most likely, free DOTA has better access to Ca^{2+} in the solution than DOTA bound to the polymer chains.

Preliminary studies on the interactions of POx-DOTA with model Gram-negative bacterial strains *E. coli* and *P. aeruginosa* were carried out and also followed by cryo-TEM microscopy. Throughout the culture of *E. coli* in the presence of POx-DOTA, the number of bacterial colonies remained unchanged at around 1×10^7 CFU/mL with time (up to 16 hours), as confirmed by microbiological test. This means that bacteria did not multiply in the presence of POx-DOTA, indicating that the conjugate exhibited bacteriostatic properties. The same trend was observed for the culture of *P. aeruginosa*. In this case, the number of bacterial colonies remained unchanged at around 9×10^7 CFU/mL throughout the culture (up to 16 hours) in the presence of POx-DOTA. Cryo-TEM images showed no damage in bacterial cells membrane up to 4 hours of incubation with POx-DOTA. Afterwards, polymeric spherical structures adhered to the bacterial membrane and the distortion of the cell was noted. The rumples in the membrane could be seen and the bacteria begin to lose their original morphology. Further incubation resulted in the disruption of the bacterial cell membrane.

3. Conclusions

A new, stable and metal-free polymeric conjugate with bacteriostatic properties was developed. It consisted of the copolymer of 2-ethyl-2-oxazoline and 2-(3-butenyl)-2-oxazoline coupled with the chelating agent DOTA. For the first time, the POx-DOTA conjugate containing a chelating compound in the side chains was prepared. POx-DOTA conjugate was able to chelate Ca^{2+} ions with good efficiency. /With the use of cryo-TEM, the changes in the morphology of *E. coli* were observed upon incubation with POx-DOTA: waving of the membrane followed by its deformation. It was found that POx-DOTA exhibited bacteriostatic properties.

It was shown that obtained chelate-functionalized poly(2-oxazoline) system is capable of affecting bacterial cell membranes. Based on these preliminary studies, we believe that the obtained conjugate will be a precursor for a new family of effective polymeric materials with antimicrobial activity.

Acknowledgements

This work was supported by the National Science Centre, project 2021/43/B/ST4/01493.



SIMULTANEOUS QUANTITATIVE DETERMINATION OF URSOLIC, POMOLIC, OLEANOLIC AND ROSMARINIC ACIDS IN PEPPERMINT EXTRACTS. A COMPARATIVE STUDY OF 2D-NMR AND HPLC DATA

Veaceslav Kulcitki,^{1*} Adrian Topala,¹ Vladilena Girbu,¹ Alic Barba,¹
Alina Nicolescu,² Calin Deleanu^{2,3}¹Moldova State University, Institute of Chemistry, Republic of Moldova²Petru Poni Institute of Macromolecular Chemistry, Romanian Academy, Iasi, Romania³Costin D. Nenitescu Institute of Organic and Supramolecular Chemistry,
Romanian Academy, Bucharest, Romania

*veaceslav.kulcitki@usm.md

1. Introduction

Peppermint (*Mentha piperita* L.) is a widespread aromatic plant exploited globally and used in a broad array of applications. Except its strong characteristic flavor, which is due to menthol, menthone and other monoterpenoids, peppermint plant contains many nonvolatile secondary metabolites that display important biological activities and represent valuable pharmaceutical and nutraceutical components [1]. Among the most relevant compounds found in peppermint, organic acids of triterpenic and phenolic structure come into focus, due to their complementary bioactivity profile and relative high abundance in the plant material. We focus in the current study oleanolic (OA), ursolic (UA) and pomolic (PA) triterpenic acids, as well as rosmarinic (RA) acid of polyphenolic structure (Figure 1).

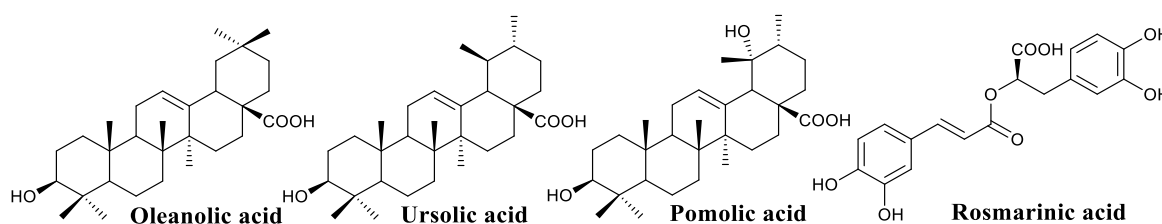


Figure 1. Chemical structures of natural acids quantified in the extract of peppermint.

Their quantitative determination in peppermint plant and derived products represents a relevant issue for quality assessment and we demonstrate a convenient 2D NMR HSQC approach based on an internal standard method with relative calibration. In order to verify the accuracy of the obtained results, an alternative analytical method based on RP HPLC was employed for comparison.

2. Experimental

The peppermint plant material (*Mentha piperita* L.) was collected in the period of July-August 2021 in the Stăuceni area of the Republic of Moldova (47°05'15"N, 28°52'13"E), then dried in a shade to constant weight and further extracted for 2 hours with EtOH 70% at 60 °C on periodic (3 x 15 min) ultrasonic irradiations. The obtained extracts have been filtered, evaporated to dryness under vacuum on a Heidolph rotary evaporator and stored in the refrigerator at -20 °C.

NMR spectra have been recorded on a Bruker Avance III spectrometer (400.13 and 100.61 MHz) in DMSO-*d*₆. NMR data processing, including T1 and s/n determinations, was performed with TopSpin 3.7.0 NMR software (Bruker). The chromatograms were sprayed with 0.1% solution of cerium (IV) sulfate in 2N sulfuric acid, and heated at 80 °C for 5 min to detect the spots. All reagents, including ethylacetate, HPLC and NMR solvents and have been purchased at Sigma-Aldrich and used as received. Ethanol was delivered

by Eladum Pharma SRL. Reagent grade OA was purchased at Sigma-Aldrich, pure UA was prepared from lavender extract as described [2], pure PA and RA were separated from a natural lavender extract.

The content of OA, UA, PA and RA in the reference samples was determined by quantitative ^1H NMR on using methyl 4-nitrobenzoate as an internal standard. HPLC analysis was performed on an Agilent HPLC system consisting of a 1200 series quaternary pump and degasser, 1100 series autosampler and UV detector, Agilent ChemStation for LC System. Separations were performed at 22 °C on a Zorbax Eclipse PAH column packed with 3.5 μm particles, 100 Å pore diameter, 150 \times 4.6 mm LT \times ID equipped with a guard column of the same material (5 μm particle size, 12.5 mm \times 4.6 mm LT \times ID) (Agilent Technologies). A gradient elution was applied, starting from 40% methanol (solvent A) – 60% water (0.6% AcOH) (solvent B) to 100% solvent A. The flow rate was kept at 0.8 mL min $^{-1}$, detection was performed at 210 nm and the injection volume was 2.5 μL . The calibration curves have been drawn basing on mixtures of OA, UA, PA and RA of known concentrations within the range of 15–250 $\mu\text{g mL}^{-1}$ (0.03–0.55 mM) in pure methanol. The R^2 values were 0.9999, 0.9997 and 1.0 for OA, UA and PA, respectively. Samples of peppermint extracts were diluted accordingly to fit the dynamic linear range of the regression line. All measurements were performed in triplicates.

3. Results and discussion

Homologation of aromatic plants varieties and industrial handling of raw extracts derived from the vegetal material requires a rigorous analytical investigation, targeting both the most abundant and minor components. Along with chromatographical methods, quantitative NMR represents a valuable tool demonstrating significant developments in the last decade. ^1H NMR is by far the most reported method for quantitative NMR assessment in diverse metabolomic studies. Unfortunately, for a rigorous quantification of secondary metabolites in the complex analytical matrix of natural product extracts, the resolution of ^1H qNMR is not sufficient, even with modern strong magnets. In this case several two-dimensional NMR experiments like COSY, TOCSY or HSQC provide handy solutions, due to the deployment of spectral data in the second dimension with an excellent resolving power. In our hands, the investigated extract of peppermint showed a strongly overlapping ^1H NMR spectrum, making quantification of bioactive organic acids non feasible (Figure 2a).

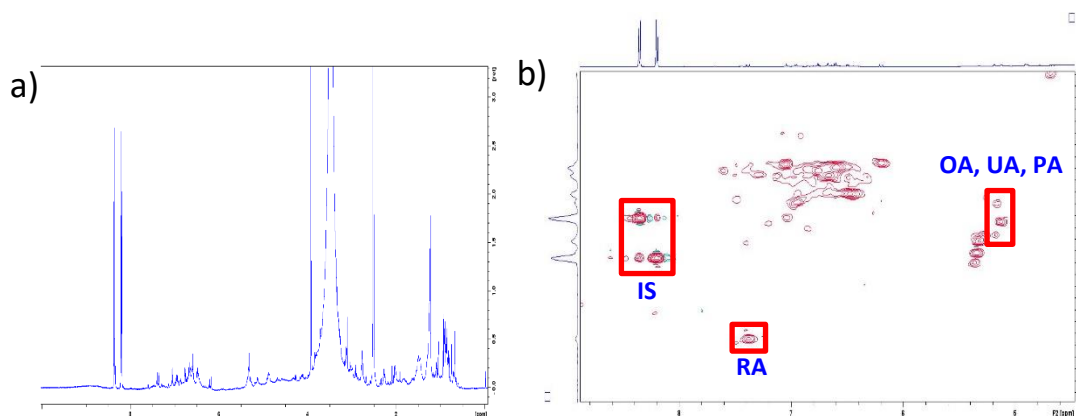


Figure 2. ^1H NMR (a) and HSQC (b) spectra of the investigated peppermint extract.

On the contrary, the HSQC spectrum (Figure 2b) showed an excellent base-line resolution of selected cross-peaks for RA at 7.4–144.9 ppm, OA at 5.2–121.9 ppm, UA at 5.1–124.9 ppm and PA at 5.2–127.1 ppm. Identification of the selected peaks was performed on the basis of the HSQC spectra of pure compounds. The quantification was achieved according to a relative calibration method on using the methyl 4-nitrobenzoate as the internal standard (IS), showing well separated peaks at 8.2–131.2 and 8.4–124.3 ppm. The determined content of the acids in the crude extract is represented in the Table 1. It also integrates the corresponding content of the acids as determined by a parallel HPLC analysis of the same extract. It is



noteworthy mentioning that HPLC analysis turned out to be problematic, due to several experimental hurdles. First of all, the separation of isomeric oleanolic and ursolic acids is very difficult and a satisfactory resolution could only be achieved on a specific PAH RP column, which required additional investments. Besides, the triterpenic acids have weak UV absorption and their detection was performed at 210 nm. At this wavelength application of a broad elution gradient results in a strong baseline drift that negatively affects separation signal-to-noise ratio, as it is illustrated in Figure 3. A more rigorous approach would include separate chromatographic runs for rosmarinic acid, which selectively absorbs at 330 nm and application of a slower gradient for quantification of triterpenic acids with detection at 210 nm. This approach is more time consuming and the described 2D NMR protocol has definitely a clear advantage.

Table 1. Content of organic acids in peppermint extract, %

Acid	Method	
	HSQC	HPLC
RA	9.1	7.3
OA	1.9	1.9
UA	4.8	7.3
PA	0.9	0.6

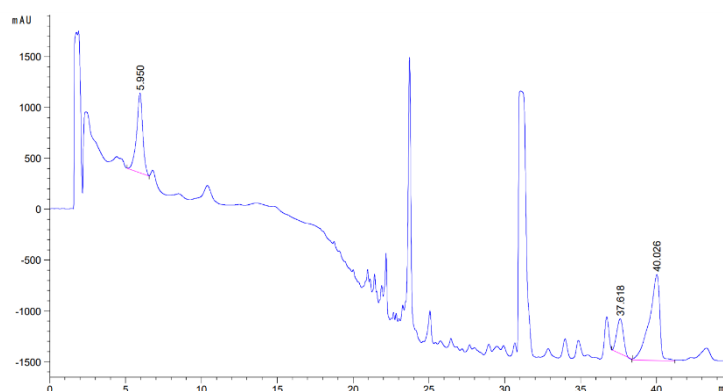


Figure 3. HPLC chromatogram of the crude peppermint extract.

4. Conclusions

The application of a 2D quantitative NMR procedure allowed for an accurate simultaneous determination of the selected bioactive organic acids in a peppermint extract. The analytical procedure is simple and robust, providing data in a close agreement to the more traditional HPLC method. Due to the advent of compact NMR equipment, the proposed analytical protocol can be integrated into the current practice of any analytical laboratory for the proper estimation of the quality of peppermint vegetal material or derived extracts for broader industrial applications.

Acknowledgements

This study was supported by a grant of the CNCS-UEFISCDI, contract no. 30ROMD/2024, project PN-IV-P8-8.3-ROMD-2023-0249 (DiMoMeD). A.T. and A.B. acknowledge financial support from the Ministry of Education and Research of the Republic of Moldova, sub-program 010601.

References

- [1]. Hudz N, Kobylinska L, Pokajewicz K, Horčinová Sedláčková V, Fedin R, Voloshyn M, Myskiv I, Brindza J, Wiczorek PP, Lipok J. *Mentha piperita*: Essential oil and extracts, their biological activities, and perspectives on the development of new medicinal and cosmetic products. *Molecules*, 28, 7444, 2023.
- [2]. Csuk R, Siewert B. A convenient separation of ursolic and oleanolic acid. *Tetrahedron Lett.*, 52, 6616–6618, 2011.



SILSESQUOXANES-BASED HYBRID MATERIALS FOR ENVIRONMENTAL APPLICATIONS (CO₂ CAPTURE)

Alexandra Bargan,^{1*} Mihaela Dascalu,¹ Bianca-Iulia Ciubotaru,^{1,2} Mirela-Fernanda Zaltariov,¹

Adrian Bele,¹ George Theodor Stiubianu,¹ Muslum Demir,^{3,4} Maria Cazacu¹

¹*Petru Poni Institute of Macromolecular Chemistry, Romanian Academy, Iasi, Romania*

²*Department of Biomedical Sciences, Faculty of Medical Bioengineering, Grigore T. Popa University of Medicine and Pharmacy, Iasi, Romania*

³*Department of Chemical Engineering, Bogazici University, Istanbul, Turkey*

⁴*TUBITAK Marmara Research Center, Material Institute, Gebze, Turkey*

*anistor@icmpp.ro

1. Introduction

In the last years the global warming has changed in a significant way the weather all over the world by modifying the length of seasons and the rainfall patterns, the melting of glaciers, the raising of the sea levels and causing waters in some regions. Greenhouse gases present in the atmosphere capture the heat from the sun rising the atmospheric temperature. Carbon dioxide (CO₂) represents 80% of these GHGs being a major contributor to global warming. Because of the progressive increase of the greenhouse gases, especially of the CO₂ caused by the anthropogenic activities, such as urbanization, deforestation, and excessive use of fossil fuels, the global warming and the climate change became one of the greatest issues today. This requires urgent practical and economical ways of projecting the best conditions for CO₂ capture processes. According to the data obtained from the Mauna Loa station, the value of this parameter is increasing: 425.25 ppm in 07.2024 and 427.87 ppm in 07.2025 (Figure 1) [1]. This situation has led to efforts being dedicated to the capture and storage of CO₂ from atmosphere. Gas separation using new silsesquioxanes-hybrid materials (POSS) seems to be attractive due to its low energy requirement and simplicity of operation.

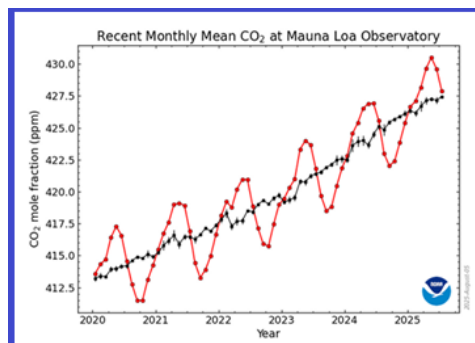


Figure 1. Monthly mean CO₂ measured at Mauna Loa Observatory, Hawaii [1]
(red lines: monthly mean values; black lines: corrected monthly mean values).

An easy method used to obtain multifunctional POSS materials starting from octavinyl-T8-silsesquioxane (V-PS) is the thiol-ene reaction because of its special characteristics, such as quick reaction rates, high oxygen and water allowance, moderate reaction conditions, low-price catalysts, high yield. Multicarboxy functionalized POSS are of interest due to their potential use in supramolecular chemistry and crystal engineering. In this study, octakis-carboxy T8-silsesquioxane monomers were synthesized via the photo-induced thiol-ene reaction of V-PS and thioalkylcarboxylic acids, and after, their transition metal complexes were obtained, confirmed, characterized and applied as new hybrid materials for selective CO₂ capture. The new silsesquioxanes based materials will be used in environmental applications as active materials with user-controlled adaptability for integrated management of the CO₂ gas separation. The



efficient capture of CO₂ due to the logical design of new silsesquioxanes-materials with enriched functionality represents a relevant step in diminishing CO₂ emissions.

2. Experimental

Silsesquioxanes hybrids based materials were prepared using the photo-induced thiol-ene reaction (Figure 2). The products as white (hybrid ligands) and colored powders (complexes) were analyzed and characterized in terms of physical, mechanical, morphological (SEM), infrared and moisture, N₂ and CO₂ sorption properties, thermal stability. The CO₂ capture property of the materials can be improved. The new POSS-materials with heteroatom doping as efficient adsorbents for the selective capture of CO₂, represent a good solution for effective CO₂ mitigation.

Materials: Octavinyl-T8-silsesquioxane (V-PS); 3-mercaptopropionic acid (MPA); thioglicolic acid (TGA) from TCI Chemicals; 2,2-dimethoxy-2-phenylacetophenone (DMPA); tetrahydrofurane, ethylacetate, acetone, copper chloride (CuCl₂) from Sigma-Aldrich.

Equipments: The NMR spectra were recorded on a 400 MHz Bruker spectrometer, in CD₃OD-d₄ or D₂O, at room temperature. The IR spectra were registered on Bruker Vertex 70 FT-IR equipment in transmission mode, in the 400-4000 cm⁻¹ range, with a resolution 2 cm⁻¹ and 32 scans, at room temperature (Figure 3). SEM images were taken on the products obtained as such. The moisture sorption capacity of the materials has been studied using the IGAcorp analyzer made by Hiden Analytical, Warrington (UK).

3. Results and discussion

The continuous requirement for new hybrid materials in environmental applications motivates the scientists in the progress of new active strategies. The efficient capture of CO₂ due to the logical design of new materials based on silsesquioxanes with enriched functionality represents an important step in increasing the CO₂ emissions. New hybrid materials (octakis(carboxyalkyl-thioalkyl)silsesquioxanes) were synthesized by using click photo-induced thiol-ene addition reaction between octavinyl-T8-silsesquioxane and thioalkylcarboxylic acids next to some of their transition metal complexes. The newly obtained materials were characterized and applied for selective CO₂ capture.

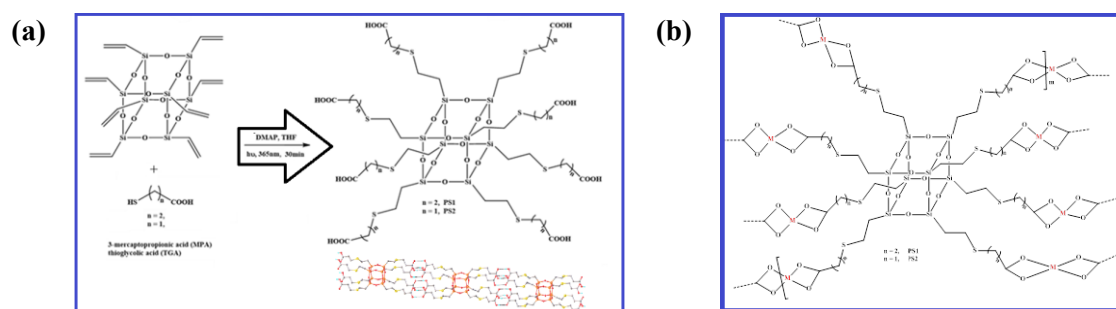


Figure 2. Schematic representation of (a) Silsesquioxanes functionalized with carboxyl groups as ligands (PSx); (b) And of the Cu-PS1 complexes.

In the FTIR spectra of hybrid silsesquioxanes ligands (Figure 3) the most useful characteristic bands are assigned to the asymmetric and symmetric stretching vibrations of COO⁻. The frequencies of these bands are responsive to the coordination modes of the carboxylate groups: ionic, monodentate, bidentate chelating or bidentate bridging coordination. As a result of coordination, the band at ~1710 cm⁻¹ in FTIR spectrum of PS assigned to the carboxylic acid C=O stretching vibration disappeared in FTIR spectra of the metal complexes, and a new strong band attributed to $\nu_{as}(\text{COO}^-)$ at around 1581 cm⁻¹ can be observed.

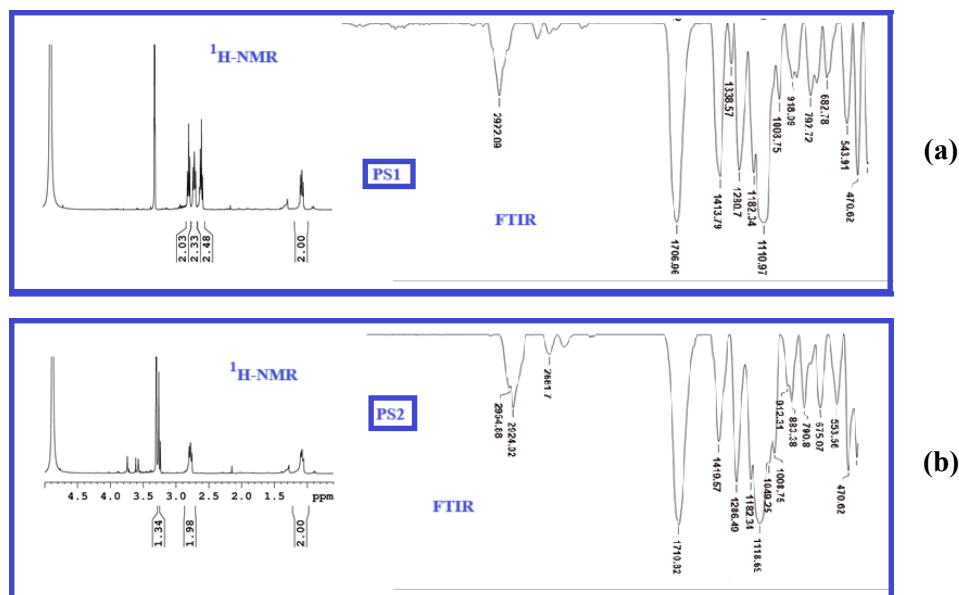


Figure 3. (a) FTIR, (b) ¹H-NMR spectra of carboxy functionalized silsesquioxanes PS1 and PS2.

4. Conclusions

New silsesquioxanes based materials were obtained using photo-induced thiol-ene reaction in order to be used for environmental applications, as active materials with user-controlled adaptability for integrated management of the CO₂ gas separation. The obtained materials and their transition metal complexes were confirmed, characterized and applied as new hybrid materials for selective CO₂ capture. The CO₂ capture property attributed to the materials' high microporosity and well-dispersed sulfur functionality throughout the carbon framework of the material can be adjusted. The new POSS-materials with heteroatom doping represent a good and valuable solution for effective CO₂ diminution.

Acknowledgements

This work was supported by a grant of the Ministry of Research, Innovation and Digitization, CCCDI – UEFISCDI, project number PN-IV-P8-8.3-PM-RO-TR-2024-0046, within PNCDI IV, Contract ctr. 8 BMTR/2025 (SynTioPOSS).

References:

- [1]. <https://www.co2.earth/22-co2-now/121-mauna-loa-co2>. Accessed 31 July 2025.
- [2]. Dumitriu AMC, Cazacu M, Bargan A, Balan M, Vornicu N, Varganici CD, Shova S. *J. Organomet. Chem.* 799–800, 195–200, 2015.
- [3]. Dumitriu AMC, Bargan A, Balan M, Varganici CD, Shova S, Cazacu M. *Rev. Roum. Chim.* 61(4-5), 385–393, 2016.
- [4]. Dascalu M, Stoica AC, Bele A, Maccim AM, Bargan A, Varganici CD, Stiubianu GT, Racles C, Shova S, Cazacu M, *J. Inorg. Organomet. Polym.* 32, 3955–3970, 2022.
- [5]. Bai J, Shao J, Yu Q, Demir M, Altay BN, Turgunov MA, Yongfu J, Wang L, Hu X. *Chem. Eng. J.* 479, 147667, 2024.

DESIGN AND ENGINEERING OF FLOATABLE HYBRID AEROGELS BASED ON CELLULOSE NANOFIBERS

**Andreea Laura Chibac-Scutaru,* Violeta Melinte, Gabriela Biliuta,
Madalina Elena Bistriceanu, Raluca Ioana Baron, Sergiu Coseri**

Petru Poni Institute of Macromolecular Chemistry, Romanian Academy, Iasi, Romania

**andreea.chibac@icmpp.ro*

1. Introduction

Aerogels possess a unique combination of properties, including a large surface area, high porosity, ultralight weight, low thermal conductivity, and excellent thermal and chemical stability, that make them highly attractive for applications such as thermal insulation, energy storage, pollutant adsorption, and catalyst support. To tailor aerogels for these diverse functions, recent research has increasingly focused on engineering their physicochemical characteristics by precisely manipulating the composition of building blocks, tuning pore architecture, and enhancing interfacial interactions. The synergistic integration of these structural elements has guided the advancing in the design and fabrication of next-generation, high-performance aerogels [1].

Our objective is to design aerogels as macroporous matrices for further used as supports for immobilizing photocatalysts, aiming to prevent catalyst leaching, increase the catalyst-loading capacity, and improve mass transfer. Unlike densely packed photocatalyst films, embedding photocatalysts within aerogels can significantly boost photocatalytic efficiency [2]. Additionally, compared to conventional polymer–photocatalyst nanocomposites, which are typically submerged in water and suffer from reduced light exposure underwater decreasing thus their photocatalytic performance, our approach focuses on creating floatable substrates. By positioning the nanocomposites at the air–water interface, they can fully harness solar radiation, benefit from higher oxygen availability promoting radical generation and oxidation reactions and enable more efficient photocatalytic process.

Cellulose nanofibers, with diameters of 4–100 nm and lengths of several micrometers, serve as excellent building blocks for aerogels due to their high crystallinity, biocompatibility, mechanical strength, low density, and versatile surface chemistry. Their high aspect ratio and entangled network enable the formation of ultralight, porous structures. To improve mechanical stability, chemical crosslinking is often applied, strengthening the network while also allowing surface wettability to be tailored. For instance, crosslinkers like epichlorohydrin and organoalkoxysilanes can impart hydrophilic or hydrophobic properties, enabling multifunctional aerogel designs [3].

To fabricate ultralight, floatable aerogels, cellulose nanofibers (CNFs) were hybridized with an organoalkoxysilane derivative, poly(vinyltrimethoxysilane) (PVTMS). Controlled hydrolysis and condensation of PVTMS generated hydrophilic silanol groups (Si–OH), which formed strong interfacial bonds with the CNF network, ensuring crosslinking of the network and enhancing the mechanical strength of the resulting hybrid aerogels. Concurrently, polycondensation produced polyvinylsilsesquioxane (PVSQ) within and on the surface of the CNF network. This modification introduced siloxane groups (Si–O–Si) on the CNFs surface transforming the inherently hydrophilic cellulose aerogels into hydrophobic structures with improved moisture stability.

2. Results and discussion

Cellulose nanofibers (CNFs) used in the aerogel network were obtained through a combination of chemical pre-treatments (alkaline–acid hydrolysis), physical treatment (ultrasonication), and TEMPO-mediated



oxidation, as illustrated in Figure 1. This oxidation selectively converts the primary hydroxyl groups of cellulose into carboxyl groups, introducing anionic functionalities that enhance electrostatic repulsion and prevent fibril aggregation, thereby improving dispersion. Following oxidation, the cellulose was mechanically processed - via homogenization, microfluidization, or fibrillation - to yield nanoscale fibers. Various cellulose sources with different degrees of polymerization were tested for CNF extraction: cotton linters (CL, DP = 465), microcrystalline cellulose (MCC, Avicel PH-101, DP = 140), alpha cellulose (α -CEL, DP = 950), and eucalyptus cellulose (EYPT, DP = 2742). The resulting CNFs were extensively characterized using zeta potential analysis, FTIR, TEM, XRD, and quantification of carboxyl group content.

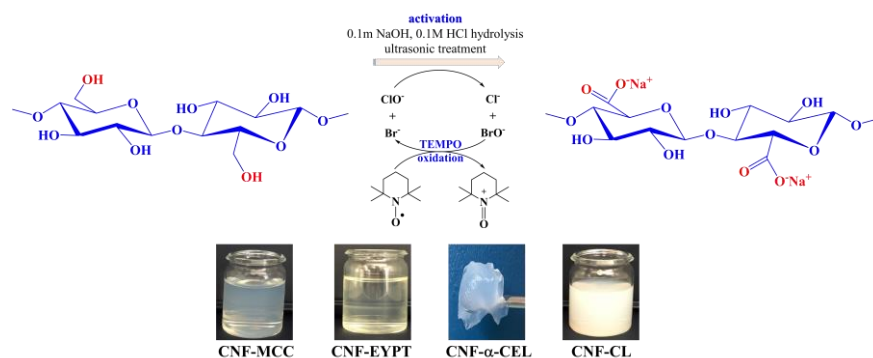


Figure 1. Schematic representation of the CNFs preparation process.

Poly(vinyltrimethoxysilane) (PVTMS) was synthesized via free radical polymerization of vinyltrimethoxysilane using di-tert-butyl peroxide as the radical initiator (Figure 2). The chemical structure of the resulting polymer was confirmed by ^1H NMR spectroscopy, and its molecular weight was determined by gel permeation chromatography (GPC).

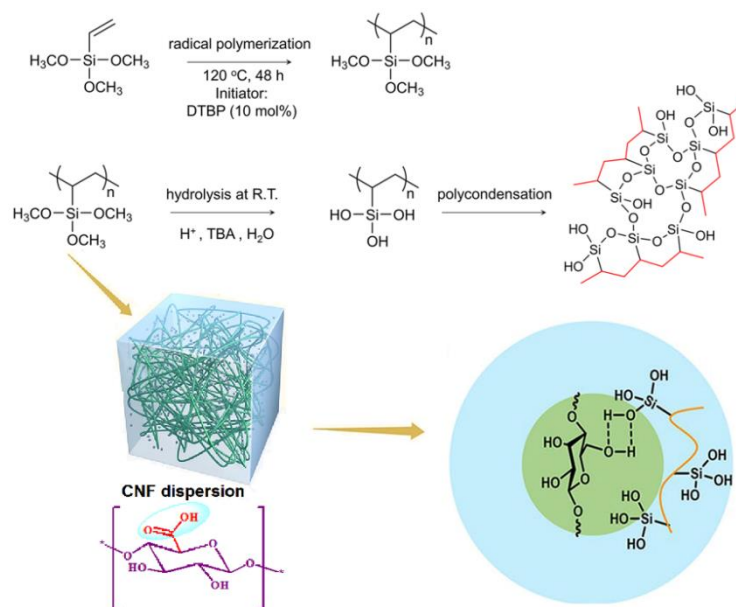


Figure 2. Synthetic routes of polysiloxane via free-radical polymerization and hydrolytic polycondensation along with the hybridization of cellulose nanofibers.

Ultralight, highly porous, and floatable aerogels were prepared as follows: an aqueous dispersion of cellulose nanofibers (CNFs) was mixed with a siloxane sol solution of poly(vinyltrimethoxysilane) (PVTMS) to form a homogeneous mixture. Acetic acid was then added to initiate hydrolysis, promoting hydrogen bonding between the hydrophilic silanol groups ($\text{Si}-\text{OH}$) and the hydroxyl groups ($-\text{OH}$) on the CNF surface (Figure 2). Subsequent freezing and freeze-drying induced polycondensation, forming polyvinylpolysilsesquioxane on the CNF nanofiber network. This process resulted in ultralight, floatable

aerogels, as shown in Figure 3. The synthesized aerogels were characterized by FTIR spectroscopy and SEM/EDX analysis to evaluate CNF–PVTMS interactions, morphology, and structural homogeneity.

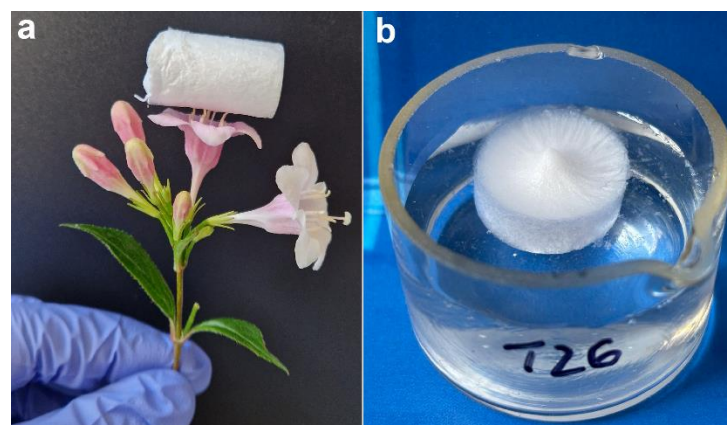


Figure 3. Photos of the prepared aerogels demonstrating their (a) ultralight character and (b) floatability on water.

4. Conclusions

Floatable, ultralight aerogels with high porosity were successfully developed by hybridizing cellulose nanofibers prepared in our laboratory with PVTMS, followed by hydrolysis and polycondensation processes. The resulting hybrid aerogels exhibited enhanced moisture stability and structural integrity, confirmed by FTIR and SEM/EDX analyses.

Acknowledgements

This work was supported by a grant of the Ministry of Education and Research, CNCS – UEFISCDI, project number PN-IV-P1-PCE-2023-1020 (6PCE08.01.2025), within PNCDI IV.

References

- [1]. Zhang J, Cheng Y, Xu C, Gao M, Zhu M, Jiang L. Hierarchical interface engineering for advanced nanocellulosic hybrid aerogels with high compressibility and multifunctionality. *Adv. Funct. Mater.* 31, 2009349, 2021.
- [2]. Lee WH, Lee CH, Cha GD, Lee B-H, Jeong JH, Park H, Heo J, Bootharaju MS, Sunwoo S-H, Kim JH, Ahn KH, Kim D-H, Hyeon T. Floatable photocatalytic hydrogel nanocomposites for large-scale solar hydrogen production. *Nat. Nanotechnol.* 18, 754–762, 2023.
- [3]. Xu C, Gao M, Yu X, Zhang J, Cheng Y, Zhu M. Fibrous aerogels with tunable superwettability for high-performance solar-driven interfacial evaporation. *Nano-Micro Lett.* 15, 64, 2023.



3D PRINTED SCAFFOLDS BASED ON FUNCTIONALISED GELATIN AND XANTHAN GUM FOR SOFT TISSUE ENGINEERING

Isabella Nacu,^{1*} Anca Toma,¹ Maria Butnaru,¹ Loredana Elena Nita,² Liliana Verestiuc¹

¹*Faculty of Medical Bioengineering,*

Grigore T. Popa University of Medicine and Pharmacy, Iasi, Romania

²*Petru Poni Institute of Macromolecular Chemistry, Romanian Academy, Iasi, Romania*

**nacu.isabella@gmail.com*

1. Introduction

Tissue engineering scaffolds have to adapt to the morphology of the targeted tissue or organ, possess a three-dimensional porous architecture with controlled design, degradation, and bioadhesive properties to promote cellular migration and proliferation, exhibiting suitable mechanical properties to uphold structural integrity and strength [1]. In this regard, 3D printing processes can be obtained biomimetic scaffolds for tissue engineering, extrusion technology being the most used method. Along with the printing method, choosing the appropriate polymeric ink is an important step [2]. All (bio)inks must possess biocompatibility, biodegradability, and appropriate rheological properties for extrusion and structural integrity. Gelatin is a common biopolymer for 3D-printed scaffolds due to its biocompatibility, biodegradability, and Arg-Gly-Asp (RGD) amino acid sequence, which enhances cellular attachment. Xanthan, a heteropolysaccharide, improves (bio)ink's rheology and mechanics along with gelatin [3]. For the development of this study was used gelatin, xanthan gum, and their chemically modified form (GelMA and XGMA) to formulate inks for soft tissue engineering scaffolds. Subsequent to fabrication, the scaffolds were evaluated for morphology, physicochemical characteristics, and biological interactions to determine their tissue engineering applicability.

2. Experimental

The structures of the biopolymers, gelatin and xanthan gum, were modified in accordance with the protocol established by Camci-Unal [5], with certain modifications to the methodology. In order to obtain the scaffolds, various polymeric inks were synthesized by combining gelatin and xanthan gum in different form and amounts. Formulations were based on two polymeric solutions of methacrylated gelatin (20%) solution and xanthan methacrylated (1%), riboflavin as a crosslinking agent and LAP as a photocrosslinking initiator. The prepared inks were added into the printer's syringes and subsequently extruded using a CellInk (bio)printer employing a selected digital model within the printer software. During the printing process, each deposited layer was crosslinked utilizing the printer's UV lamp ($\lambda = 365$ nm). Then, the scaffolds were freeze-dried for subsequent characterization.

3. Results and discussion

Scaffolds characterization: Scaffolds were characterized through different methods, including: FT-IR spectroscopy, morphology, swelling degree, degradation and their compatibility with cell cultures. Figure 1 presents the Gel/GelMA_XG/XGMA FT-IR data table, gelatin being identifiable through the characteristic protein bands: amide I (1658 cm^{-1}), amide II (1542 cm^{-1}), and amide III (1243 cm^{-1}). The scaffolds exhibit N-H group specific bands at 3467 cm^{-1} corresponding to amide A and C-H group specific bands at 2933 cm^{-1} associated to the amide B. Bands at 3492 cm^{-1} , 1646 cm^{-1} (indicative of the carbonyl group), 1330 cm^{-1} (associated with COO^- groups), and 1070 cm^{-1} (related to ether groups) is also observable. The absorptions at 3567 cm^{-1} were attributed to the stretching of the amino ($-\text{NH}_2$) and hydroxyl ($-\text{OH}$) groups in the methacrylated xanthan gum and methacrylated gelatin within the GelMA_XGMA



scaffolds. The morphological analysis of the scaffolds highlighted their shape. It was found that the scaffolds preserved their structural integrity.

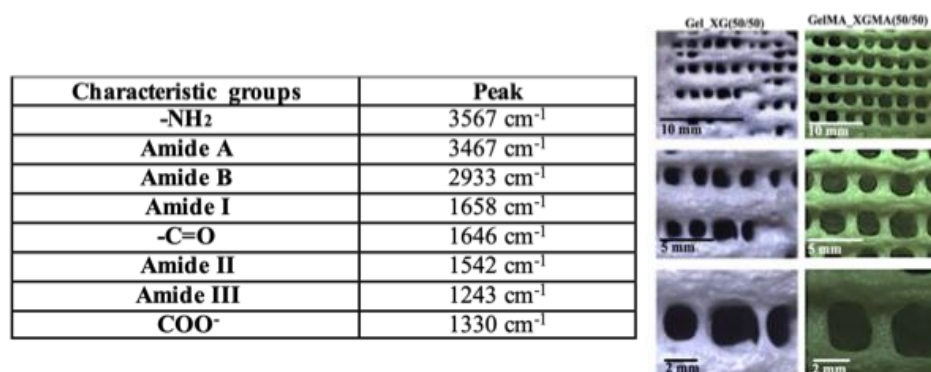


Figure 1. FT-IR and optical microscopy results for scaffolds based on XG/XMA_Gel/GelMA.

The interaction of scaffolds with simulated biological fluids and their water absorption capacity are critical factors for their application in the medical field. According to the Table 1, scaffolds based on chemically modified polymers, presented higher absorption capacity over time, reaching over 250% after 24 hours, indicating more efficient crosslinking and increased stability.

Table 1. Equilibrium degree of swelling (SD, %) and enzymatic degradation process for porous scaffolds with different ratios between polymers.

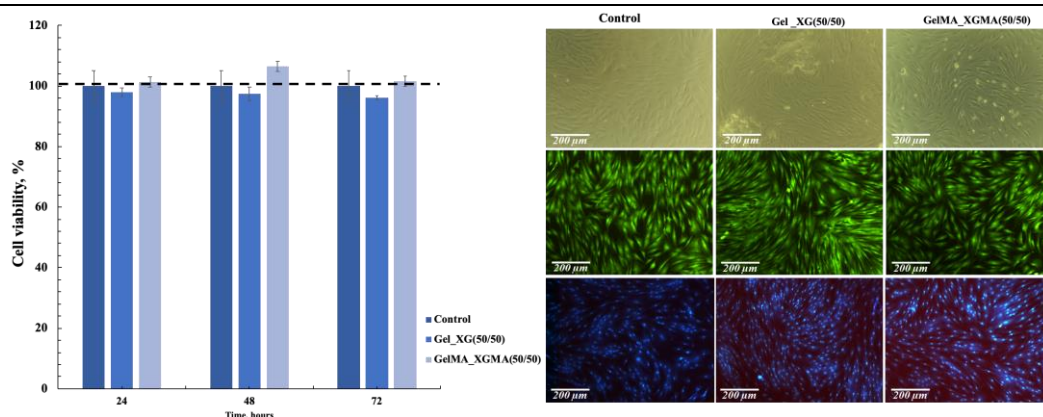
Sample	Swelling degree (%)	Concentration of degraded gelatin, 72h (mg/mL)	Sample	Swelling degree (%)	Concentration of degraded gelatin, 72h (mg/mL)
Gel_XG (25/75)	309±20.4	0.076±0.002	GelMA_XG MA (25/75)	2296±70.545	0.064±0.002
Gel_XG (50/50)	-	0.066±0.001	GelMA_XG MA (50/50)	937±45.420	0.065±0.005
Gel_XG (75/25)	-	0.070±0.005	GelMA_XG MA (75/25)	1064±60.793	0.065±0.0005

Also, hydrogels formulated based GelMA and XGMA exhibited reduced degradation kinetics compared to those composed of unmodified gelatin and xanthan, due to an increased crosslinking degree due to polymeric chain modification, leading to a complex three-dimensional structure with improved mechanical strength. From the bioadhesive point of view, the scaffolds composed of unmodified gelatin and xanthan (Gel_XG) exhibits low detachment force values, indicating a poorly crosslinked network. In contrast, the GelMA_XGMA scaffold demonstrates enhanced bioadhesion properties attributed to an improved crosslinked network resulting from interactions between the modified polymers.

The cytocompatibility of cell cultures was assessed through direct contact and MTT assays, with cell viability evaluated accordingly ISO-10993-5. Figure 2. illustrates that the cell viability exceeding 85% in fibroblast cultures after 72 hours scaffolds direct contact. According to the morphology images in Figure 2, it can be seen that the cells exhibit normal morphology, maintain their shape, and preserve cell density over time. The cells adhered to the substrate by forming a uniform monolayer and exhibited a morphology typical of normal human dermal fibroblasts. Bioadhesive properties of printed porous scaffolds with different ratios between polymers are presented in Table 2.

Table 2. Bioadhesive properties of printed porous scaffolds with different ratios between polymers.

Sample	Force of detachment (mN)	Work of adhesion (mN·s)	Sample	Force of detachment (mN)	Work of adhesion (mN·s)
Gel (100)	0.051±0.003	0.036±0.007	GelMA (100)	0.034±0.001	0.024±0.003
Gel_XG (25/75)	0.037±0.001	0.023±0.002	GelMA_XGMA (25/75)	0.078±0.010	0.049±0.002
Gel_XG (50/50)	0.045±0.002	0.016±0.005	GelMA_XGMA (50/50)	0.042±0.013	0.015±0.002
Gel_XG (75/25)	0.029±0.001	0.011±0.002	GelMA_XGMA (75/25)	0.071±0.015	0.026±0.001
XG (100)	0.048±0.006	0.270±0.013	XGMA (100)	0.117±0.029	0.654±0.015

**Figure 2.** Cell viability (%) and morphology of viable cells after 72 h of cell culturing.

4. Conclusions

In this study we obtained scaffolds based on polymeric inks, including gelatin and xanthan gum, for tissue engineering applications. The results revealed 3D architectures, and the influence of composition upon morphology and swelling extent. The printed scaffolds' architectures enhance nutrient flow and cellular proliferation. The matrices were found to be cytocompatible, supporting their use as scaffolds in regenerative medicine for repairing damaged epithelial tissue.

Acknowledgments

This research was funded by the Ministry of Research, Innovation and Digitization, CCCDI- UEFISCDI, project number 613 PED/2022, PN-III-P2-2.1-PED-2021-3003, as part of PNCDI III.

References

- [1]. Zhou F, Hong Y, Liang R, Zhang X, Liao Y, Jiang D, Zhang J, Sheng Z, Xie C, Peng Z, Zhuang X, Bunpetch V, Zou Y, Huang W, Zhang Qm Alakpa EV, Zhang S, Ouyang H. Rapid printing of bio-inspired 3D tissue constructs for skin regeneration. *Biomaterials*, 258, 120287, 2020.
- [2]. Wang Z, Kapadia W, Li C, Lin F, Pereira R, Granja PL, Sarmiento B, Cui W. Tissue-specific engineering: 3D bioprinting in regenerative medicine. *J. Controll. Rel.*, 329, 237–256, 2021.
- [3]. O'Connell CD, Konate S, Onofrillo C, Kapsa R, Baker C, Duchi S, Eekel T, Yue Z, Beirne S, Barnsley G, Di Bella C, Choong PF, Wallace GG. Free-form co-axial bioprinting of a gelatin methacryloyl bio-ink by direct in situ photo-crosslinking during extrusion. *Bioprinting*, 19, e00087, 2020.

MACRO Iași 2025





Finanțat de
Uniunea Europeană
NextGenerationEU



Planul Național
de Redresare și Reziliență

POLYSACCHARIDE-BASED (BIO)HYBRID NANOSTRUCTURES

Marcela Mihai,¹ Stergios Pispas^{1,2}

¹*Petru Poni Institute of Macromolecular Chemistry, Romanian Academy, Iasi, Romania*

²*Theoretical and Physical Chemistry Institute,
National Hellenic Research Foundation, Athens, Greece*

*hybsac.pnrr@icmpp.ro

Polysaccharide based (Bio)Hybrid Nanostructures (HYBSAC) is a project being implemented by the “*Petru Poni*” Institute of Macromolecular Chemistry (ICMPP), Iasi, Romania, project no. 760082/23.05.2023, project code CF201/28.11.2022, funded by the National Recovery and Resilience Plan, Component C9 - Support for the private sector, research, development, and innovation, Investment I3: Development of a program for attracting highly specialized human resources from abroad for research, development and innovation activities.



The goal of the HYBSAC project is to increase the competitiveness of Romanian research, at the national and international level, and build a research core with high-level scientific competence, under the coordination of an international expert, and build a new research field within ICMPP. Top methods will be addressed for synthesizing, characterizing and testing polysaccharides with synthetic polymer components using RAFT polymerization methodologies.

The HYBSAC research project aims to develop new hybrid nanomaterials that will be formed from the combination of natural polysaccharides, synthetic/soluble responsive and biocompatible polymers. The synthesis will be specifically achieved by growing the synthetic polymers in a covalent manner to polysaccharide chains using the RAFT polymerization mechanism. RAFT polymerization is a controlled radical polymerization process that allows for sophisticated tuning of both the structure and functionality of the polymer.

Two synthetic strategies were developed.

- **Grafting-from**, in which polymer grow directly from the polysaccharide backbone.
- **Grafting-to**, in which pre-synthesized polymers will be chemically attached to the polysaccharide.

Either of these approaches was obtain **hybrid synthetic-biological polymers** for advanced functional properties. We will also study the **self-assembly and co-assembly** of these hybrid materials producing well-organized nanostructures through polymer physical chemistry principles, informed by the study of these assemblies in aqueous environments and their structural features and formation mechanisms.

The resultant nanoassemblies was assessed for a variety of high-impact applications such as:

- **Drug delivery, bioimaging and protein transport.**
- **Environmental restoration** as nanocontainers for capturing organic/inorganic pollutants.
- **Surface functionalization** for high-performance material interfaces.



Furthermore, co-assembly with **proteins and antibodies** allow us to create **biofunctional nanoparticles** with biomimetic architecture for diagnostic and treatment purposes. The project also generate **hybrid organic–inorganic and bio–inorganic nanostructures** by co-assembly of functionalized polysaccharides and inorganic nanoparticles, in attempts to create materials that possess **magnetic, optical, catalytic** or **antimicrobial** properties.

The project is coordinated by Dr. Stergios PISPAS, Research Director at the Institute of Theoretical and Physical Chemistry, National Hellenic Research Foundation, Greece (TPCI/NHRF). Dr. Pispas has expertise in polymer synthesis using controlled polymerization techniques, with innovative results applicable in nanomedicine and the delivery of drugs/genes/proteins for therapy, bioimaging, detection, and water treatment. As further evidence of his scientific achievements, Dr. Pispas was included in the *Top 2% Scientists Worldwide in Chemistry* in the field of polymers for the years 2018–2022.

The project team is mainly formed by *Functional Polymers Laboratory* members from ICMPP (<https://icmpp.ro/laboratories/l4/description.php>), coordinated by Dr. Marcela Mihai, one of Romania's leading research groups with internationally recognized interests on multifunctional (composite) materials mainly through the synthesis and utilization of a variety of synthetic and natural ionic polymers with predetermined functional groups and architectures. In addition, two members of the HYBSAC team originate from TPCI/NHRF, as part of Dr. Pispas's team, to assist with implementing the project. Dr. Pispas' collaborations with Romanian team members date back to 2012 with a number of research visits performed at TPCI/NHRF on subjects aligned with the HYBSAC project.

The project implementation period is 60 months, from July 1, 2023, to June 30, 2026.

The total value of the financing contract is 7,551,991.04 RON, non-reimbursable funds from the European Union – NextGenerationEU, of which the non-reimbursable financing amount is 7,000,000 RON and the VAT related to eligible expenses from PNRR is 551,991.04 RON.

The **general objective** of the HYBSAC project is to increase the capacity and quality of research and development activities at ICMPP by attracting specialists with advanced skills from abroad, opening a new research direction in the field of biomaterials, and creating a research excellence group.

Specific objectives of the HYBSAC project include, but are not limited to:

- Polysaccharides containing rationally designed synthetic polymer constituents obtained by controlled RAFT polymerization. Graft copolymers made with controlled composition and structure. Structural elucidation, self-assembly, and morphology will be evaluated in aqueous media and on substrates.
- Development of biocompatible, synthetic-biological polymer constituents with temperature-triggered and pH-triggered properties that can be co-assembled with biologically relevant materials, namely therapeutic payloads, enzymes, and pre/in-situ created inorganic nanoparticles, for hierarchical control of nanostructures, responsive and environmental conditions, external stimulation, and reaction of the hybrid nanostructures to a specific environmental condition (i.e. those found in living tissue).
- Studying the external controlling/stimulating effects facilitated by the interactions of inorganic components that are responsive, e.g., light and NIR, (ex. gold nanoparticles) embedded in hybrid polysaccharides, or those controllable by an external magnetic field or other forms of radiation (for example, magnetic iron oxide nanoparticles), to regulate their enzymatic activity and analyze/evaluate the combined effects of simultaneous hyperthermic, photothermic, and photodynamic therapy for combined/synergistic therapy and diagnostics.



Specific objectives of the HYBSAC Project (*Aligned with PNRR – Pillar III Strategic Priorities*)

- Enhance the National and International Competitiveness of Romanian Research by establishing a research core with high-level performance indicators (performance center) emphasizing polysaccharide hybrid materials, which was started under the supervision of an internationally renowned researcher and expert, and a new research pathway on hybrid materials based on polysaccharides in high technology. Also, advanced RAFT polymerization techniques have been developed, which will yield polysaccharides with synthetic polymer components to determine the synthesis, characterization, and testing proportions of pure polysaccharide and hybrid polysaccharides and how much of the synthetic polymers are the same.
- Develop the International profile of ICMPP and allow for the new performance Hybrid Materials Research Core to work on EU and national research programs so that it increases the profile of the institution and becomes active in working with other studies.
- Increase the quality and specialization of the human resources by scientific training and collaborative research under different disciplines. The project will be the vehicle where world-class research will be undertaken. It can allow members of the team to acquire competencies as well as improve their practice for those researchers who have more experience in the field of the project.

The activities in HYBSAC will enhance the team knowledge in producing nanomaterials/nanostructures with more desirable properties and functions, greater diversity, and durability. This knowledge will be readily adopted in industry. The group of young researchers (Postdocs and PhD students) engaged in HYBSAC will receive training in a multidisciplinary context within a state-of-the-art research field, concerning a contemporary issue of material sustainability and ecological social development.

Acknowledgements

We also acknowledge the support provided by the Romanian National Authority for Research, with project number PNRR-III-C9-2022-I8-201, within the National Recovery and Resilience Plan.

Contact

Website: <https://icmpp.ro/hybsac/index.php>; E-mail: hybsac.pnrr@icmpp.ro

” The content of this material does not necessarily represent the official position of the European Union or the Government of Romania”



“PNRR. Finanțat de Uniunea Europeană – Următoarea Generație UE”

NRPP. Funded by European Union-Next Generation EU

<https://mfe.gov.ro/pnrr/>

<https://www.facebook.com/PNRROficial/>



Finanțat de
Uniunea Europeană
NextGenerationEUPlanul Național
de Redresare și Reziliență

INTELLIGENT SYSTEMS FOR CANCER DIAGNOSIS AND TREATMENT - IntelDots

Adina Coroaba,* Narcisa-Laura Marangoci

Petru Poni Institute of Macromolecular Chemistry, Romanian Academy, Iasi, Romania

**adina.coroaba@icmpp.ro*

1. Introduction

As the project Beneficiary, the Petru Poni Institute of Macromolecular Chemistry in Iasi is implementing the project **“Intelligent Systems for Cancer Diagnosis and Treatment (IntelDots)”**, under contract no. 760081/23.05.2023, CF 291/30.11.2022. The project is funded through Romania’s National Recovery and Resilience Plan (NRRP), Component C9 – Support for the private sector, research, development, and innovation, under Investment I8 – Development of a program to attract highly specialised human resources from abroad in research, development and innovation activities. Financing is provided by the European Union through the NextGenerationEU initiative.

IntelDots project aims to capitalize the scientific skills of a renown Spanish PI, Dr Maria Concepcion Ovin Ania, and the interdisciplinary and complementary expertise of a Romanian team working in academia and at “Petru Poni” Institute of Macromolecular Chemistry, to develop new and advanced theranostic systems, contributing thus at finding efficient solutions for a societal problem placed among the financing priorities of the European Union, the diagnosis and treatment of cancer. The assumed task will enrol the Romanian team in the joint efforts hosted by the Horizon Europe programme under „Cancer” mission. Theranostic products for oncological use recently entered on the drug market, and, according Market Data Forecast, an annual increase of their market share by 12 % is envisioned, reaching more than 40 million Euro until 2027. Based on an original approach, IntelDots project will develop a revolutionary theranostic nanomedicine platform for imaging-guided and drug delivery, applicable in oncology under the syntagm of “visible cancer therapy”. An intelligent combination of two non-invasive imaging techniques, nuclear magnetic resonance and fluorescence, is envisaged for the early detection of malignant evolution at cell and tissue level, to support the establishment of efficient individualized treatments.

2. State-of-the-art and project objectives

Cancer is a global health and life threat that is escalating, with often an intractable and deadly character [1]. Due to this, a lot of efforts have been invested in order to continue to research cancer, making Cancer one of the important Mission in the framework of Horizon Europe (H EU) [2], supporting researches aimed to understand, prevent, and optimize cancer diagnosis and treatment. Poor early diagnosis, high systemic toxicity, significant side effects, and difficulty to evaluate therapeutic responses have hampered surgery, chemotherapy, and radiotherapy [1]. Developing a revolutionary nanomedicine platform for imaging-guided and drug delivery, “visible cancer therapy”, can increase therapeutic efficiency and reduce side effects. Magnetic resonance (MR) and fluorescence imaging have received attention recently, and the combination between them is remarkable. Non-invasive imaging analysis can detect cancer early and establish individualized treatment. Importantly, fluorescence probe design can be used to create therapeutic nanomaterials that can identify cancer cells and deliver image-guided cancer treatment. Therefore, magnetofluorescent nanomaterials (MF) are effective biomedical research probes [3,4]. In this context, the project aims to experimentally and theoretically design, develop, and test two new intelligent systems based on multi-functional carbon dots that combine delivering and imaging abilities, providing carrying system for drugs and promote targeted and triggered effects for cancer diagnosis and treatment. The originality and



innovation of the IntelDots project derive from the ambitious goal to design new intelligent systems by combining in a synergistic manner the intriguing fluorescence properties of carbon with the magnetic properties given by the manganese ions.

The IntelDots project's general objective is to attract high-level personnel from abroad, and launching a new research area at IntelCentru, an ICMPP department, by implementing a project related to the field of intelligent systems for cancer diagnosis and treatment, based on MF Cdots, and therefore to support and increase the quality and capacity of the research, development, and innovation (RDI) activity. The project aims at integrating the experimental studies with the theoretical investigations in order to establish, strengthen, and exploit collaboration between experimentalists and theoreticians by assembling a strong and truly interdisciplinary team, under the supervision of a top-level specialist. These actions aim to increase Romanian research competitiveness at the European level, thereby significantly contributing to the accomplishment of general objectives of the National Strategy for Research, Innovation and Smart Specialization.

A set of specific objectives (SO) are considered in order to attempt this ambitious goal:

- SO1: Development and advancement of fundamental scientific research in Romania by creation of a strong research group under the supervision of a top-level specialist, and establishment of a new RDI area at IntelCentru;
- SO2: Encouraging the training of competent human resources and the creation of interdisciplinary research group under the supervision of a high-level specialist;
- SO3: Increasing the number of publications with high international impact and successful participation in the competitions of the H EU framework program.

3. Project implementation and expected outcomes

The scientific Mission of IntelDots project is to develop of a theranostic platform for image-guided drug delivery, applicable in oncology under the concept of “visible cancer therapy.” The project envisions an intelligent combination of two non-invasive imaging techniques – magnetic resonance imaging and fluorescence – for the early detection of malignant evolution at the cellular and tissue levels, with the aim of establishing highly efficient, personalized treatments. The nanometer-scale theranostic system to be developed within the IntelDots project is based on so-called carbon dot entities, capable of acting both as molecular “reporters” and as drug carriers.

The IntelDots project is multidisciplinary per se (implying chemistry, cancer biology, engineering and computational chemistry), and has a major objective to gain an increased knowledge and expertise in designing and producing nano-tools for cancer diagnosis and treatment, addressed to EU Cancer Mission Recommendations No.: 4 – advances in new diagnostic technology, 5 – providing effective therapies with minimal harm, and 6 – increasing the diagnostic and offering a minimally invasive treatment. Besides its scientific objectives, IntelDots project intends to build up a team of high expertise in understanding and providing solutions for both diagnostic and treatment in personalized medicine. Moreover, during the implementation, IntelDots project intends to disseminate the obtained scientific results and to promote its available infrastructure at the European level for both scientific and general publics. According to the SOs, the IntelDots work program includes 5 work packages (WP):

- WP 1 PROJECT MANAGEMENT
- WP 2 INTELLIGENT SYSTEMS based on peptide, cyclodextrin, and Mn@CND with anticancer activity:
 - Obtaining and testing manganese-doped carbon dots from imidic precursors, usable as nanoplatforms for cancer diagnosis and treatment.
 - Development of intelligent systems based on carbon dot functionalized with cyclodextrins, which can form inclusion complexes with hydrophobic moiety connected to particular cell targeting



- peptides.
 - In vitro/in vivo testing of the selected intelligent systems.
 - Magnetic resonance (MR) investigations of the selected intelligent systems.
- WP 3 LIPOSOMAL FORMULATIONS containing hemp oil nanoemulssions and Mn@CND:
 - Development of liposomes containing hemp oil nanoemulssions and Mn@CND.
 - In vitro/in vivo testing of the selected intelligent systems.
 - MR investigations of the selected intelligent systems
- WP 4 MULTISCALE MODELLING of the INTELLIGENT SYSTEMS:
 - Development of liposomes containing hemp oil nanoemulssions and Mn@CND.
 - In vitro/in vivo testing of the selected intelligent systems.
 - MR investigations of the selected intelligent systems
- WP 5 SUPPORT AND DISSEMINATION OF THE SCIENTIFIC RESEARCH

4. Conclusions

The IntelDots project develops innovative theranostic nanoplatforms for “visible cancer therapy,” combining magnetic resonance and fluorescence imaging for early detection and personalized treatment. By combining international expertise with Romanian team interdisciplinary research, the project strengthens national RDI capacity and aligns with Horizon Europe’s Cancer Mission. Expected outcomes include high-impact publications, advanced nanomedicine tools, and increased European visibility of ICMPP.

Acknowledgements

The authors are thankful for the financial support of the grant of the Romanian National Authority for Research, project no. PNRR-III-C9-2022-I8-291, contract no. 760081/23.05.2023, within the National Recovery and Resilience Plan.

References

- [1]. Hoop M, Ribeiro AS, Rösch D, Weinand P, Mendes N, Mushtaq F, Chen X, Shen Y, Pujante CF, Puigmartí-Luis J. Mobile magnetic nanocatalysts for bioorthogonal targeted cancer therapy. *Adv. Funct. Mater.* 28, 1705920, 2018.
- [2]. EU Mission, https://research-and-innovation.ec.europa.eu/funding/funding-opportunities/funding-programmes-and-open-calls/horizon-europe/eu-missions-horizon-europe/eu-mission-cancer_en. Accessed November 30, 2022.
- [3]. Xu Y, Jia X-H, Yin X-B, He X-W, Zhang Y-K. Bridging biodegradable metals and biodegradable polymers: A comprehensive review of biodegradable metal–organic frameworks for biomedical application. *Anal. Chem.* 86, 12122–12129, 2014.
- [4]. Mishra SK, Kannan S. Microwave synthesis of chitosan capped silver-dysprosium bimetallic nanoparticles: a potential nanotheranosis device. *Langmuir* 32, 13687–13696, 2016.





Finanțat de
Uniunea Europeană
NextGenerationEU



Planul Național
de Redresare și Reziliență

METAL COMPLEXES AS MICROTUBULE- AND DUAL MICROTUBULE-R2 RNR-TARGETING DRUGS FOR CANCER TREATMENT - Metubin

Mihaela Dascalu,^{1*} Vladimir Arion^{1,2}

¹Petru Poni Institute of Macromolecular Chemistry,
Romanian Academy, Iasi, Romania

²Institute of Inorganic Chemistry, University of Vienna, Vienna, Austria
*amihaela@icmpp.ro

1. Introduction

Petru Poni Institute of Macromolecular Chemistry (ICMPP), Iasi, Romania is implementing the project “**Metal complexes as microtubule- and dual microtubule – R2 RNR-targeting drugs for cancer treatment** (Metubin), ID 99/31.07.2023, contract no. 760284/27.03.2024, project financed through the National Recovery and Resilience Plan, Component C9 – Support for the private sector, research, development and innovation, Investment I8: Development of a program to attract highly specialized human resources from abroad in research, development and innovation activities.



The **Metubin** project's *general objective* is to attract high-level staff from abroad, and develop a new research area in ICMPP, by implementing a project related to antiproliferative activity and tubulin polymerization inhibition of indolobenzazocine based Schiff bases, TSCs and their metal complexes, and therefore to support and increase the quality and capacity of the research, the development and innovation (RDI) activity. Although modern anticancer chemotherapy has made progress, there are still many problems caused by drug resistance and by the low selectivity of anticancer drugs generating serious side

effects. Therefore, the search for new chemotherapeutics remains an essential challenge. Tubulin, the repeating subunit of microtubules (MTs), and R2 ribonucleotide reductase (RNR) are validated molecular targets for anticancer drugs, as they play crucial roles in cell proliferation and other vital cellular processes. MT-targeted agents (MTAs) and R2 RNR inhibitors lead to disruption of cell cycle progression and cell death via cell cycle arrest in G2/M and S-phase, respectively. The project leader's team recently discovered that Cu(II) complexes with indolobenzazocine-based Schiff bases show good antiproliferative activity and act as colchicine site inhibitors [1], while highly antiproliferative Cu(II) complexes with thiosemicarbazones (TSCs), sharing with the previous agents a similar tridentate binding motif, had both tubulin- and R2 RNR inhibitory activity [2] (Scheme 1). These latter compounds impaired different phases of the cell cycle and were without precedence in the literature.

2. Project objectives

The aim of **Metubin** project is to further refine the electronic and geometric structure of the two prototype metal complexes [3,4] with modified indolobenzazocine and TSC ligands sharing a similar metal binding motif as inhibitor of tubulin polymerization or as dual agent with tubulin- and R2 RNR inhibiting properties endowed with high antiproliferative activity.

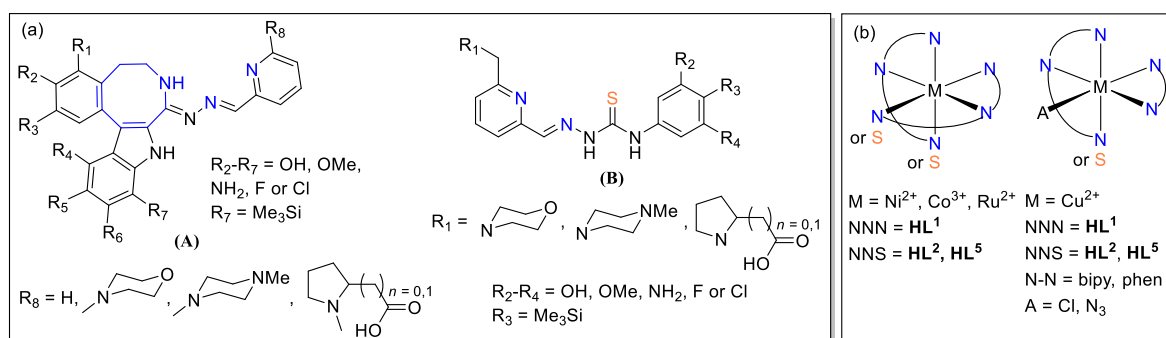
The *specific research objectives* (RO) of the project:

RO1. Preparation and characterization of the two prototype ligands bearing a trimethoxyphenyl group and copper(II) complexes thereof.



- RO2.** Design, synthesis and characterization of the second generation of the two modified prototype ligands bearing electron withdrawing and donating groups including Me₃Si and metal(II) complexes thereof.
- RO3.** Design, synthesis and characterization of the third generation of the two modified prototype ligands and metal complexes thereof.
- RO4.** Design, synthesis and characterization of the fourth generation of the two modified prototype ligands and metal complexes thereof.
- RO5.** Evaluation of stability and extended biological investigation of two lead Schiff bases and two metal complexes.

Based on the initial *in silico* screening, the two prototype molecules are structurally modified through four sequential iterations by attaching electron-withdrawing and donating groups, as well as solubilizing substituents (R₈ and R₁ in Scheme 1). The power of coordination chemistry to build structures with well-defined globular shapes, matching the 3D structure of the colchicine pocket, is exploited to complement the molecular diversity offered by purely organic scaffolds. Kinetic stability of the coordination sphere in biological media will be achieved by using both multidentate ligands and kinetically inert metal ions, e.g., Co(III), Ru(III). This approach was not used for the development of tubulin polymerization inhibitors so far, but proved to be successful for the development of efficient protein kinase inhibitors [3,4]. The synthesis and chemical modification will be followed by full analytical, spectroscopic and structural characterization, as well as biological evaluation of the isolated compounds. The lead drug candidate will be tested *in vivo*.



Scheme 1. Envisaged structural modification of the two main prototypes based on 5,6,7,9-tetrahydro-8H-indolo[3,2-e]benzazocin-8-one and TSCs and metal complexes thereof.

3. Project implementation and expected outcomes

The project objectives will be approached a competent, well-structured team from “Petru Poni” Institute of Macromolecular Chemistry, with top chemistry expertise and infrastructure, under the guidance of a recognized specialist in medicinal chemistry from the University of Vienna, and with strong external collaborative support. Thus, the design of specific compounds start with *in silico* calculations, which will be performed in collaboration with Dr. J. Reynisson (Keele University, UK), **EC1**. The substitution will be considered favorable if the docking scores (e.g., binding free energy) of the newly designed compounds, as well as their ADMET parameters (e.g., aqueous solubility, lipophilicity, physicochemical properties, Lipinski’s rule of five), are not inferior to those of the prototype compounds and remain within the drug-like chemical space. The designed compounds that successfully go through this preliminary *in silico* screening will then be synthesized, fully characterized and tested for antiproliferative activity on several cancer cell lines (breast MCF-7, lung A549, ovarian CH1) and normal MRC-5 human embryonal lung fibroblasts and analyzed for effects on tubulin assembly. This theoretical preselection of relevant structures will make the synthesis work more effective and less time-consuming. Analysis of the results of this full cycle will allow the next iteration, which again will consist of design, molecular docking calculations with determination of molecular descriptors, synthesis, characterization and biological evaluation. The tests will

be performed within ICMPP (IntelCentre) and University of Belgrade, Serbia, and validated at NCI/NIH, USA, based on pre-established collaboration agreements.

The achievement of the scientific objectives is also expected to lead to broader goals (GO):

GO1: Development and progress of fundamental research in Romania through the establishment of a new RDI area at ICMPP conducted by an excellent research group led by a recognized specialist in medicinal chemistry from abroad.

GO2: Training of competent human resources and the formation of an interdisciplinary research group under the supervision of a highly qualified specialist, increasing the ICMPP international visibility.

GO3: Increase of the number of publications with high international impact and participation in the competitions of the European Union's Horizon Europe framework programme competitions.

4. Conclusions

This project aims to develop a new class of compounds based on indolobenzazocines and thiosemicarbazones and their copper(II) complexes, capable of selectively inhibiting tubulin and/or R2 RNR, offering an innovative alternative to existing anticancer agents. Through a structural optimization strategy guided by *in silico* screening, followed by full characterization and biological evaluation, the project will lead to the identification of promising candidates for preclinical development. The originality of the approach, combined with the expertise of the project team and cutting-edge research infrastructure, gives the project a high potential to contribute to the progress of medicinal chemistry and the discovery of new anticancer therapies.

Acknowledgements

The paper was supported by a grant of the Romanian National Authority for Research, project no. PNRR-III-C9-2023-I8-99/31.07.2023 within the National Recovery and Resilience Plan (Romania).

References

- [1]. Wittmann C, Dömötör O, Kuznetcova I, Spengler G, Reynisson J, Holder L, Miller GJ, Enyedy EA, Bai R, Hamel E, Arion VB. Indolo[2,3-*e*]benzazocines and indolo[2,3-*f*]benzazonines and their copper(II) complexes as microtubule destabilizing agents. *Dalton Trans.* 52, 9964–9982, 2023.
- [2]. Wittmann C, Bacher F, Enyedy EA, Dömötör O, Spengler G, Madejski C, Reynisson J, Arion VB. Highly antiproliferative latonduine and indolo[2,3-*c*]quinoline derivatives: complex formation with copper(II) markedly changes the kinase inhibitory profile. *J. Med. Chem.* 65, 2238–2261, 2022.
- [3]. Meggers E. Exploring biologically relevant chemical space with metal complexes. *Curr. Opin. Chem. Biol.* 11, 287–292, 2007.
- [4]. Anand R, Maksimoska J, Pagano N, Wong EY, Gimmotty PA, Diamond SL, Meggers E, Marmorstein R. Toward the development of a potent and selective organoruthenium mammalian sterile 20 kinase inhibitor. *J. Med. Chem.* 52, 160216–11, 2009.





Finanțat de
Uniunea Europeană
NextGenerationEU



Planul Național
de Redresare și Reziliență

MULTIFUNCTIONAL HYBRID 3D ARCHITECTURES BASED ON HOLLOW GaN NANO-MICRO-TETRAPODS FOR ADVANCED APPLICATIONS AT PETRU PONI INSTITUTE OF MACROMOLECULAR CHEMISTRY (MultiPodGaN)

Narcisa-Laura Marangoci,¹ Alexandru Rotaru,¹ Tudor Braniste,^{1,2} Ion Tighineanu,^{1,2*}

¹Petru Poni Institute of Macromolecular Chemistry, Romanian Academy, Iasi, Romania

²Technical University of Moldova, Chisinau, Moldova

*ion.tighineanu@icmpp.ro

The **MultiPodGaN** project aims at the creation of an interdisciplinary research group at Petru Poni Institute of Macromolecular Chemistry under the supervision of Prof. Acad. Ion Tiginyanu in the exciting field of 3D GaN nano-micro-architectures. The established research team will be involved in fundamental research in the bio-micro-fluidics of liquid marbles and self assembled membranes. The advanced multifunctional liquid marbles will be built on the basis of aerogalnite with a view of using them in exploring fundamental bio- and/or chemical processes as well as the interaction of living cells in specific conditions of spatial confinement. Tunable shell material properties will be reached by diminishing the sizes of aero-GaN hollow tetrapods fabricated by direct epitaxial growth of GaN on sacrificial templates consisting of ZnO micro- or nano-tetrapods. Thus, the obtained aero-GaN hollow tetrapods will be subsequently functionalized with macromolecules (synthetic amphiphilic polymers) or biomacromolecules (DNA, proteins or peptides) and investigated for controlled formation of programmed assemblies. Polymer-guided decoration of functionalized GaN units with nanomaterials (metal nanoparticles or carbon nanomaterials) will be examined to produce hybrid materials suitable for the preparation of sensing elements in smart sensors. The current proposal foresees testing of a series of applications for the proposed biocompatible functional 3D GaN nano- and microsystems, including applications as cell supports in supramolecular matrices or design and demonstration of GaN electrochemical or Raman-based sensors.

The **general objective** of the current proposal is to support and increase the quality and capacity of the research development and innovation (RDI) activity by *attracting high-level personnel from abroad, broadening the areas of research at the ICMPP by implementing a project related to the field of 3D GaN-based micro- and nanomaterials, and creating a competitive research group working in this highly competitive field*. These actions aim to *stimulate Romanian research competitiveness at the European level, thus strongly contributing to the fulfilment of the objectives set out in the Romania's National Recovery and Resilience Plan*. Besides the general objective, the proposal also includes **Specific Objectives (SO)**:

- **SO 1.** *Development and advancement of fundamental scientific research in Romania by creation of a high competency scientific group under the supervision of a top-level specialist, and establishment of a new RDI area at ICMPP.* The foreign specialist will pursue the development of new hybrid materials consisting of 3D GaN micro/nanomaterials, and synchronize this field with the research performed at **ICMPP** to provide new interdisciplinary directions for the 3D GaN-based technologies.
- **SO 2.** *Encouraging the training of competent human resources and the creation of interdisciplinary research group under the supervision of a high-level specialist.* Involvement of specialists at the PhD/Postdoc levels in the project tasks will be strongly motivated.
- **SO 3.** *Increasing the ICMPP international visibility and successful participation in the competitions of the European Union's Horizon Europe framework program.* The foreseen results include: **7 high level** scientific publications; **1 National** and **1 European project** submitted; **10 participations** at national and international conferences.



The proposed work strategy and objectives are closely aligned with the main aim of the project, ensuring a unified integration of efforts. The investigation methods and tools are well-founded and well-established, drawing upon several key factors: (i) the project benefits from the extensive expertise of the PI in the field of 3D GaN micro/nanomaterials, and guarantees a strong foundation for the project's success; (ii) the research tasks outlined in the project proposal leverage the interdisciplinary capabilities of the **ICMPP** team, which further strengthens the project's potential for innovative breakthroughs; (iii) the **ICMPP** modern infrastructure, the availability of cutting-edge facilities and resources provides a robust and well-equipped environment for the successful execution of the project; (iv) outstanding previous experience of both the PI and the project manager in projects management; (v) rigorous planning of envisioned project activities. By combining these key elements, the project demonstrates a clear advantage in achieving its objectives, ensuring that the proposed investigation will be conducted with rigor and excellence, providing significant contributions to the field of 3D GaN micro/nanomaterials.

Hollow tetrapods: State-of-the-art and prospects

Aero-GaN within the Aero-Semiconductor Landscape: Aero-semiconductors fabricated from sacrificial ZnO templates offer versatile structural motifs like rods, tetrapods, and multipods, that preserve a hierarchical 3D network (Figure 1). Compared to carbon-based analogues such as aerographite and graphene aerogels, semiconductor aero-architectures bring new properties, including optical transparency, piezoelectricity, photocatalysis, and tunable band structures [1]. Among these, aero-GaN is unique in several respects [2-4]: (i) dual wettability: it exhibits both hydrophobic and hydrophilic domains, enabling novel self-healing and self-assembly phenomena; (ii) biocompatibility: hollow GaN units can interact with living cells, paving the way for biomedical integration; (iii) piezoelectric activity: characteristic to GaN, suitable for applications in pressure sensing and electromechanical systems; (vi) electromagnetic shielding: aero-GaN can provide >40 dB shielding efficiency in the THz range.

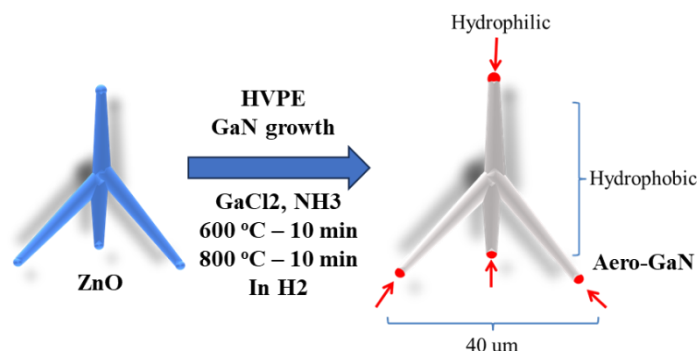


Figure 1. Technological route for the fabrication of aero-GaN.

Functionalization and Hybrid Architectures: To expand the new materials versatility and applicability, aero-GaN can be functionalized via several strategies: (i) polymeric coatings: amphiphilic polymers tune wettability and allow supramolecular assembly; (ii) biomacromolecules: DNA, proteins, and peptides confer biocompatibility and programmable biofunctionality; (iii) nanomaterial decoration: metallic nanoparticles and carbon nanostructures add plasmonic, catalytic, or conductive properties. These hybrid approaches transform aero-GaN into a multifunctional building block. Its tetrapod morphology, with high surface-to-volume ratio and open porosity, is particularly suited for controlled attachment of functional species or nanomaterials.

Prospective Applications:

- *Bio-microfluidics and liquid marbles* - Aero-GaN-based “liquid marbles” assemblies are envisioned as robust, semi-permeable capsules for isolating and studying biological and chemical processes. Their self-healing ability on aqueous surfaces makes them attractive for micro-bioreactor applications, drug testing, and synthetic biology [3].
- *Self-assembled membranes* - Networks of functionalized tetrapods can self-organize into membranes



with tunable hydrophobic/hydrophilic balance. Thus assembled membranes are promising for selective separation, microfluidics, and as bio-inspired scaffolds [2].

- *Smart sensing platforms* - Decorated with various noble metals, the aero-GaN individual entities, or assemblies could be successfully used as: (i) electrochemical sensors for the detection of biologically relevant analytes: decoration with catalytic nanoparticles enhances charge transfer; (ii) Raman sensors for environmental contaminants: GaN frameworks act as stable substrates for SERS-based detection; (iii) pressure and piezoelectric sensors: exploiting the piezoelectric nature of GaN within ultralight, flexible architectures [4].
- *Electromagnetic shielding and optoelectronics* - Owing to their high porosity and dielectric properties, aero-GaN structures and their assemblies serve as efficient THz shields, while transparent aero-Ga₂O₃ complements this family with internet of things (IoT)-oriented applications. The potential for integration into photonic and optoelectronic devices is vast.

Conclusions and Outlook

Aero-GaN hollow tetrapods represent a new edge in ultraporous functional materials. As a member of the broader aero-semiconductor family, it uniquely combines structural lightness, multifunctional semiconductor properties, and unprecedented dual wettability. Functionalization with polymers, biomolecules, and nanomaterials transforms aero-GaN into a platform technology, bridging disciplines from bio-microfluidics to nano-optoelectronics. The MultiPodGaN project is consolidating interdisciplinary expertise to advance these concepts from fundamental research toward demonstrator systems. In future, challenges such as large-scale fabrication, stability in complex biological environments, and integration into device architectures will determine the development of this fascinating material.

Acknowledgements

This work was financially supported by the Romanian National Authority for Research, project no. PNRR-III-C9-2023-I8-161, contract no. 760285/27.03.2024, within the National Recovery and Resilience Plan.

References

- [1]. Ursaki V, Braniste T, Marangoci N, Tiginyanu I. Emerging aero-semiconductor 3D micro-nano-architectures: technology, characterization and prospects for applications. *Appl. Surf. Sci. Adv.* 26, 100708, 2025.
- [2]. Tiginyanu I, Braniste T, Smazna D, Deng M. Self-organized and self-propelled aero-GaN with dual hydrophilic-hydrophobic behaviour. *Nano Energy* 56, 759–769, 2019.
- [3]. Braniste T, Ciobanu V, Schutt F, Mimura H, Raevschi S, Adelung R, Pugno NM, Tiginyanu I. Self-propelled aero-GaN based liquid marbles exhibiting pulsed rotation on the water surface. *Materials* 14(17), 5086, 2021.
- [4]. Dragoman M, Ciobanu V, Shree S, Dragoman D, Braniste T, Raevschi S, Dinescu A, Sarua A, Mishra YK, Pugno N, Adelung R, Tiginyanu I. Sensing up to 40atm using pressure-sensitive aero-GaN. *Phys. Status Solidi RRL* 13, 1900012, 2019.



BIOMAT4CAST DEVELOPMENT ALIGNED WITH CUTTING-EDGE SCIENTIFIC PERSPECTIVES

Teodora Rusu,^{1*} Mariana Pinteala,¹ Ana – Nicoleta Bondar,^{1,2,3} Aatto Laaksonen^{1,4}

¹*Petru Poni Institute of Macromolecular Chemistry, Romanian Academy, Iasi, Romania*

²*Bucharest University, Faculty of Physics, Bucharest, Romania*

³*Forschungszentrum Jülich, Germany*

⁴*Department of Chemistry, Stockholm University, Stockholm, Sweden*

**teia@icmpp.ro*

1. Introduction

Since its inception, the BioMat4CAST project has consistently aligned its activities with the most advanced trends and perspectives in modern science. By combining excellence in biomaterials research with a strong focus on sustainability, the project has fostered new opportunities for growth, collaboration, and innovation. The period 2023–2025 has been particularly dynamic, marked by the initiation and implementation of diverse research projects, extensive networking activities, and international partnerships. These efforts have not only reinforced the team's visibility and expertise but have also ensured that BioMat4CAST remains at the forefront of emerging scientific developments, ready to contribute to the future of biomaterials and beyond.



2. Setting up and Strengthening the BioMat4CAST Team

The future of the BioMat4CAST team is built on a vision of growth, collaboration, and scientific excellence. Under the guidance of Prof. Aatto Laaksonen, together with the BioMat4CAST Management Team coordinated by Dr. Teodora Rusu and Dr. Marian Pinteală, the project has taken important steps towards consolidating its position in the scientific community. As the project evolves, the team is not only strengthening its expertise in biomaterials and advanced computational approaches, but also expanding its capacity to connect with the wider European research community. By combining innovative research, continuous professional development, and strong networking activities, the BioMat4CAST group is shaping a sustainable path forward—one that ensures long-term integration within the scientific landscape of ICMPP and beyond. The strategic steps, initiatives, and opportunities that guide the team towards becoming a driving force in modern science and innovation are summarized below.

Strengthening Sustainability through Research Projects

A key pillar of sustainability has been the proactive approach to securing additional funding. Between 2023–2024, the BioMat4CAST team implemented **five research projects** and submitted **six new proposals** to national and international funding calls. By the end of 2025, several of these proposals were successfully financed, ensuring a research budget of approximately **€350,000 for the following three years**. Other proposals remain under evaluation, while some were not selected, yet every submission has contributed to improving the team's expertise in research funding applications and increasing its chances of future success.

Networking and Sustainability Activities

Equally important has been the role of **networking events, training, and workshops**. The BioMat4CAST consortium organized and co-organized a variety of activities that fostered collaboration with academic,



industrial, and policy actors. Highlights include the **REVERT Project Consortium Seminar (July 2024)**, a **BioMat4CAST Seminar on Modern Trends in Chemistry (October 2024)**, a **Technology Transfer Training (November 2024)**, and a **Networking Workshop on Protein Folding (June 2025)**. These events enhanced scientific exchange, promoted innovation culture, and supported the transfer of knowledge into practical applications. In addition, the team hosted **round-table discussions** that connected researchers and stakeholders across diverse sectors. Examples include the **round table within the PRECISEU Personalised Medicine School (July 2025)**, and exchanges with representatives of the **OMRI PNRR Project (February 2025)**.

Guest Researcher Engagements

The BioMat4CAST project also welcomed a series of **renowned guest researchers**, creating opportunities for direct knowledge transfer and long-term cooperation. Visits included: **Danny O'Hare**, (Imperial College, London); **Dr. Marc Baaden** (Institute of Physical and Chemical Biology, Paris), **Prof. Jozef Uličný** (University of P. J. Safarik, Košice, Slovakia), **Dr. Francesca Mocci** (Cagliari University, Italy), **Prof. Peter Kusalik** (University of Calgary, Canada); **Dr. Fredrik Hedman** (Noruna AB, Stockholm, Sweden); **Dr Szilard Fejer** (Pro-Vitam Diagnostics and Research Centre, Sfantu Gheorghe, Romania), Prof. **Anna Marabotti** (University of Salerno), Prof. **Ana Nicoleta Bondar** (University of Bucharest & Forschungszentrum Jülich), Dr. **Teodoro Laino** (IBM Research Zurich), **Prof. William Wimley** (Tulane University), USA and Prof. **Kalina Hristova** (Johns Hopkins University, USA), Prof. **Paolo Carloni** (Forschungszentrum Jülich & Aachen University). These exchanges provided valuable expertise in computational biomedicine, chemistry, and biomolecular modelling, while anchoring BioMat4CAST within an active international scientific community. Beyond the immediate scientific insights gained, the visits laid the foundation for stronger collaborative links, fostering co-authorship opportunities, joint project proposals, and future training activities. They also helped expose the BioMat4CAST team to diverse methodological approaches and state-of-the-art perspectives, enriching both its research capacity and its visibility within the European and global scientific arenas. By bringing together experienced researchers and early-stage scientists, these engagements have strengthened not only the project's knowledge base but also its long-term sustainability through collaboration and innovation.

3. Shaping the future of BioMat4CAST Team

From October, the BioMat4CAST project will enter a new phase of growth, with its team being further strengthened through the recruitment of **Prof. Dr. Ana Nicoleta Bondar** as Team Leader. Prof. Bondar brings extensive experience in the field of **computational biochemistry and biomolecular simulations**, with a particular focus on **protein-ligand interactions, membrane protein dynamics, and multiscale modeling approaches**. Her dual expertise in scientific research and research management will complement the existing leadership of **Prof. Aatto Laaksonen**, enhancing the project's capacity to coordinate complex studies, attract new funding opportunities, and foster international collaborations. By integrating Prof. Bondar's skills, the BioMat4CAST team will not only consolidate its research excellence but also strengthen its long-term sustainability, ensuring the continuity and growth of innovative activities within ICMPP and its broader European network.

Two new topics will be also to be implemented in close collaboration with **Prof. William Wimley** (Tulane University), USA and Prof. **Kalina Hristova** (Johns Hopkins University, USA), Prof. **Paolo Carloni** (Forschungszentrum Jülich & Aachen University). During the visit at the Petru Poni Institute in June 2025 the team discussed a collaboration on combining experiment and computation to study inhibitors that bind to receptor tyrosine kinases (RTKs) implicated in cancer disease. The laboratory of Prof. Kalina Hristova has the documented expertise to study RTKs homo- and hetero-interactions in cells using three different methods: i) a fluorescence fluctuation spectroscopy method called Number and Brightness, which is used to report the co-diffusion of receptors in the plasma membrane; ii) Forster Resonance Energy Transfer



(FRET), sensitive to close approach of the receptors in the plasma membrane; iii) in vitro phosphorylation assay to measure phosphorylation as a function receptor complex formation. These experiments will be combined with extensive computations performed by the BioMAT4CAST colleagues, as follows. i) classical mechanical computations to study the motions of the membrane-embedded RTK hetero-complex; ii) combined quantum mechanical/molecular mechanical computations using methods developed by Paolo Carloni to study inhibitor binding and the effect of inhibitors on the reaction coordinate of the phosphorylation reaction; iii) computational screening and prediction of new inhibitors. These new predicted inhibitors will be synthesized by the experimental team of BioMAT4CAST and tested for RTK heterocomplex binding by the Hristova laboratory. We envision that, once successful, we may proceed with developing an inhibitor cargo delivery system together with the Wimley and Hristova laboratories.

4. Conclusions

Between 2022 and 2025, BioMat4CAST has demonstrated remarkable progress in enhancing sustainability, advancing scientific excellence, and fostering international collaboration. The team has successfully implemented multiple research projects, submitted and secured additional funding proposals, and actively engaged in trainings, workshops, and networking events—both nationally and internationally. These efforts have strengthened the team's research capacity, expanded its visibility, and consolidated its position within ICMPP and the broader European research landscape.

Collectively, these achievements provide a solid foundation for BioMat4CAST to continue shaping the future of biomaterials research. The combination of strong leadership, a skilled and growing team, international partnerships, and a proactive approach to securing funding positions the project as a driving force in the field, capable of delivering innovative solutions and contributing significantly to the European Research Area. The period 2022–2025 thus represents a transformative phase for BioMat4CAST, setting the stage for continued growth, scientific impact, and sustained excellence in the years to come.

Acknowledgements

We also acknowledge the support provided by European Union's Horizon Europe Research and Innovation Programme under grant agreement No 101086667, project BioMat4CAST (BioMat4CAST - "Petru Poni" Institute of Macromolecular Chemistry Multi-Scale In Silico Laboratory for Complex and Smart Biomaterials).



Funded by the
European Union

Talent Pass



FOSTERING EUROPEAN TALENTS FOR WIDENING CIRCULAR ECONOMY

Magdalena Aflori,* Raluca-Oana Andone,* Dan-Radu Rusu,

Tachita Vlad-Bubulac, Valeria Harabagiu

*Petru Poni Institute of Macromolecular Chemistry, Romanian Academy, Iasi, Romania***talent_pass@icmpp.ro*

1. Talent Pass idea and Consortium

The HORIZON-WIDERA ERA Talents Action was developed to address the goals formulated by the Horizon Europe Work Programme [1] and represents the most suitable tool to incubate the Talent Pass idea. Talent Pass Project, a €3 million Horizon Europe-funded project is designed to advance talent mobility, foster knowledge transfer, and accelerate innovation within the circular economy. The Talent Pass consortium incorporates 4 academic and 6 non-academic beneficiaries from 4 widening countries (Romania, Portugal, Slovenia, Turkey) and 3 non-widening countries (Italy, Estonia, United Kingdom).

The consortium coordinated by the Petru Poni Institute of Macromolecular Chemistry, Iasi, Romania brings together academic and non-academic partners: Institutul National de Cercetare Dezvoltare pentru Ecologie Industrială, Bucharest, Romania, Kemijski Institut, Ljubljana, Slovenia, IST-ID Associacao Do Instituto Superior Tecnico Para a Investigacao e o Desenvolvimento, Lisboa, Portugal, Asociación Para La Investigación y Desarrollo Tecnológico de la Industria de Castilla la Mancha, Tomelloso Ciudad Real, Spain, Opencom I.S.S.C., Arezzo, Italy, Unismart - Fondazione Università Degli Studi di Padova, Padova, Italy, Crowdhelix Limited, London, United Kingdom, Farplas Otomotiv Anonim Sirketi, Kocaeli, Türkiye, Chimcomplex SA Borzesti, Onesti, Romania (Figure 1a). This geographical diversity within the Consortium ensures a comprehensive approach to research and innovation, blending different levels of expertise and creating a rich environment for collaboration across various academic, non-academic, and socio-economic backgrounds (Figure 1b).

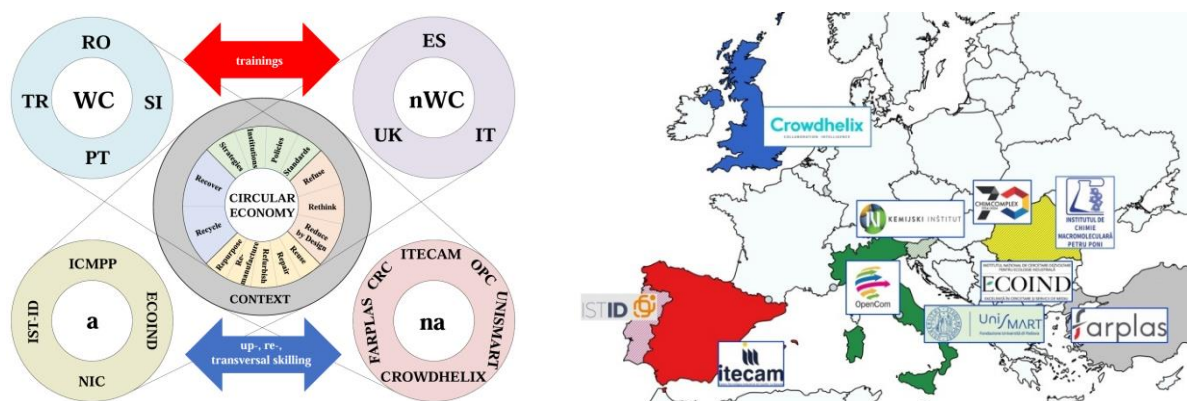


Figure 1. Talent Pass Consortium: (left) Talent Pass drone methodology; (right) geographical diversity within the Talent Pass consortium.

2. Context and overall objectives

The specific needs that triggered the Talent Pass project are:

- Reskilling and upskilling personnel in sustainability, project management, knowledge and technology transfer, intellectual property rights, open science, data management, entrepreneurship, research ethics and integrity, risks management and digital skills
- Increase mobility of R&I staff, particularly to non-academic sectors
- Revert brain-drain
- Tackle challenges in attracting and retaining top research talent
- Build motivation tools and increase focus on career development for R&I staff to reduce the gaps in services for private sector partnerships and limited cross-sectorial cooperation
- Increase the low benefit/cost ratio for technology transfer
- Boost external communication and networking, leading to poor knowledge circulation.

In this context, the Talent Pass initiative is designed to:

- strengthen the innovation ecosystem towards a borderless research, innovation (R&I) and technology market by addressing the critical need for geographically balanced talent circulation and increased cross-sectorial interoperability, as outlined in Action 4 of the ERA Policy Agenda (2022-2024)
- cultivate and support cross-sectorial partnerships between academic and non-academic organizations that operate in areas of proven scientific excellence, particularly within the realm of the circular economy.

The Talent Pass project objectives are:

- O1. To develop a critical mass of human resources (researchers, innovators, research managers and other R&I talents) by up-skilling, re-skilling and transferable knowledge circulation in the framework of circular economy.
- O2. To enhance employability and sustainable career prospects within a dynamic innovation ecosystem for R&I talents.
- O3. To advance R&I organizations' support capacity through a sound collaboration between academic and non-academic stakeholders via collaborative/supportive structures.
- O4. To facilitate two-way access for talents from (non)academic R&I entities to know-how and infrastructures across and beyond the European Research Area via equitable geographical and cross-sectorial talent circulation.
- O5. To establish excellent research organizations in widening countries through inter- and multi-disciplinary cross-sectorial collaborations in circular economy.

3. Expected impact

Talent Pass project aims to:

- Significantly enhance talent mobility and expertise development within circular economy, particularly focusing on researchers, innovators, and other R&I academic/non-academic talents from widening countries.
- Build a critical mass of competent researchers having the necessary high-quality knowledge, skills, and tools to drive forward innovation and sustainability in the circular economy.
- Improving access to excellence by consolidating an interdisciplinary network of highly skilled human resources and enhance the efficient utilization and valorisation of complementary research capacities, infrastructure and results, aligning with the Horizon Europe Work Programme (2023-24) - WIDERA and the Circular Economy Action Plan for a Cleaner and More Competitive Europe (2020) [2].
- Bridge the gap between research and application and effectively translate advancements in circular economy into real-world solutions, by fostering collaboration between academia and industry.



Impact of the Talent Pass project may be observed through different perspectives:

- Networking impact: strengthened research community, enhanced innovation at national, regional, and European levels.
- Scientific impact: increased visibility, competitiveness, scientific output, innovation capacity, and improved access to European funding and financing tools.
- Economic/technological impact: enhanced collaboration, regenerative growth model, sustainable job creation, and reduced resource pressure.
- Societal impact: balanced brain circulation, improved R&I careers, reduced brain drain, and enhanced motivation tools for R&I staff.

Acknowledgements

We acknowledge the financial support received from the European Union through the Horizon Europe Research and Innovation Programme, under the Talent Pass Project, Grant Agreement No. 101217448 – HORIZON-WIDERA-2024-TALENTS-03.

Contact

Email: talent_pass@icmpp.ro; Website: <https://www.talentpass-project.eu/>

References

- [1]. Horizon Europe Work Programme 2023-2025, 11. Widening participation and strengthening the European Research Area, https://ec.europa.eu/info/funding-tenders/opportunities/docs/2021-2027/horizon/wp-call/2023-2024/wp-1-general-introduction_horizon-2023-2024_en.pdf. Accessed 15 Aug 2025
- [2]. https://environment.ec.europa.eu/strategy/circular-economy-action-plan_en. Accessed 15 Aug 2025



MACRO Iași 2025

